REPUBLIQUE ALGERIENNE DEMOCRATIQUE ET POPULAIRE

Ministère de l'Enseignement Supérieur et de la Recherche Scientifique

Ecole Nationale Polytechnique

Department of Electronics

Laboratory of Communication Devices and Photovoltaic Conversion

Doctoral thesis 3rd Cycle LMD

Option: Solar electricity

Implementation on FPGA of an algorithm for the characterization of solar modules

Presented by:

TCHOKETCH KEBIR Selma

Master in Automatics, University of Blida1

Presented and publicly supported on 14 / 07 / 2021

Jury members:

Chair	M .ADNANE Mourad,	Professor	ENP
Supervisor	M .AIT CHEIKH Mohamed Salah,	Professor	ENP
Supervisor	M .HADDADI Mourad,	Professor	ENP
Examiner	M .LARBES Cherif,	Professor	ENP
Examiner	M .BELMILI Hocine,	Doctor	UDES/CDER
Examiner	Mrs .HASSAINE Linda,	Doctor	CDER
Guest	Mrs .CHEGGAGA Nawal,	Doctor	USDB1

ENP 2021

REPUBLIQUE ALGERIENNE DEMOCRATIQUE ET POPULAIRE

Ministère de l'Enseignement Supérieur et de la Recherche Scientifique

Ecole Nationale Polytechnique

Department of Electronics

Laboratory of Communication Devices and Photovoltaic Conversion

Doctoral thesis 3rd Cycle LMD

Option: Solar electricity

Implementation on FPGA of an algorithm for the characterization of solar modules

Presented by:

TCHOKETCH KEBIR Selma

Master in Automatics, University of Blida1

Presented and publicly supported on 14 / 07 / 2021

Jury members:

Chair	M .ADNANE Mourad,	Professor	ENP
Supervisor	M .AIT CHEIKH Mohamed Salah,	Professor	ENP
Supervisor	M .HADDADI Mourad,	Professor	ENP
Examiner	M .LARBES Cherif,	Professor	ENP
Examiner	M .BELMILI Hocine,	Doctor	UDES/CDER
Examiner	Mrs .HASSAINE Linda,	Doctor	CDER
Guest	Mrs .CHEGGAGA Nawal,	Doctor	USDB1

ENP 2021

REPUBLIQUE ALGERIENNE DEMOCRATIQUE ET POPULAIRE

Ministère de l'Enseignement Supérieur et de la Recherche Scientifique

Ecole Nationale Polytechnique

Département D'Electronique

Laboratoire de Dispositifs de Communication et de Conversion Photovoltaïque

Thèse de doctorat en 3ème Cycle LMD

Option : Electricité solaire

Implémentation d'un algorithme pour la caractérisation de modules solaires

Présentée par :

Selma TCHOKETCH KEBIR

Master en Electronique, Université de Blida

Présentée et soutenue publiquement le 14/07/2021

Composition du Jury :

Président	M .Mourad ADNANE,	Professeur	ENP
Promoteur	M .Mohamed Salah AIT CHEIKH,	Professeur	ENP
Co-Promoteur	M .Mourad HADDADI,	Professeur	ENP
Examinateur	M .Cherif LARBES,	Professeur	ENP
Examinateur	M .Hocine BELMILI,	Docteur	UDES
Examinatrice	Mme .Linda HASSAINE,	Docteur	CDER
Invitée	Mme .Nawal CHEGGAGA,	MCA	USDB1

ENP 2021

ملخص: المولد الكهروضوئي، الذي يعتبر قلب أي تركيب كهروضوئي، يعرض أحيانًا أعطالًا أثناء حياته مما يؤدي إلى تدهور التركيب الكهروضوئي بأكمله. لذلك، هناك حاجة إلى تقنيات التشخيص لضمان اكتشاف الأخطاء وتجنب المخاطر الخطيرة وتوفير الحماية وإطالة العمر الصحي. ولهذه الغايات، يساهم هذا العمل في دراسة أنواع تدهور المولدات الكهروضوئية وأنواع أعطالها وتقنيات التشخيص الرئيسية. تم تطوير هذه الرسالة في جزأين رئيسيين، الجزء الأول "المولدات الكهروضوئية: نظرة عامة، الأداء، الإنتاجية، الأعطال، التشخيص، النمذجة، التصنيف ". تم تنظيم هذا الجزء الأول في ثلاثة فصول. بينما يتضمن الجزء الثاني "الذكاء الاصطناعي والتنفيذ" فصلين. الفصل 4: تطبيق الشبكات العصبية لتشخيص عيوب PVG. في هذا الفصل، يتم تقديم وصف عام للشبكات العصبية وتطبيقها على تشخيص الأعطال التي تحدث في PVG. إنها شبكة من الشبكات العصبية الاصطناعية، تم تطويرها لنمذجة أنواع مختلفة من الأخطاء التي يمكن أن تظهر عند تشغيل نظام PV في الوقت الفعلي. تم تقديم عمليات المحاكاة والاختبارات التجريبية، وقد أظهرت هذه الطريقة نتائج جيدة لنمذجة وتشخيص المجال الكهروضوئي الصحي والمعيب. كمرحلة أخيرة من هذه الأطروحة، يحتوي الفصل الخامس على منهجية تجميعية للتنفيذ على لوحة FPGA لإحدى الشبكات العصبية المطورة. يعتمد وصف VHDL المقترح على بنية بسيطة ومنتظمة ومتوازية.

الكلمات المفتاحية ـ مولد كهروضوني، المراقبة الآلية، كشف الأعطال، التشخيص الإلكتروني، الذكاء الاصطناعي، الشبكات العصبية، FPGA.

Résumé : Le générateur photovoltaïque, considéré comme le cœur de toute installation photovoltaïque, présente parfois des dysfonctionnements durant leur vie qui entraînent des dégradations sur l'ensemble de l'installation photovoltaïque. Par conséquent, des techniques de diagnostic sont nécessaires pour garantir la détection des pannes, permettent d'éviter les risques dangereux, permettent une protection et prolongent leur vie saine. A ces fins, ce travail contribue à l'étude des types de dégradations des générateurs photovoltaïques, de leurs types de défauts et de ces principales techniques de diagnostic. Ce travail de thèse a été développé en deux parties principales, la première partie « Générateurs Photovoltaïques : Généralité, Performances, Productivité, Défauts, Diagnostic, Modélisation, Caractérisation, & Identification ». Cette première partie est organisée en trois chapitres. Tandis que la deuxième partie « Intelligence Artificielle & Implémentation » comprend deux chapitres. Le chapitre 4 : Application des réseaux de neurones au diagnostic des défauts de PVG. Dans ce chapitre, une description générale des réseaux de neurones et de leur application au diagnostic des défauts survenant en PVG est présentée. Il s'agit d'un réseau de réseaux de neurones artificiels, développé afin de modéliser différents types de défauts qui peuvent paraître lors de l'exploitation d'un système PV en temps réel. Des simulations et des tests expérimentaux ont été présentés, cette méthode montre de bons résultats pour la modélisation et le diagnostic du champ photovoltaïque sain et défectueux. Comme phase finale de ce mémoire, le chapitre 5 renferme une méthodologie de synthèse pour l'implémentation sur carte FPGA de l'un des réseaux de neurone développé. La description VHDL proposée est basée sur une architecture simple, régulière et parallèle.

Keywords- Générateur photovoltaïque, surveillance automatique, détection de défauts, diagnostic, intelligence artificielle, réseaux de neurones, FPGA.

Abstract: The photovoltaic generator, considered to be the heart of any photovoltaic installation, exhibits sometimes malfunctions during their life cycle, which lead to degradation of the entire photovoltaic installation. Therefore, diagnostic techniques are needed to ensure fault detection, prevent dangerous risks, provide protection and prolong their healthy life. To these ends, this work contributes to the study of the types of degradation of photovoltaic generators, their types of faults and these main diagnostic techniques. This thesis work has been developed into two main parts, the first part "Photovoltaic Generators: Generality, Performances, Productivity, Faults, Diagnosis, Modelling, Characterization, & Identification". This first part is organized in three chapters. While the second part "Artificial Intelligence & Implementation" includes two chapters. Chapter 4: Application of neural networks to the diagnosis of PVG defects. In this chapter, a general description of neural networks and their application to the diagnosis of faults occurring in PVG is presented. It is a network of artificial neural networks, developed to model different types of faults that can appear when operating a PV system in real time. Simulations and experimental tests have been presented, this method shows good results for the modelling and the diagnosis of the healthy and defective photovoltaic system. As a final phase of this thesis, chapter 5 contains a synthesis methodology for the implementation on an FPGA board of one of the neural networks developed. The proposed VHDL description is based on a simple, regular and parallel architecture.

Keywords- Photovoltaic generator, automatic monitoring, faults detection, diagnosis, artificial intelligence, neural networks, FPGA.

ACKNOWLEDGEMENTS

First, I thank *ALLAH* for letting me live to see this thesis through.

I would like to thank my thesis supervisor Mr *Med Salah AIT CHEIKH*. His availability and generous help during some of my difficult times have been of very high quality, and of immense comfort, thank you very much, Professor, who is like another father to me.

My Co-thesis supervisor Mr *Mourad HADDADI* for his excellent supervision, guidance and continuous help.

My sincere thanks to Mr *Cherif LARBES* for his help, support and encouragement throughout my doctoral studies.

I thank Mrs *Nawal CHEGGAGA* teacher at the *University Saad Dahleb of Blida1 (USDB1)*, for her support and help. She helped me find solutions to move forward and had always pointed me in the right direction. I am forever indebted to her unwavering support, and encouragements through this process.

I would also like to thank the *Laboratoire de Recherche en Energie Eolienne (LREE)* of the *University of Quebec At Rimouski (UQAR)* in *Canada* to have accepted me as a visiting researcher since November 2017; and particularly his director Mr *Adrian ILINCA*, for his high quality of help, orientation, generosity and kindness.

I would like to thank Mr *Hocine BELMILI* who allowed me to use the facilities of the *Multi-Sources-System (SMS)* laboratory at *Unité de Développement des Equipements Solaires (UDES)* and for his direction during the realization of some tasks.

I thank by the way Mrs *Nouma IZEBOUDJEN* researcher from *Centre de Développement de technologies Avancées (CDTA)*, for her help in finalising this work.

I would like to thank the members of my thesis committee: *Mourad ADNANE* at *ENP*, *Cherif LARBES at ENP*, *Linda HASSAINE at CDER*, *Hocine BELMILI at UDES, and Nawal CHEGGAGA at USDB1* for kindly evaluating my work.

I address my sincere thanks to all the people who by their words and advices guided my reflections during my research. Moreover, to all of my near colleagues at *UDES*.

Thank you to the people who believed in me and who allowed me to complete this thesis. My sincere gratitude goes to my family and all my close ones without their continued encouragement and moral support I would not have gotten to where I am, especially those who make me happy.

Finally, I could not end these thanks without a thought to all of my teachers who are the source of all knowledge.

Dedication

To

My ALLAH

My Family

My Parents " Mohamed & Fatma-Zohra ZEMIR"

My Sisters & Brothers

My Closed Persons

TABLE OF CONTENTS

Part 2

Artificial Intelligence & Implementation

LIST OF TABLES

LIST OF FIGURES

LIST OF SYMBOLS

I_{dc}: Current of the direct side

V_{dc}: Voltage of the direct side

P_{dc}: Power outputs of the direct side

T_{amb}: Ambient temperature

I_{ac}: Current of the alternative side

V_{ac}: Voltage of the alternative side

P_{ac}: Power outputs of the alternative side

T_c: Cell's temperature

G: Solar irradiation

Y_f: Final yield

Y_r: Reference yield

E_t: Consumed PV energy (Wh)

P_{STC}: System rated power at STC (Wp)

H_t: Total in-plane irradiance (Wh/m^2)

G_{STC}: Reference irradiation at STC

Y_a : Array yield

E_{dc}: Energy generated by the PV array (Wh)

P_{ref} : Maximum power output of the PV array

I_{MPP}: Current at the MPP

V_{MPP}: Voltage at the MPP

P_{MPP}: Power at the MPP

I_{SC}: Current at Short-Circuit

V_{OC}: Voltage at Open-Circuit

R_s: Series resistance

R_{sh}: Shunt resistance

I_L: Light current.

I_{ds1}: Diode saturation current (*Diffusion phenomenon*)

I_{ds2}: Reverse diode saturation current (*Recombination phenomenon*)

n_1: Diode ideality factor (*Diffusion phenomenon*)

n_2: Second diode ideality factor (*Recombination phenomenon*)

V_t: Thermal voltage constant

K_B: Boltzmann's constant (1.380650*10 -23 J/K)

q: Electronic charge (1.6021764*10-19 C) and

T_c: Cell's temperature.

N_s: Number of series cells

N_{ms}: Number of panels in series branches

N_{mp}: Number of panels in parallel branches

η: Efficiency

C_r: Current ratio

V_r: Voltage ratio

LIST OF ABREVIATIONS

RE: Renewable Energy

CSP: Concentrated Solar Power

PV: Photovoltaic

FDD: Fault detection and diagnosis

C-Si: Crystalline-Silicon

PVG: Photovoltaic generator

GHI: Global Horizontal Irradiation

UV: Ultraviolet

IR: Infrared

Mono-C-Si: Mono-Crystalline-Silicon

a-Si: Amorphous

Poly-C-Si: Polycrystalline-Silicon

CdTe: Cadmium Telluride

CIGS: Copper Indium Gallium Selenide

DSSC: Dye-Sensitized Solar Cell

PEC: Photo-electrochemical

GaAs: Gallium Arsenide

PSC: Perovskite solar cell

NREL: National Renewable Energy Laboratory

STC: Standard Test Conditions

BPD: Bypass diode

BD: Blocking diode

JB: Junction Box

DC: Direct Current

AC: Alternative Current

DC-DC: Converter from direct to direct

DC-AC: Converter from direct to alternative (Inverter)

MPPT: Maximum Power Point Tracking

IEA: International Energy Agency

IEC: International Electronic Committee

PR: Performance ratio

DAQ: Data acquisition system

BBP: Blocking and bypassing diode

HS: Hot-Spot

PS: Partial-Shading

OC: Open-Circuit

SC: Short-Circuit

LLF: Line-to-Line Fault

GF: Ground-Fault

AF: Arc-Fault

EVA: Ethylene vinyl acetate

PID: Potential Induced Degradations

I-V: Current-Voltage

P-V: Power-Voltage

MPP: Maximum Power Point

ELS: Energy loss stress

LIT: Lock in thermography

EL: Electroluminescence

PL: Photoluminescence

TDR: Time-domain reflectometry

AI: Artificial intelligence

ANN: Artificial neural networks

PCA: Principal component analysis

DWT: Discrete wavelet transform

GFPD: Ground-fault-protection-device

OCPD: Over-current-protection-device

SVM: Support vector machine

AFCI: Arc-fault-circuit-interrupter

IoT: Internet of Thing

SDM: Single Diode Model

DDM: Double Diode Model

FF: Fill factor

MPPT: Maximum Power Point Tracking

NR: Newton Raphson

EA: Evolutionary Algorithm

DE: Differential Evolutionary

GA: Genetic Algorithms

PS: Pattern Search

SA: Simulated Annealing

Rcr-IJADE: Repaired Adaptive Differential Evolution

EFO: Electromagnetic Field Optimization

GSA: Gravitational Search Algorithm

EMA: Electromagnetism-Like Algorithm

WSA: Weighted Superposition Attraction

HS: Harmony Search

AI: Artificial intelligence

BFA: Bacterial Foraging Algorithm

STLBO: Simplified Teaching-Learning-Based Optimization

DSOS: Discrete Symbiosis Organism Search

AIS: Artificial Immune system

PSO: Particle Swarm Optimization

BMO: Bird Mating Optimization

ABSO: Artificial Bee Swarm Optimization

CWOA: Chaotic Whale Optimization Algorithm

CSO: Cat Swarm Optimization

CA: Cluster Analysis

EHA-NMS: Hybrid adaptive Nelder-Mead simplex algorithm based on eagle strategy

NM-MPSO: Nelder-Mead and Modified Particle Swarm Optimization

ABC-DE: Artificial Bee Colony-Differential Evolution

ABC-TRR: Trust-Region Reflective deterministic algorithm with the Artificial Bee Colony

TLABC: Teaching–learning–based Artificial Bee Colony

HPSOSA: hybrid particle swarm optimization combined with simulated annealing

LM: Levenberg-Marquardt

GWO: Grey Wolf Optimizer

LSM: Least-squares mean

SD: Steepest-Descent

GN: Gauss-Newton

LMGWO: Levenberg-Marquardt combined with Grey Wolf Optimizer

ANNs: Artificial Neural Networks

NN: Neural-network

NANNs: Networks of Artificial Neural Networks

PNNs: Probabilistic Neural Networks

CDER: Centre of Development of Renewable Energies

G: Solar irradiance

T: Panel's temperature

PDF: Probability Density Function

MLP: Multi-Layer Perceptron

RBF: Radial basis functions

RMSE: Root mean square error

MRE: Mean relative error

SMS : Multi-Sources-System laboratory

UDES : Unité de Développement des Equipements Solaire

VLSI: Very Large Scale Integrated

VHDL: Very High speed integrated circuits Hardware Description Language

FPGA: Filed Programmable Gate Array

RTL: Register transfer level

PLD: Programmable Logic Device

PAL: Programmable Array Logic

GAL: Generic Array Logic

EPLD: Erasable Programmable Logic Device

CPLD: Complex Programmable Logic Device

CLB: Configurable logic blocks

IO: Configurable input/output blocks

SRAM: Static Random Access Memory

ISE: Integrated Software Environment

MUX: Multiplexers

LUT: Look Up Table

MAC: Multiply Accumulate circuit

ROM: Memory circuit

DSP: Digital Signal Processor

GENERAL INTRODUCTION

GENERAL INTRODUCTION

The threats of fossil energies such as dangers of nuclear energy, pollution, high emissions of Co2, increasing prices of petroleum, have motivated many utilities for developing and harnessing new forms of energy sources that are highly reliable, in order to satisfy the increasing energy demand in the world. In this context, renewable energy (RE) is the form that responds to this subject and can be produced through resources that naturally replenish themselves by natural processes from sunlight (Photovoltaic & thermal: Concentrated Solar Power (CSP)), wind (On-shore & Off-shore), rain, wave power, ocean energy, flowing water (Hydropower) and geothermal heat (Geothermal), hydrogen and fuel cells (Bioenergy). All of the RE forms have been installed with evolution during the last period (2015-2019), as indicated in Figure 0.1, with global renewable power capacity totalled 2378 GW by 2018 [1].

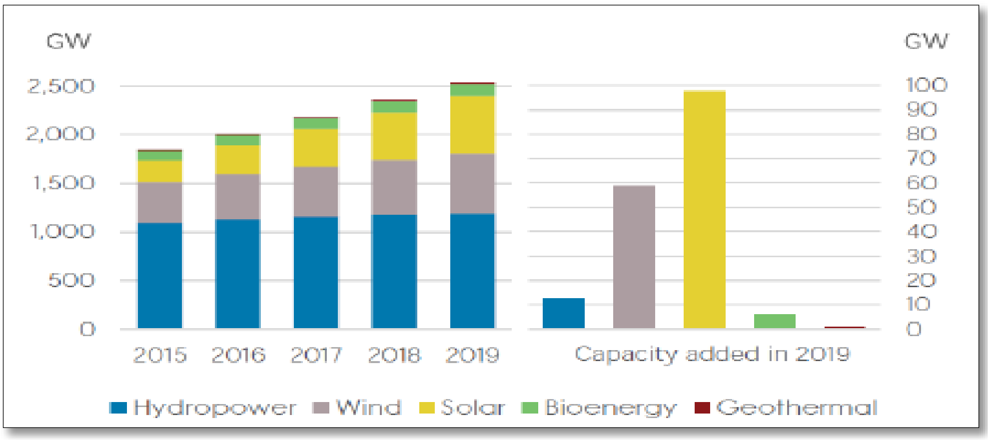

Figure 0.1 Evolution of installed technology capacity from RE in the world (2015-2019) and the last addition (2019) [1].

Renewable energy is considered not only as a source of energy but also as a promising solution to many problems such as energy security, creating jobs and reducing poverty, etc. Therefore, these sources have become the subject of advanced research for extracting power with high reliability, lower cost and increased energy efficiency. Power generation from solar energy is one of the most promising renewable energies that attract the attention of researchers, which is clean, renewable, inexhaustible, free and abundant in most parts of the world, and it has proven to be an economical source of energy in many applications. Solar energy can be exploited into two major forms: the first form is the captured heat (CSP) that can be used as solar thermal energy. The second form is photovoltaic (PV), which converts the incident solar irradiance into electrical energy, and which is the most usable form of energy. Figure 0.2 illustrates the evolution of cumulative PV capacity (GW) installed: a) around the world; b) per region in the world, with projection to 2050, as indicated in the trends of the International Energy Agency (IEA) in [2].

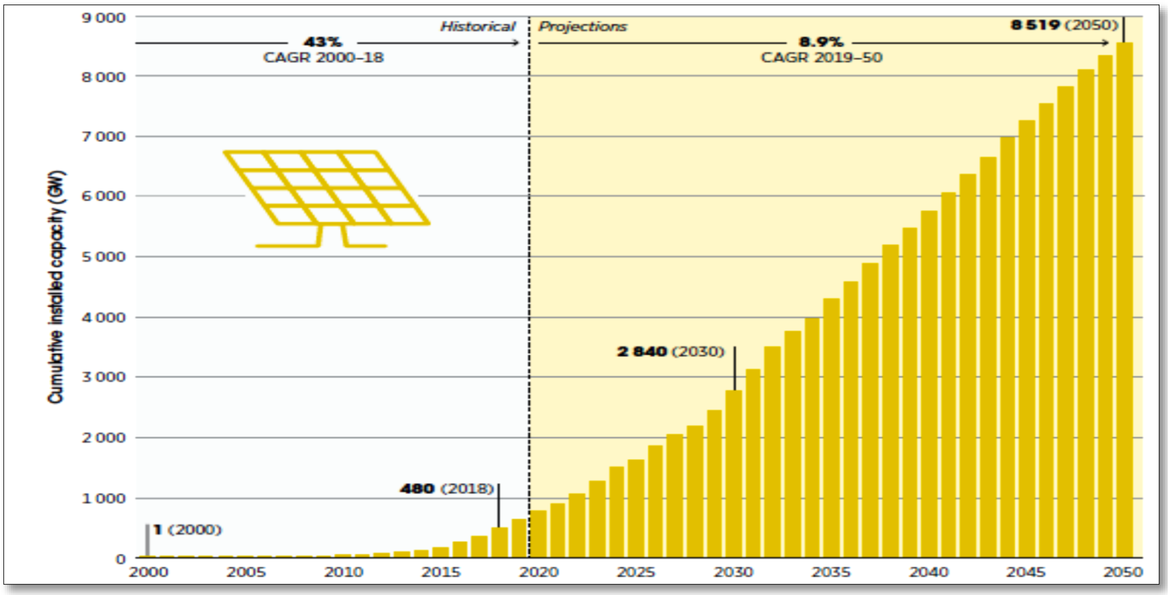

a)

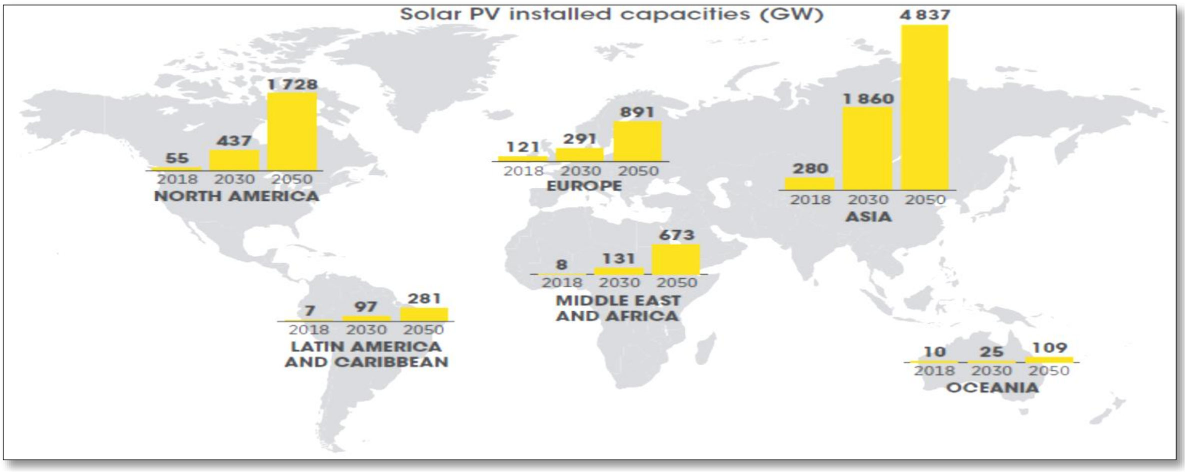

b)

Figure 0.2 Evolution of cumulative PV capacity installed: a) around the world; b) per region in the world, with projection to 2050 [2].

Solar photovoltaic energy is the most well-known and widely spread renewable energy across the globe, where it has achieved a cumulative capacity of 635 GW by the end of 2019 [3]. In this energy, researchers and laboratory have interested on the development of different axes such as, material's composite, cells and amelioration of their yields, panels and their characterization, on the global installation and its optimization, identification, and diagnosis of state. In this issue, the installed PV plants are subject to failures, malfunctions, and damages during their life cycle [4], [5]. In this regard, proper diagnosis is crucial, to avoid any loss of efficiency, safeguard the system, and guarantee service continuity. The failures detected in any solar PV system are due to different internal, external, and ageing causes [4], [6], [7]. Fault detection and diagnosis (FDD) methods for PV plants are needed to detect and identify abnormal conditions at early stages to reduce the risks associated with a long-term operation. Many research works have been focused on developing diverse FDD techniques, to guarantee efficient and intelligent monitoring and supervision in PV plants. Figure 0.3 shows the growing number of reference documents concerning the diagnosis of PV systems published since 2005. This shows how much research on this subject has increased over the years and remain strong.

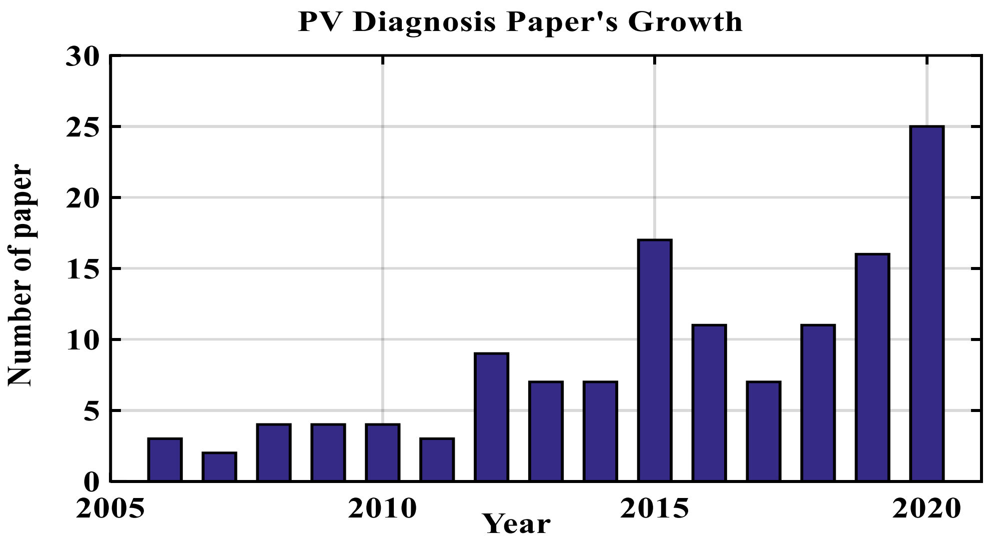

Figure 0.3 Growth of PV diagnosis published papers per year, since 2005.

This thesis work has been developed in two main parts, structured as cited below:

1st Part « ***Photovoltaic Generators: Generality, Performances, Productivity, Faults, Diagnosis, Modelling, Characterization, & Identification*** »

This first part contains three chapters as bellowed.

- Chapter 1: Photovoltaic Generators: Generality, Applications, & Productivity.

This chapter presents a study of the photovoltaic generation unit, known as a photovoltaic generator (PVG). The study of PVG encloses generalities, behaviors, performances, their main applications, and productivity. We have seen the importance of using such PVG, from the interest done with years in the historical point, the many advantages cited with some limitations, the abundance of energy from the sun, and the focus of researchers to get a very high yield from the used material technology. The performances and several applications of PV systems have been also detailed. Before termination of this chapter, a presentation has been enlarged of the losses and productivity in a special PV application containing the major elements of the PV chain.

- Chapter 2: Fault Detection and Diagnosis Techniques for PVG.

After seeing generalities in the first chapter, particularly seeing that the productivity of a PV system, is affected by many factors and that PVG necessitates protections. This chapter summarizes the different causes and types of degradations of photovoltaic generators, the major types of faults and their main diagnosis techniques. Various fault detection and diagnosis techniques have been presented. Besides, some envisaged diagnosis solutions have been discussed.

- Chapter 3: Modelling, Characterization, & Identification.

In previous chapter, the performances of PVG affected by different faults that can occur on it, has been presented. Among these faults the parasitic resistances effect and others electrical parameters, which have shown a prodigious influence on performances. Besides, the exact PV parameters values are essential for precise mathematical modelling, simulation, and control of the photovoltaic generation systems. In this chapter, a presentation is done about the modelling and identification of the different electrical parameters of the PVG. With a detail about different methods used for obtaining the best values of photovoltaic parameters.

2nd Part « ***Artificial Intelligence & Implementation*** » The second part contains two chapters as bellowed.

- Chapter 4: Application of Neural Networks to Faults Diagnosis of PVG.

In this chapter, a general description of neural networks and their application to the diagnosis of faults occurring in PVG is presented. An artificial neural network has been developed in order to model different types of faults (Short-circuit, shading) that have appeared in a photovoltaic generator, then detect and diagnose them. Simulation and experimental testing have been presented, the results prove the high performance of the proposed approach. We obtained very satisfactory results. The approach has proven its strength while injecting noises (*e.g* presence of perturbations from inverter) and notice the presence or absence of confusion.

- Chapter 5: FPGA implementation of FDD for PV-Generator.

Through this chapter, we have presented a synthesis methodology for FPGA implementation of a digital neural-network diagnosing faults (at short-circuit) in PVG. We were interested in the study of FPGA circuits, their structures, the different circuits, the VHDL, and the ISE Xilinx software environment, which integrates the ISim simulation module (ISE Simulator). VHDL description of the network begins by creating a component neuron, then a component layer, and finally a network. The neuron being the essential nucleus of a neural network, we are therefore interested in the architecture of the latter. We first checked, validated the operation and implemented the VHDL code of the neuron architecture based on the activation function (sigmoid). The proposed VHDL description is based on a simple, regular and parallel architecture. The use of the parametric VHDL description offers a high flexibility to the designer. These implementation results have been getting very good performances.

Lastly, the conclusion of this thesis is made and proposes the scope of future work.

Part 1

Photovoltaic Generators: Generality, Productivity, Faults, Diagnosis, Modelling, Characterization, & Identification

Chapter 1

PV Generators (Generality, Applications, &Productivity)

CHAPTER 1: PV Generators (Generality, Applications, & Productivity)

Introduction

Photovoltaic energy is one of the energy challenges policy in our century, which results from the direct transformation of sunlight to electricity, using a solar PV cell. The current available preliminary data for the world solar PV cell production in 2019 vary between 120 GW and 135 GW, as illustrated in Figure 1.1. The figure shows the evolution of annual PV productions in the world [3].

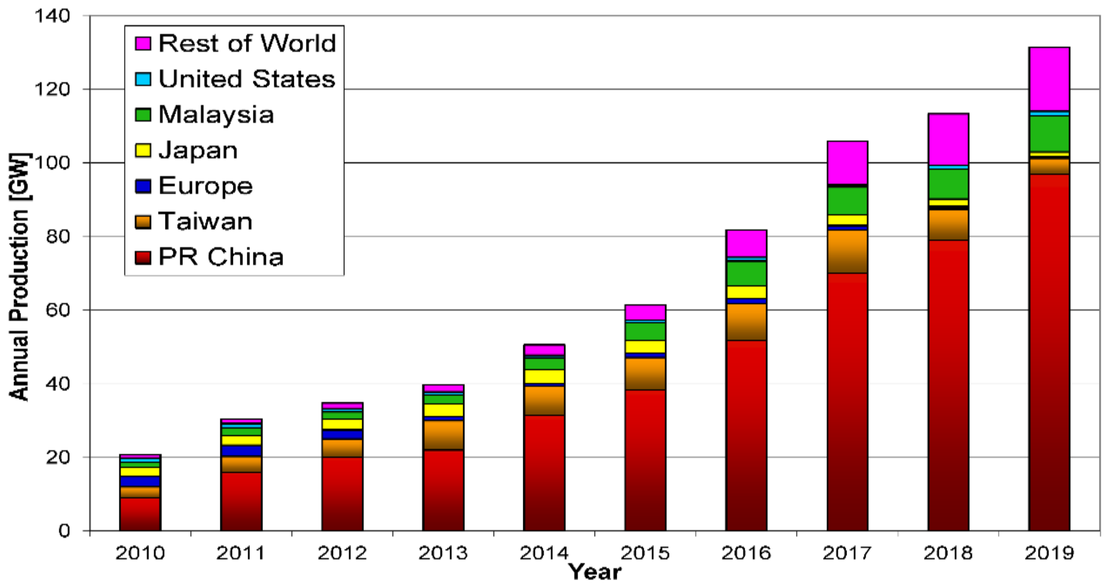

Figure 1.1 World PV Module Production from 2010 to 2019 (Data source: [3] and new analysis).

Besides, the cost of PV energy has shown a major decrease, which rounds it the lowest source of energy during 2020 [8]. The average price per watt dropped drastically for solar PV cells in the last decades. While in 1977 prices for Crystalline-Silicone (C-Si), cells were about $77 per watt, average spot prices in August 2018 were as low as $0.13 per watt or nearly 600 times less than forty years ago [9]. This price trend was seen as evidence supporting *Swanson*'s law (an observation similar to the famous *Moore*'s Law) which states that the per-watt cost of solar PV cells falls by 20 per cent for every doubling of cumulative photovoltaic production [10]. In this subject, this chapter presents a study of the photovoltaic generation unit, known as a photovoltaic generator (PVG). The study of PVG encloses generalities, behaviors, performances, and their main applications.

1.1 History research

The French scientist *Becquerel* was the first to discover the photoelectric effect in 1839. *Becquerel* has observed the electrical behavior of electrodes immersed in a conductive liquid exposed to light [11]. Subsequently, in 1905, *Albert Einstein* discovered, working on the photoelectric effect, that light has not only an undulation character but also that, its energy was carried by particles, photons. It was not until 1954 that the first solar PV cells producing electricity appeared, thanks to the work of Bell Laboratories in the United States [12]. From the photoelectric effect to the design of the photovoltaic cell, we had to wait a century. Photovoltaic energy had a renewed interest in the 1960s during the first space launches of satellites and then during lunar missions [13]. The economic crises of the 1970s, then the accidents of nuclear power plants increased the interest of the public towards renewable energies, and in particular photovoltaic energy [11], which is emerging as one of the most promising sources of renewable energies.

1.2 Advantages of PV systems

- It provides green, renewable, free and available energy.
- Can be used locally which reduces losses.
- Operation and maintenance costs are low.
- PV is silent (No noise), static.
- PV has no mechanical parts and easy to install.
- Used in spacecraft applications.
- Reliability and long lifetime.
- Improving efficiency and decreasing prices.
- The flexibility of construction with a modular nature.
- Availability of government support and incentives.

1.3 Limitations of PV systems

- No power at night or during cloudy or rainy weather.
- It requires additional equipment as inverters and batteries.
- Low efficiency of 15 to 18%.
- Needs continuous cleaning.
- For high power, PV requires a large area, which is difficult inside cities.

1.4 Solar resource

The sun is a great natural resource of energy. The incoming irradiation on earth from the sun is shown in Figure 1.2 bellow [14].

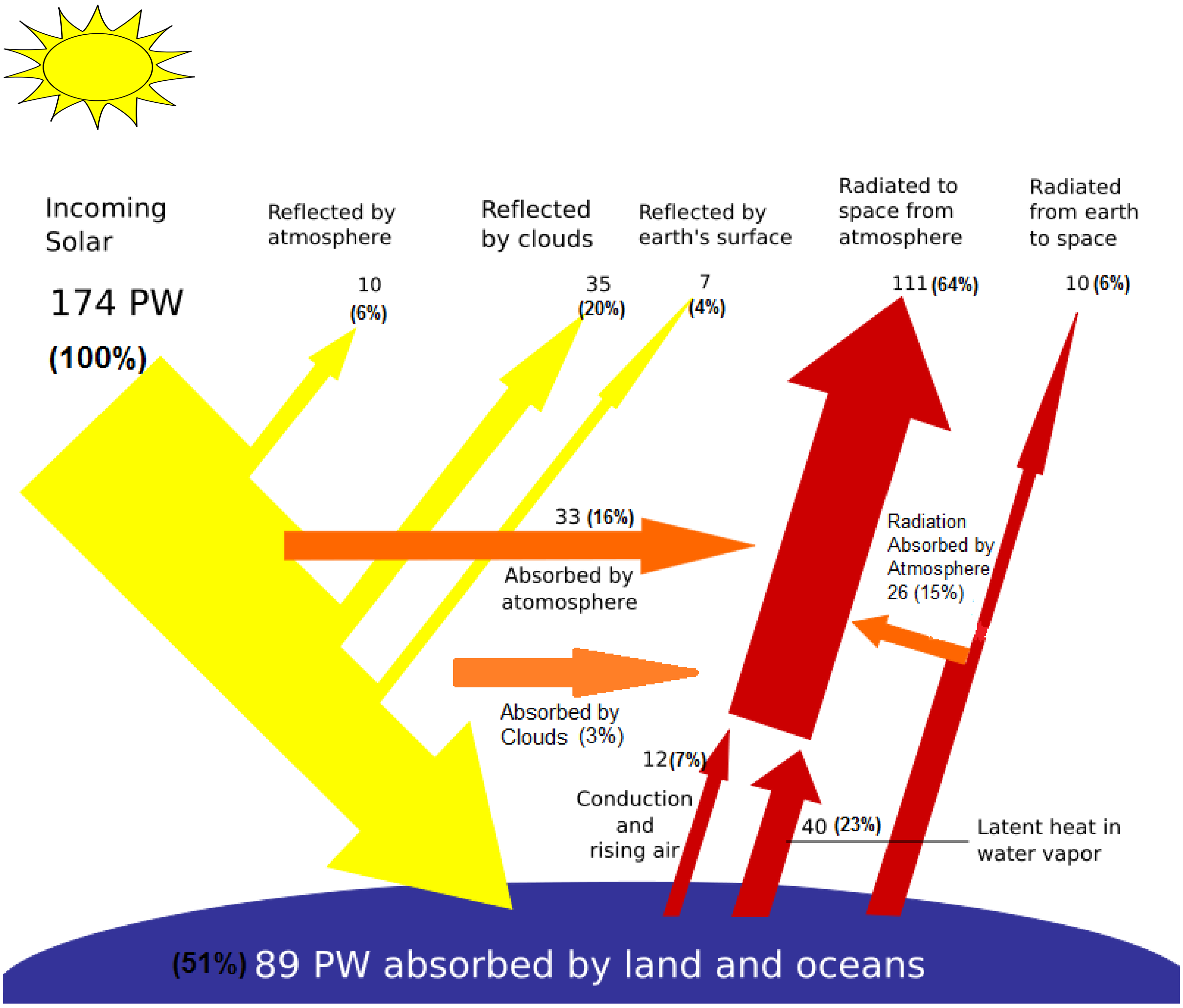

Figure 1.2 Breakdown of incoming solar energy on earth [14].

- The earth receives 174 Peta-watts (10^{15} Watts) of solar radiation in the upper atmosphere.
- Nearly 30% are reflected space while clouds, oceans and land absorb the rest.

Due to its geographic location, Algeria possesses one of the highest solar deposits in the world. The most important of the entire Mediterranean basin as shown in Figure 1.3 [15]. It is, therefore, legitimate to take advantage of it. It is mentioned that the global horizontal irradiation (GHI)* received in Algeria and all around the world is in an interval of about 3.5-7KWh/ m^2 per day.

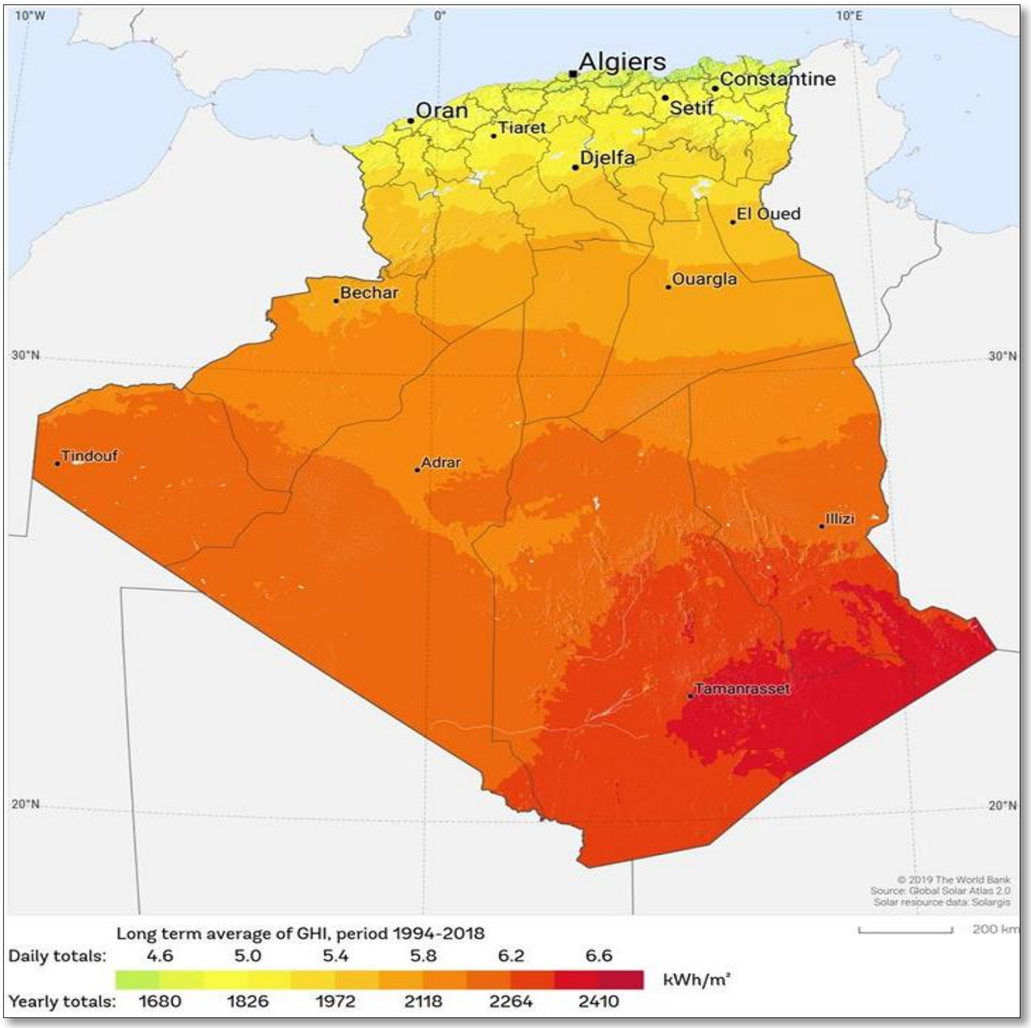

Figure 1.3 Global horizontal irradiation (GHI) received in Algeria [15].

The sun emits electromagnetic radiation called the solar spectrum, which extends from the ultraviolet into the infrared (~300nm – 2500nm). Figure 1.4 shows the variation of the spectral solar distribution [16]. The diagram shows a plot of the solar spectrum, indicating the ultraviolet (UV), visible, and infrared (IR) portions of the spectrum, as well as showing where the bandgap of silicon (for solar PV cells) is located. The energy, associated with this solar radiation, decomposes approximately as 9% in the UV band (<0.4 µm), 47% in the visible band (0.4 to 0.8 µm), and 44% in the IR band (> 0.8 µm).

The use of solar radiation as an energy source, therefore, poses a very special problem. Solar radiation is not always available; moreover, it cannot be stored or transported. The design of a PV system that uses solar radiation as an energy source must therefore determine the quantity of solar energy available at the target location, and the moment when this energy is available.

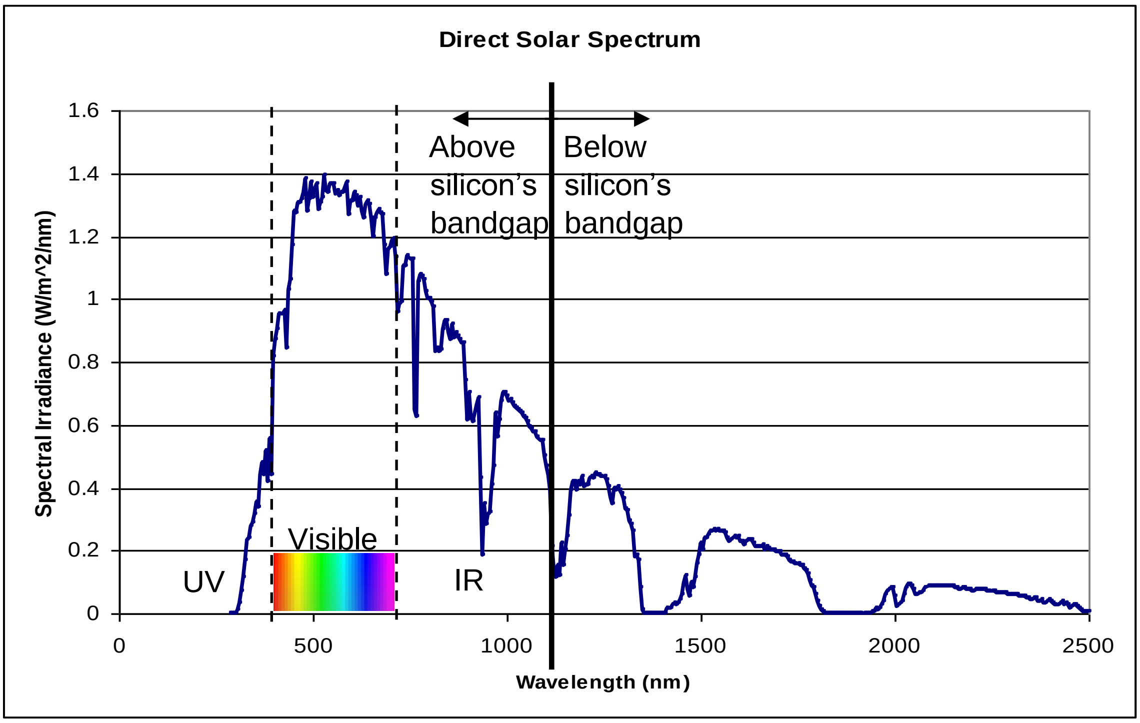

Figure 1.4 Spectral analysis of solar radiation [16].

1.5 Photovoltaic energy

Photovoltaic energy is a physical phenomenon, which converts light (photons) from the sun into electricity using semiconductor material. The latter has special electronic properties. Therefore, the photovoltaic system can supply electric energy to a given load by directly converting sun energy through the photovoltaic effect, as shown in the following Figure 1.5.

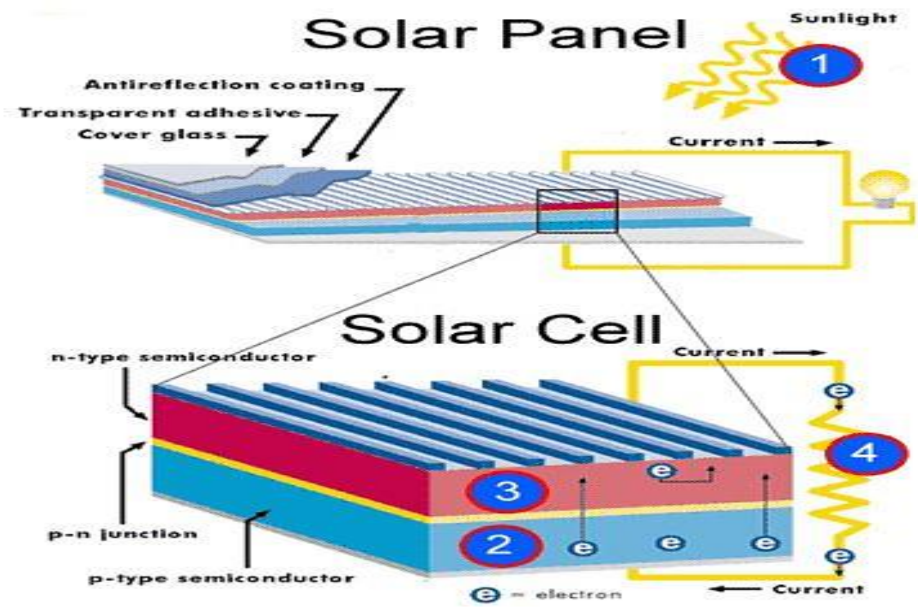

Figure 1.5 The basic PV cell/panel functioning principal.

Figure 1.5 shows that the photovoltaic process is based on three important principles: The first is the excitation of free mobile charge carriers due to light absorption, the second is the separation of the charge carriers and the third one is the collection of the charge carriers at the contacts. The fourth is to feed the load with electricity.

1.6 Types of photovoltaic technologies

A variety of PV technologies exists today. There are four generations according to technological developments.

1.6.1 First generation

This generation represents around 90% of the current PV market and belongs to the first generation PV technology, which is based on using very pure bulky semiconductor materials, like crystalline-silicon (C-Si), particularly the Mono-Crystalline-Silicon (Mono-C-Si) [17]. This first generation is considered as the most effective of the solar PV cells with 15% efficiency. They also last longer than other panels and perform better at low light. The main disadvantages are the cost, which often means that it is not the first choice for homeowners. It can also be affected by dirt or shade, which can break the circuit. Bifacial is the trending from this first technology.

- Bifacial solar PV panels

Bifacial are one of the newest product trends in the PV industry [18]. In fact, unlike the mono facial cells, bifacial cells are light-sensitive on both sides (Figure 1.6).

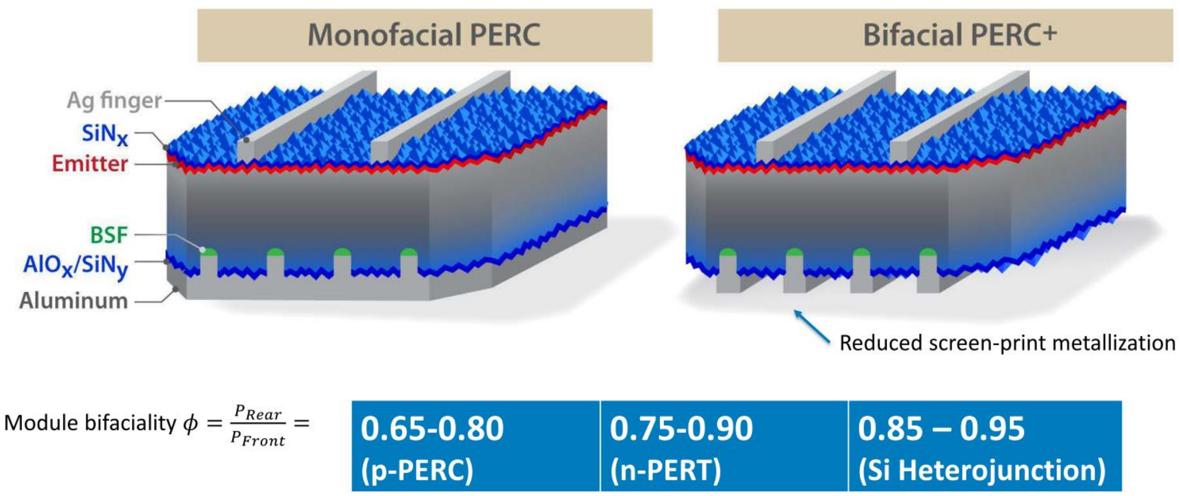

Figure 1.6 Mono-facial & bifacial structure of PV cell [18].

In the mono-facial back surface field solar cell, the rear surface is covered with aluminium. In a bifacial solar cell, a finger grid is used, so the sun can reach the rear side. Unlike the opaque back sheet that features on the mono facial solar panel, they are made with a transparent back sheet or dual tempered glass. Framed or frameless, bifacial panels are usually made from mono-crystalline cells, but polycrystalline can be used as well. Bifacial solar panels have solar cells that absorb light from both the front and the back. That means that besides capturing sunlight from the front of the panel, they also capture all the valuable sunlight that is reflected from the ground, as well as any diffused light that hits the back of the solar cells. Thus, they absorb more sunlight and provide higher efficiency than mono-facial solar cells.

1.6.2 Second generation

These solar cells are manufactured using cheaper processing technology based on thin-film [19]. Consequently, the materials have more defects resulting in lower performances. In this case, no C-Si wafers are used but very thin layers of silicon, which are deposited on glass or a flexible substrate. The silicon does not have the same lattice structure and can be amorphous (a-Si), Polycrystalline (Poly-C-Si) or Nano-crystalline.

- An alternative thin-film PV technology is based on an II-VI semiconductor, the cadmium telluride (CdTe). The CdTe has currently the largest market among the thin-film PV technologies.
- Another thin-film PV technology, based on a chalcogenide alloy is copper indium gallium selenide (CIGS). It has the highest demonstrated conversion efficiency on the lab scale, just above 20%.
- Another thin-film PV technology is based on organics, also referred to as the plastic solar cell. The absorption and charge transport in the solar cell occurs in conductive organic polymers or molecules.

With an efficiency of 13% polycrystalline (multi-crystalline) solar panels are often seen as a better economic choice, particularly for homeowners. At 7%, thin-film (amorphous) solar panels are among the least efficient on the market but they are the cheapest option. The main advantage is that it can be mass-produced at a much cheaper cost but is more suitable for situations where space is not a big issue. The main disadvantage for thin-film solar panels are not generally used for residential purposes and will degrade quicker than crystalline cells.

1.6.3 Third generation

The third generation PV technology would be solar organic [20] cells with higher conversion efficiencies about the first and second generations. Furthermore, the cost price of the materials and processing techniques are expected to be cheap as well. The dye-sensitized solar cell (DSSC) is a kind of photo electrochemical (PEC) system of a third technology, in which a semiconductor material based on molecular sensitizers is placed between a photo-anode and an electrolyte [21-22]. Third-generation PV technology covers a wide range of novel and innovative ideas, the most successful being multi-junctions.

1.6.4 Fourth generation

It is based on a hybrid process from inorganic crystalline [22]. Inorganic–organic hybrid solar cells (hybrid solar cells) have attracted considerable interest as a result of the synergistic properties of organic and inorganic semiconductors, which also take advantage of lightweight, robust, flexible, and inexpensive properties. The final PV technology is based on III-V semiconductor materials such as gallium arsenide (GaAs). III-V materials are being used in multi-junction devices, often processed on germanium wafers as substrate. The multi-junction based on III-V semiconductors are the most efficient solar cells today. The record conversion efficiency of 44% was obtained with a metamorphic triple junction in 2012. The III-V semiconductor solar cells are being used in concentrator PV technology and space applications. Hybrid solar cells are made from a mix of amorphous and monocrystalline cells to generate maximum efficiency. There are a variety of hybrid cells and they are still very much at the research and development stage which is why they are currently a more expensive option. Perovskite panels are trending from this fourth technology recently.

- Perovskite solar cell (PSC):

A PSC is a type of the fourth generation of solar cell which includes a Perovskite structured compound, most commonly a hybrid organic-inorganic lead or tin halide-based material, as the light-harvesting active layer (Figure 1.7) [23]. Perovskite materials, such as methyl-ammonium lead halides and all-inorganic caesium lead halide, are cheap to produce and simple to manufacture. Solar cell efficiencies of devices using these materials have increased from 3.8% in 2009 to 25.2% in 2020 in single-junction architectures, and, in silicon-based tandem cells, to 29.1%, exceeding the maximum efficiency achieved in single-junction silicon solar cells. Perovskite solar cells are therefore currently the fastest-advancing solar technology. With the potential of achieving even higher efficiencies and very low production costs, perovskite solar cells have become commercially attractive.

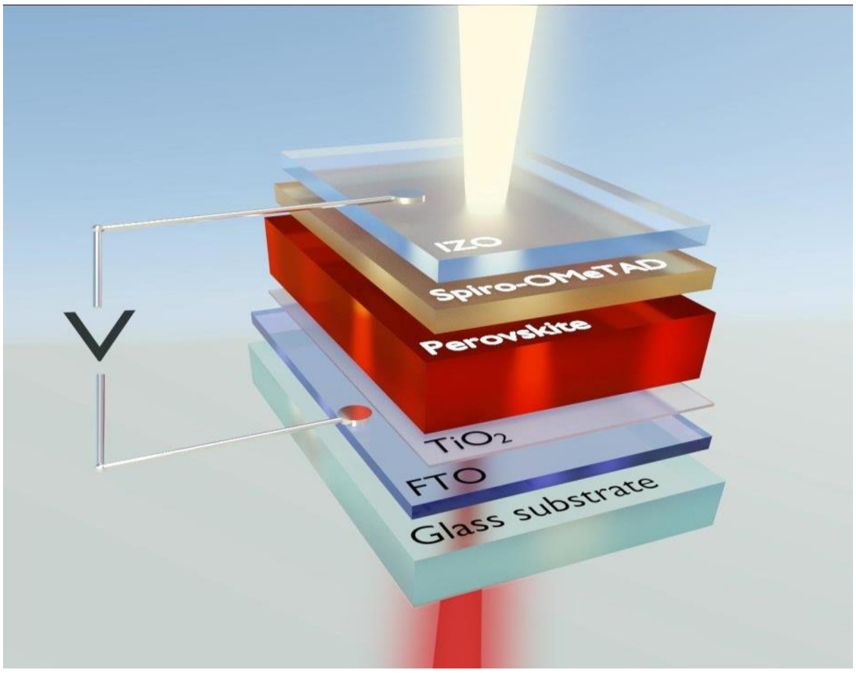

Figure 1.7 Structure of Perovskite PV cell.

1.7 Yield of PV generations

There has been steady progress in improving conversion yields for many PV tgenerationes in recent decades. This has caused competition between the developers of each technology to increase their returns, as shown in Figure 1.8 bellow. This figure shows the famous chart of the National Renewable Energy Laboratory (NREL) [24], which represents the evolution of the yield of each PV cell technology obtained in the laboratory for all sectors from 1975 to the present. It summarizes the worldwide research effort of the last 40 years and shows the current record efficiencies of solar PV cells at a research scale.

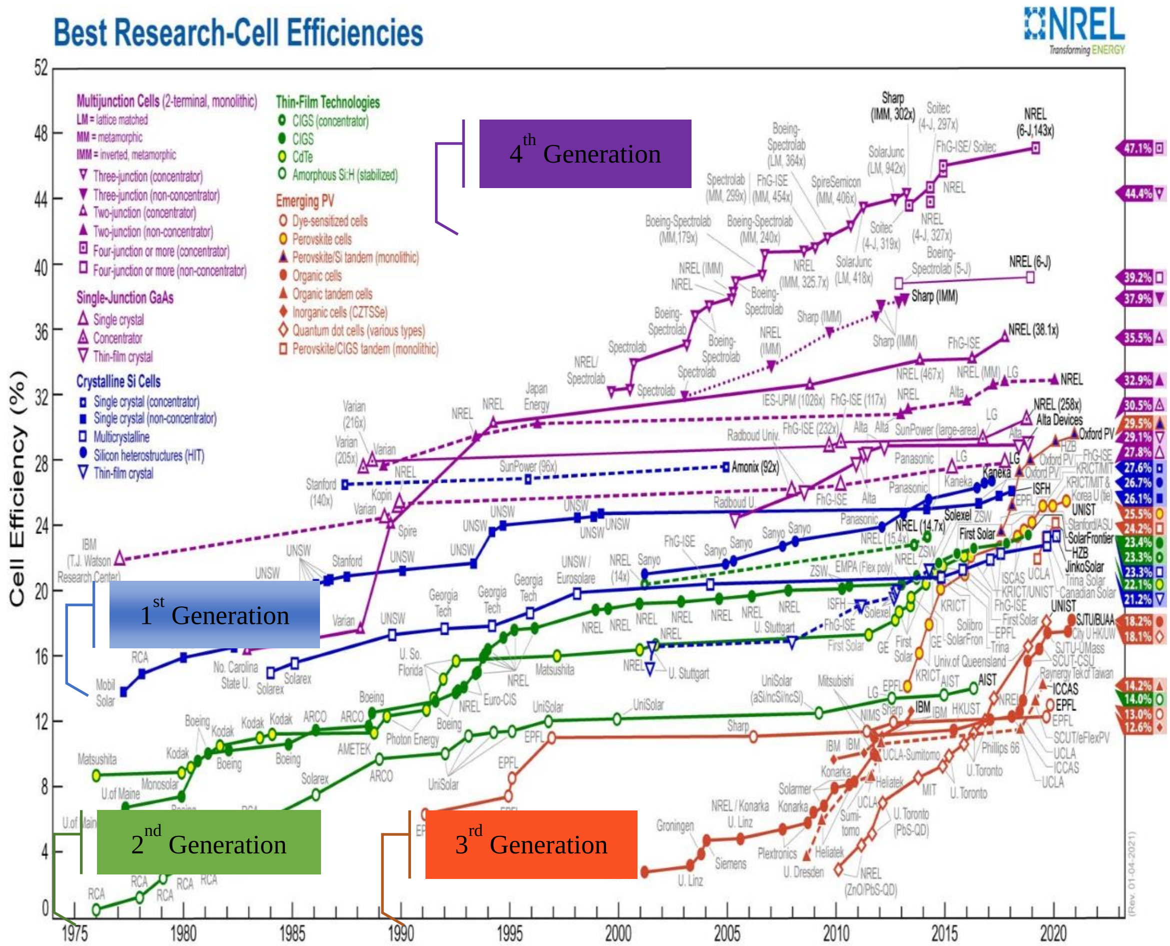

Figure 1.8 Evolution of PV yield over time (Source: NREL) [24].

- The **blue** (1st generation) lines and dots represent the crystalline silicon technology based on mono-crystalline and multi-crystalline silicon. The record efficiency ranges from 20% up to 25% under the standard one sun illumination conditions and 27% can be achieved under 92 suns illumination.
- The inorganic thin-film technologies, like thin-film silicon, CdTe and CIGS are indicated by the **green** (2nd generation) markers and their record efficiencies range from 13.4 % up to 20%.
- The **red** (3rd generation) colored lines and markers indicate the emerging PV technologies, like organic solar cells.
- The **purple** (4th generation) colored markers represent the III-V technology based on single, double and triple junctions and have efficiencies ranging from 26% up to 44% under concentrated light conditions.

The following table summarizes the different types of photovoltaic cells under standard test conditions (STC: 1000 W/m^2 & 25°C).

Table 1.1 Summarized classification of several photovoltaic technologies.

	Type of cell	Yield	Advantages	Disadvantages	Picture
1st Generation	**Mono-Crystalline Silicone (Mono-C-Si)**	13-17%	Good performance for a cell	High manufacturing cost, loss of material during fabrication	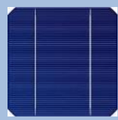
	Poly-Crystalline Silicone (Poly-C-Si)	11-15%	Good performance for a module	High manufacturing cost, loss of material during fabrication	
	Amorphous Silicone (a-Si)	5-9%	Easy to fabricate	Poor performance	
2nd Generation	**CdTe**	7-11%	Absorb 90% of incident photons	Cadmium highly polluting	
	CIGS	20%	Adjustable gap energy, 99% of the photons absorbed	Lack of raw material	
3rd Generation	**Organic**	$\leq 5\%$	Low manufacturing cost, flexible	Yield still too low	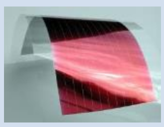
4th Generation	**Hybrid**	18%	Most efficient	Most expensive	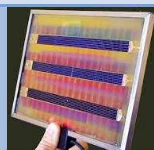

Each PV generation has its appropriate fabricant in the world. Most fabricants are summarized in Figure 1.9.

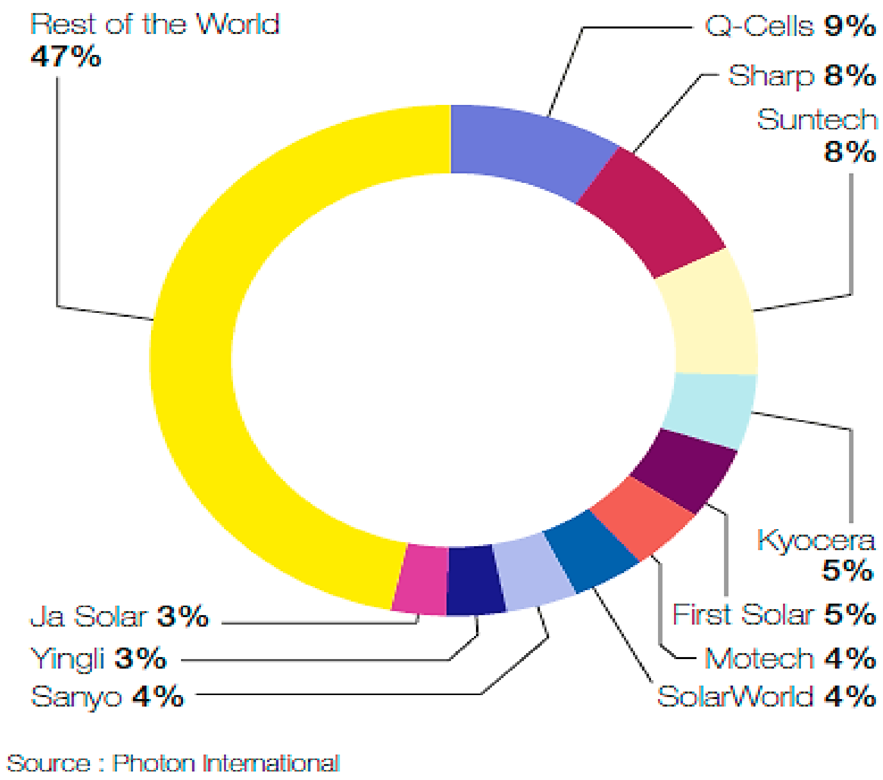

Figure 1.9 Fabricant of PV panels in the world.

- Q-Cells, Solar World from Germany.
- Sharp, Kyocera, Sanyo from Japan.
- Suntech, Yingli, JA Solar from China.
- Motech from Taiwan.

After the process of manufacturing of any PV modules they are tested under standard test conditions (STC), with some norms IEC (61215 for C-Si, 61646 for a-Si), with a solar simulator* and then a datasheet* containing the major characteristics (electrical and mechanical) and some performances are added on the bellowed surface of PV modules. This process occur in a specific laboratory of testing*.

1.8 Protection of PV generator

Mounting of PV generator can be in various configurations as seen in Figure 1.10 [25].

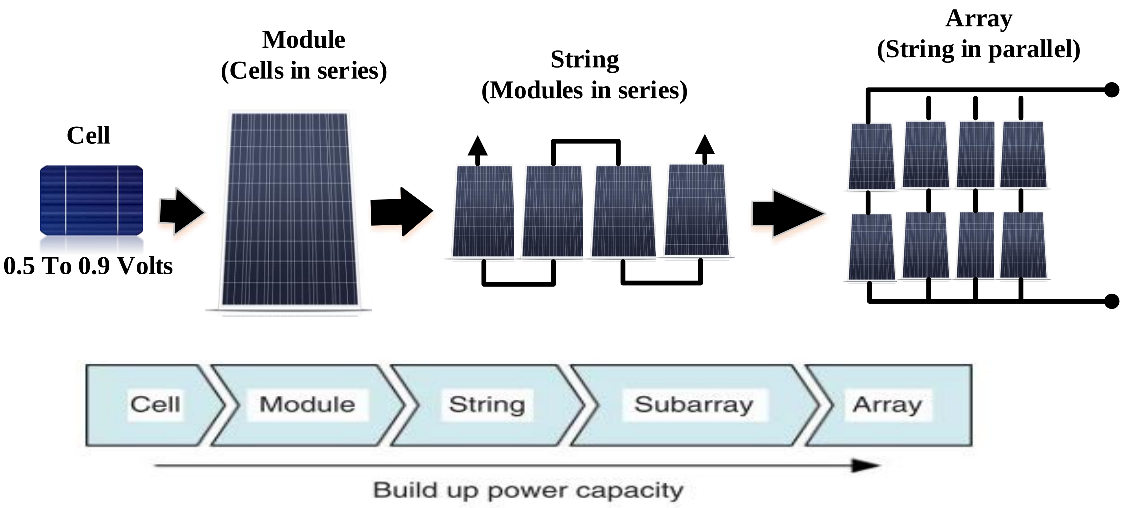

Figure 1.10 Mounting of PV generator: Cell, Module, String, Subarray, and Array [25].

From solar PV cell, module (cells in series associations), string (modules in series association), an array (strings in parallel association). Hence, after the manufacturing process for a given PV module with a certain anatomy*, several types of protection for a PVG exist. The components used for protecting the PV generator are cited below.

1.8.1 Bypass diode (BPD)

The bypass diode is connected in antiparallel with a group of cells (Figure 1.11), in order to protect the weakest between them against reverse polarization, as explained in Figure 1.12.

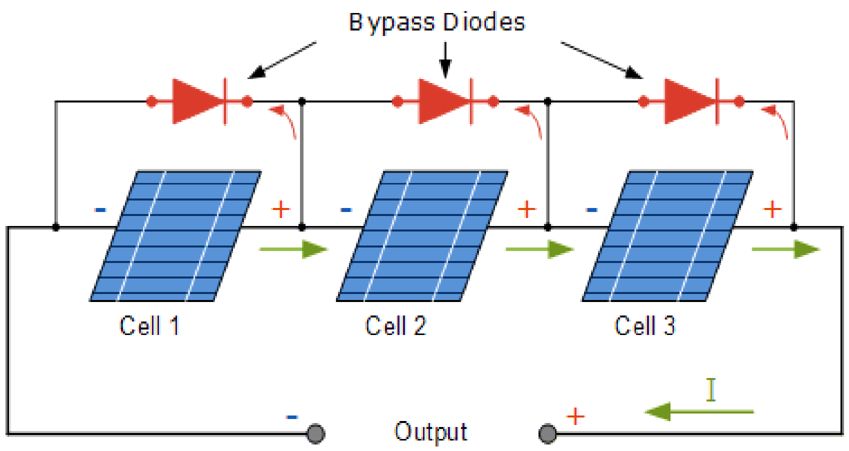

Figure 1.11 Protection of PVG with BPD diodes.

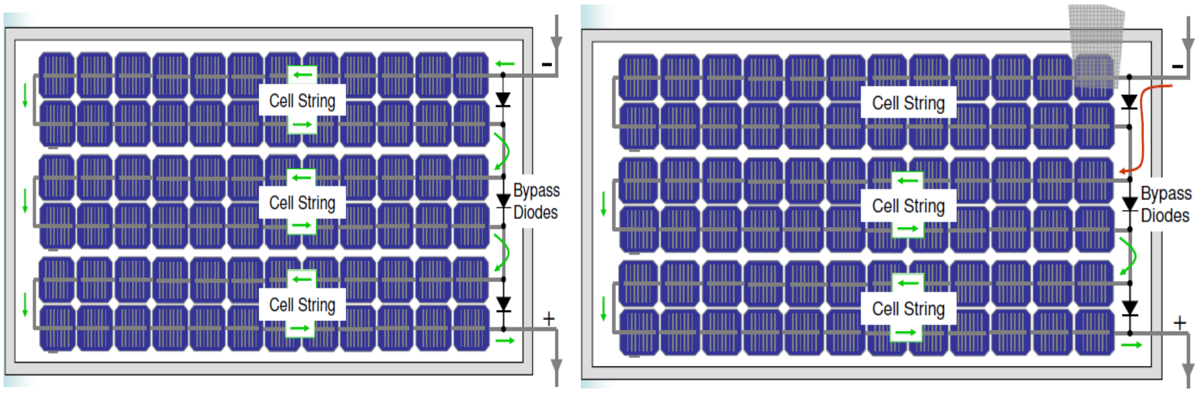

Figure 1.12 Explanation of bypass diode's role (Shade of one cell in 72-cell of PV module).

1.8.2 Blocking diode (BD)

The voltage produced by each string can be different. When paralleling these strings to form a PV field, the string with the lowest voltage can absorb a reverse current from the other strings. Therefore, this leads to a drop in production. The modules of the string crossed by the reverse current could also be susceptible to failure. To avoid these reverse currents, a blocking diode is placed at the end of each string, Figure 1.13.

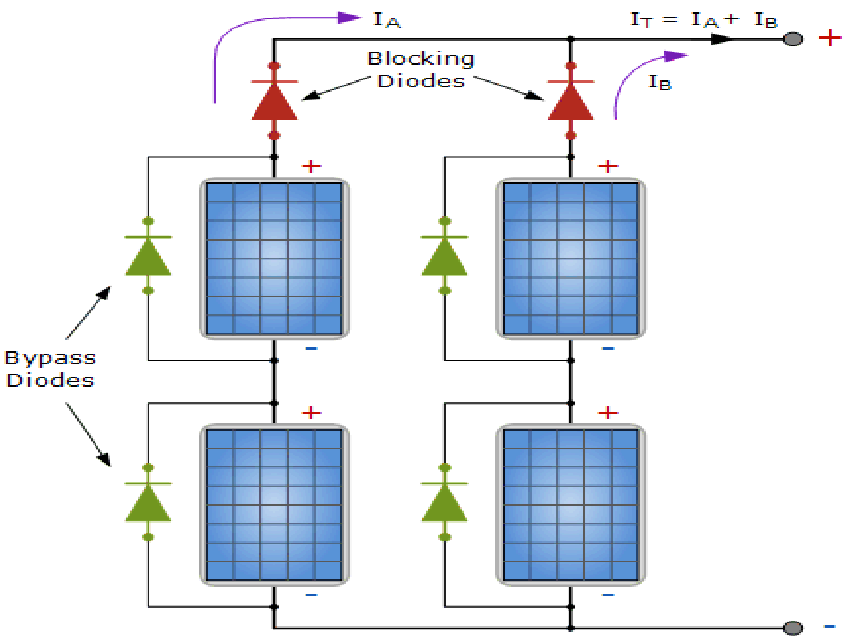

Figure 1.13 Protection with blocking diodes.

The use of the blocking diode introduces a loss in production due to the voltage drop caused by this diode during normal operation of the PV field. Besides, these diodes can go into the fault and therefore require regular control; a fuse is sometimes used in place of the non-return diode. However, the use of the fuse does not protect the string against the reverse current.

1.8.3 Junction Box (JB):

A junction box (Figure 1.14) containing connectors, fuses and switches is strongly recommended. Besides, the majority of PV systems are equipped with circuit breakers placed between the PVG and the inverter to simplify isolation in the event of a failure.

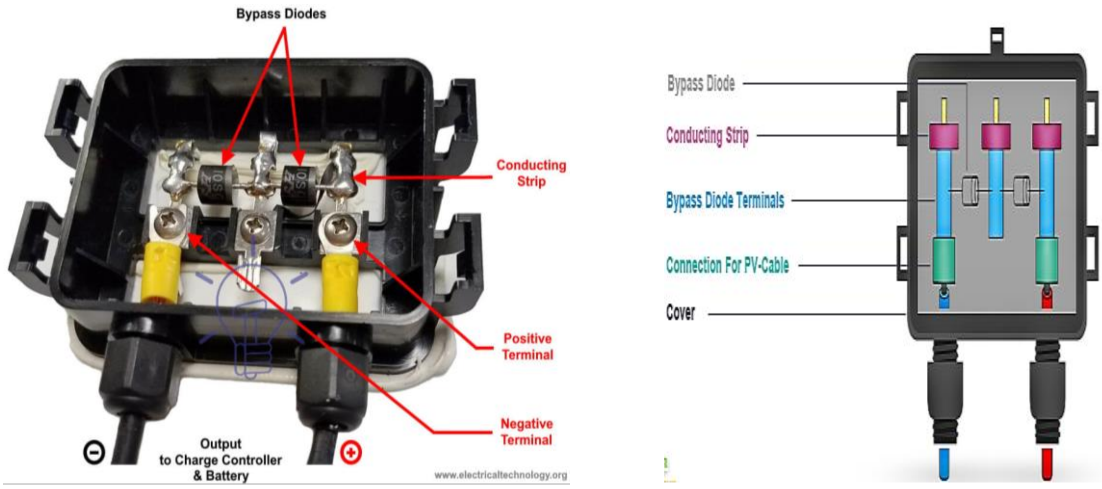

Figure 1.14 Constitution of a junction box.

1.8.4 Solar PV cables

These cables with MC4 connectors shown in Figure 1.15 are designed and tested to operate at a normal maximum conductor temperature of 90°C and for 20 000 hours up to 120°C.

Figure 1.15 Cables with MC4 connectors used for connection of PV panels in series and/or parallel association.

They are suitable for permanent outdoor long-term use under variable and harsh climatic conditions.

1.9 PV system Applications

Two main types of PV system applications exist Grid-connected, and Off-Grid (Figure 1.16). In either case, basic PV system principles and elements remain the same.

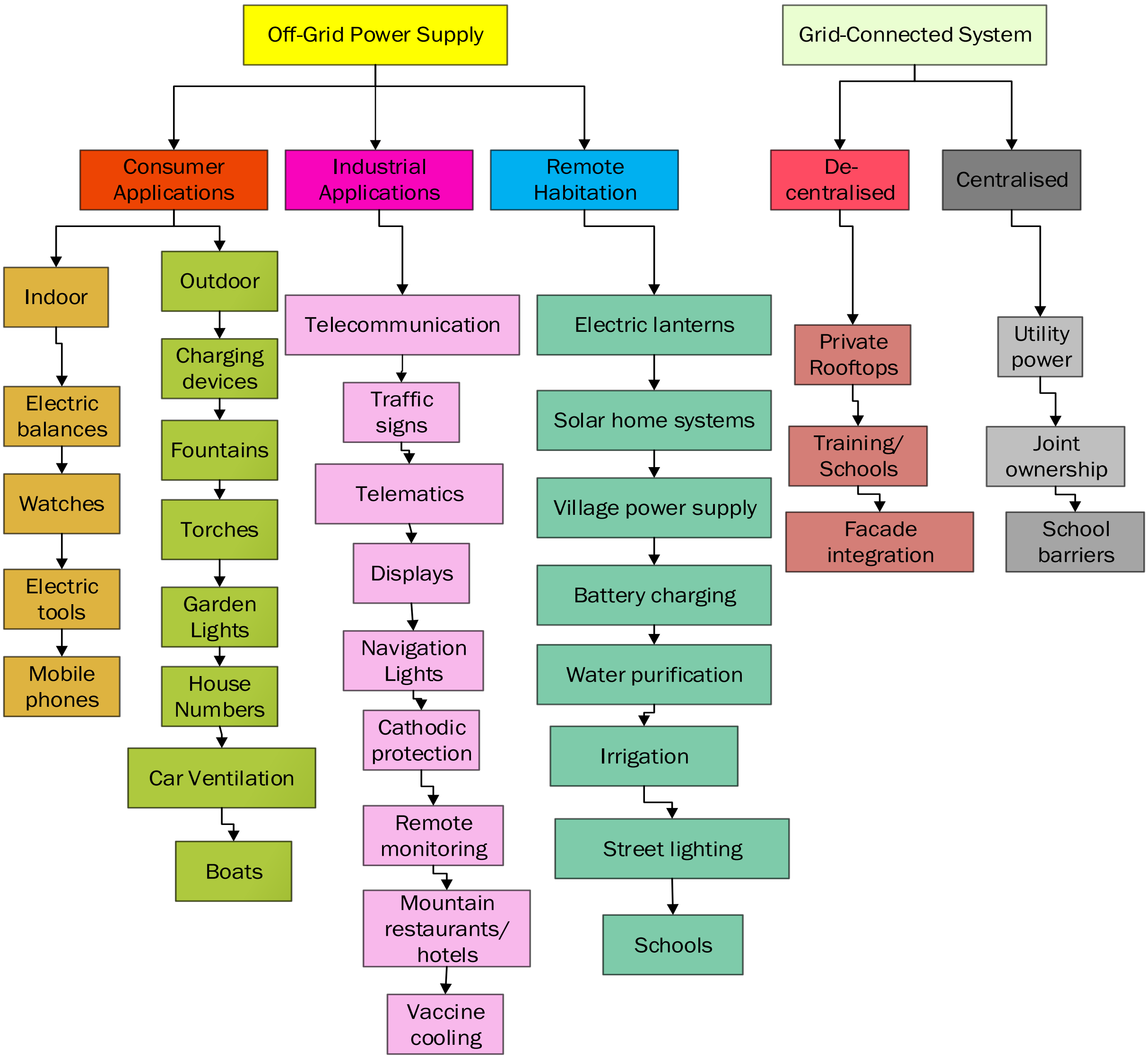

Figure 1.16 Various kinds of PV applications.

In what follow, some details are given about the different kinds of application of PV systems.

1.9.1 Off-Grid PV application (Stand-alone)

In this type, the PV system is isolated from the electric grid (remote area). The basic block diagram of a stand-alone PV system is described in Figure 1.17. It includes all the elements necessary to serve direct and alternative charges appliances in a common isolated household.

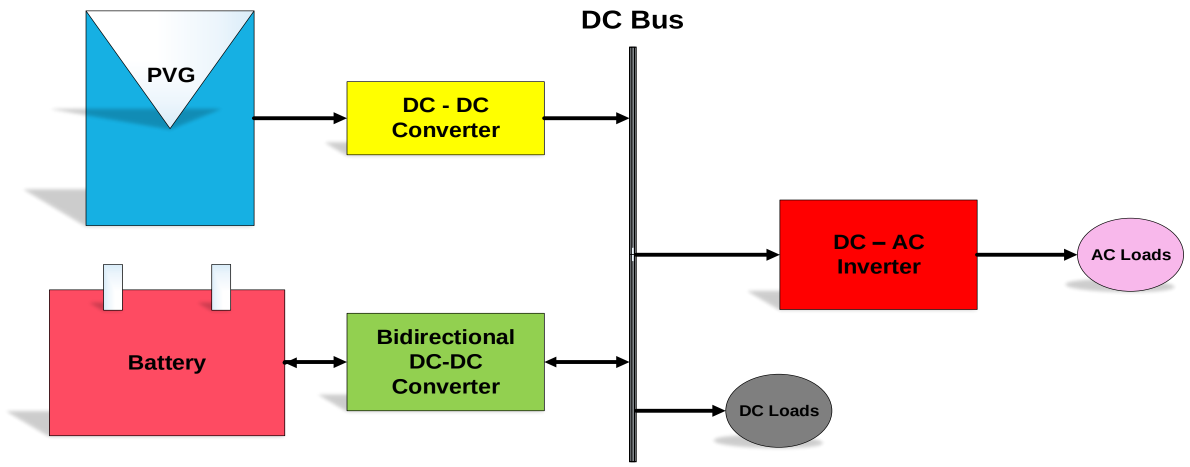

Figure 1.17 Block diagram components of Off-Grid PV installation (Stand-alone).

It consists of a PVG, DC-DC (from direct to direct) converter, DC-AC (from direct to alternative) inverter, and a bank of storage with a regulator (Bidirectional DC-DC converter).

1.9.2 Grid-Tied PV applications

The grid connection PV systems are directly tied to the electric distribution network, with two major configurations as detailed below.

a) Integrality injection

The basic system configuration is depicted in Figure 1.18. Electric energy is either sold or bought from the local electric utility depending on the local energy load patterns and the solar resource variation during the day.

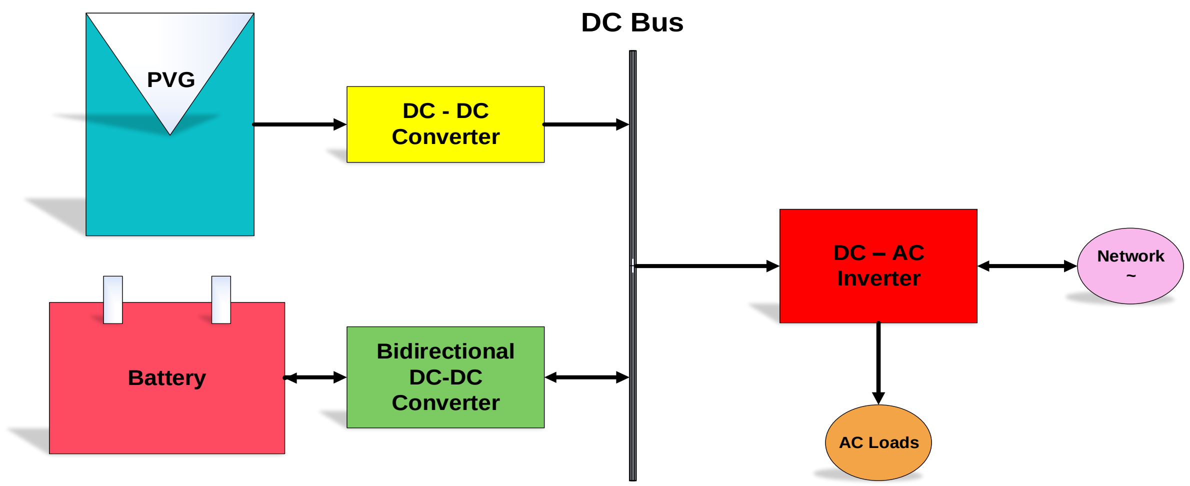

Figure 1.18 Block diagram of Grid-Tied photovoltaic system with battery (injection to the network of integrality).

b) Total injection:

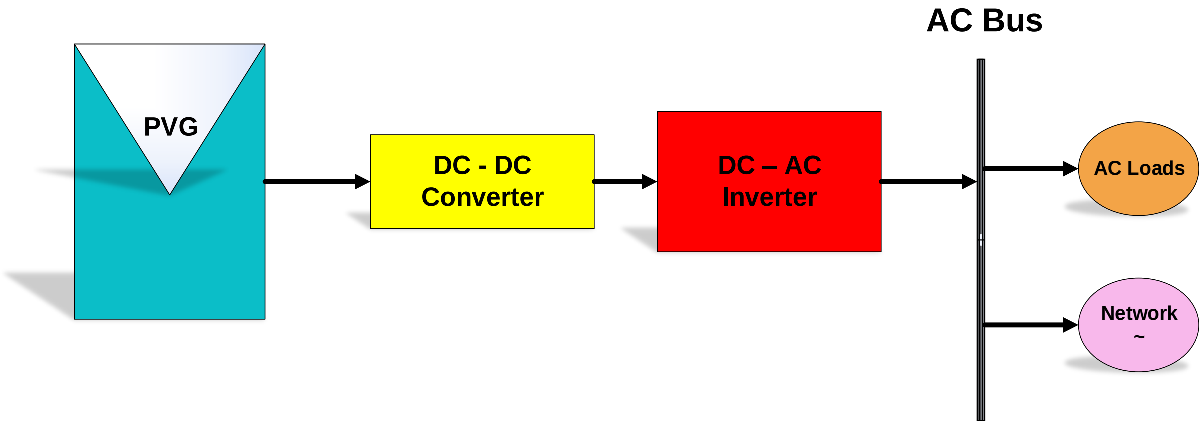

Figure 1.19 Block diagram of Grid-Tied Photovoltaic System without battery (Direct/pure injection to the network).

In the grid-connected system, dump heaters are not required, as all excess power is fed to the grid lines [26]. The battery is also eliminated. The DC power is first converted into AC by the inverter, ripples are filtered and then only the filtered power is fed into the grid lines.

1.9.3 Hybrid application (Multisource)

These systems consist of combination of two or more sources of energy, such as photovoltaic modules and a complementary means of electricity generation such as a diesel, gas or wind generator [26-27] (Figure 1.20).

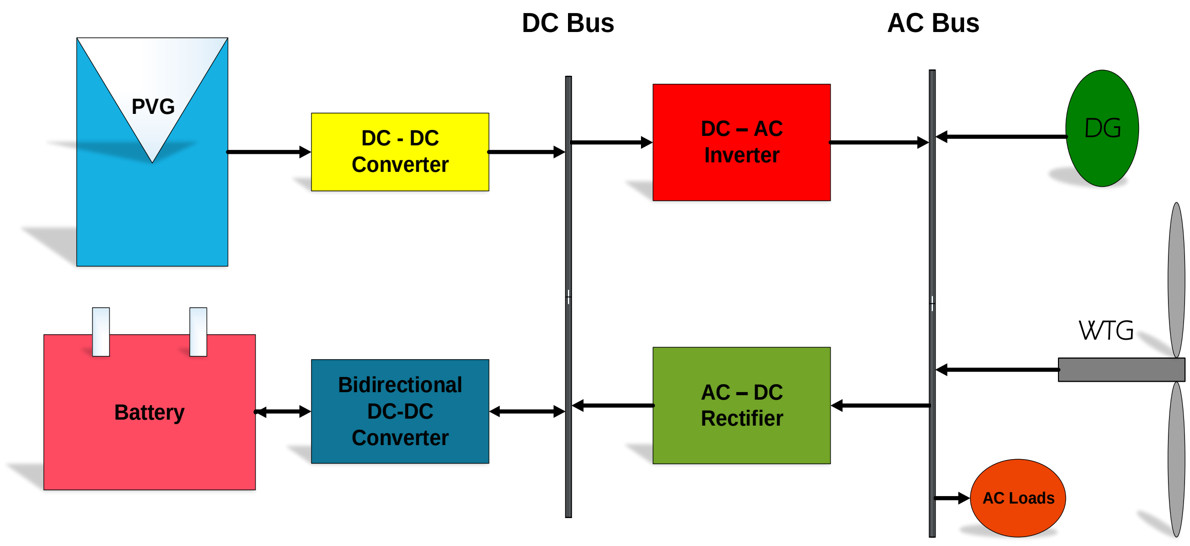

Figure 1.20 Block diagram representation of a multisource (hybrid) system.

To optimize the operations of the different generators, hybrid systems typically require more sophisticated controls than stand-alone PV systems.

1.10 PV system components & productivity

The PVG by itself does not constitute the PV power system. It must also have a structure to mount it, point to the sun, and the components that accept the Direct Current (DC) power produced by the array and condition the power in the form that is usable by loads. If the loads are Alternative Current (AC), the system needs an inverter to convert the DC power into AC, generally at 50 or 60 Hz [21]. The electrical block diagram of a PV system supplying a load, and containing the major components is illustrated in Figure 1.21.

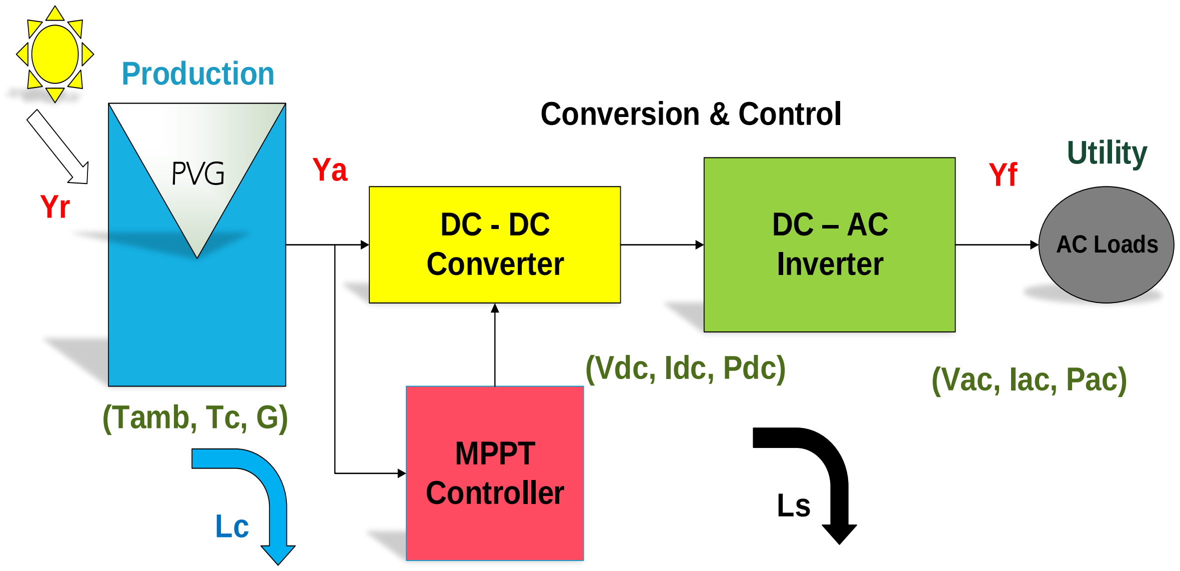

Figure 1.21 Schematic components of PV system's components with productivity.

Figure 1.21 shows the necessary components of a PV power system, which are:

- Production part: PV generator.
- Conversion & control part: Converters (DC-DC & DC-AC) with MPPT (Maximum Power Point Tracker) controller.
- Utility part: Loads.

The peak power tracker (MPPT) senses the voltage, current, and/or power outputs of the PV array (I_{dc},V_{dc}, P_{dc}) and continuously adjusts the operating point to extract the maximum power under the given climatic conditions (ambient temperature: T_{amb}, cell's temperature: T_c, and solar irradiation G). The output of the array goes to the inverter, which converts the DC into AC (I_{ac},V_{ac}, P_{ac}).

The productivity of a PV installation is relied on two main factors: the performance and the availability of the installation [28]. The later availability is affected by the ratio between the period of service continuity and a total observed period [29]. Whereas, the performance is affected by the global efficiency of the chain of conversion, and can be deduced through a performance ratio indicator, proposed by the European directive [30] and the International Electronic Committee (IEC) 61724 [31].To study the PV system's performance, the International Energy Agency (IEA) Photovoltaic Power System Program established four performance parameters concerning the energy production, solar resources, rated power and overall effect of system losses. The performance ratio (PR) can be expressed by the following expression [32], and is defined as a ratio of the measured system efficiency and the nominal efficiency of the PV modules:

$$PR = \frac{Y_f}{Y_r} = \frac{E_t/P_{STC}}{H_t/G_{STC}} = \frac{P_{MPP}/P_{MPP\_STC}}{G/G_{STC}} \tag{1.1}$$

Where:

Y_f & Y_r are the final and reference yields (Hours). E_t is the consumed PV energy (Wh), P_{STC} is the system rated power at STC (W_p), H_t is the total in-plane irradiance (Wh/m^2), G_{STC} is reference irradiation at STC (1000 W/m^2).

The performance of PV system is also affected by losses [33], which can be:

- Capture losses (L_c): in PVG from the DC side.
- System losses (L_s): in converters along the chain (AC part).

L_c occurs in the DC side of PVG and are given by the sum of thermal (L_{ct}: high functioning temperature, more than 25°C) and miscellaneous (L_{cm}: Operation of PVG: soiling, shading, wiring mistakes, etc.) losses [33].

The losses may be calculated by the following expressions [34]:

$$L_c = Y_r - Y_a \tag{1.2}$$

$$L_s = Y_a - Y_f \tag{1.3}$$

Where:

$$Y_a = \frac{E_{dc}}{P_{Ref}} \tag{1.4}$$

Where: Y_a is the array yield, E_{dc} is energy generated by the PV array (Wh), and the P_{ref} is the maximum power output of the PV array (W_p).

The productivity of a PV system is affected by several factors [28, 32]:

- The performance of the PV installation.
- From one season to another (Climatic conditions of the place).
- Electrical, mechanical and geometric configurations of PVG/plant.
- Shading (Partial or total).
- Several technologies of manufacturing PV modules.
- Damage in protection and wiring components.
- Damage in PV inverter.

For the best productivity of the PV installation, many solutions exist as choosing PV components of high reliability and also insert a sophisticated diagnosis system for detecting damages occurring in PV plants and correcting them.

Conclusion

In this chapter, a small overview of the photovoltaic generator's generality has been presented. We have seen the importance of using such PVG, from the interest done with years in the historical point, the many advantages cited with some disadvantages, the abundance of energy from the sun, and the focus of researchers to get a very high yield of the used material technology. The performances and several applications of PV systems have been also detailed. Before termination of this chapter, a presentation has been enlarged of the losses and productivity in a special PV application containing the major elements of the PV chain. This chapter has been elaborated on, to include our studied photovoltaic generator, and situate the readers to the developed thematic. After seeing generalities in this chapter, particularly seeing that the productivity of a PV system, which is affected by many factors and that PVG necessitates protections, we choose to develop in the next chapter, the different forms and causes of faults in PV generator, and the techniques to diagnose them.

Chapter 2

Fault Detection and Diagnosis in PVG

CHAPTER 2: Fault Detection and Diagnosis in PVG

Introduction

From the last chapter we have seen that the productivity of a photovoltaic system is affected by its performance, where the PR is the formulas that indicate it. Along a PV chain the PR is subject to different sort of losses and attenuation as illustrated in Figure 2.1 [35]. Where the PV generator can got a remarkable diminution of the total PR (about 19.5%).

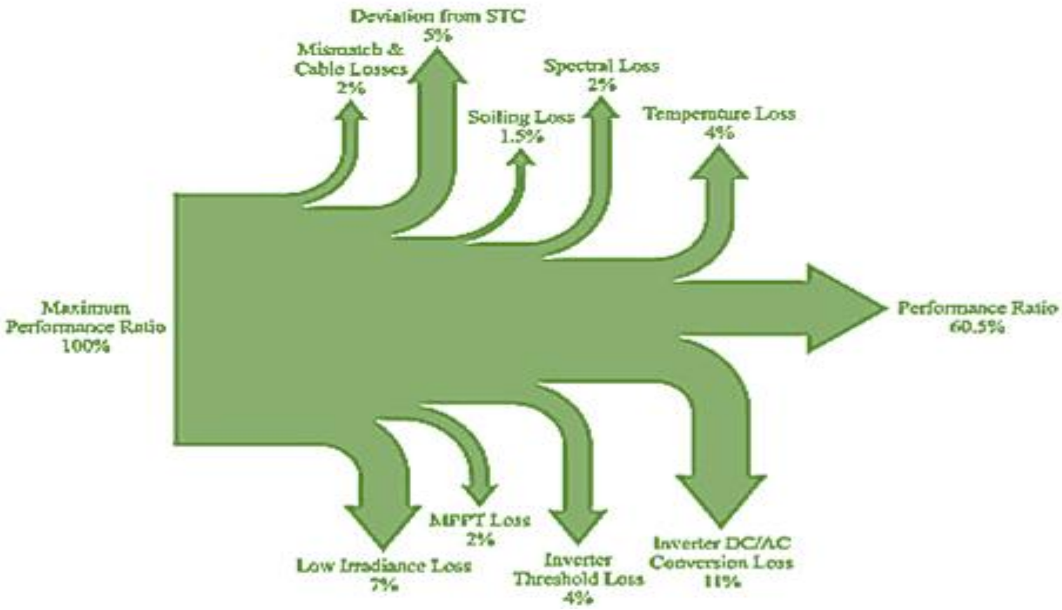

Figure 2.1 Different system losses and overall performance ratio [35].

Therefore, photovoltaic systems are subjected to different sort of losses, malfunctions, and failures during their lifecycle, particularly the PVG. Fault analysis in the PVG is a fundamental task to eliminate any kind of dangerous and undesirable situations arising in the operation due to the presence of faults. They must be detected and cleared off rapidly. Without proper fault detection, non-cleared faults in PVG not only cause power losses but also might lead to safety issues and fire hazards. This chapter summarizes the different causes and types of degradations of photovoltaic generators, the major types of faults and their main diagnosis techniques.

2.1 Causes and classification of faults

The failures detected in any solar PV system are due to different effects such as internal, external, and aging [3], [5], [6] (Figure 2.2). Internal PV faults originate from the PV plant itself and include all components failures such as generators, cabling, converters, protections, batteries, inverter and data acquisition system (DAQ) [6]. External PV faults, which lead to several degradations [36] and annual power losses [37, 38], are due to outer unfavourable conditions, such as shading effect [39], high temperature [40], low irradiance, high humidity, suboptimal tilt or orientation, corrosion [41] and accumulation in the surface of soil, dirt, or snow [42].

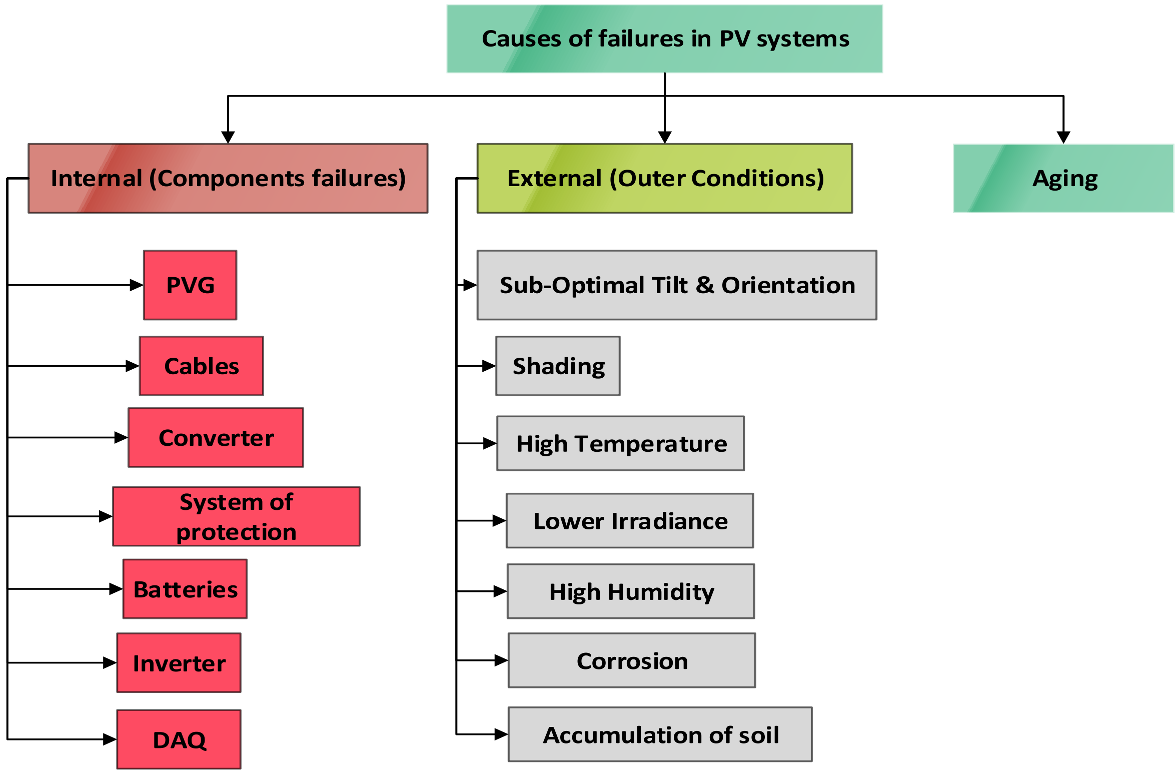

Figure 2.2 Causes of faults in PV systems [41].

Many studies have been developed that deal only with the faults occurring in the PV generator (cell, panel, string, and array), due to dangerous failures that can occur on it [7] (electrical shock and fire risks). The later faults can be classified into physical, environmental, and electrical faults [43-44], (Figure 2.3). Physical faults are caused by internal failures (damages on PV panel or on blocking and bypassing diode (BBP)) or external failures (cracks in PV panels, junction box (JB) damages or other degradations) [45]. Environmental faults are caused by soiling [46], permanent shading (Hot-Spot (HS)) [47], or temporary shading (Partial-Shading (PS)) [48]. Electrical faults [5], and their catastrophic threat [43] are caused by Open-Circuit (OC), Short-Circuit (SC) Line-to-Line Fault (LLF), Ground-Fault (GF), and Arc-Fault (AF).

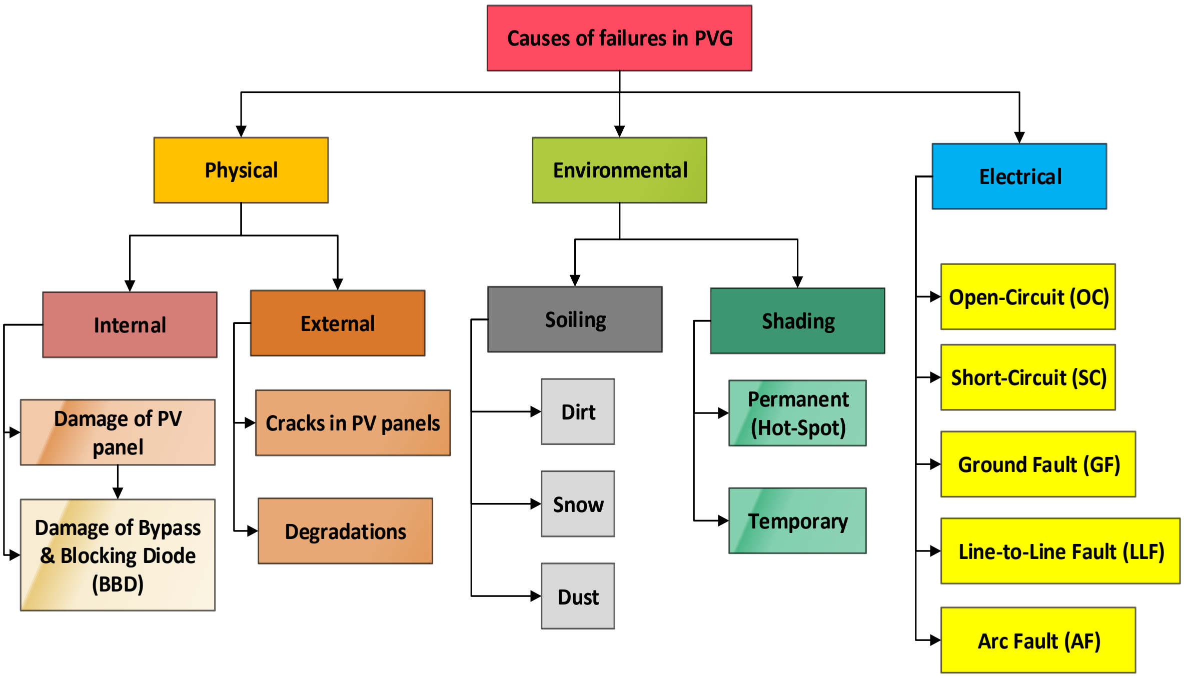

Figure 2.3 Causes of faults in PV generator [44].

Faults in a photovoltaic generator (PVG) [7], [38], [49], [50] can occur due to discoloration, corrosion, delamination, broken glass [45], [49], bubbles, disconnection, encapsulation, leakage currents, wiring mistakes, installations faults, and manufacturing defects.

2.2 Kind of degradations in PVG

Gradual deteriorations of PV plants components involve lower performances, power losses and hazardous risks. Several factors cause different degradations that can occur in a photovoltaic generator [7, 41, 49 and 50]. The major kinds of degradations are summarized below (Figure 2.3):

a) Oxidation phenomenon.

b) Corrosion phenomenon.

c) Metal corrosion phenomenon.

d) Dirt in PV panels.

e) Dust in PV panels.

f) Snow in PV panels.

g) Uniform and non-uniform soiling.

h) Brocken/shattered glass.

i) Junction box degradations.

j) Mechanical breakage & degradation of JB: burnt diode phenomenon.

k) Fire damage.

l) Temporary shading (PS).

m) Discoloration of Ethylene vinyl acetate (EVA) phenomenon.

n) Detachment of EVA phenomenon.

o) Snail tracks phenomenon.

p) Back sheet-chalking phenomenon.

q) Catastrophic bond failure phenomenon.

r) Degradation of antireflection coating of photovoltaic cells, caused by water vapor ingress.

s) Burn marks phenomenon.

t) Delamination phenomenon.

u) Bubbles phenomenon.

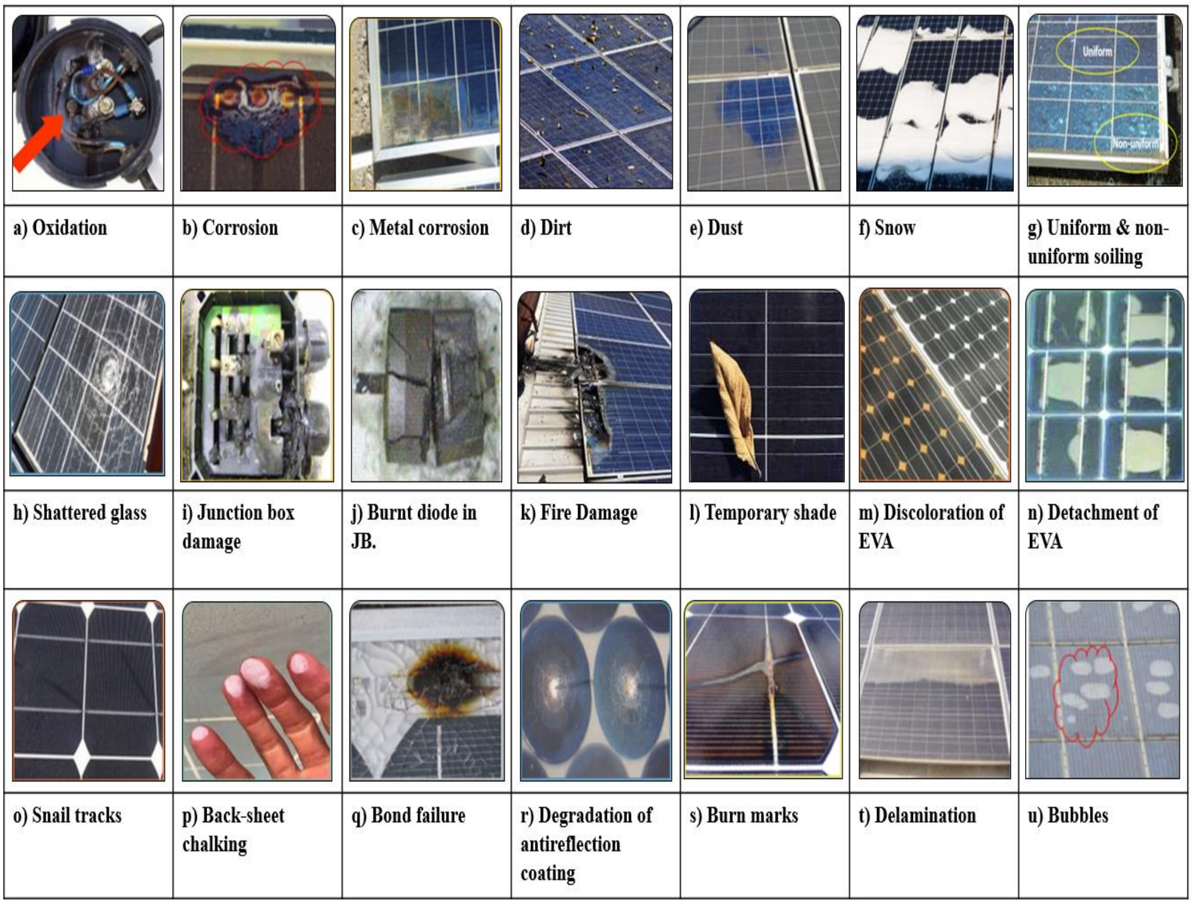

Figure 2.4 Kinds of degradation in photovoltaic generator.

Other PV degradations observed through microscopic way are summarised in Figure 2.5.

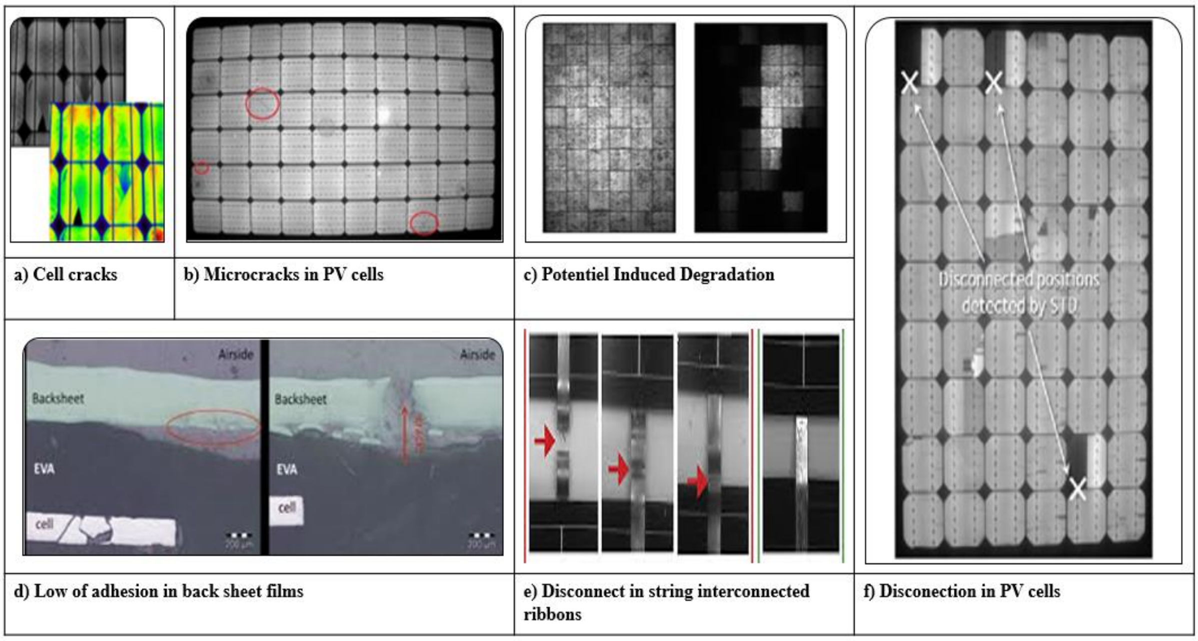

Figure 2.5 Microscopic degradations in photovoltaic generator.

a) Cell cracks.

b) Micro cracks.

c) Potential Induced Degradations (PID) [51].

d) Low of adhesion in back sheet film.

e) Disconnection of interconnected ribbon.

f) Disconnection in PV cells.

Other PV degradations exist such as encapsulation failures, improper installations, wiring mistakes, leakage currents, installations damages, manufacturing defects, and transportation destructions.

2.3 Types of faults in PVG

The non-linear behaviour of the PV generator and its intermittent operation due to environmental conditions (temperature and irradiance), involves the occurrence of many faults. Therefore, it is necessary to find out the techniques to detect them. The following Figure 2.6 illustrates some Current-Voltage (*I-V*) characteristics curves. The red curve represents the normal *I-V* characteristic whereas the other ones represent faulty *I-V* characteristics.

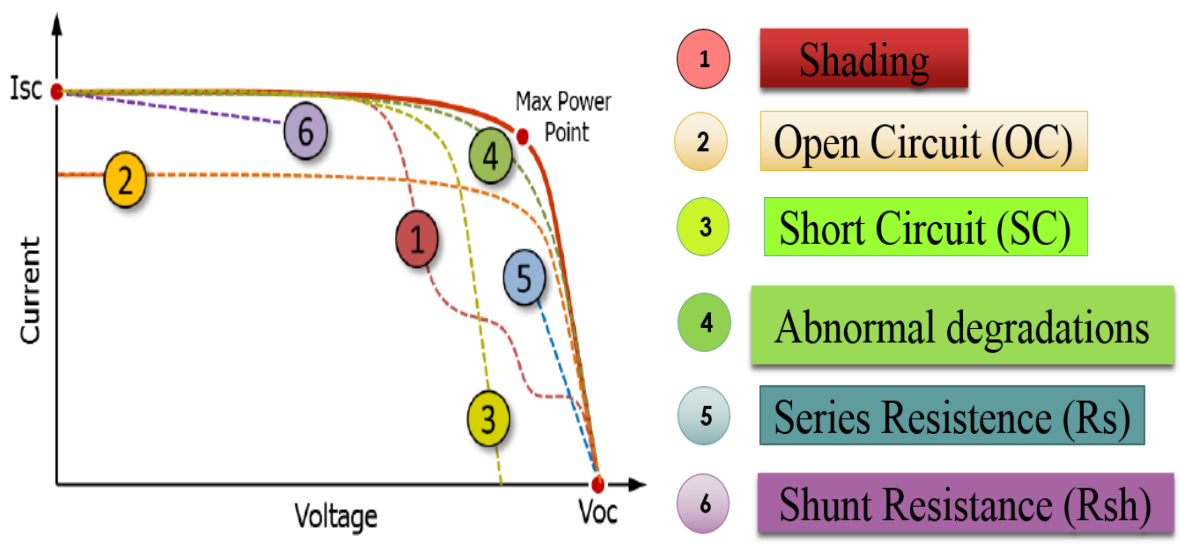

Figure 2.6 *I-V* curves indicating various types of faults.

The six deviations curves have multiple causes, which are detailed bellow.

2.3.1 Shading

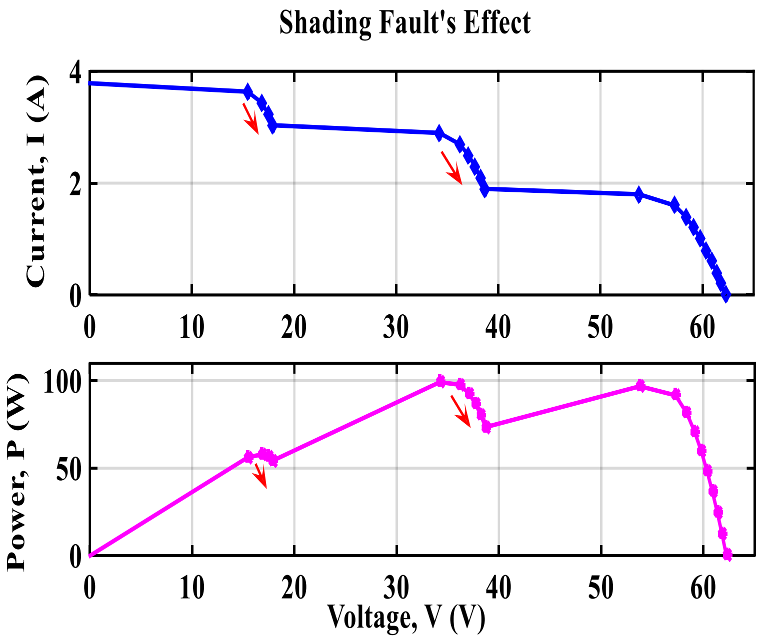

Figure 2.7 *I-V* and Power-Voltage (*P-V*) characteristics of PV generator with shading fault effect.

Shading fault may involve severe damages [48]. It can decrease the current, voltage, and power at the maximum power point (MPP): I_{MPP}, V_{MPP} & P_{MPP} (Figure 2.7).

2.3.2 Open-Circuit (OC)

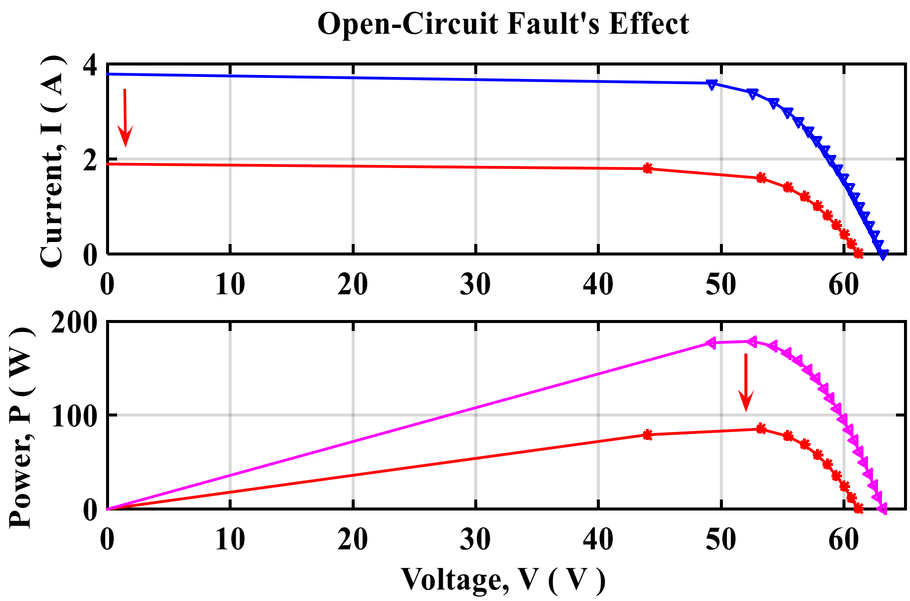

Figure 2.8 *I-V* and *P-V* characteristics with Open-Circuit fault effect.

Open-circuit fault affect short-circuit and MPP currents (I_{SC}, I_{MPP}), causing a decline of their values (Figure 2.8). Cracks in PV cells, weakness, due to thermal stress, and wind loading lead to interconnection, affects the occurrence of Open-Circuit fault [52]. Figure 2.9 gives an example of OC fault in a PV string.

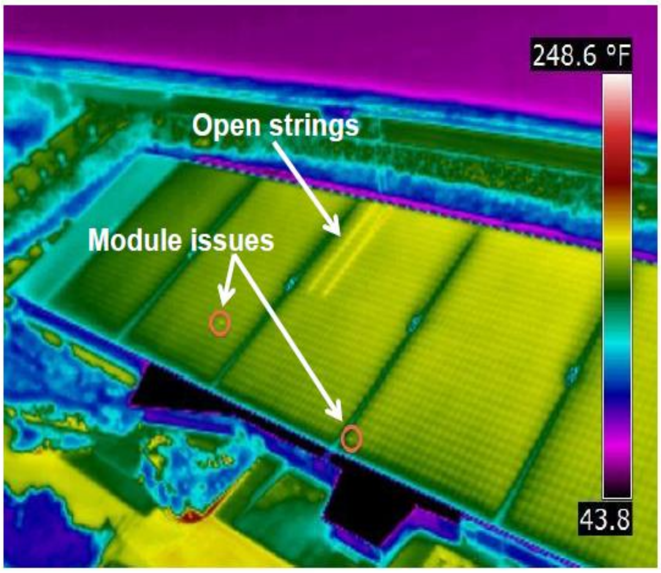

Figure 2.9 Example of Open-Circuit in a PV string (OC).

2.3.3 Short-Circuit (SC)

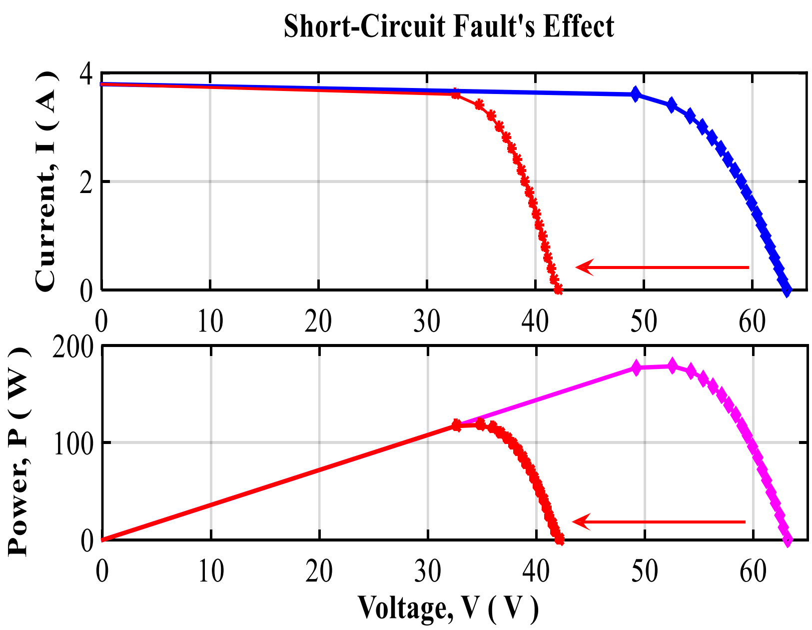

Figure 2.10 *I-V* and *P-V* characteristics with Short-Circuit fault effect.

Figure 2.10 shows that Short-Circuit fault reduces PV voltages at Open-Circuit and MPP (V_{OC}, V_{MPP}). It appears at PV cell interconnections, causing excessive heating (Figure 2.11). Besides, it can also be caused by bad wiring during installation or handling [52].

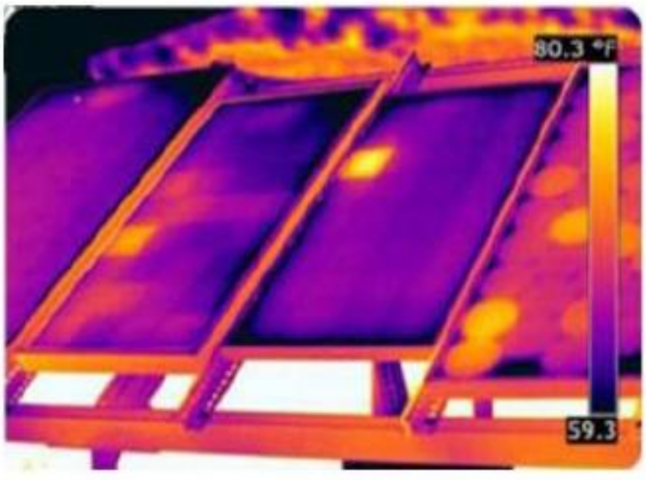

Figure 2.11 Example of Short-Circuited PV cell (SC).

2.3.4 Abnormal degradations

Abnormal degradations reduce PV generator efficiency (Figure 2.12). They are mainly due to the aging effect under harsh environment condition [53].

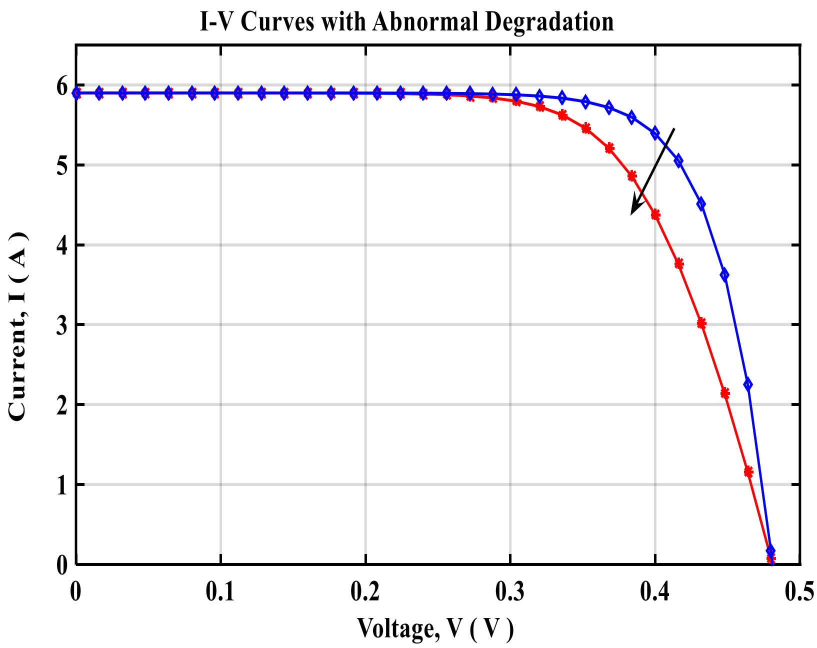

Figure 2.12 Effect of abnormal degradations in the *I-V* characteristic.

2.3.5 Increasing series resistance (R_s)

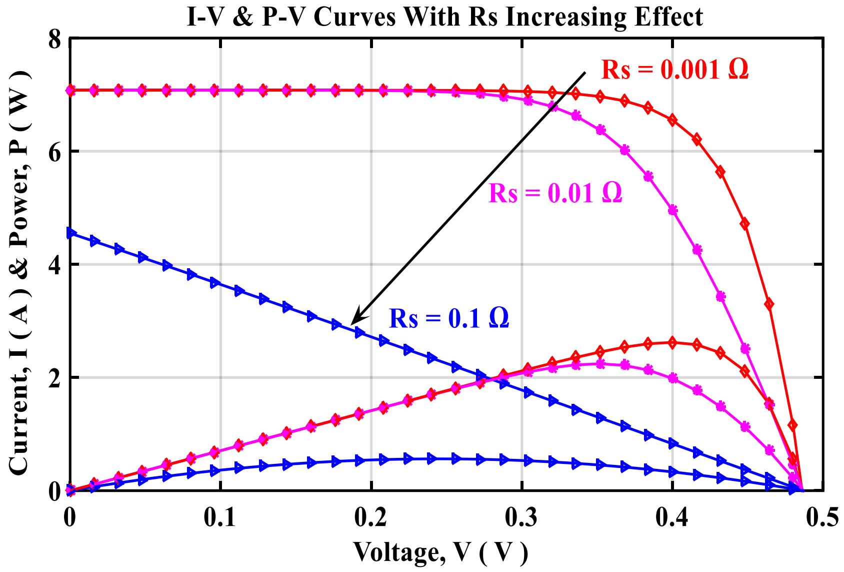

Figure 2.13 Effect of increasing the series resistance in the *I-V* and *P-V* characteristics.

Degradations, such as bond failure and resistive heating, influence series resistance value. From Figure 2.13 we can see that an increase of the series resistance value causes a decrease of the slope of OC (Increased slope in horizontal leg), getting a severe damage in reality (Figure 2.14). Series losses are caused by excessive resistance in the circuit. This can be due to degradation in a particular component, or the wiring between them. The increased resistance can result in further degradation and permanent damage. Bypass diodes help to mitigate this.

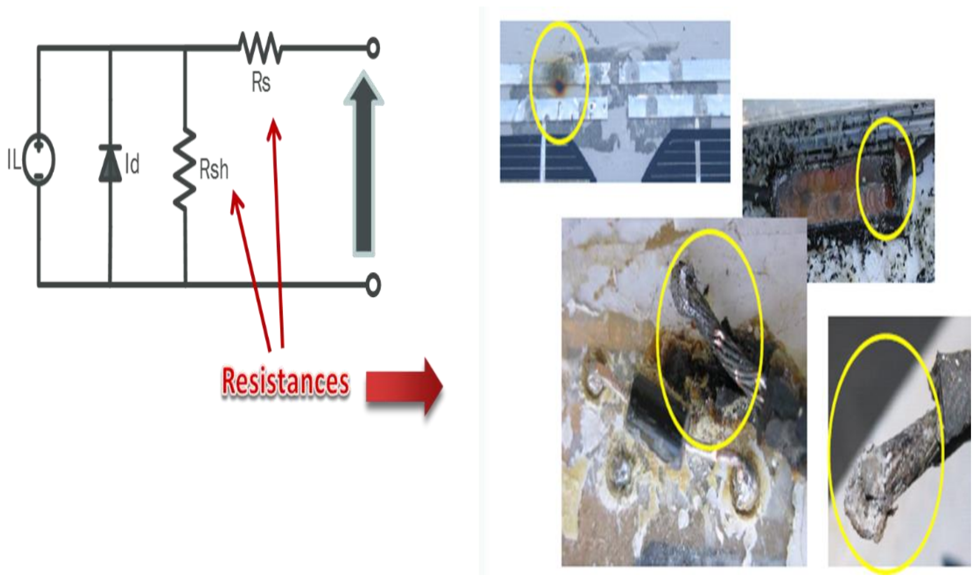

Figure 2.14 Real effect of parasitic resistances of PV cells.

2.3.6 Decreasing shunt resistance (R_{sh})

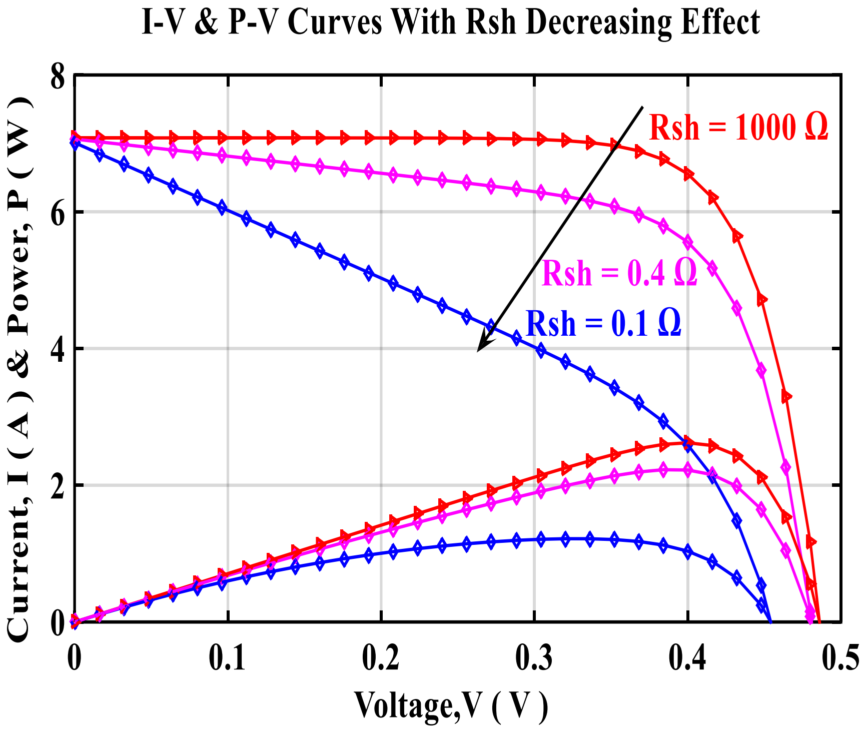

Figure 2.15 Effect of decreasing shunt resistance in the *I-V* & *P-V* characteristics.

From Figure 2.15 one can see that a high shunt resistance value induces a poor fill factor. The decrease in shunt resistance value causes a decrease at the slope of SC (Reduced slope in vertical leg) and then severe damage. A shunt causes power losses by providing an alternate current path and short-circuiting a module or cell. Such a diversion causes significant heating of the affected component.

2.3.7 Other dangerous faults

It is shown from the above figures that each type of PV fault influences a special part of the characteristics and therefore depend on specific parameters. This implies that we need to treat each fault in a specific manner. In addition to the above-mentioned PV faults, there are other dangerous electrical failures, which are cited bellow.

2.3.7.1 Ground-Fault (GF)

To prevent electrical shocks in PV plants, the user connects all non-current carrying and metal parts to the common ground. When a high current passes through the metal parts, the photovoltaic installation must stop since this can generate electrical shocks for users. This is known as Ground-Fault [40, 41]. Figure 2.16 presents a descriptive schematic of a GF example.

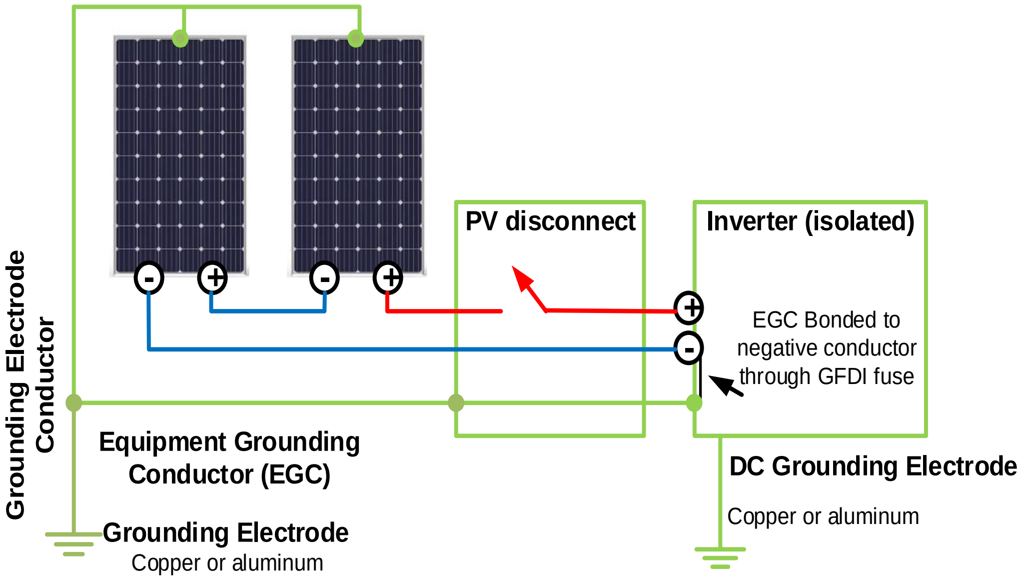

Figure 2.16 Descriptive schematic of a Ground-Fault (GF).

2.3.7.2 Line to Line Fault (LLF)

A line-to-line fault, also known as a double ground fault can be defined as a Short-Circuit fault among the PV panel's cables with diverse potential [56, 57]. Figure 2.17 presents a descriptive schematic of LLF examples.

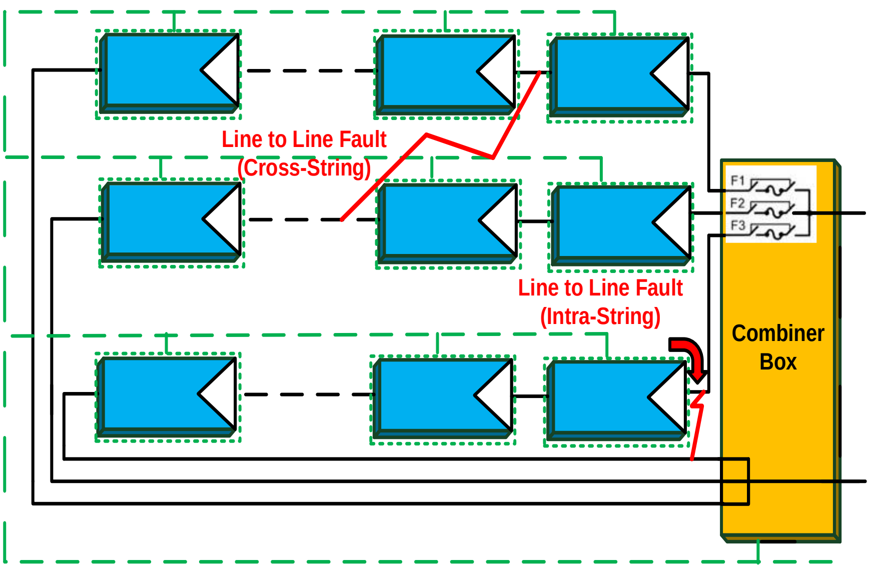

Figure 2.17 Descriptive schematic of Line-to-Line Fault (LLF).

2.3.7.3 Arc Fault (AF)

A rise in temperature leads to combustible material in PVG and therefore the risk of an arc fault. It can be series or parallel AF [58, 59]. Figure 2.18 presents a descriptive schematic of AF examples.

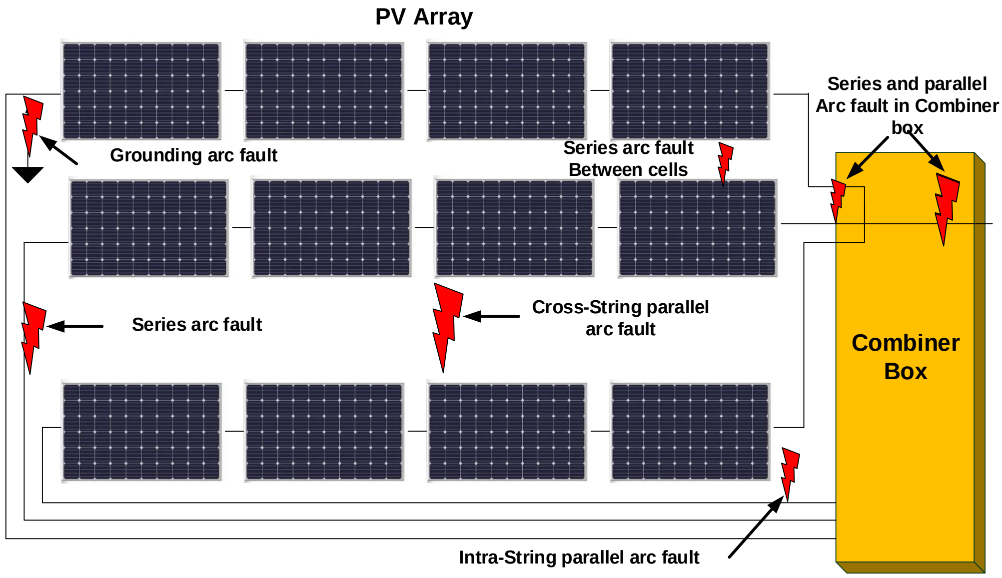

Figure 2.18 Descriptive schematic of Arc-Fault (AF).

2.3.7.4 Blocking and bypassing diode (BBP)

The blocking and bypassing diodes are integrated into PV panels to protect them (Figure 1.11 & Figure 1.13). The faults associated with these diodes can be due to Short-Circuit or Open-Circuit in them [43].

2.3.7.5 Junction box fault (JB)

The energy loss stress (ELS) is the major cause of JB faults. Other causes are from bad cabling during installation, or to the ageing effect [41]. Figure 2.19 gives an example of JB Fault.

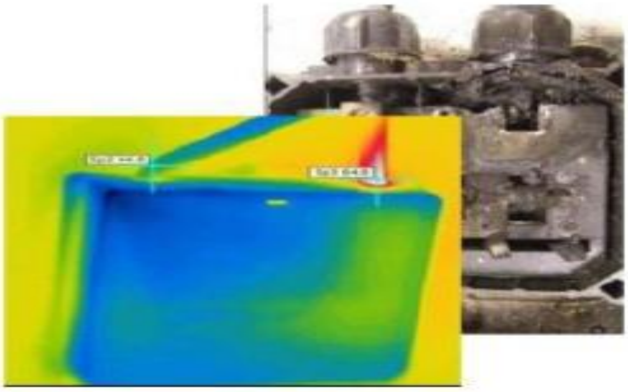

Figure 2.19 Example of fault in the JB: Corrosion.

The next section detail the elaborated techniques in the literature to diagnose all of the above-mentioned PV faults.

2.4 Fault Detection and Diagnosis techniques in PVG

Researchers have focused in inventing different methods to detect and diagnose failures coming in PV generators in order to prevent main hazards such as fire risks [41], electrical shocks [5], physical danger, and PV panels cracking [44] and so on. FDD-based techniques can be classified into two main categories (visual and electrical). Details are given in what follows.

2.4.1 FDD visual-based techniques

These techniques require human factor intervention [49, 50, 60, and 61]; and consists of inspecting PV generator visually through:

- Thermal imaging process [62, 63] by using infrared (IR) camera* (e.g. detection of hot spots in PVG, Figure 2.19).

- Lock in thermography (LIT) [50].

- Electroluminescence (EL) [60] & Photoluminescence (PL) tests [41].

- Ultrasound scanners and X-ray tomography [41].

2.4.2 FDD electrical-based techniques

These techniques are based on supervised algorithms to be implemented in PV plants [64, 65]. Several electrical-based FDD techniques have been developed [65]. These techniques can be classified also into five groups [43].

• The first group is based in statistics and signal process [66]: these techniques use signal analysis tools, such as time-domain reflectometry (TDR) [67] and Fourier analysis [68].

• The second group is based on the observation and analysis of the *I-V* characteristic of the PVG [41]. The *I-V* curve provides information such as short-circuit current, open-circuit voltage, series and shunt resistors, fill factor and presence of shading and soil. These parameters allow distinguishing several faults.

• The third group is based on power losses analysis [69-72]. These fault diagnosis techniques are based on parameters such as thermal and miscellaneous capture losses, which allow generating an indicative signal of faults in the PV plant [69]. Besides, other diagnosis techniques are based on the performances ratio, by developing mathematical parameters indicators of voltage and current in [73].

• The fourth group is based on the measured *I-V* curve [74]. The techniques compare the real and modelled PVG. The created models are obtained using real measured values of healthy/faulty PVG.

• The fifth group is based on artificial-intelligence (AI) techniques. They have been successfully used for diagnosing all kinds of renewable energy systems [75], and particularly for PV systems [76]. In [60], [74], [77], [78] and [79], artificial neural networks (ANN) based techniques were used to classify different types of failures occurring in the photovoltaic field. Researchers in this order have developed different model types (multi-layer perceptron, radial basis network, feed forward, recurrent neural-network, etc.) with different structures (number of the hidden layer, number of neurons in the layer) and through the use of a different kind of learning process (supervised/non-supervised). All of the developed ANN-based techniques have proven good accuracy and efficiency in PV diagnosing. In [80], a decision tree-based approach is developed to detect many types of failures (LLF, Shading, and OC). Fuzzy logic controllers are used in [81] and [82] for diagnosing SC, OC, BBP, snow and shading. Combined Neuro-fuzzy based controllers are used in [83] to diagnose earth fault, diode SC, and PS. Besides, the combination of neural networks with a heuristic approach is presented in [84], for diagnosing SC, aging, and shading. In [85], authors used wavelet packets for the detection of faults under low irradiance. It differentiates the shading fault from other ones by the use of variations in voltage array, energy array, and variable impedance. Metaheuristics are developed for FDD in [86] and [87] for diagnosing BBP, SC, disconnection, and shading.

Other methods are presented in [88-89]. All of the developed electrical FDD based techniques can be done through offline adaptation (test of the technique's effectiveness) [66] or on-line adaptation at real-time [89-91]. It is clear that online fault diagnosis is important because: it is the essential for any array dynamical reconfiguration and it contains key state of health information useful for system maintenance. Besides, supervision of PV plants can be done in situ through the use of *I-V* solar tracers* or from distance (tele-monitoring) by recuperation of collected data through DAQ system. In what follows, details about the developed FDD electrical-based for each of the cited PV faults presented in section 2.3.

a) Shading fault-based FDD:

The measured *I-V* curve is generally used to diagnose this type of fault [52]. Such as the standard analysis error in [92], vertices principal component analysis (PCA) [93], and discrete wavelet transform (DWT) [94].

b) SC-based FDD:

ANN-based are the most used techniques for failures identification of Short-Circuit fault in PV panels [61], [81]. These techniques have proven good performances in diagnosing SC.

c) OC-based FDD:

The work in [4], identifies and localizes failures at Open-Circuits in PV plant. The ANN-based technique has been developed in [94] with success to diagnose OC fault, using two NNs with a multilayer NN. Furthermore, in [93] a backpropagation neural-network have provided effective detection of OC and other faults.

d) Abnormal degradations-based FDD

Abnormal degradations have been diagnosed using several techniques in [52, 96]. In [84], a heuristic technique has been proposed for diagnosing several faults and particularly the aging one. Besides, the NNs based are elaborated for diagnosing aging fault in [96].

e) GF-based FDD:

Some equipment is created to be inserted in the PV plants such as the fuse-based ground-fault-protection-device (GFPD) [54]. Some simulations are investigated in [55] to present the limits of GFPD and suggest other solutions. Other techniques for GF are presented in [5].

f) LLF-based FDD:

The over-current-protection-device (OCPD) is inserted in PV plants for protection from LLF [55]. LLF was also treated by the use of a support vector machine (SVM) in [56]. Other techniques for LLF are suggested in [5], [43], and [65].

g) AF-based FDD:

Some equipment for protection from AF are inserted such as arc-fault-circuit-interrupter (AFCI) in [97]. Besides, it is treated through time and frequency characteristics of a capacitor current [58] using wavelet transform and mathematical morphology [59]. Other techniques for AF are suggested in [5], [43].

h) BBP-based FDD:

Some AI-based techniques are developed to diagnose the BBP fault, such as the fuzzy controller [82], and meta-heuristics [87]. Other techniques are proposed in [43], [65].

i) JB-based FDD:

In addition to the control users of the JB, visual-based techniques give more precision about the health state of JB [43], [65].

The following Table 2.1 presents the different faults occurring in PVG with their associated FDD techniques.

Table 2.1 Several PVG faults with their developed diagnosis techniques.

PVG Faults	Detection and diagnosis used techniques
Shading	AI: decision-tree [80], fuzzy[80-81], neuro-fuzzy [83], heuristic [84], Meta-heuristic [87-88], Standard analysis error in *I-V* [92], PCA [93], DWT [94]
Short-circuit (SC)	AI based on *I-V* curve: ANN [74], [79], Fuzzy [81-82], Heuristic [84], Meta-heuristic [86,87]
Open-circuit (OC)	AI based on *I-V* curve [78], Decision-tree [80], Fuzzy [80-81]
Abnormal degradations	Visual inspections and drones, IR, EL, PL
Line to Line Fault (LLF)	Wavelet-Packets [80], Support vector machine (SVM) [95]

Arc-Fault (AF)	*I-V* test curve tracers* [92], Frequency domain reflectometry [67]
Blocking and bypassing diode fault (BBP)	AI: Fuzzy [82], Meta-heuristic [86-87]
Junction-box fault (JB)	User checking, Temperature sense, Visual-based: IR [43], Multi-meter
Hot-spot (HS)	Thermal inspections [43]: IR
Ageing effect	AI [81], Visual inspections

2.4.3 Material-based techniques

In reality, when faults occur and PV system stop functioning, we can give instruments of measurements such as multi-meters and test the current/voltage at each level of cascading the PV installation.

Moreover, to avoid PV degradations some trending solutions are mentioned bellow.

a) Cleaning PV panels.

Solutions such as cleaning [98, 99] PV panels are used. Cleaning can be dry or wet, related to the type of region. PV plants cleaning can be either through a manual manner, automatic, semi-automatic, or using truck (Figure 2.20).

Figure 2.20 Example of PV cleaning.

- Dry cleaning is observed in desert regions, due to water rarefaction but it is limited because of scratches on the glass of the PV panels, which appear after the passage of sand wind.
- Wet cleaning is done in a region rich of water.

b) Including protections equipment in PV plants.

To protect PVG from overcurrent, fuses and overcurrent protection device as OCPD [80] are inserted. Besides, devices such as GFPD [51] is capable of GF detection, fault current interruption, indication, and provide fire hazard prevention. Furthermore, equipment named AFCI is developed in [97] to protect PV plants from an arc fault.

c) Tele-monitoring

Controlling and diagnosing the PVG from long distance using new smart protocols such as ZigBee technology [96] and Internet of Thing (IoT) [100].

Cost reduction is required for any envisaged solutions for diagnosing PV generators. In industry, some solutions are integrated into PV plants. Some of them have been implemented and some others have not been implemented by the cause of their high complexity or great cost estimation. In this order, cost estimation, efficiency, robustness, availability to the PV site, low complexity of implementation, integration in the whole PV system have a major influence in the choice of the appropriate FDD technique for diagnosing the faults in PVG.

2.4 Process of FDD techniques in PVG

Many anomalies, degradations, and faults, presented above, can occur in PV generators. A challenge is required to detect automatically these faults and diagnose them in early stages before dangerous risks and severe damages appear. PV plants inspections and alarms allow the users, when failures are detected, to take decisions for correcting the process. In general, operators do some visual PV inspections (detection of bubbles, delamination, detachment of the frame, discolouring) before system start-up. As for thermal fault and defects, like a hotspot, it is necessary to use instruments such as infrared (IR) camera mounted on drones* [80-82] for image thermography inspections to detect hotter areas within PVG. Drones can detect anomalies with high precision. This process is also required for electrical-based FDD, by using the images stored in a database, taken from drones. Researchers developed further techniques analysis, as electrical FDD-based, to be implemented with the PV plant to detect, diagnose, correct failures, and protect the system. The major faults diagnosis steps, using FDD electrical-based techniques, are cited bellow (Figure 2.21):

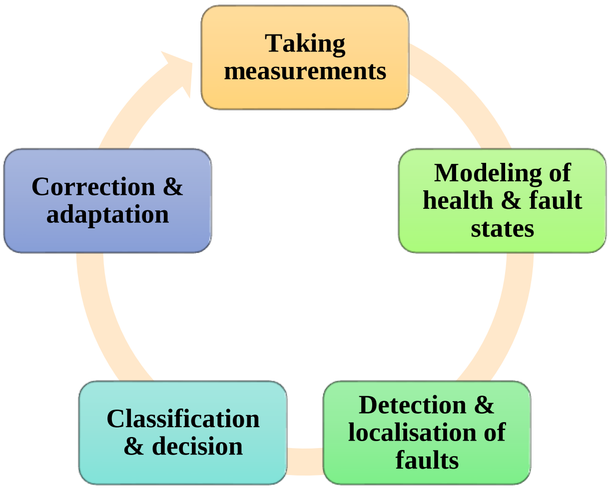

Figure 2.21 Process of diagnosis in the PV plant.

- Measurements through sensors and data acquisition system.
- Modelling of the health and fault states.
- Detection and localization of faults.
- Classification and decision about the health state.
- Correction, protection, and adaptation.

Conclusion

This chapter has contributed to the diagnosis techniques of faults occurring in the PV generator. It presents the major forms of degradations in PVG and gives details about the different types of PV faults taking into consideration their causes, as detailed in my work in [101]. Various FDD techniques have been presented. Besides, some envisaged diagnosis solutions have been discussed. Some criteria (low cost, simple implementation, high efficiency, availability, robustness) are required for any envisaged solutions for diagnosing a PV generator/plant. From the study in this chapter, the major influences of faults caused by parasitic resistances have attired our interest to model and identify parameters of PVG, in the next chapter.

Chapter 3

PV Generator (Modelling, Characterization & Identification)

CHAPTER 3: PVG (Modelling, Characterization, & Identification)

Introduction

In previous chapter, the performances of PVGs affected by different faults that can occur on it, has been presented. Among these faults the parasitic resistances effect and others electrical parameters, which have shown a prodigious influence on performances. Besides, the exact PV parameters values are essential for precise mathematical modelling, simulation, and control of the photovoltaic generation systems. In this chapter, a presentation is done about the modelling and identification of the different electrical parameters of the PVG.

3.1 Modeling of electrical equivalent circuit of PVG

There are several electrical circuit models, used by researchers, describing the physical behaviors of solar PV cells. They are represented in Figure 3.1. The corresponding PV panel and PV generator's electrical schematics are then represented as in Figure 3.2 [102], [103].

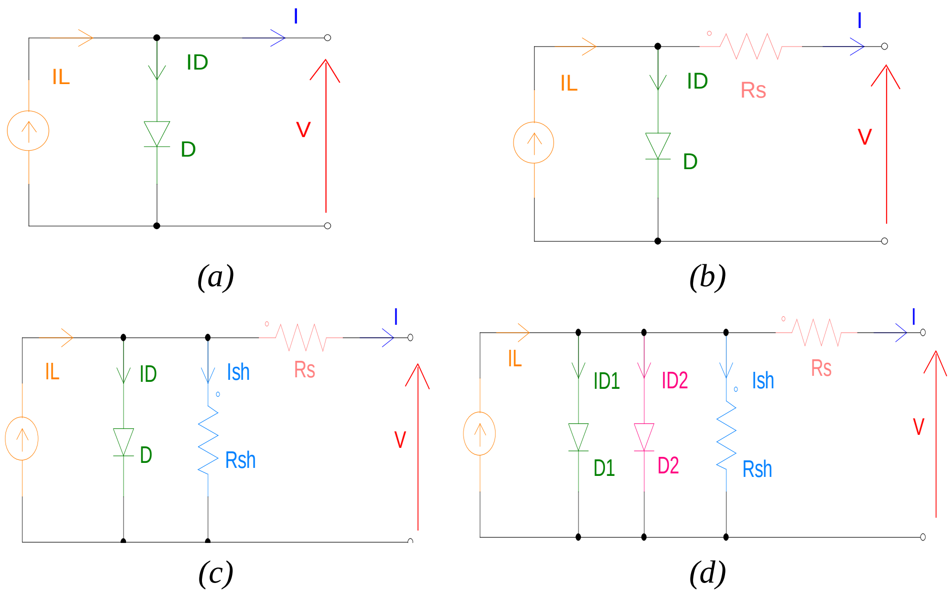

Figure 3.1 Solar PV cell's electrical equivalent circuits:
(a) Ideal model. (b) Single diode model with series resistance R_s*. (c) Single diode model with series* R_s *and shunt* R_{sh} *resistances. (d) Double diode model.*

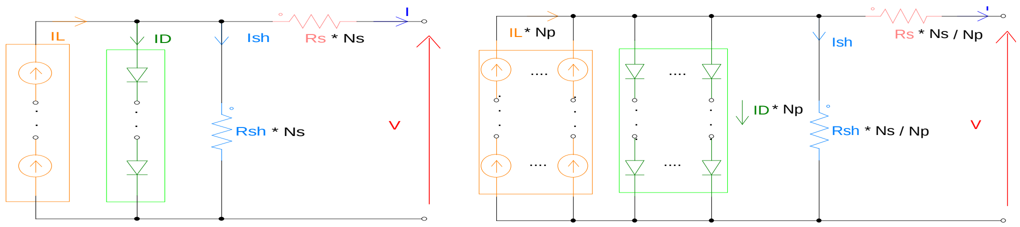

(a) *(b)*

Figure 3.2 PV panel and PV generator's electrical equivalent circuits:
(a) Panel of N_s *cells in series. (b) Generator composed of* N_s *and* N_p *branches.*

The mathematical expressions related to the Current-Voltage, (*I-V*) relationship of the different electrical models are given bellow. Then the equations (3.1) through (3.9) could be obtained.

First case « Cell: Single Diode Model (SDM)»

a) Ideal Model (*contains **three** unknown parameters*)

$$I = I_L - I_D \tag{3.1}$$

$$I = I_L - I_{ds}.\left(exp\left(\frac{V}{n.V_t}\right) - 1\right) \tag{3.2}$$

b) Single diode model with series resistance (*contains **four** unknown parameters*)

$$I = I_L - I_{ds}.\left(exp\left(\frac{V + R_s.I}{n.V_t}\right) - 1\right) \tag{3.3}$$

c) Single diode model with series and shunt resistances (*contains **five** unknown parameters*)

$$I = I_L - I_D - I_{sh} \tag{3.4}$$

$$I = I_L - I_{ds}.\left(exp\left(\frac{V + R_s.I}{n.V_t}\right) - 1\right) - \frac{V + R_s.I}{R_{sh}} \tag{3.5}$$

Second case « Cell: Double Diode Model (DDM)»

d) Double diode model (*contains **seven** unknown parameters)*

$$I = I_L - I_{D1} - I_{D2} - I_{sh} \tag{3.6}$$

$$I = I_L - I_{ds1}.\left(exp\left(\frac{V + R_s.I}{n_1.V_t}\right) - 1\right) - I_{ds2}.\left(exp\left(\frac{V + R_s.I}{n_2.V_t}\right) - 1\right) - \frac{V + R_s.I}{R_{sh}} \tag{3.7}$$

Third case « Panel »

a) Panel of N_s cells in series

$$I = I_L - I_{ds}.\left(exp\left(\frac{V + R_s.N_s.I}{n.V_t.N_s}\right) - 1\right) - \frac{V + R_s.I.N_s}{R_{sh}.N_s} \tag{3.8}$$

Fourth case « ***Generator*** »

b) Composed of $\boldsymbol{N_{ms}}$ and $\boldsymbol{N_{mp}}$ branches.

$$I = I_L N_{mp} - I_{ds}.N_{mp}\left(exp\left(\frac{V.N_{mp} + R_s.I.N_s.N_{ms}}{n.V_t.N_s.N_{ms}}\right) - 1\right) - \frac{V.N_{mp} + R_s.I.N_s.N_{ms}}{R_{sh}.N_s.N_{ms}} \tag{3.9}$$

All of the above mathematical equations are in non-linear form (contain exponential terms) and contain a set of unknown parameters. These later are usually unknown to the users since they are not directly measurable and are not mentioned in the PV manufacturers' datasheet. They are closely related to the internal physical behaviors of solar PV cells, where:

- $\boldsymbol{I_L}$*:* Light current.
- $\boldsymbol{I_{ds1}}$: Diode saturation current (*Diffusion phenomenon*).
- $\boldsymbol{I_{ds2}}$: Reverse diode saturation current (*Recombination phenomenon*).
- $\boldsymbol{n_1}$: Diode ideality factor (*Diffusion phenomenon*).
- $\boldsymbol{n_2}$: Second diode ideality factor (*Recombination phenomenon*).
- $\boldsymbol{R_s}$: Series resistance.
- $\boldsymbol{R_{sh}}$: Shunt resistance.

With $V_t = K_B * T_c$: Thermal voltage constant, K_B: Boltzmann's constant (1.380650*10 -23 J/K), *q*: Electronic charge (1.6021764*10-19 C) and T_c: Cell's temperature. N_s: Number of series cells. N_{ms}: Number of panels in series branches. N_{mp}: Number of panels in parallel branches.

3.2 Photovoltaic electrical characteristics

Current–Voltage (*I–V*) curves are obtained by exposing the cell to a constant level of light, while maintaining a constant cell temperature, varying the resistance of the load, and measuring the produced current (Figure 3.3).

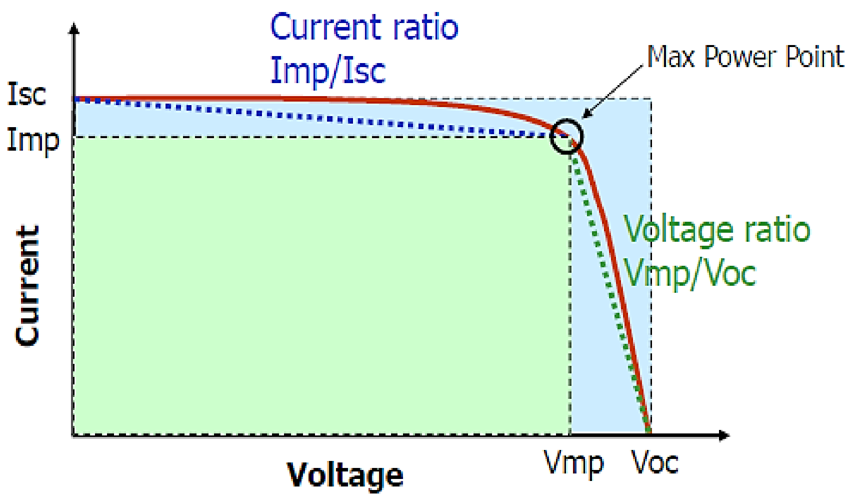

Figure 3.3 Solar *I-V* curve characteristic.

The *I–V* curve typically passes through two points:

- ***Short-circuit current* (ISC):**

$$I_{sc} = N_p(\frac{I_{sc\_STC}}{1000}\mathrm{G} + K_i(T - T_{STC}) \tag{3.10}$$

- ***Open-circuit voltage* (VOC):**

$$V_{oc} = N_s(V_{oc_{STC}} + K_v(T - T_{STC}) + V_{th}\ln\left(\frac{I_{sc}/N_p}{I_{sc\_STC}}\right)) \tag{3.11}$$

Some other electrical interesting parameters can be obtained from the *I-V* characteristic such as:

➢ ***Efficiency (η):***

Maximum efficiency in the solar PV cell context means the ratio between incident light power and maximum power. The equation 3.12 depicts efficiency clearly.

$$\eta = \frac{electrical\ power\ output}{solar\ power\ impinging\ the\ cell} = \frac{P_{Max}}{P_{in}} = \frac{I_{Max}.V_{Max}}{A.G_a} \tag{3.12}$$

Where: A is the cell area and G_a is the ambient irradiance.

➢ ***Fill factor (FF):***

The fill factor is considered as key metric for comparing *I-V* curve shapes. Fill-factor is easy to understand graphically (Figure 3.3). Just divide the area of the green rectangle (defined by the max power point) by the area of the blue rectangle (defined by I_{sc} and V_{oc}). Fill-factor is a measure of the square-ness of the *I-V* curve. A squarer curve (less rounded) means higher output power (and higher module efficiency).

$$FF = \frac{I_{mpp} * V_{mpp} (Watts)}{I_{sc} * V_{oc} (Watts)} \tag{3.14}$$

The fill factor for some specific materials is bellowed:

$$\begin{cases} aSi: 0.50 - 0.70 \\ xSi: 0.75 - 0.85 \\ GaAs: 0.85 - 0.9 \end{cases} \tag{3.15}$$

- ***Current ratio & voltage ratio***

Indicators of slope differences. If a PV string or module has a low fill factor compared with the population, and there are no steps in the curve, the current and voltage ratios are clues that can help you troubleshoot the problem and are calculated by the following expressions [92].

$$Cr = \frac{I_{mpp}}{I_{sc}} \tag{3.16}$$

$$Vr = \frac{V_{mpp}}{V_{oc}} \tag{3.17}$$

3.3 Influence of factors

PV generator's performances are affected by many factors, where some of them are external, related to the environmental conditions like the weather's variations (solar irradiance and temperature). Others are internal, related to the electrical, physical and mathematical modelling.

3.3.1 External effect (Climatic conditions)

Power, voltage, and current outputs of the PV modules are affected by environmental outdoor conditions such as solar irradiance and temperature, Figure 3.4 and 3.5.

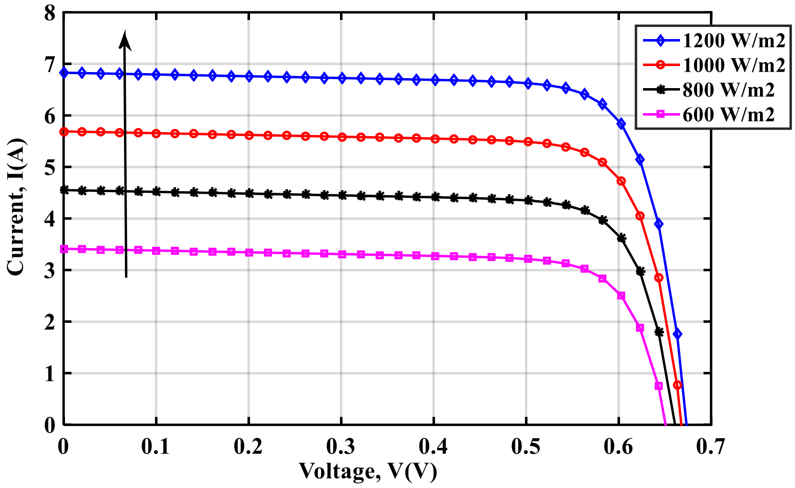

a)

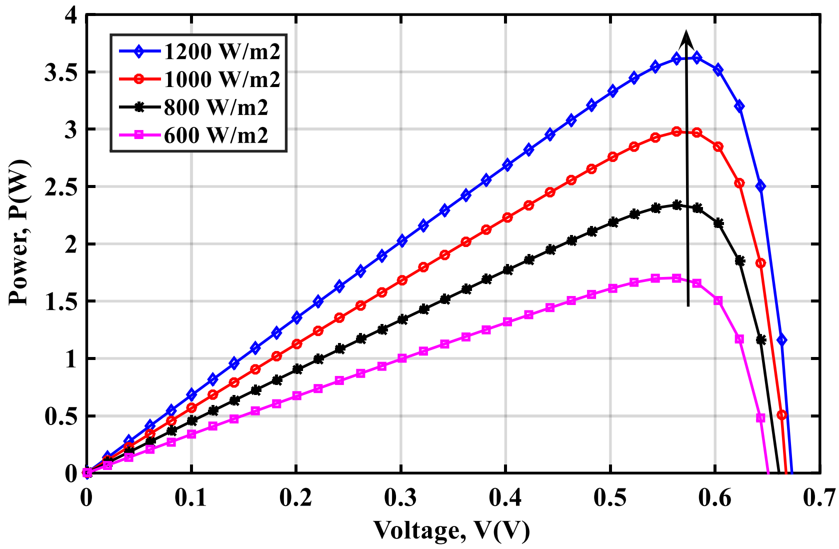

b)

Figure 3.4 PV curve characteristics under different solar irradiance: a) *I-V; b) P-V*.

It is observed from Figure 3.4 that the irradiance have a proportional influence on the *I-V* and *P-V* characteristics.

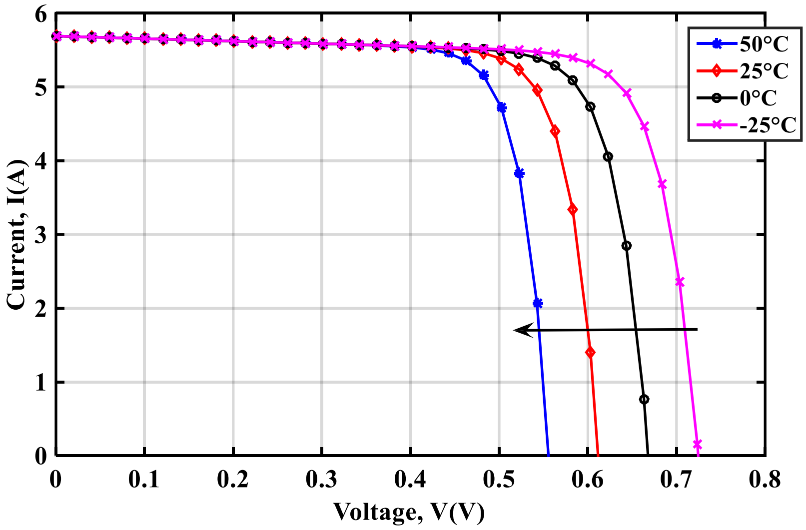

a)

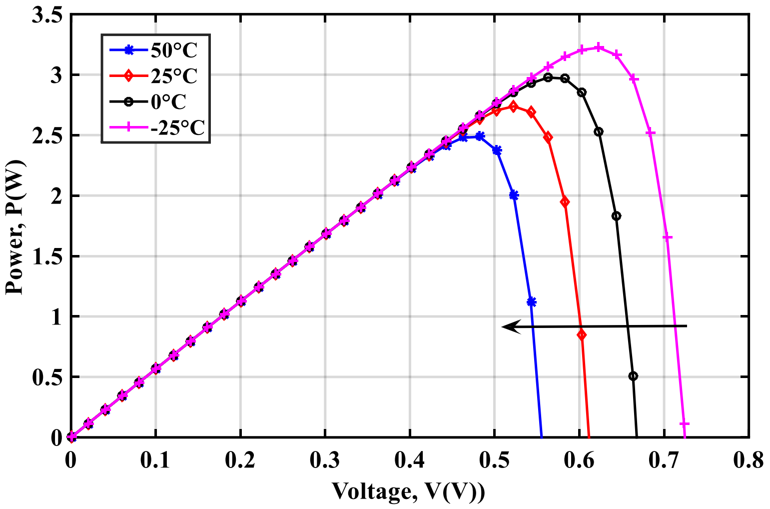

b)

Figure 3.5 PV curve characteristics under different temperature: a) *I-V; b) P-V.*

It is observed from Figure 3.5 that the temperature have an inverse proportional influence on the *I-V* and *P-V* characteristics.

3.3.2 Internal effect (Electrical parameters)

The overhead electrical governing equations (from 3.1 to 3.9) contain several unknown parameters (I_L, I_{ds1}, I_{ds2}, n_1, n_2, R_s, R_{sh}). Each of the PV parameters has a crucial influence on the performances and PV power production. The effects of variation of the internal five PV electrical parameters on the solar photovoltaic cell's performances [104] are shown in Figure 3.6.

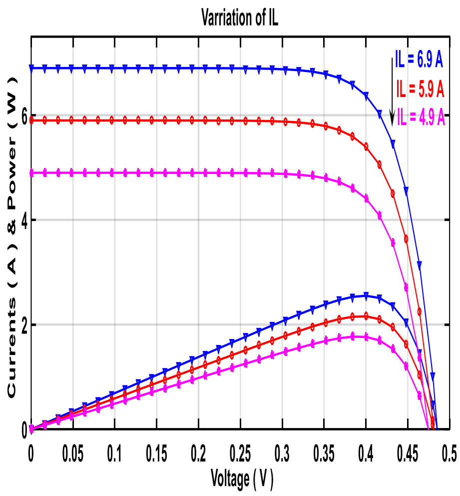
Varriation of IL
IL = 6.9 A
IL = 5.9 A
IL = 4.9 A
Currents (A) & Power (W)
Voltage (V)

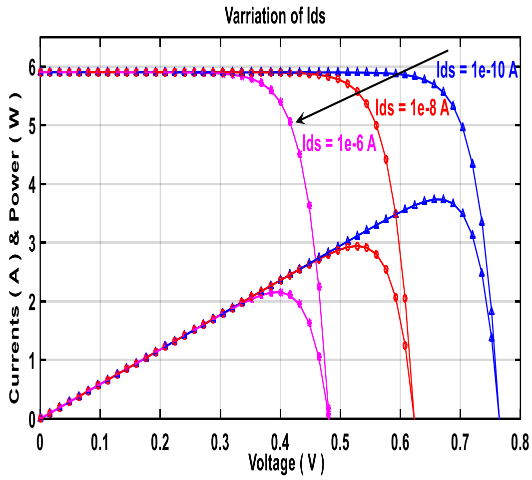
Varriation of Ids
Ids = 1e-10 A
Ids = 1e-8 A
Ids = 1e-6 A
Currents (A) & Power (W)
Voltage (V)

(a)

(b)

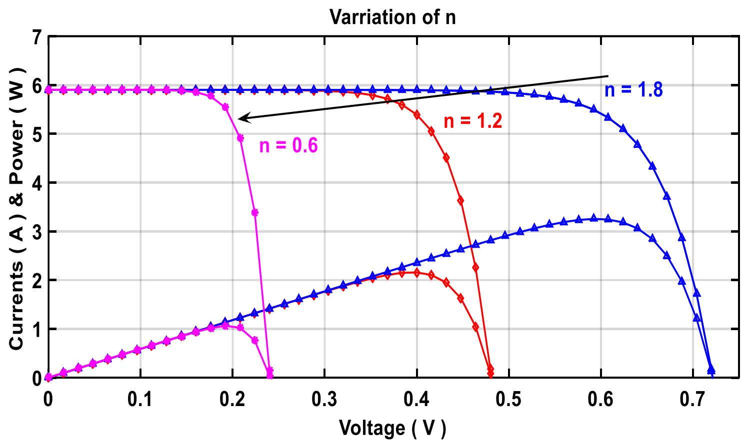
Varriation of n
n = 1.8
n = 1.2
n = 0.6
Currents (A) & Power (W)
Voltage (V)

(c)

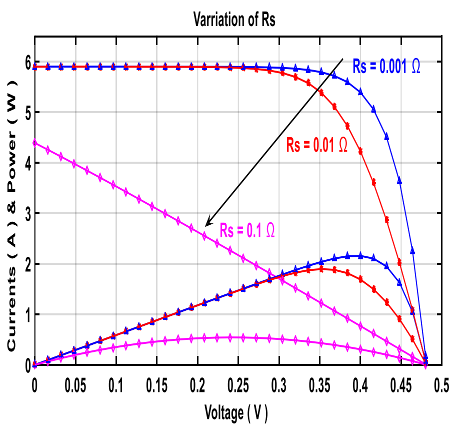
Variation of Rs
Rs = 0.001 Ω
Rs = 0.01 Ω
Rs = 0.1 Ω
Currents (A) & Power (W)
Voltage (V)

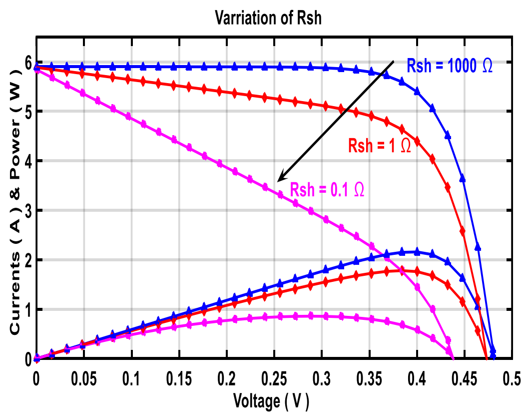
Varriation of Rsh
Rsh = 1000 Ω
Rsh = 1 Ω
Rsh = 0.1 Ω
Currents (A) & Power (W)
Voltage (V)

(d)

(e)

Figure 3.6 Variations effects of the electrical parameters on the (*I-V*) & (*P-V*) curves characteristics of solar PV cells: *(a)* Light current 'I_L'. *(b)* Diode saturation current 'I_{ds}'. *(c)* Diode ideality factor 'n'. *(d)* Series resistance 'R_s'. *(e)*. Shunt resistance 'R_{sh}'.

Figure 3.6 (a) illustrates the light current I_L effect, which is similar to that of the solar irradiance effect, so it has a proportional relationship with the generated current. Figure 3.6 (b), illustrates that diode saturation current I_{ds} has a proportional relationship with the voltage as shown, so it has an inverse effect compared to the temperature effect. In Figure 3.6 (c), the diode ideality factor n shows an effect on the obtained maximum power point (MPP). Figure 3.6 (d) and (e) illustrate that series R_s and shunt R_{sh} resistances have an effect on the slope at the open and short circuit points respectively. Consequently, each of these parameters has a crucial influence on the performances and the PV power production. This information involves the importance of accurate PV parameters values.

After the modelling step of any PV generator, their identified parameters values are used in an established model. Therefore, it is necessary to find the accurate values of the unknown electrical PV parameters by an appropriate approach. Besides, accurate parameters value of PV cells are essential for the development of good controlling techniques for Maximum Power Point Tracking (MPPT) based power electronic converters [105]. As shown in the following Figure 3.7 the importance of PV parameters' obtaining accurate values for a whole PV system.

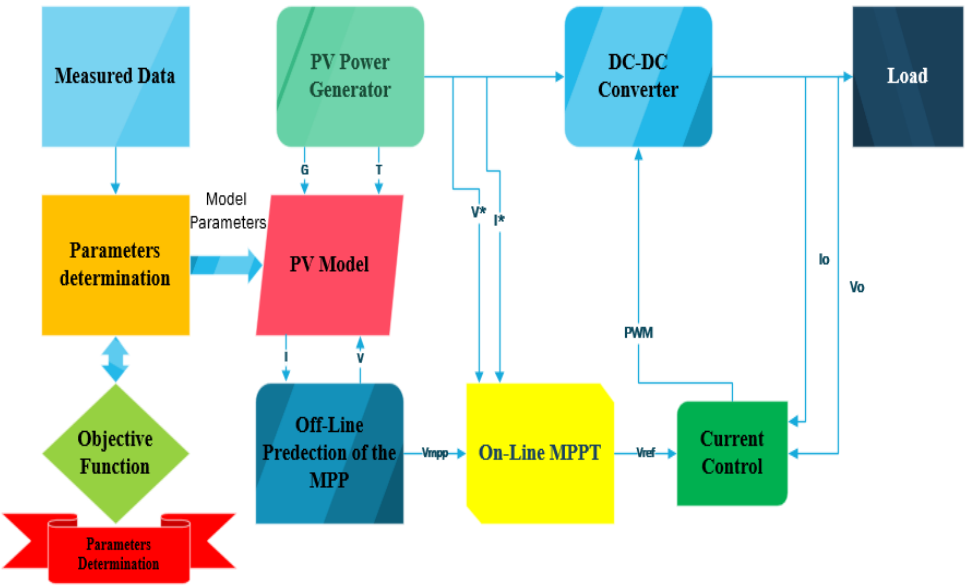

Figure 3.7 Importance of accurate PV parameters determination values in PV systems [105].

With the problem of non-linearity found in PV models and the dependence of environmental conditions [106], the determination of PV parameters becomes a complex problem, which necessitates an appropriate approach to find the best accurate values of the unknown PV parameters. The next section give more details about PV parameters obtaining methods.

3.4 Classification of identification methods

Earliest, numerous research workings have been developed only for getting the series and shunt resistances values (parasitic effects), by the cause of their high influences in the PV performances [107]. Afterthought, it has been observed that some other electrical parameters (Light current, diode saturation current, and diode ideality factor) have also an effect in PV performances [104]. For this reason, researchers have done many works to get the electrical unknown PV parameters [108] values with high precision and fast computational process. From the literature, these methods can be classified as the following Figure 3.8 [109].

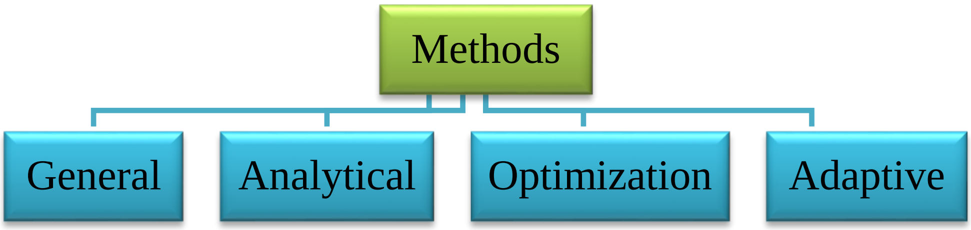

Figure 3.8 Classification of the PV panel's electrical parameters getting methods.

3.4.1 General methods

In a general way, *Duffie* obtained each parameter individually [110]. The parasitic resistances (series and shunt) are found graphically through the calculation of the slopes at open and short-circuits respectively [110, 111]. The diode ideality factor is taken in an interval depending on the used material's technology for the PV selected panels, for different manufacturers and different PV technologies (Si-Mono, Si-Poly, CDTE, Amorphous, CIS, Multi-junctions) [111, 112]. Light current and diode saturation current are obtained by the use of mathematical expressions [108], and by the use of PV manufacturer's datasheet information.

3.4.2 Analytical methods

Analytical methods such as *Carrero*'s method [113], are based on the analytical resolution of mathematical non-linear expressions through some simplifications and approximations [114],

[115]. The use of explicit formulas such as in [116] leads to reasonable PV parameters values. The PV parameters can be found through an analytical way through the use of three points at the current-voltage (*I-V*) characteristic. These points are found at the short-circuit, open-circuit, and maximum power points (MPP) [116]. This lead to obtain a set of expressions at each point. Then, through a suitable estimation to the problem, the problem can be approximated to a series of decoupled equations representing each parameter's value. This approach requires the datasheet information. The major analytical methods have a similar way of getting off the PV parameters expressions values and lead usually to similar results [113-115].

3.4.3 Optimization methods

The optimization algorithms are categorized into numeric-traditional, meta-heuristics, and hybrid methods. By the cause of limits of the analytical method to achieve with high precision the PV parameters values, our interest is gone for the optimization-based methods. This latter can be classified as in Figure 3.9.

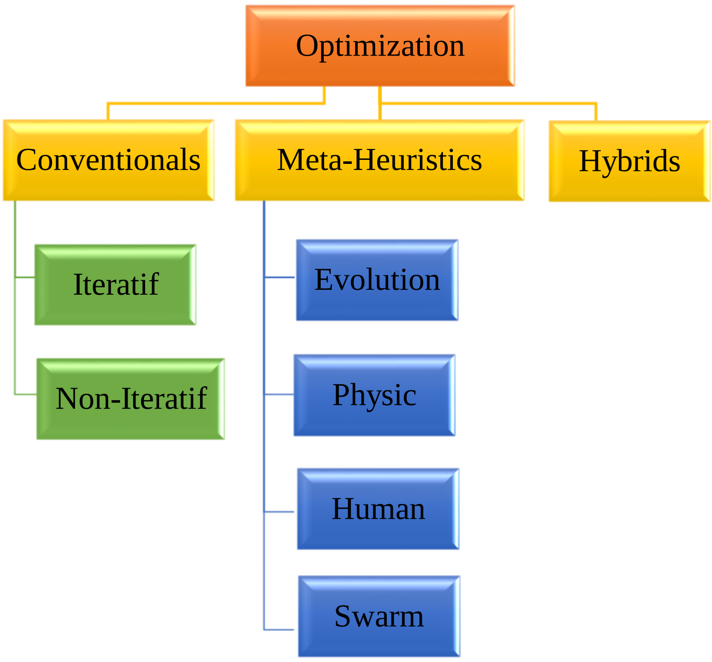

Figure 3.9 Classification of PV cell's electrical parameters determination optimization-based methods.

3.4.3.1 Numeric conventional

Numeric conventional optimization-based methods for PV parameters getting values, such as *Kashif*'s one [117], are based on the reduction of the number of parameters to be evaluated.

The conventional Newton-Raphson (NR) method can also be used as developed in [118, 119]. It necessitates an iterative process with good initialization guess of PV parameters values, to converge to the best solutions. Besides, the traditional methods are used to obtain the optimum of the function using the gradient or the hessian. A presentation of three numeric methods' obtained parameters values is in Table 3.1 [120].

Table 3.1 Extracted single-diode PV model parameters using three numerical algorithms.

Parameters **Models**	**T. Esram**	**Vilalva**	**Vika**
I_L ***(A)***	1.220	5.500	5.532
I_{ds} ***(mA)***	1.6e-6	2.0e-08	2.0e-8
n	1.833	1.200	1.200
R_s ***(Ω)***	0.164	0.372	0.370
R_{sh} ***(Ω)***	461.962	200.602	169.789

3.4.3.2 Metaheuristics

In recent times, meta-heuristic optimization-based methods, using Artificial-Intelligence (AI) inspired algorithms, have attracted the care of researchers to obtain with good precision, the unknown PV parameters values. The metaheuristic methods use evolution-based [120], physics-based [121], or immune-human-based [122] and swarm-based [123], algorithms in the search process, which are presented in the subsections below.

a) Evolution-based

Evolutionary Algorithm (EA) [124], Differential Evolutionary (DE) [125], Genetic Algorithms (GAs) [126], Pattern Search (PS) [127], Simulated Annealing (SA) [128], Repaired Adaptive Differential Evolution (Rcr-IJADE) [117].

b) Physics-based

Electromagnetic Field Optimization (EFO), Gravitational Search Algorithm (GSA), Electromagnetism-Like Algorithm (EMA), Weighted Superposition Attraction (WSA) [129].

c) Human-based

Harmony Search (HS) [130], Bacterial Foraging Algorithm (BFA) [131], Simplified Teaching-Learning-Based Optimization (STLBO) [132], Discrete Symbiosis Organism Search (DSOS) [133], Artificial Immune system (AIS) [134].

d) Swarm-based

The swarm-based, Particle Swarm Optimization (PSO) [135, 136], Bird Mating Optimization (BMO) [137], Artificial Bee Swarm Optimization (ABSO) [138]. Grey Wolf Optimizer (GWO) [139], Chaotic Whale Optimization Algorithm (CWOA) [140], Cat Swarm Optimization (CSO) [141], and Cluster Analysis (CA) [142].

The metaheuristics are more attractive than the traditional deterministic methods in terms of accuracy and robustness, by the cause of their good global research achieving. In addition, they do not require a gradient or differentiable of the objective function. Besides, the initial guess of parameters values is not a necessity but it necessitates the upper and lower limits of an interval of research. An evaluation of some metaheuristics methods for PV parameters getting values is carried out as in [143]. Table 3.2 bellow presents a comparison between different metaheuristics parameters getting methods for SDM.

Table 3.2 Comparison among different metaheuristics parameters getting methods for SDM.

Parameters/Models	GA	PS	SA	HS	ABSO
I_L (A)	0.7619	0.7167	0.7620	0.76070	0.7608
I_{ds} (mA)	0.8087	0.9980	0.4798	0.30495	0.3062
n	1.5751	1.6000	1.5172	1.47538	1.4758
R_s (Ω)	0.0299	0.0313	0.0345	0.0345	0.0366
R_{sh} (Ω)	42.3729	64.1026	43.103	43.1034	52.2903

The metaheuristic methods transformed the difficult model of PV parameters getting values into a simple non-linear optimization problem. In addition, they use inspired algorithms from artificial intelligence to finding their precise values, which professionalism more the process of research [143].

3.4.3.3 Hybrid

To improve the effectiveness of methods, researchers have combined a mix between different simple methods such as (analytical and numerical, analytical and optimization, numerical and optimization, so on). Hybrid adaptive Nelder-Mead simplex algorithm based on eagle strategy (EHA-NMS) [144], Nelder-Mead and Modified Particle Swarm Optimization (NM-MPSO) [145], Artificial Bee Colony-Differential Evolution (ABC-DE) [146], Trust-Region Reflective deterministic algorithm with the Artificial Bee Colony (ABC-TRR) [146], Teaching–learning–based Artificial Bee Colony (TLABC) [146]. Those methods, which are called hybrid, have excellent performances because they restrict the universe in the search process without losing precision (without losing the optimum). They achieve the best results in less number of iterations compared to simple optimization-based methods. Therefore, an evaluation between the obtained PV parameters values from simple PSO and the hybrid particle swarm optimization combined with simulated annealing (HPSOSA) is presented in the following Table 3.3.

Table 3.3 Comparison between PV parameters results from PSO and HPSOSA.

Parameters **Models**	**PSO**	**HPSOA**
I_L (A)	0.7619	0.7167
I_{ds} (mA)	0.8087	0.9980
n	1.5751	1.6000
R_s (Ω)	0.0299	0.0313
R_{sh} (Ω)	42.3729	64.1026

From the works in [147], it is proved that the HPSOA has better performances compared to simple PSO and has achieved the global optimum in all test runs.

3.4.4 Adaptive

As the physical behavior of solar PV cells/panels is influenced by environmental conditions. There are several other methods in literature capable of finding the parameters of a more general model, in which the physical parameters models change dynamically concerning with irradiance and temperature values. Those models and their respective methods are called adaptive models and methods [144, 145].

After seeing the major methods developed, we have seen that there is a compromise of some characteristics for obtaining high effectiveness and precision of PV parameters values. It is necessary that the method chosen to be applied should ensure simplicity, rapidity, popularity, robustness, and high accuracy. For this reason, we opted in the following section to develop a hybrid optimisation-based method.

3.5 Hybrid optimization-based method

The identification process is based on the development of a mathematical representation for a physical system by the use of experimental data [148], through details explained in the major steps cited in the points below of Figure 3.10.

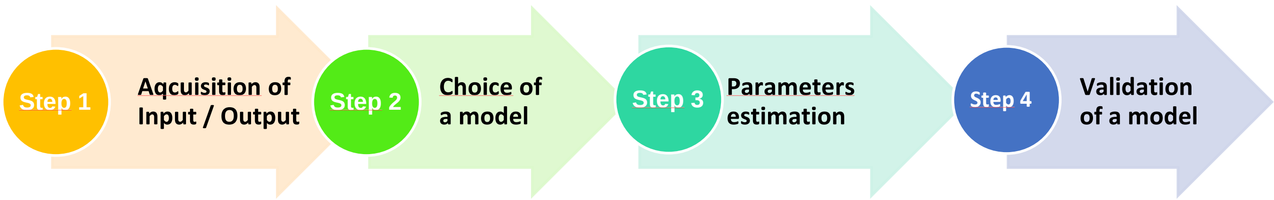

Figure 3.10 Major steps of parameters identification in systems.

- ***First Step***: *Acquisition of real Data.*
- ***Second Step***: *Choice of an appropriate model.*
- ***Third Step***: *Parameters estimation.*
- ***Fourth Step:*** *Validation of the model.*

In the third step, the application of the chosen optimization algorithm to identify and obtain the optimal values of PV parameters. The idea is based on a prediction error between the output of the real PV process and the output predicted by the PV model [149].

The combination of a traditional method and a recent smart swarm-based optimization method is done, with a big focus on the application of the topic of artificial intelligence algorithms into solar photovoltaic production. The combined approach was done between the traditional method, which is the non-iterative *Levenberg-Marquardt* (LM) technic and between the recent meta-heuristic optimization technic, called by Grey Wolf Optimizer (GWO) algorithm.

Our focus is to estimate the PV parameters values of the SDM model using RTC France data at the conditions of irradiance about 1 000 W/m^2 and of temperature about 300^{0}C. Only the third part of identification process is detailed, which is the estimation of PV parameters values. The big focus is to optimize the damping factor of LM through GWO. The estimation/identification process can be gotten in three major phases, such as the initial step of prediction through the use of least-squares mean (LSM), the getting of optimal PV parameters values through LM, and the optimization of a dominant factor through GWO as detailed below [150].

3.5.1 Least Squares Mean (Initial phase of prediction)

Prediction of initial PV parameters values using LSM [151] for the two parts of the introduced real experimental points of *I-V* curve characteristics as described below.

- For the linear part:

The prediction in the linear part [152] of the model can be obtained simply through the use of the following expressions.

$$I_{Model}(i) = a * V_{Model}(i) + b \tag{3.18}$$

$$Error(i) = I_{\mathrm{Re}al}(i) - I_{Model}(i) \tag{3.19}$$

$$J(i) = J(i-1) + error(i)^2 \tag{3.20}$$

Where *a* and *b* are constants depending on a determinant and others constants introduced by user. *J* is the Jacobian and is defined below.

- For the non-linear part:

The prediction in the non-linear part [153] of the model can be obtained with a logarithmic way through the use of the following logarithmic expression.

$$I_{Model}(i) = C_0 + C_1 * I_{Model}(i) + C_2 * \log(1 - \frac{I_{\mathrm{Re}al}(i)}{b}) \tag{3.21}$$

$$Error(i) = I_{\mathrm{Re}al}(i) - I_{Model}(i) \tag{3.22}$$

$$J(i+1) = J(i) + error(i)^2 \tag{3.23}$$

Where C_0, C_1, C_2 and b are constants depending on a determinant, on the hessian and other constants introduced by the user. J is the Jacobian and is defined below.

Once obtaining initial values of PV parameters values, we introduce them on the LM in order to optimize their values, as explained in the following subsection.

3.5.2 Levenberg Marquardt (Get of optimal PV parameters values)

The traditional *Levenberg-Marquardt* approach is a gradient order from Steepest-Descent (SD) in its first step and from Gauss-Newton (GN) in its second step [153]. It is mainly based on an optimization of the error between real data and data from the model through the following expression.

$$Ecart - Quad = \sum_{i=1}^{N} Error(i)^2 \tag{3.24}$$

Where N is the number of measured I-V data.

$$Error = I_{\mathrm{Re}al}(i) - I_{Model}(i) \tag{3.25}$$

The real and simulated data are denoted by I_{Real} and I_{Model}, respectively. While I_{Model} is the objective function given as Equation (2).

$$I_{Model}(i) = f(I, V, \theta) \tag{3.26}$$

Evaluate the objective function $f(\Theta)|_{\Theta = \Theta k}$.

Where Θ is considered as the PV parameters vector.

$$\theta = \{I_L, I_{ds}, n, R_s, R_{sh}\} \tag{3.27}$$

Calculus of Jacobian of *f(I,V,Θ)* for Θ_k, as the derivative calculation of I (Eq.2) with respect to parameters.

$$J = -\left[\frac{\partial f(\theta)}{\partial \theta}\right]_{\theta=\theta_k} \tag{3.28}$$

For (damping optimized) update Θ_k. The PV parameters to be found are updated at each iteration by the use of the expression bellow.

$$\theta_{k+1} = \theta_k - [\frac{J^{'} * \varepsilon}{J^{'} * J + \lambda_k * I}]_{\theta=\theta_k} \tag{3.29}$$

The dominant factor λ is considered as responsible parameters for switching from SD to GN in the LM process [154].

For this reason, it is important to get an optimal value of this damping factor by the use of another optimization-based method, our choice was for the recent swarm-based method called GWO, through the following idea.

$$Ecart - Quad(I, V, \theta, \lambda) \rightarrow Ecart - Quad(\lambda)\big|_{\theta=\theta_k} \tag{3.30}$$

In addition, it is mentioned that at each iteration of the LM process that the damping factor must be found and is considered as crucial factor for the convergence process of the algorithm. Therefore, its value must be optimized by the use of another approach such as the GWO approach.

3.5.3 Grey Wolf Optimizer (optimize of damping factor's value)

In this subsection, our focus is on the evolution of the function *f(I,V,Θ,λ)* indicated by *f(λ)* for Θ fixed at Θ_k, as regards with various varied values of the damping factor, at each iteration of the LM. As it is observed that at each iteration different local minimums values of *f(λ)* exist. So, for obtaining the global minimum of *f(λ),* which correspond to the best minimal value of the objective function *f(I,V,Θ),* we suggest using the swarm-based meta-heuristic GWO method.

3.5.4 LMGWO

The main steps of the used hybrid LMGWO method applied for the PV parameters obtaining values are presented in Figure 3.11, below.

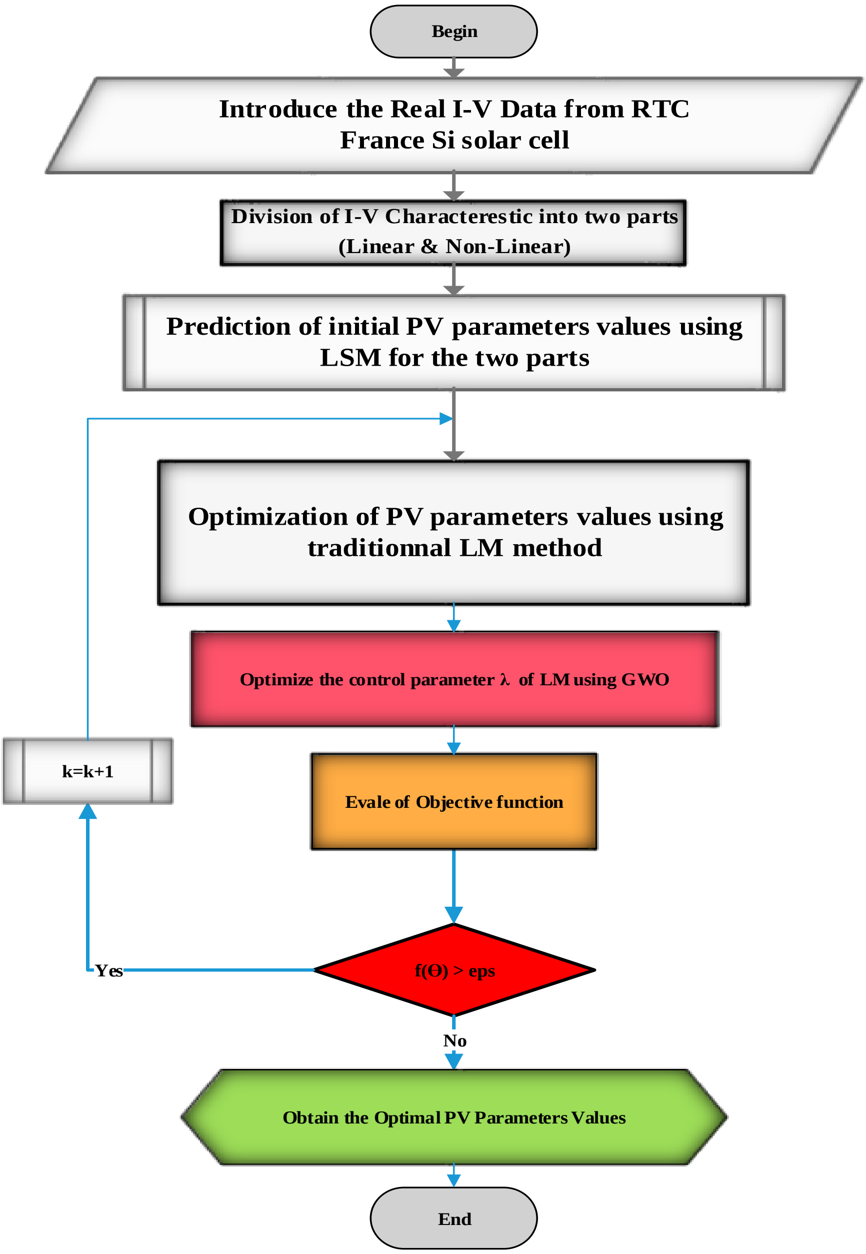

Figure 3.11 PV parameters identification steps using the hybrid LM approach with GWO approach.

The following Table 3 presents PV parameters results for the all classified optimization-based method discussed in section 2.

Table 3.4 Parameters extraction results for 57-mm diameter R.T.C. France commercial silicon solar cell using the single diode model.

Parameters/Methods	***I_L (A)***	***I_{ds}(μA)***	***n***	***R_s(Ω)***	***R_{sh}(Ω)***	***RMSE***
LM-GWO	0.760776	0.32306	1.48118	0.03637	53.7222	.8601E-04

The fitting obtained curves of real and simulated data are illustrated in Figure 3.12 bellow.

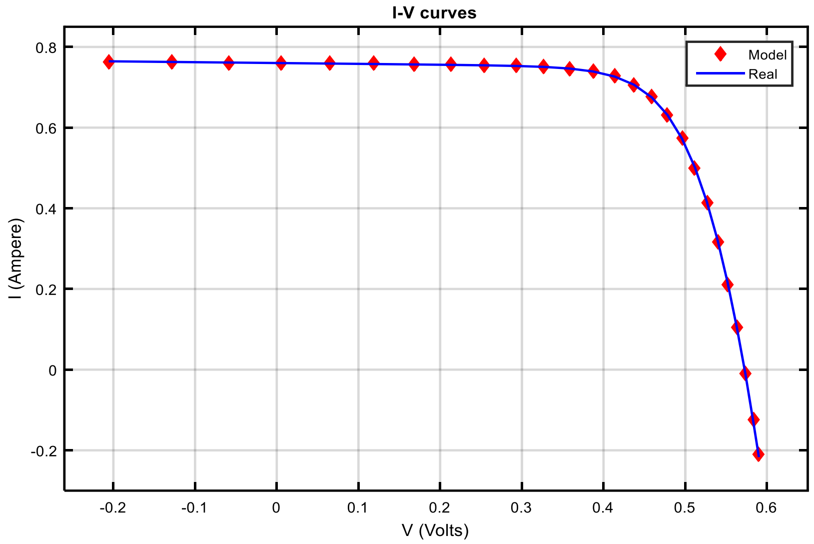

Figure 3.12 Fitted I-V curve characteristic for the RTC silicon solar cell, using the hybrid LM-GWO method.

The best approximation gotten from the fitted curves in Figure 3.12 has proved the effectiveness of our hybrid LMGWO method.

Conclusion

In this chapter, accurate parameters values of PV cells/panels are essential for researchers in the modelling and the development of good controlling techniques for Maximum Power Point Tracking based power electronic converters. This chapter has presented a comprehensive study of a new hybrid method developed for obtaining the electrical unknown parameters of solar PV cells. The final obtained results show that the used hybrid method outperforms the classical methods.

Part 2

Artificial Intelligence & Implementation

Chapter 4

Application of Neural-Networks to fault diagnosis of PVG

CHAPTER 4: Application of Neural-Networks to fault diagnosis of PVG

Introduction

Intelligence is too complex to be described by any single theory. Instead, researchers are constructing a hierarchy of theories that characterize it at multiple levels of abstraction and called it artificial intelligence (AI) [155]. At the lowest levels of this hierarchy, neural networks, genetic algorithms and other forms of emergent computation have enabled us to address the processes of adaptation, perception, embodiment, and interaction with the physical world that must underlie any form of intelligent activity. Since the appearance of artificial intelligence, researchers have been constantly competing with each other to invent new methods. Neural network computing is an intelligent information processing paradigm, inspired by the biological system, composed of a large number of highly interconnected processing elements (neurons) working in unison to solve specific problems. Indeed, the greatest advantage of ANN compared to other modelling approaches is their ability to model complex non-linear processes, without having to learn the form of the relationship between the input and output variables. In this chapter, a general description of neural networks and their application to PVG diagnosis will be presented.

4.1Biological neuron

The brain is made up of approximately 10^{12} (one trillion) interconnected neurons, with 1 000 to 10 000 synapses (connections) per neuron. The human brain consists of a large number; more than a billion neural cells that process information. Each cell works like a simple processor. The massive interaction between all cells and their parallel processing makes the brain's abilities possible. The structure of the neural cell is detailed as follow (Figure 4.1.a) [156]:

- **Dendrites** are branching fibres that extend from the cell body or soma.
- **Soma or cell body** of a neuron contains the nucleus and other structures, support the chemical production of neurotransmitters.
- **Axon** is a singular fibre carries information away from the soma to the synaptic sites of other neurons (dendrites and somas), muscles, or glands.

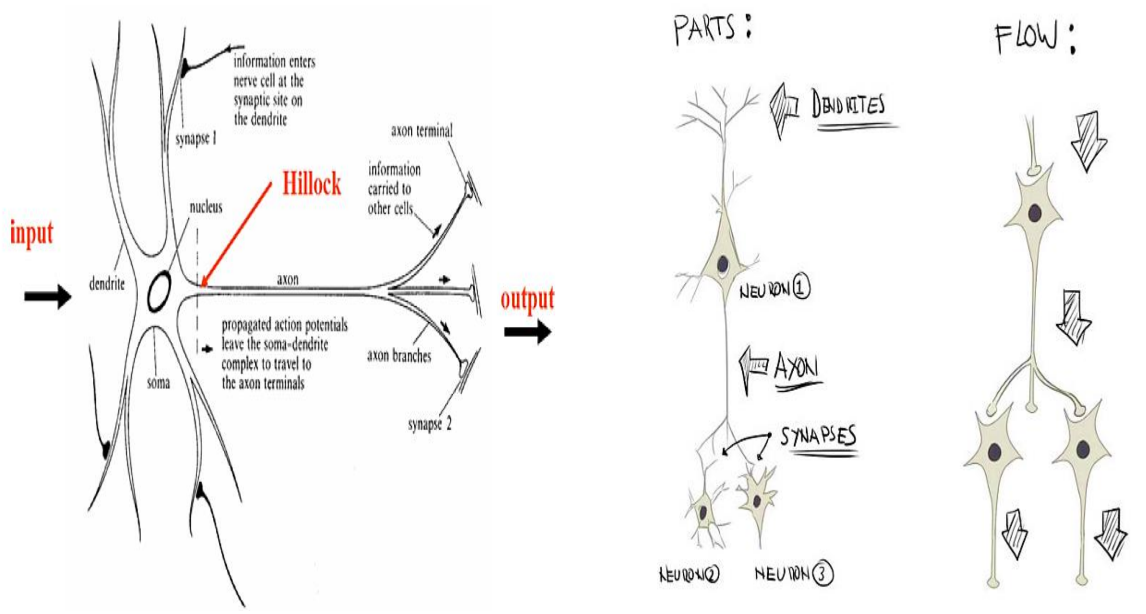

a) b)

Figure 4.1 a) Structure of biological neuron; b) Flow of information.

Each neuron is an autonomous unit within the brain. The neuron continuously receives inputs. The cell body of the neuron is the control centre. This is where the information received is interpreted. The unique response to these signals is sent through the axon (Figure 4.1.b). The axon synapses on other neurons (a thousand). The transmitted signal can have an excitatory or inhibitory effect. The nerve impulse is comparable to an electrical signal propagating like this:

- Dendrites receive nerve impulses from other neurons.
- The neuron evaluates all of the stimulation received.
- If it is sufficient, it is excited: it transmits a signal (0/1) along the axon.
- The excitement is propagated to the other neurons connected to it via the synapses.

4.2Artificial neuron

The three main regions of biological neuron: cell body, dendrites, and axon, are modelled mathematically to get the artificial neuron, Figure 4.2 [157].

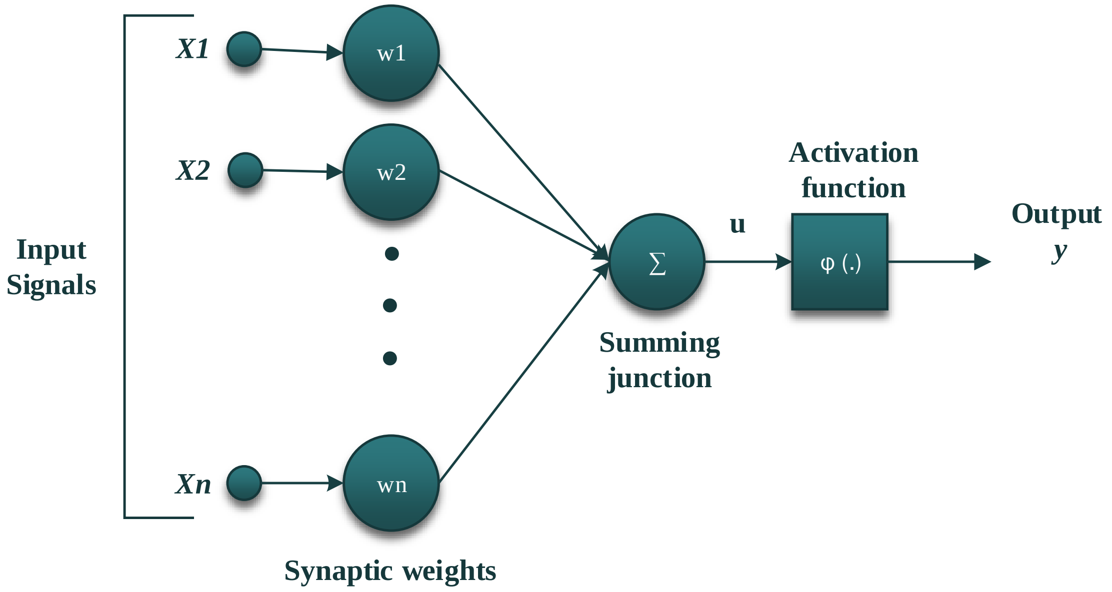

Figure 4.2 Basic components of an artificial neuron.

An artificial neuron is a mathematical function conceived as a simple model of a real (biological) neuron. The total synaptic input, *u*, to the neuron is given by the inner product of the input and weight vectors by the following formulas:

$$u = \sum_{i=1}^{I} w_i * x_i \tag{4.1}$$

Where the threshold of the activation is incorporated in the weight vector. The output activation *y* is given by.

$$y = \phi(u) \tag{4.2}$$

Where:

- *y*: is the output of the neuron.
- *u*: is the *i* input of the neuron, it characterizes the data communicated by the sensor (test of detection) or by the expert (diagnosis and base of facts and knowledge).
- ϕ: activation function.
- w_i: weight of connections with inputs.

4.3Artificial neural networks

An artificial neural network is an elementary processor, which receives a variable number of inputs from the upstream (afferent) neurons or pattern of input (Figure 4.3). Each weight is associated with a weight *w*, abbreviation of weight, representative of the strength (or weighting) of the connection. Each elementary processor has a unique output, which then branches out to supply a variable number of downstream (efferent) neurons or pattern of output, which is like the biological neuron [157].

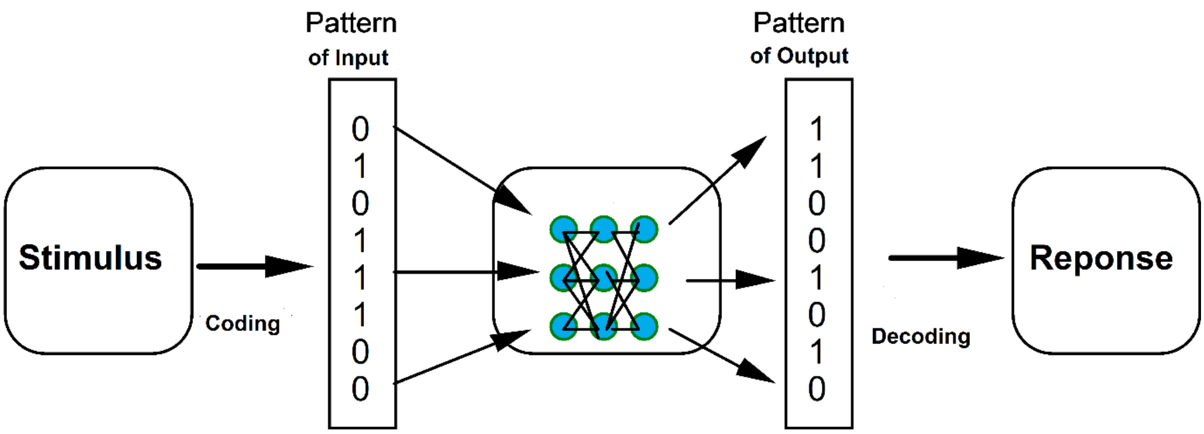

Figure 4.3 Basic structure of ANN.

An Artificial Neural Network (ANN) is often called a "Neural Network" or simply Neural Net (NN), which is an artificial representation of the human brain that tries to simulate its learning process. ANN is an adaptive system that changes its structure based on external or internal information that flows through the network.

4.4 Characteristics of NNs

A neural network can be fully described by specifying the following four elements:

- Architecture or topology of the network (number of hidden layers, number of neuron in the layers).
- Type of learning process.
- Processing element (activation function).

4.4.1 Learning and adaptation

Learning is the process by which the neural network acquires the ability to perform certain tasks by adjusting its internal parameters (synaptic weights) according to a specific learning pattern. At the end of this learning process, the network is likely to provide us with outputs as close as possible to the desired outputs. It also allows the network to dynamically modify its behaviour in order to meet new situations. The learning methods in neural networks are classified into three basic types (supervised, unsupervised, and reinforced learning), Figure 4.4.

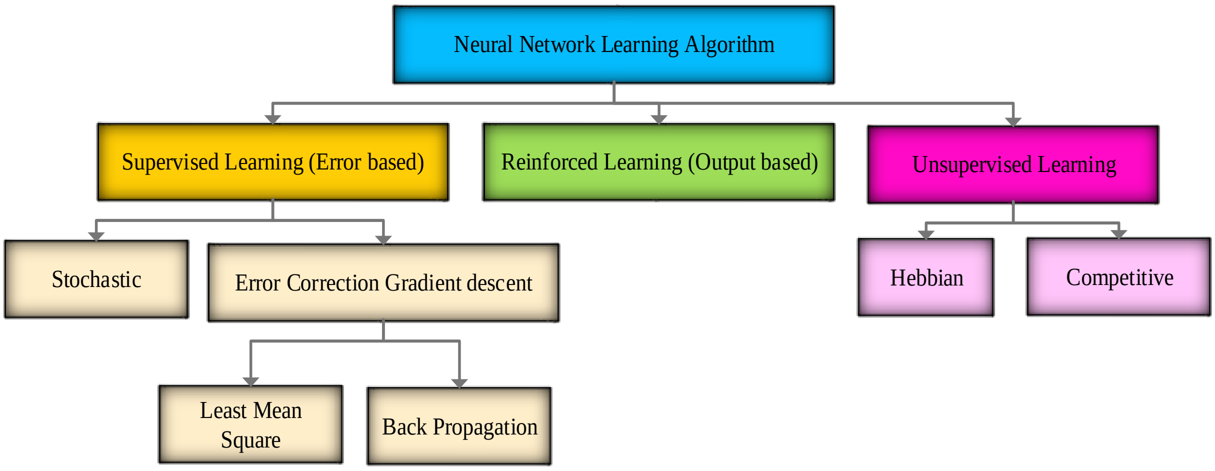

Figure 4.4 Classification of learning algorithms [159].

The learning phase is a decisive step in the design of the neural network. For this, appropriate algorithms have been developed, each of which is found to be specific to a specific type of network. There are several types of algorithms, the most frequently used are:

- Back-Propagation algorithm.
- Levenberg-Marquardt algorithm.

4.5 Some practical considerations for choosing the right neural network

Before the use of an artificial neural network, a certain number of parameters must be set, among others: dimensioning of the network, no learning, etc. this could risk generating and / or compromising the training process in the event of a bad choice. To configure a neural network, we must determine the following variables:

- Number of input neurons.
- Number of hidden layers and the number of hidden neurons.
- Number of training samples.

4.6 Types of NNs

The major types of NNs are summarized in Figure 4.5 [158], [159].

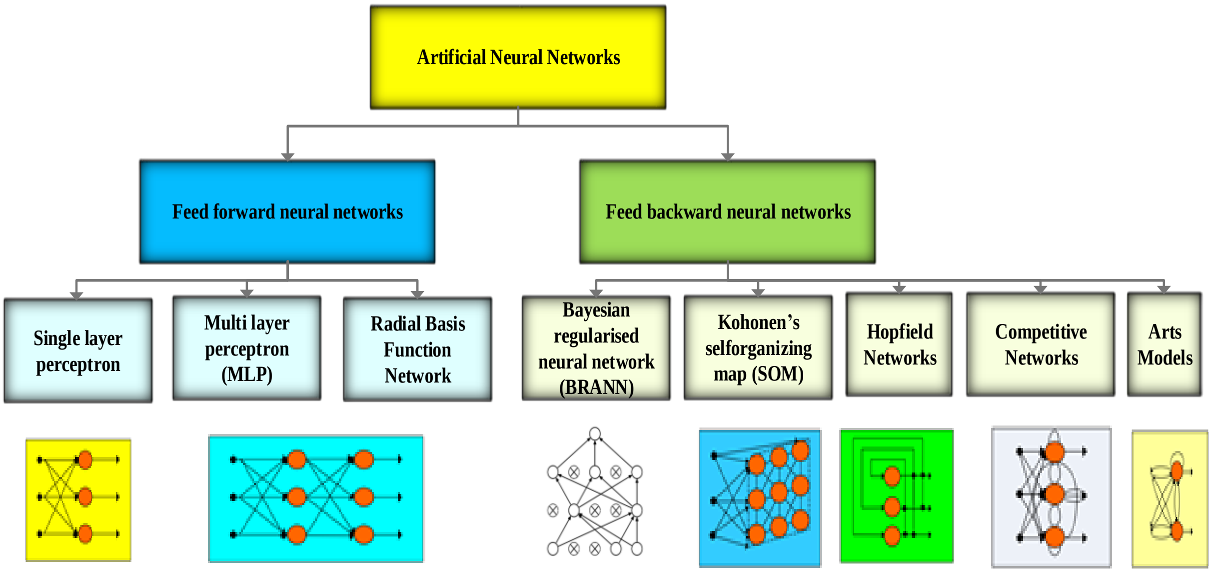

Figure 4.5 Types of NNs.

4.7 Application of neural network

Neural network applications are several, as can be cited in what follow [159]:

- Clustering.
- Classification/Pattern recognition.
- Function approximation.
- Identification.
- Control.
- Diagnosis.

4.8 Application of NNs for diagnosing PVG

In this section, a novel neural network-based method is developed for the detection of all short-circuit (SC) failures along the faulty PV string, using real data [160]. To achieve this, three major steps (injection of data, faults modelling, and decision) are elaborated. For the data injection step, measured data are used, namely, the PV panel's temperature, solar irradiance, voltage, and current at Maximum Power Point (MPP). The second step consists in modelling and fault detection, two Networks of Artificial Neural Networks (NANNs), named NANN1 and NANN2 are used to detect the faults from the injected data, and generate outputs (currents and voltages), which will be injected into two Probabilistic Neural Networks (PNNs), called PNN1 and PNN2. Therefore, the role of PNN1 and PNN2 will be to classify the current and voltage modelled values from the model based on the NANN1 and NANN2, respectively. It is mentioned that the PNN1 is a PNN used to classify the data related to current at its maximum value, into two classes (healthy and faulty), and the PNN2 will rank the voltage data at its maximum value into five classes. The third step deals with the online diagnosis of the PV system by combining the outputs from both PNNs and carrying out the final decision about the state of the PV system.

4.8.1 Modeling and diagnosis of PV faults

The proposed PV monitoring system is depicted in Figure 4.6. The overall block diagram shows the intelligent global monitoring and fault diagnosis structure for the PV system.

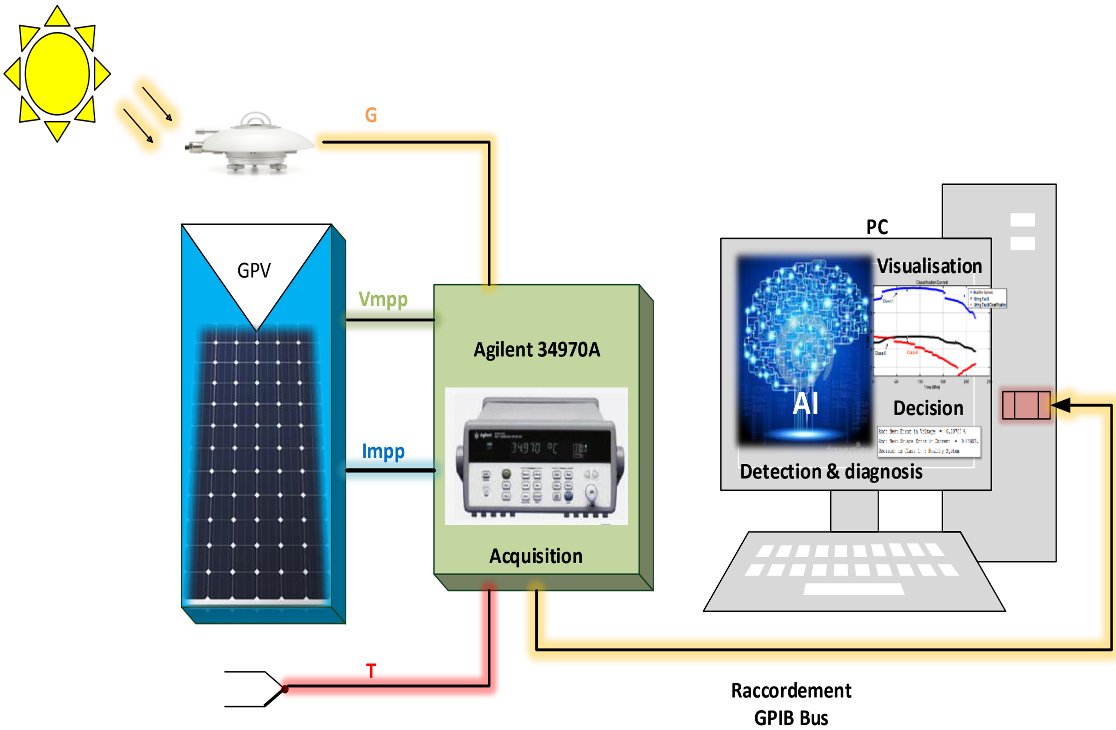

Figure 4.6 Global structure of the monitored PV system for fault detection and diagnosis.

The PV system under study is located at the Centre of Development of Renewable Energies (CDER) of Algiers, Algeria [161]. It is organized according to three sub-arrays where each subarray is connected to a single-phase inverter. Each sub-array consists of 30 PV Isofoton panels (106W-12V). Table 4.1 summarizes the specifications of the used Isofoton PV panel. The panels are arranged according to two parallel strings with 15 series-connected panels for each string. This PV plant is endowed with a monitoring system using an Agilent 34970A card* for data acquisition. A pyranometer* is used for measuring the solar irradiance (G) in the horizontal plane. For the temperature (T) measurements, a set of k-type thermocouples* is used. The measurements were carried out for 11 months in the year 2018.

Table 4.1 Specifications of Isofoton 106-12.

Parameters	Value
Maximum Power (P_{mpp})	106 W
Short-Circuit Current (I_{sc})	6.54 A
Open Circuit Voltage (V_{oc})	21.6 V
Coefficient of temperature at Isc (α)	0.060%/°C
Coefficient of temperature at Voc (β)	-0.36%/°C
Maximum Current (I_{mpp})	6.1 A
Maximum Voltage (V_{mpp})	17.4 V

In PV plants, faults usually occur from the electrical grid (instability of the grid), from the storage system, most widespread are from inverters and/or from the photovoltaic generator. This work deals with the generators' connections short-circuit failure types, which are common in PV systems. The names of these failures and their symbols are summarized in Table 4.2.

Table 4.2 Type of faults and their symbols in PVG.

Name of Faults	Symbols
Healthy model	C1
Fault detection due to voltage of one panel short-circuited	C2
Fault detection due to voltage of two panels short-circuited	C3
Fault detection due to voltage of four panels short-circuited	C4
Fault detection due to voltage of six panels short-circuited	C5
Fault detection due to current of string short-circuited	C6

To detect these faults, two operational modes are considered, the first mode refers to a healthy PV generator (Class1) while the second mode refers to the faulty PV generator (Class2-Class6). The fault diagnosis process for the above PV plant can be explained through two organigrams, as mentioned below:

- The first organigram (Figure 4.7): for exploitation of the developed method.
- The second organigram (Figure 4.8): for the developed method.

The exploitation process of the developed diagnosis method follows three main steps namely, data injection, faults modelling, and decision about fault classification, as depicted in Figure 4.7.

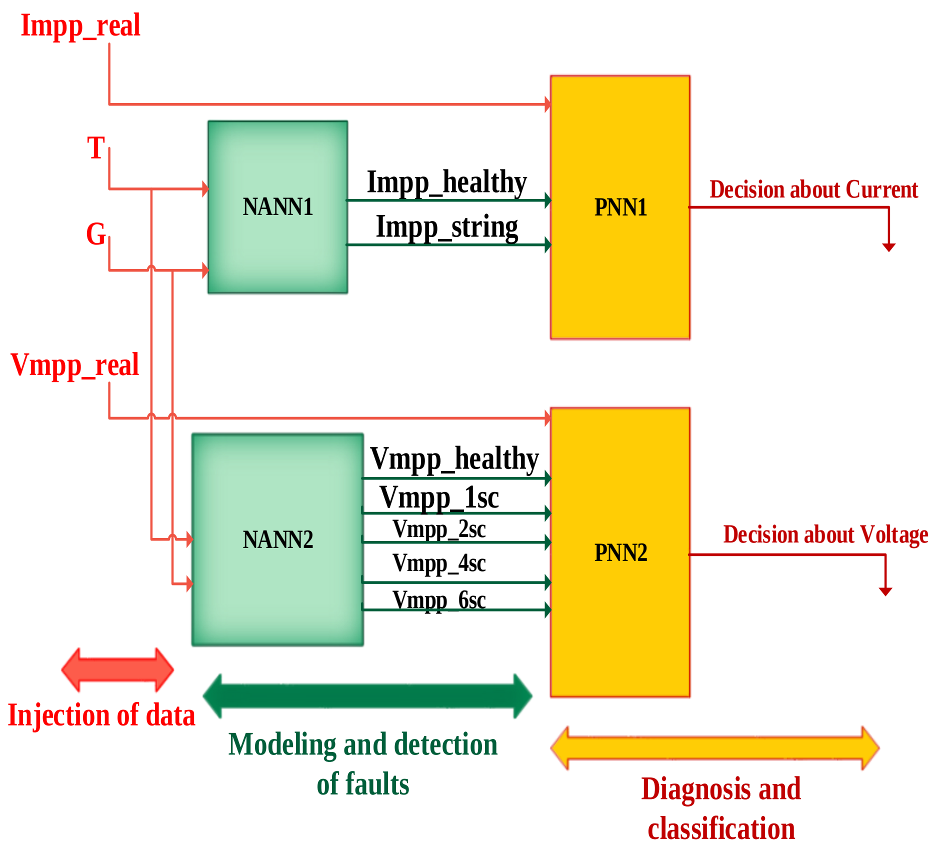

Figure 4.7 Exploitation process of diagnosis in the PV array.

In the modelling step, real data are feed into two networks of artificial neural networks, NANN1 and NANN2. Afterward, the diagnosis is carried out through failure classification using probabilistic neural networks (PNNs) from the NANNs outputs. The following subsections give more details about each step.

It can be seen from Figure 4.7, that the exploitation process is done through the major following steps:

- Collection of real meteorological data (G & T) with sensors, & their injection to NANNs.
- Production of classes from NANNs.
- Acquisition of real data from the PV array (I_{mpp} & V_{mpp}) & their injection to PNNs.
- Classification of the later measured data to their convenient classes by PNNs.
- Decision about the health state of the PV array.

The development process of the developed method given by the chart of Figure 4.8, describes in details the working principle of the PV diagnosis process.

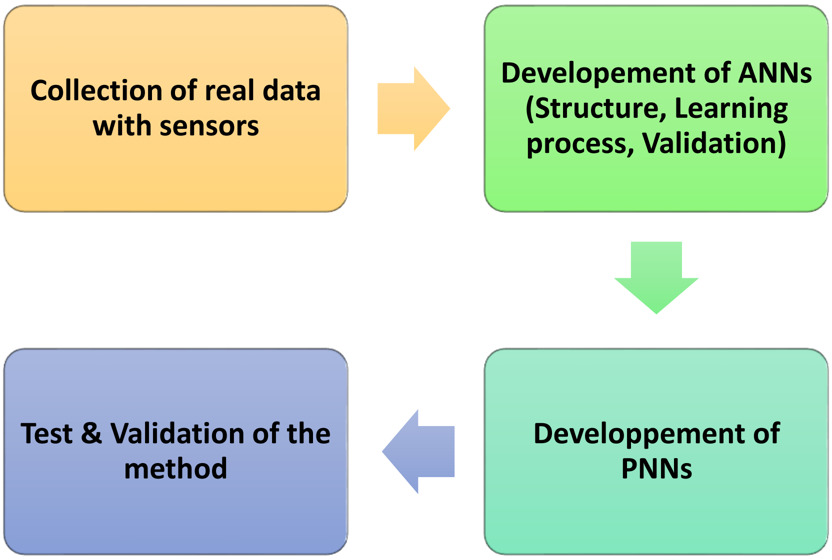

Figure 4.8 Global organigram of developing functioning of PV diagnosis process.

The following subsections provide additional details about PV diagnostic steps.

4.8.1.1 Injection of real data

In the first step, experimental data, namely, panel's temperature, solar irradiance, current and voltage at their maximum values (T, G, I_{mpp}, V_{mpp}) are feed to the created NANNs and PNNs for learning, the time variation of these parameters are summarized in Figure 4.9. The experimental setup of the PV plant, located at the Renewable Energies Development Centre (CDER) of Algiers, Algeria, is detailed at section 4.8.1 [160], [161]. The measurements were taken in March 2018 with a sampling period of one minute, which is equivalent to 220 data points for each parameter.

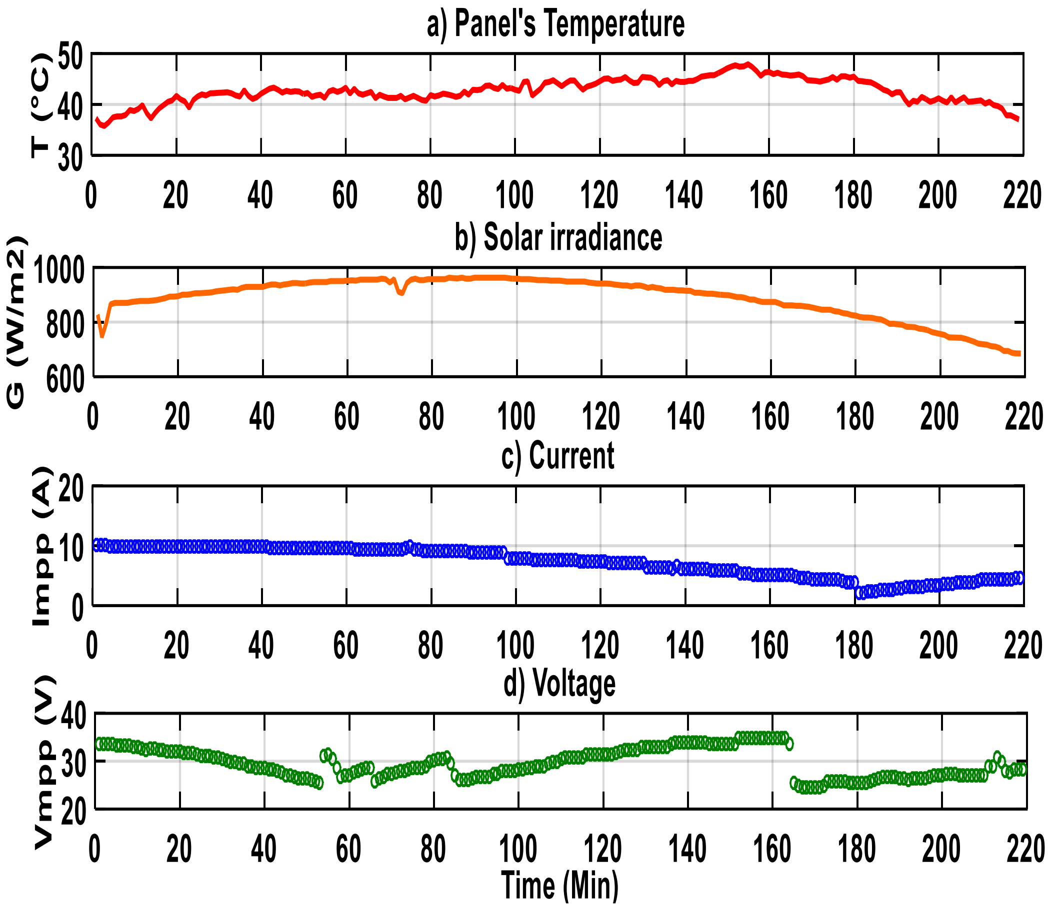

Figure 4.9 Real data of (a) Panel's temperature; (b) Solar irradiance; (c) Current; (d) Voltage.

For the meteorological data, it can be seen that the temperature varies between 36 and 48 °C while the irradiance reaches 1000 W/m^2. For the electrical parameters, the current varies in the range (6; 12 A), while the voltage varies in the range (20; 30 V).

4.8.1.2 Modelling and detection of faults using NANNs

The primary process of modelling, fault detection and classification is presented in Figure 4.10, and is described in detail in [163]. As illustrated in Figure 4.10, we used multiple neural networks (NNs) for the healthy operation and multiple-fault modelling. Therefore, every fault is modelled by a neural network. The output of every model is compared with the real (healthy or faulty) state, which will be classified using a probabilistic neural network.

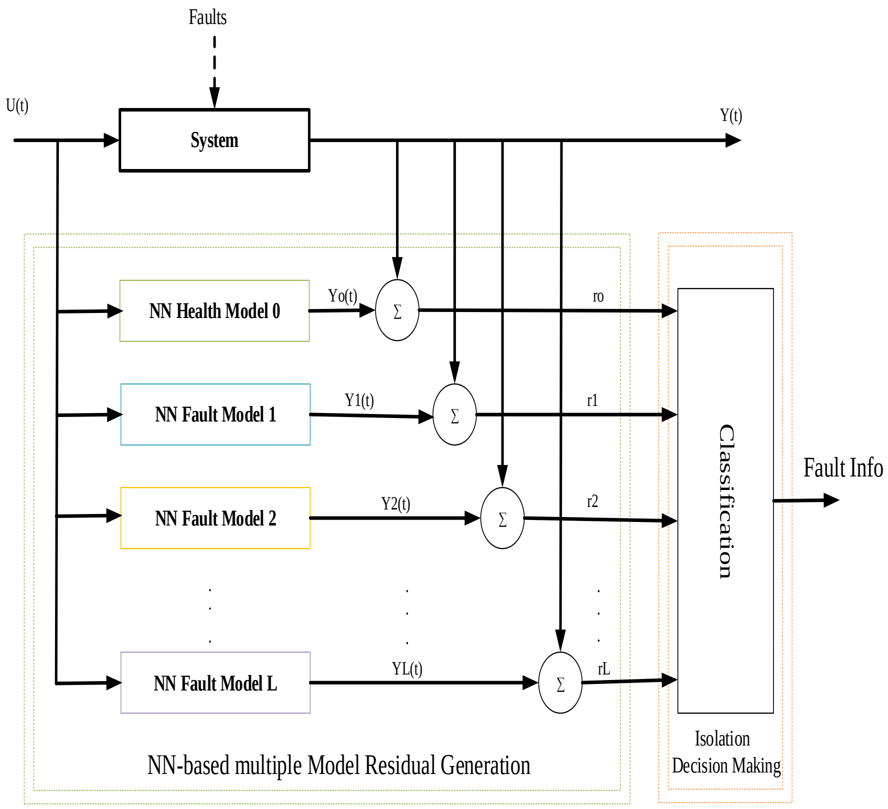

Figure 4.10 Ageneric neural network-based multiple-model fault detection and isolation scheme [163].

In this work, two networks of artificial neural networks (NANN1, NANN2) are used for modelling current and voltage at their maximum values (I_{mpp} and V_{mpp}). The followed approach consists of modelling a healthy mode and five defective modes. The first NANN is used to model current outputs while the second NANN is used to model voltage outputs under variable operating conditions as shown in Figure 4.11 and Figure 4.12.

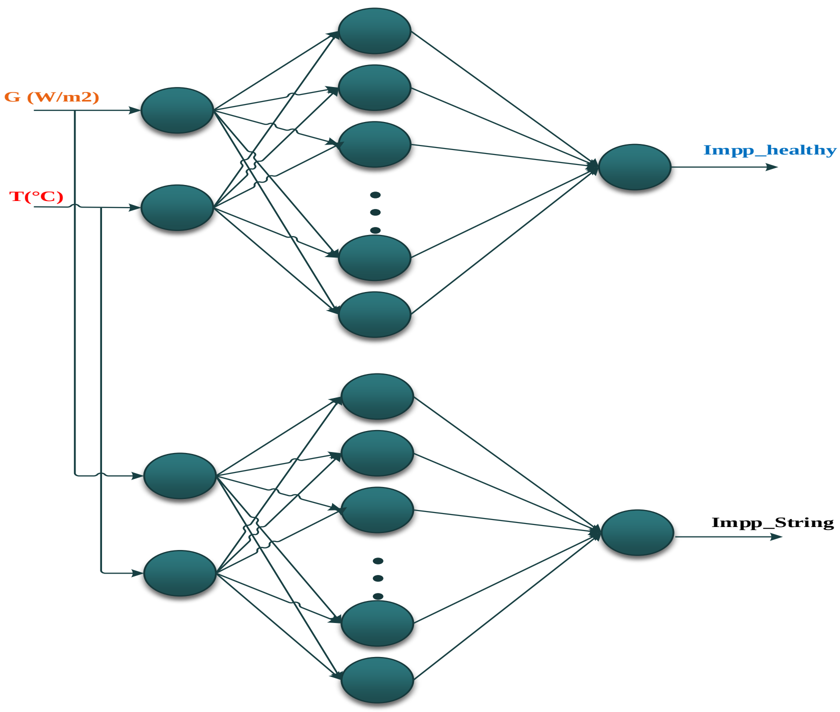

Figure 4.11 The current modelling structure by network of artificial neural network 1 (NANN1).

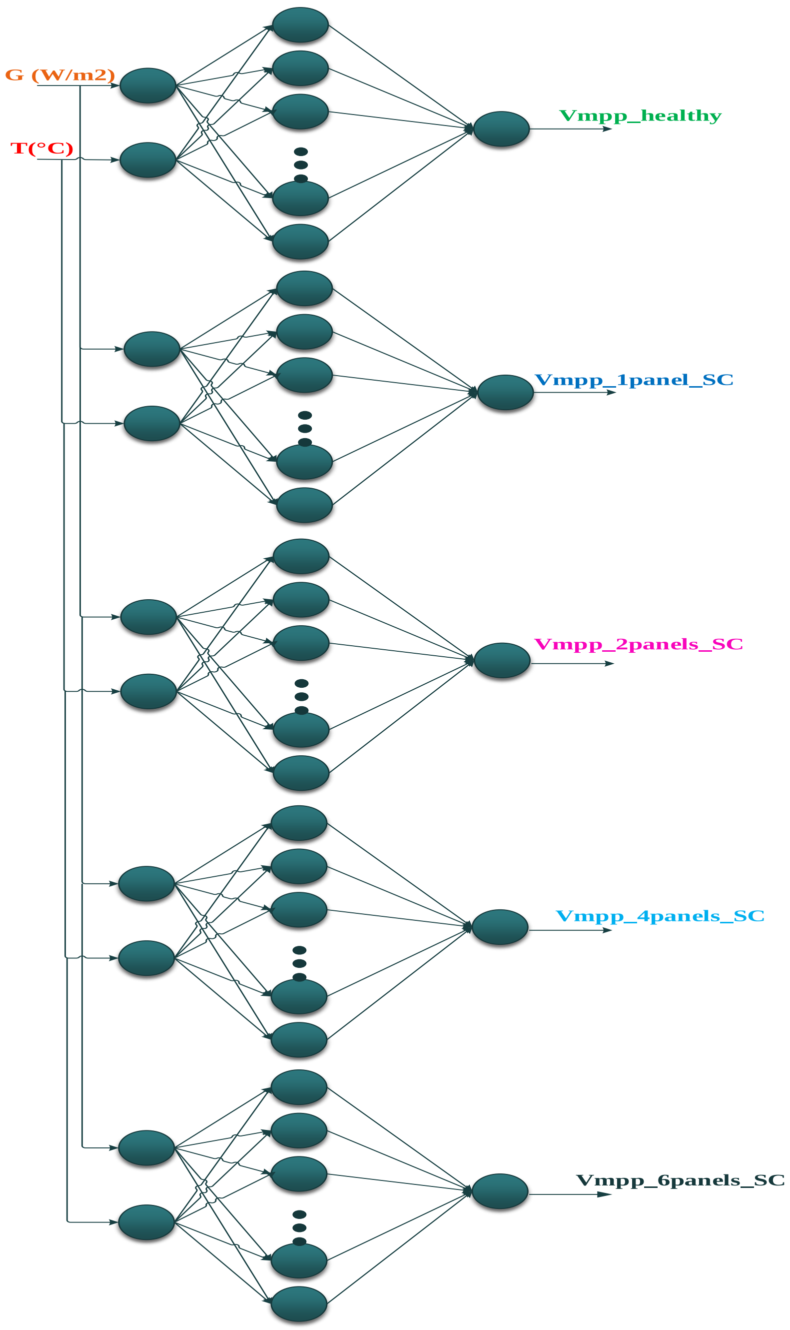

Figure 4.12 The voltage modelling structure by network of artificial neural network 2 (NANN2).

Each proposed NANN contains ANNs. Where each ANN contains three layers: the input layer, hidden layer, and output layer. While considering the injection of temperature and irradiance in the input layer for each mode and accommodate both current and voltage at the MPP at the output layer. The networks are trained by providing inputs and outputs to match the different models (healthy and faulty). More details on the elaboration of ANNs will be provided in section 4.10; the architectures of each NANNs are summarized in Table 4.3 and Table 4.4.

Table 4.3 Architecture of two ANNs developed in NANN1.

Numbers	ANNs of NANN1	Input layer	Hidden layer	Output layer
ANN1	Healthy current	2	40	1 ($I_{mpp\_healthy}$)
ANN2	Fault in current of string short-circuited	2	40	1 (I_{mpp_string})

Table 4.4 Architecture of five ANNs developed in NANN2.

Numbers	ANNs of NANN2	Input layer	Hidden layer	Output layer
ANN1	Healthy voltage model	2	40	1($V_{mpp\_healthy}$)
ANN2	Fault in voltage of one panel SC	2	40	1 (V_{mpp_1SC})
ANN3	Fault in voltage of two panels SC	2	40	1 (V_{mpp_2SC})
ANN4	Fault in voltage of four panels SC	2	40	1 (V_{mpp_4SC})
ANN5	Fault in voltage of six panels SC	2	40	1 (V_{mpp_6SC})

The NANN1 contains two ANNs, each ANN has two nodes in the input layer, one for temperature and one for the irradiance, the hidden layer contains 40 neurons, and the output layer contains one neuron to get current vector at the maximum power point (healthy and faulty mode, Figure 4.10). The NANN2 contains five ANNs, each ANN has two nodes in the input layer, one for temperature and one for the irradiance, the hidden layer contains 40 neurons, and the output layer contains one neuron to get voltage vector at the maximum power point (for healthy and the four faulty modes, Figure 4.11). Both healthy and defective modes were modelled by artificial neural networks, using temperature and irradiance data inputs as shown in Figure 4.10 and Figure 4.11. For each introduced data, the NANNs are developed to give seven outputs according to seven estimates states shown in Table 4.5 below.

Table 4.5 Type of parameters with symbols and classes.

Symbols	Parameters	Classes
I_{mpp_h}	Healthy current at the maximal power point	Class 1
V_{mpp_h}	Healthy voltage at the maximal power point	Class 1
V_{mpp1sc}	Voltage at maximum power point of 1 panel short-circuited	Class 2
V_{mpp2sc}	Voltage at maximum power point of 2 panels short-circuited	Class 3
V_{mpp4sc}	Voltage at maximum power point of 4 panels short-circuited	Class 4
V_{mpp6sc}	Voltage at maximum power point of 6 panels short-circuited	Class 5
I_{mpp_s}	Current at maximal power point of string fault	Class 6

- **Obtained classes from ANNs:**

The different classes for healthy and faulty operation are built using a Matlab/Simulink model for the PV array (Figure 4.13) [164]. The healthy case uses real data as inputs (temperature and irradiance) and determines the corresponding outputs ("healthy" current and "healthy" voltage). After that, we introduce the desired fault, one for the current with a string fault and four for the voltage with a different number of short-circuited panels, into this Simulink model [164]. With the same input data, we obtain the faulty outputs. Finally, all the results are recorded (one healthy and five faulty cases) and used as a dataset for learning the neural networks (NNs). Using the Matlab/Simulink model is preferable as it would be impossible to reproduce experimentally the same meteorological conditions for all healthy and faulty operation scenarios.

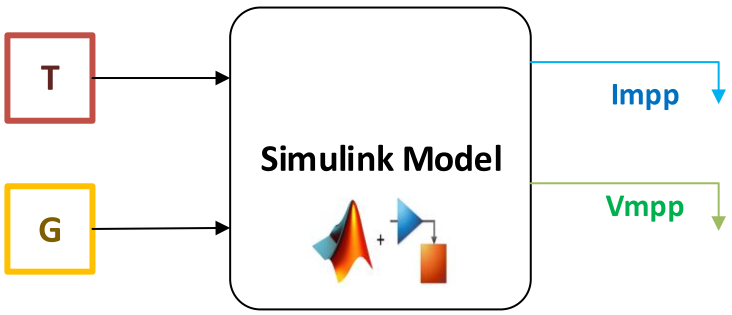

Figure 4.13 Classes obtained for the current/voltage modelled at MPP.

The classes obtained from the NANN1 are shown in Figure 4.12, the classed are described by two graphs that represent the values of two current modelled at the maximum power point with 220 data points, we see that two classes for the MPP current are obtained from the NANN1 described in Figure 4.14.

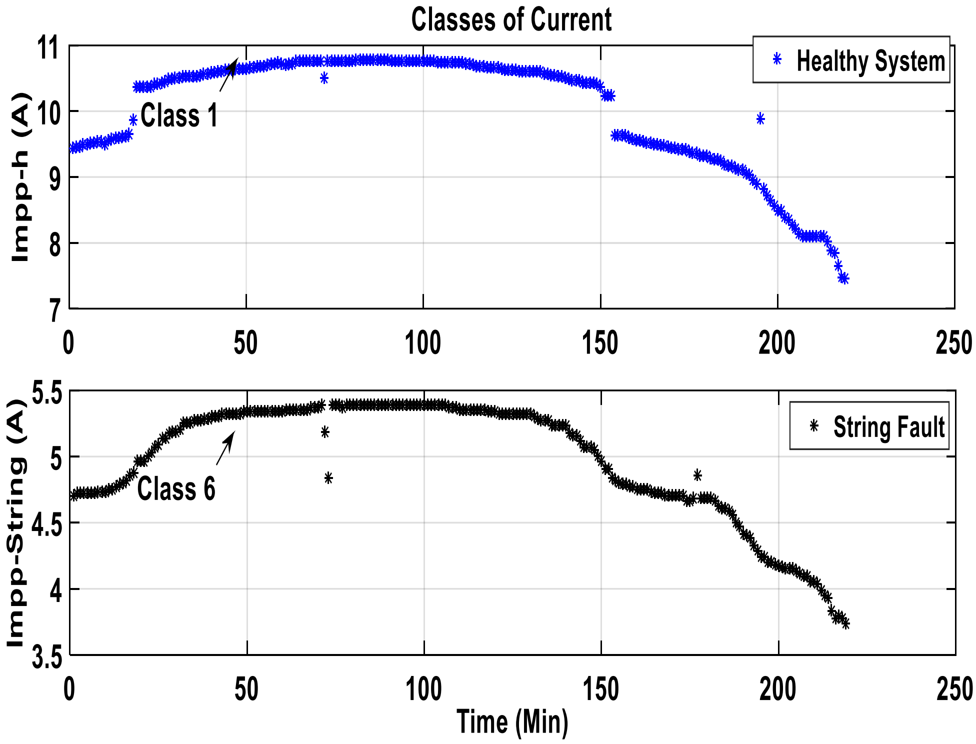

Figure 4.14 The classes obtained for current modelled at MPP.

- The first graph (in blue line) represents the Class1, which models the MPP current at the healthy state.

-The second graph (in black line) represents the Class6, which models the MPP current at a faulty state where a string is short-circuited.

Figure 4.15 gives the graphs that represent the values of the different voltages modelled at the MPP using the NANN2 described in Figure 4.12 with a period of 220 data points.

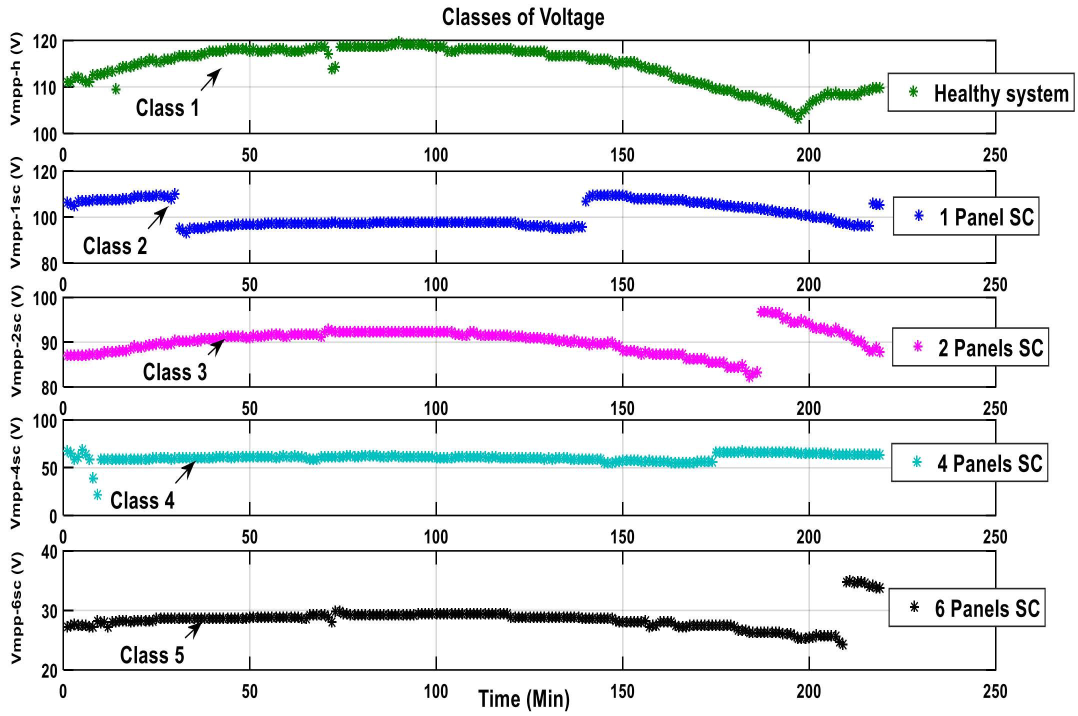

Figure 4.15 The classes obtained for voltage modelled at MPP.

- The first graph (in green line) represents the Class1, which stands for the healthy voltage model at MPP.
- The second graph (in blue line) represents the Class2, which stands for the faulty voltage model at MPP for one panel short-circuited.
- The third graph (in magenta line) represents the Class3, which stands for the faulty voltage model at MPP for two short-circuited panels.
- The fourth graph (in cyan line) represents the Class4, which stands for the faulty voltage model at MPP for four panels short-circuited.
- The fifth graph (in black line) represents the Class5, which stands for the faulty voltage at MPP where six panels are short-circuited.

Therefore, by combining the results from the two figures, the following fault models can be drawn.

- The healthy model (Figure 4.14 I_{mpph} with blue, V_{mpph} with green Figure 4.15).
- The string faulty model (Figure 4.14 I_{mpp_string} with black, V_{mpph} with green Figure 4.15).
- The faulty model 1 panel short-circuited (V_{mpp1sc} with blue Figure 4.15).

- The faulty model 2 panels short-circuited (V_{mpp2sc} with magenta Figure 4.15).
- The faulty model 4 panels short-circuited (V_{mpp4sc} with cyan Figure 4.15).
- The faulty model 6 panels short-circuited (V_{mpp6sc} with black Figure 4.15).

From this second step, six classes have been obtained as presented in Table 4.5.

4.8.1.3 Diagnosis online, classification and decision using PNNs

The third step is the diagnosis and decision step, it consists of injecting the outputs from the NANNs into two probabilistic neural networks, PNN1 and PNN2, the data to be injected is:

• The actual data from NANN1 (I_{mpp_h}, I_{mpp_string}) shown in Figure 4.15.

• The actual data from NANN2 (V_{mpp_h}, V_{mpp_1SC}, V_{mpp_2SC}, V_{mpp_4SC}, V_{mpp_6SC}) shown in Figure 4.16.

• The real data from the PV system to be monitored (I_{mpp}, V_{mpp}) shown in Figure 4.9.c and Figure 4.9.d.

The main role of these PNNs is to classify, in real-time, both the real measured currents and voltages compared with original models from NANN1 and NANN2. The fault detection algorithm compares the real measured data and the output modelled from the NANNs by using PNNs to determine the location of the fault. The analysis of the main attributes in characteristic I_{mpp} and V_{mpp} of each branch leads to the identification and isolation of failures. Along with the measured data under real conditions from the solar station. The PNN is a monitored neural network, which is widely used in pattern recognition; it has the potential in fault diagnosis for its distributed parallel processing, self-organization, and self-learning ability. The following characteristics distinguish PNN from the other networks in the learning process [165].

- A PNN is implemented using the probabilistic model, Bayesian classifiers.
- A PNN is guaranteed to converge to a Bayesian classifier when enough training data are provided.
- No learning process is required in PNNs.
- No need for initializing the weights of the PNN.
- There is no relationship between learning and recall process.

The PNNs receive nine data points at a time (Figure 4.7), three for the PNN1 and six for the PNN2. The PNN1 will classify the current data into two classes while the PNN2 will classify the voltage data into five classes. For each data vector, the PNN will work over a range of least 220 data points by using data in memory. The final decision will be taken by the last step as explained in the following Table 4.6.

Table 4.6 Diagnosis and decision about PV system.

I_{mpp}	V_{mpp}	**Decision about PV system**
I_{mpph}	V_{mpph}	2Healthy system
I_{mpph}	V_{mpp1sc}	Fault detection due to one panel short-circuited
I_{mpph}	V_{mpp2sc}	Fault detection due to two panels short-circuited
I_{mpph}	V_{mpp4sc}	Fault detection due to four panels short-circuited
I_{mpph}	V_{mpp6sc}	Fault detection due to six panels short-circuited
$I_{mppstring}$	V_{mpph}	Fault detection due to string

- **Obtained classification**

Two types of faults have been chosen to be classified, one at current and the other at voltage. In the first fault classification, the outputs from the PNN1 classification are illustrated in Figure 4.16 which shows the classification for fault at I_{mpp}. It shows that a fault in a string has a direct impact on the output current of the PV system.

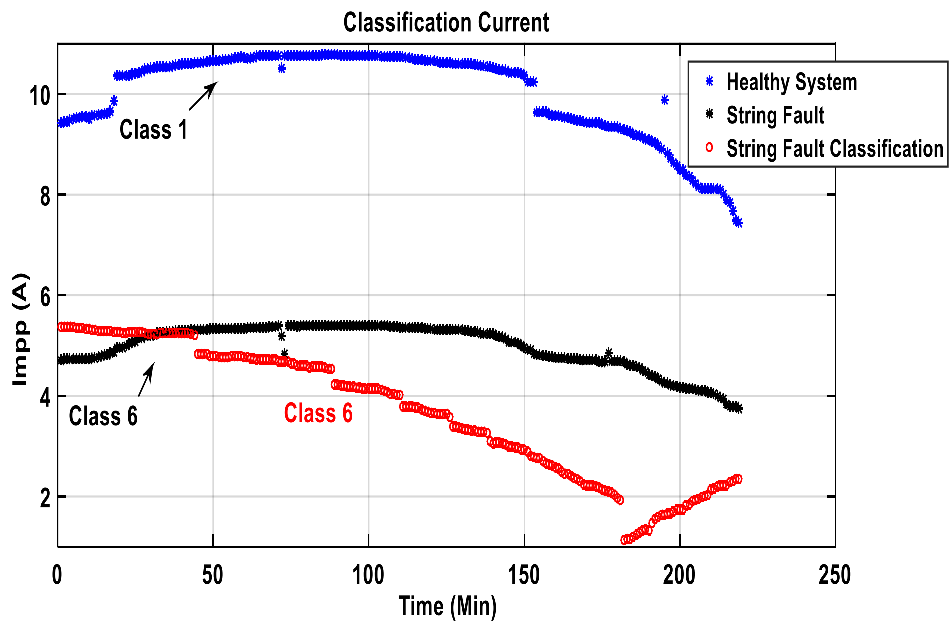

Figure 4.16 Classification of current fault at the maximum power point.

In the second fault classification, the outputs from the PNN2 classification are illustrated in Figure 4.16. It shows the classification for fault in V_{mpp}.

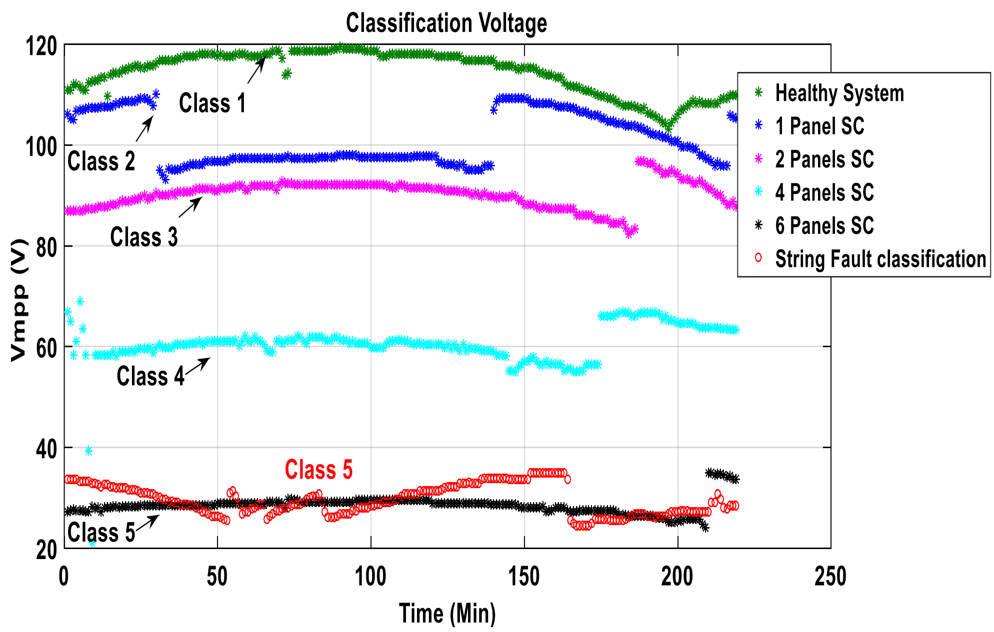

Figure 4.17 Classification of voltage faults at the maximum power point.

After removing Figure 4.6 and Figure 4.7, the PNNs classes the real data injected into them, as shown in Figure 4.9 and Figure 4.10. Where we noticed in Figure 4.9 a new graph presented with red colour, which represents the new classified current at MPP with Class6. Besides, in

Figure 4.10 we notice a new graph presented in red colour that represents the new classified voltage at MPP with Class5.

In this third stage of diagnosis, there is a routine that collects decisions from both PNNs following Table 4.6 and thus calculates the Probability Density Function (PDF) [166].

Unlike Multi-Layer Perceptron (MLP) networks, radial basis (RBF) functions (including PNNs) use radial functions instead of sigmoidal activation functions to build a local decision function centred at a subset of the input space [167]. The global decision function is the sum of all local functions [165], [168].

In the context of pattern classification, every observed vector *x* (*x* is a d-dimensional vector) is placed inside one the predefined cluster classes:

$$C_i, i = 1, 2, ..., m \ ;$$

Where *m* is the number of possible classes that *x* can belong to (six in this study).

The efficiency of the classifier is limited by the length of the input vector *x* and the number of possible classes *m*.

The Bayes classifier uses the *Bayes* conditional probability rule that is the probability $P(C_i/x)$ for *x* to belong to a class C_i.

This probability is given by:

$$P(C_i/x) = \frac{P(x/C_i)P(C_i)}{\sum_{j=1}^{m} P(x/C_j)P(C_j)} \tag{4.3}$$

Where:

- $P(C_i/x)$ is the conditional probability density function of *x* given C_i.
- $P(C_j)$ is the probability of choosing a sample from the class C_j.

An input vector *x* is classified to belong to the class C_i if:

$$P(C_i/x) > P(C_j/x) : \forall j = 1, 2, ..., m; \ j \neq i \tag{4.4}$$

The estimation process of the later probabilities from a learning set uses *Parzen's* windowing technique to determine the PDF. Therefore, the estimator used for the PNN networks, $f_A(x)$, is given by:

$$f_A(x) = \frac{1}{2\pi^{P/2}\sigma^P}\frac{1}{m}\sum_{i=1}^{m}\exp\left[-\frac{(x-x_{ai})'-(x-x_{ai})}{2\sigma^2}\right] \tag{4.5}$$

Where x_{ai} represents the i^{th} sample belonging to the class C_A and σ is a smoothing parameter.

When the diagnosis algorithm is executed, it will display the errors and gives the decision about the state of the system, as shown in Figure 4.18.

```
Root Mean Error in Voltage  =  0.20787 %
Root Mean Square Error in Current  =  0.06657.
Decision is Class 1  : Healthy System
```

Figure 4.18 Snapshot of the classification result and estimation errors about the PV system.

All of the above three steps (data injection, faults modelling, and decision about diagnosis) should be reiterated at each classification.

4.9 Details about elaboration of NANNs for PV diagnosis

This section presents more details for modeling the ANNs used in NANNs. The approach given may work well for a whole life cycle of the system but requires a substantive prior work, which includes:

- The collection of real measured data (T, G, I_{mpp}, V_{mpp}), reserved for learning and validation of NANNs.

- The choice of the type of ANNs (Multi-layer Perceptron (MLP)) and their architectures.

- The choice of the learning type (Supervised learning).

- The validation of NANNs.

- The exploitation of the results.

In what follows, more details about each of these steps are provided.

4.9.1 Collect of real measured data

The data from the Station at the CDER including panel' temperature, solar irradiance, current, and voltage are collected on 20 March 2018, for a period about 460 data points as presented in Figure 4.19.

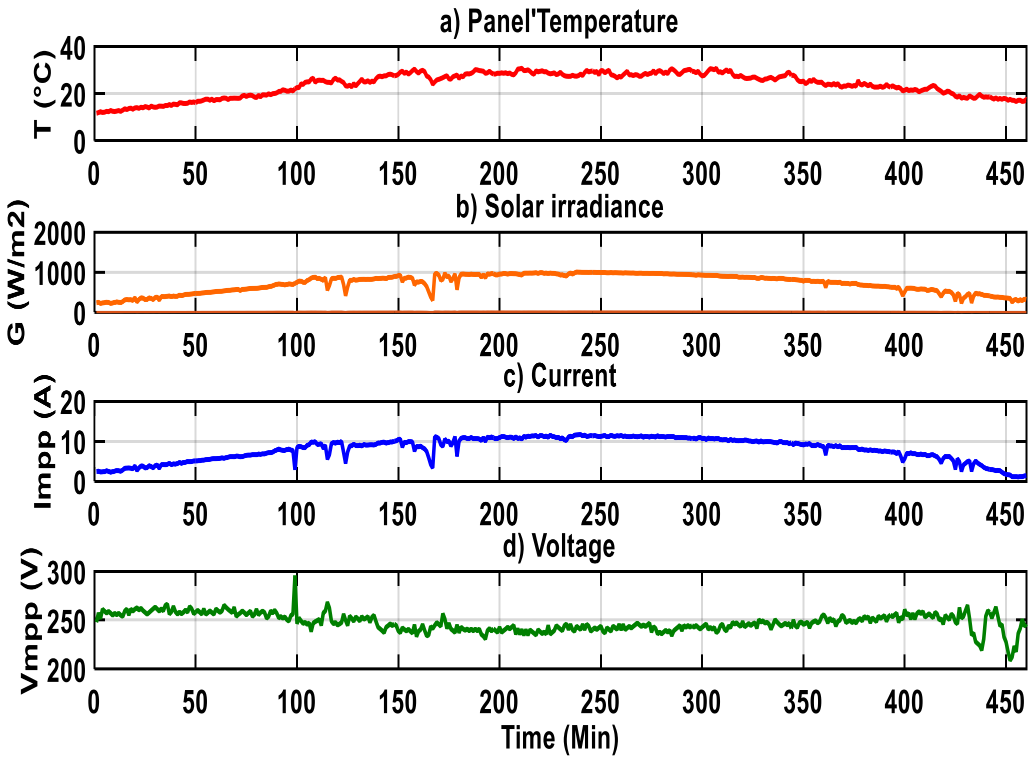

Figure 4.19 Collected meteorological and electrical data for 460 data points.

4.9.2 Choice of type of ANNs and their architectures

The developed ANNs are based on a Multi-Layer Perceptron (MLP). To find the optimal network architecture, several simulations were carried out, varying the number of hidden layers and the number of neurons in each hidden layer. Table 4.3 and Table 4.4 summarize the obtained architectures of each ANN.

4.9.3 Choice of learning type

From the 460 introduced data points of Figure 4.13, only 220 points are used for learning the NANNs. The type of learning used in this paper is called the "supervised learning" in which the network is formed by providing the input and output to match the model. During the learning process, the network is likely to produce outputs that are as close as possible to the desired real outputs. The weights of the network are adjusted progressively based on the error signal, which represents the difference between the real output and the model output, this adjustment is done by using an appropriate algorithm called the learning algorithm. The following Figure 4.19 presents the process of supervising the ANNs.

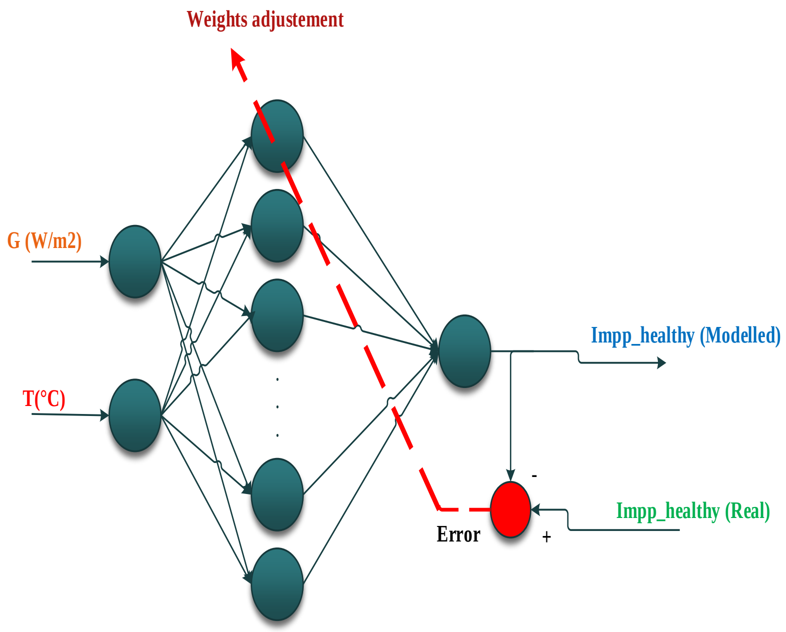

Figure 4.20 Process of supervising and weight adjustments in ANN1 for a healthy system.

The inputs to the ANNs are the temperature, irradiance while the outputs are I_{mpp} (supervised following real healthy and real faulty) and V_{mpp} (supervised following real healthy and reals faulty). Besides, faults are introduced in the real PV system to obtain real current and voltage data for each faulty mode. These real electrical data are matched using ANNs to generate their modelled electrical outputs. In Figure 4.21 and Figure 4.22, the data provided for ANN1 of NANN1 and ANN1 of NANN2 are presented.

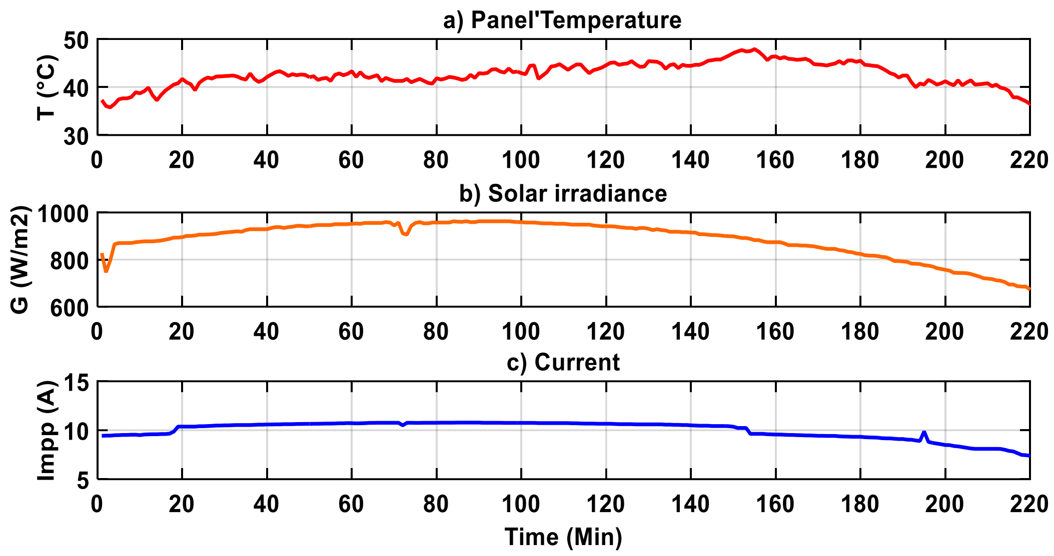

Figure 4.21 Data provided to the ANN1 of NANN1 in a healthy system for the current learning process.

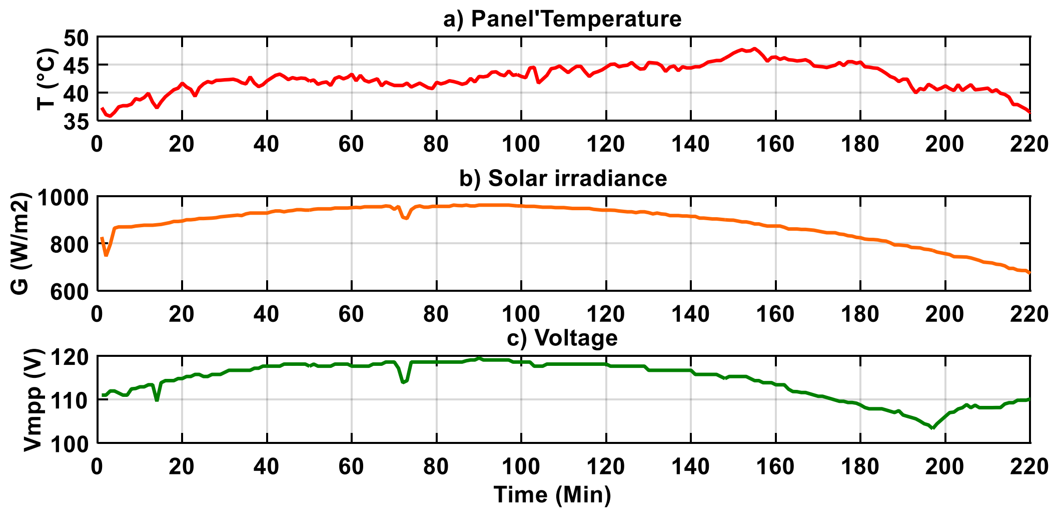

Figure 4.22 Data provided to the ANN1 of NANN2 in a healthy system for the voltage learning process.

The weights adjustment is achieved using the *Levenberg-Marquardt* (LM) [154] backpropagation algorithm using Matlab 2015a Software environment. Results after learning from a healthy ANN are summarized in Figure 4.23 bellow, which shows good training performance.

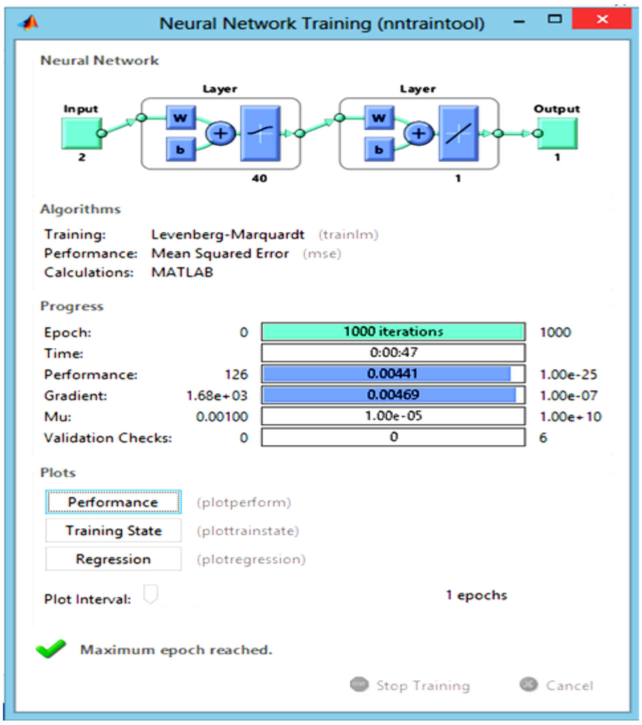

Figure 4.23 Generated toolbox interface for the developed NNs training on Matlab.

The appropriate neural structure is characterized by the transfer function a hyperbolic tangent in the first hidden layer (for ANNS) and a linear transfer function in the second hidden layer (for PNNs).

Regression of complex training process of NNs based controllers is shown in the following Figure 4.24.

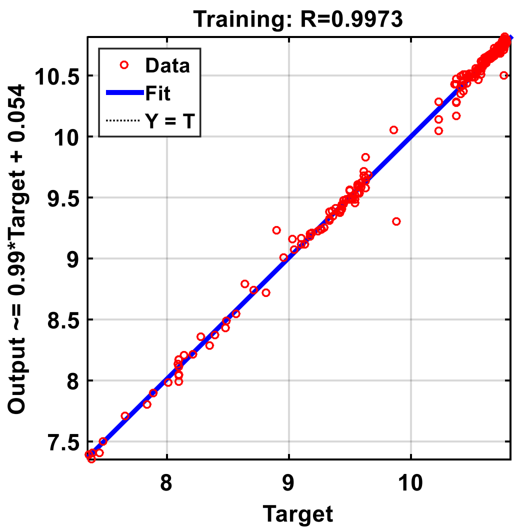

Figure 4.24 Generated regression of training process.

Figure 4.22 illustrates that the major points of scatter (Target output) are regrouped around the right (Y=T), which demonstrates the good efficiency of the approach.

Figure 4.22 and 4.23 clearly show that the weights of the network are well adjusted and the model could reproduce the output data with good accuracy.

4.9.4 Validation of ANNs

The remaining data points out of 460 from Figure 4.18 are used for validation. In what follow, some cases for healthy and faulty scenarios are presented.

4.9.4.1 Healthy system validation

a) Validation of model from ANN1 of NANN1 (I_{mpp} of healthy system):

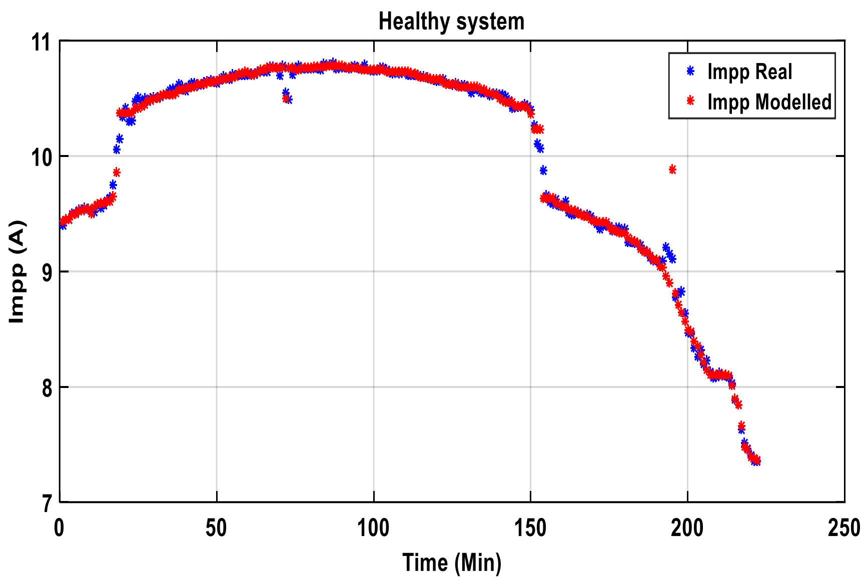

Figure 4.25 Real vs modeled data from current, I_{mpp} in a healthy system.

The following Figure 4.26 shows the error between real and modelled currents data. Error is given by the following equation:

$$Error = I_{MPP,Real} - I_{MPP,Model} \tag{4.6}$$

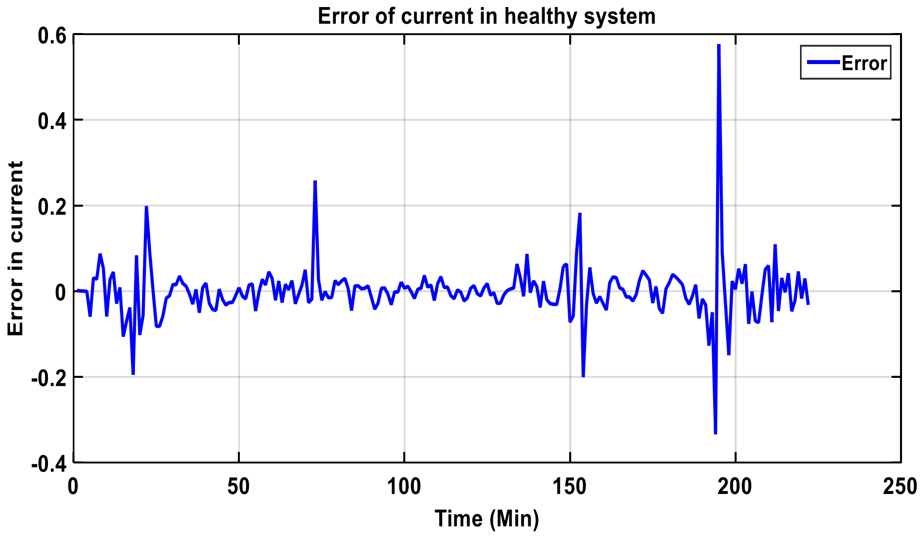

Figure 4.26 Error between I_{mpp_Real} and $I_{mpp\_modelled}$.

b) Validation of model from ANN1 of NANN2 (V_{mpp} of healthy system)

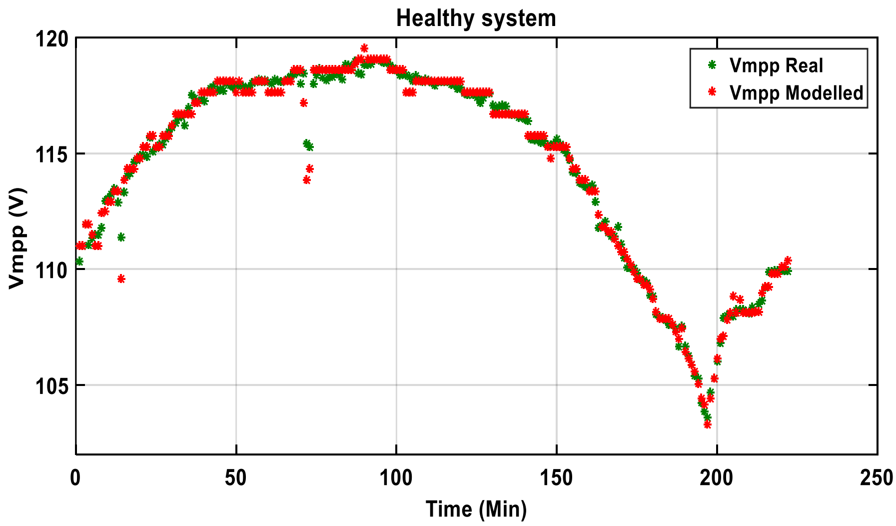

Figure 4.27 Real and modelled data from voltage, V_{mpp} in a healthy system.

Modeling by ANNs as shown in results of Figure 4.25 and Figure 4.27 involved how a high fitting comparison between the real data (current and voltage), and the ones estimated by the modeled ANNs in a healthy system.

The error between real and modelled voltage data for a healthy system is depicted in Figure 4.28 bellow.

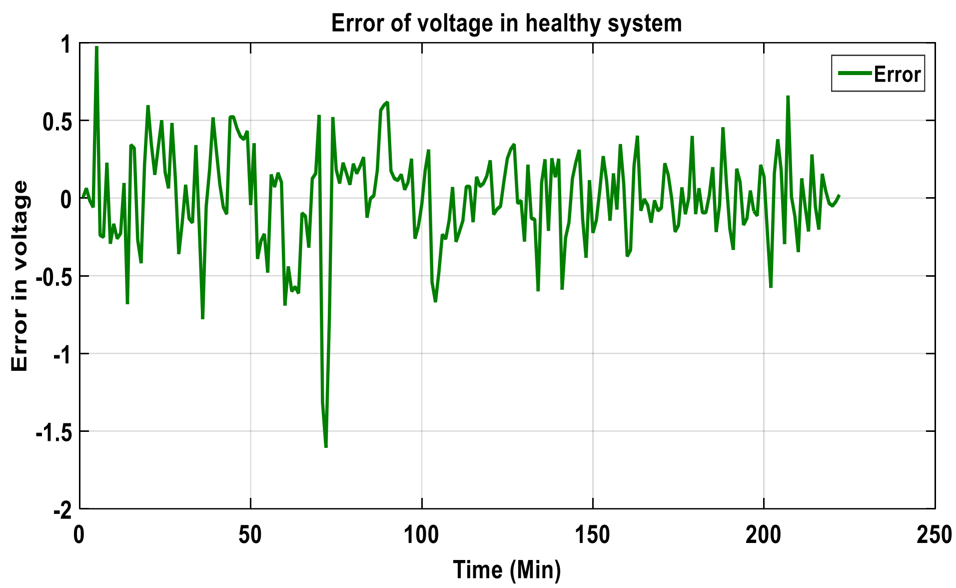

Figure 4.28 Error between V_{mpp_Real} and $V_{mpp\_modelled}$.

It can be seen from errors of Figure 4.26 and Figure 4.28 that there is a good agreement between modelled and real data, which indicates the good performance of the developed NANN1-model and NANN2-model. Therefore, the network weights and bias of the network are well adjusted and the model is able to reproduce the output data with good accuracy.

4.9.4.2 Faulty system validation

a) Validation of model from ANN2 of NANN1 (I_{mpp} faulty string)

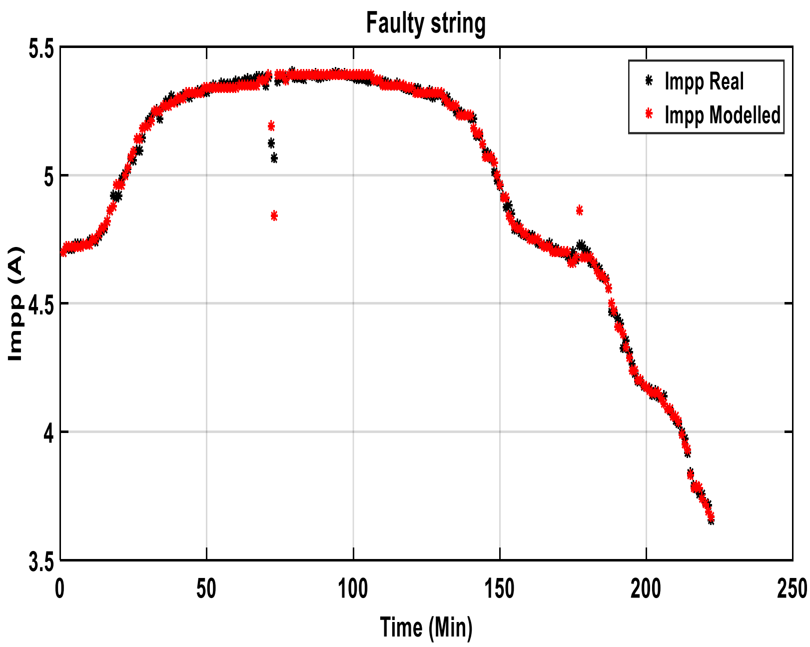

Figure 4.29 Real and modelled data from current, I_{mpp} in a faulty string system.

b) Validation of model from ANN2 of NANN2 (V_{mpp} of one panel short circuited)

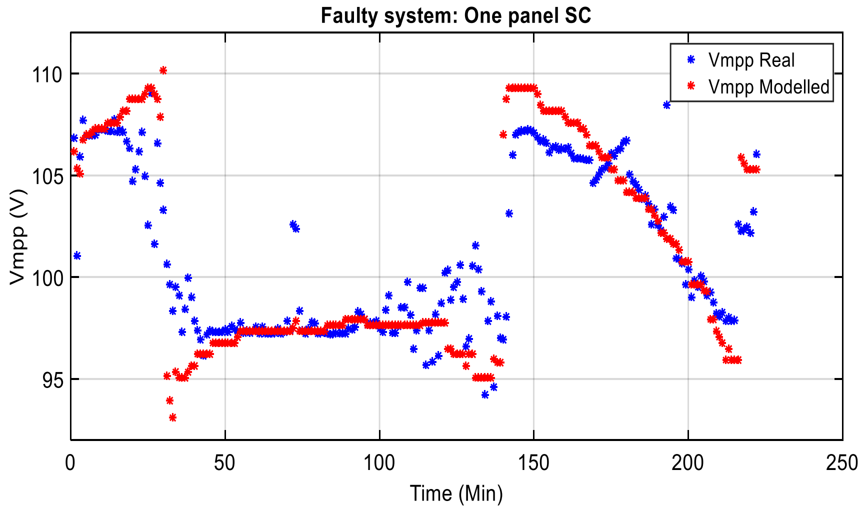

Figure 4.30 Real and modelled data from voltage, V_{mpp} in a faulty system (1 Panel SC).

4.9.5 Exploitation of results:

The diagnosis step of the PV system, using the classification method, consists of using the root mean square error (RMSE) and the mean relative error (MRE) methods in order to display the state about the PV system. For example, for a faulty PV system, Figure 4.31 and Figure 4.32 show the state of faulty current and voltage respectively.

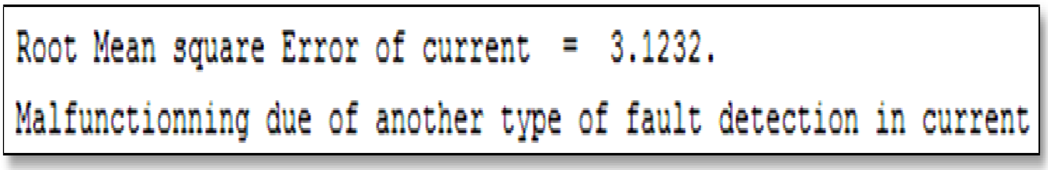

Root Mean square Error of current = 3.1232.

Malfunctionning due of another type of fault detection in current

Figure 4.31 RMSE command window results for a fault at current.

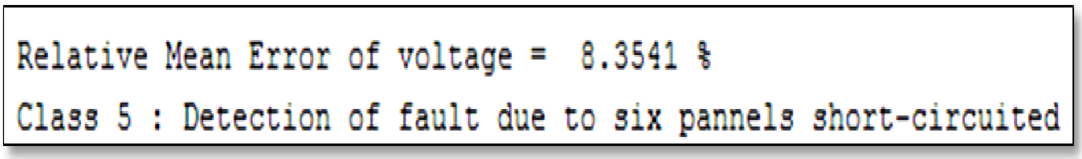

Relative Mean Error of voltage = 8.3541 %

Class 5 : Detection of fault due to six pannels short-circuited

Figure 4.32 MRE command window results for fault at six panels SC.

The expression of Root Mean Squared Error (RMSE) can be written as:

$$RMSE = \sqrt{\frac{1}{N} \times \sum_{i=1}^{n} \left(Data_{Real} - Data_{Model}\right)^2} \tag{4.7}$$

Where:

- N: number of data points.

The equation of the Relative Mean Error (MRE) is expressed as follow:

$$MRE = \left(\frac{1}{N} \sum_{i=1}^{N} \frac{\left| Data_{Real} - Data_{Model} \right|}{Data_{Mean}} \right) \times 100 \tag{4.8}$$

Where:

- $Data_{Mean}$: Mean of real data points.

The relative mean error has no unit; it tells us the quality (accuracy) of the results voltage obtained. It is usually expressed in percentage (%).

More results values of obtained errors (RMSE, MRE) for each class of the real PV system are presented in Table 4.7 bellow.

Table 4.7 RMSE (Root Mean Square Error) and MRE (Mean Relative Error (%)).

	Current Healthy System	**Current String Fault**	**Voltage Healthy System**	**Voltage 1 Panel SC**	**Voltage 2 Panels SC**	**Voltage 4 Panels SC**	**Voltage 6 Panels SC**
RMSE	0.5737	0.8264	2.4928	2.4493	1.1601	1.7280	**0.8201**
MRE (%)	**3.21**	**1.62**	**1.78**	**1.02**	**1.51**	**1.54**	**1.67**

4.10 Test of robustness

The robustness of the ANNs based fault diagnosis method is assessed by introducing noises in the PV system and showing the effect of injected data. Moreover, noise can be perceived as an error, a statistical uncertainty or an undesired random disturbance of a useful modeled response of the PV system. Several different effects can cause such noise such as thermal noise, device type, or manufacturing quality.

4.10.1 Presence of noise from inverter

In this subsection, the PV system is related to the grid through an inverter, this leads to noises on the current and the voltage at the level of the vector to be classified. Figure 4.33 and Figure 4.34 show the classification of the overall system (current and voltage) along with the results from the faulty string model in the presence of noise from the inverter.

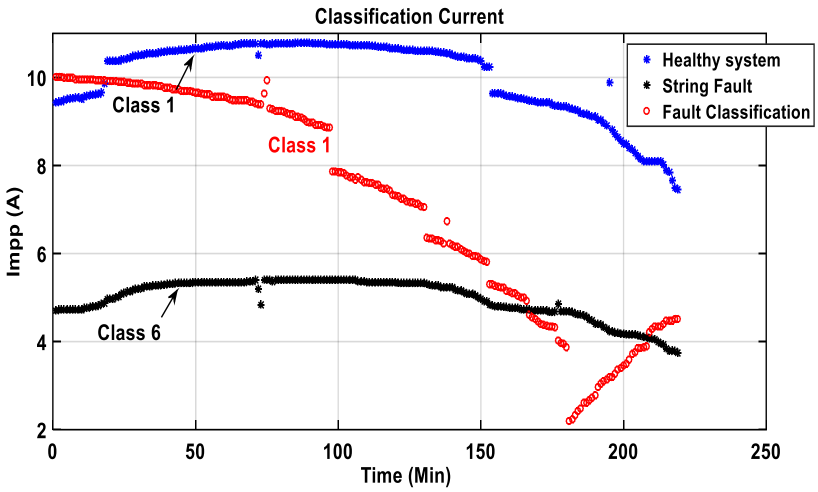

Figure 4.33 Classification of current at maximum power point in the presence of noise from the inverter.

Figure 4.33 illustrates that the classification of current (in red) is closer to the healthy current (in blue) than the defective current (in black). The most important data belong to class 1 (for a healthy system).

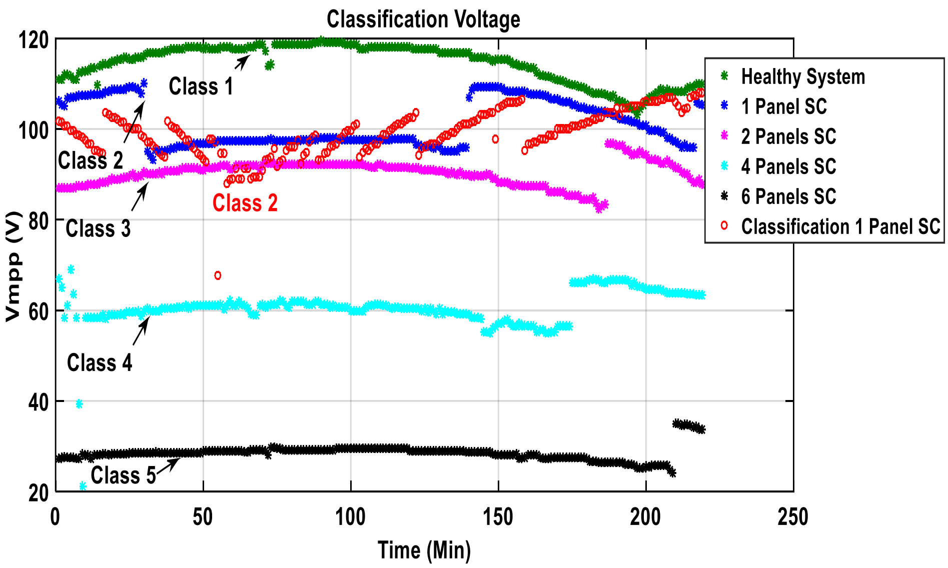

Figure 4.34 Classification of voltage at maximum power point in the presence of noise from the inverter.

Figure 4.34 shows that the classification of voltage (in red) is closer to the healthy voltage (in green) than the other defective voltages (in blue, magenta, cyan, and black). Besides, even though the data to be classified is corrupted by noise from the inverter, the proposed approach was able to classify it correctly (Figure 4.33 and Figure 4.34), which shows the effectiveness of PNNs in classification.

4.10.2 Effect of detection time

It is worth mentioning also that the classification can be carried out in a reduced time interval such as chosen 10 data points as shown in Figure 4.34 and Figure 4.35.

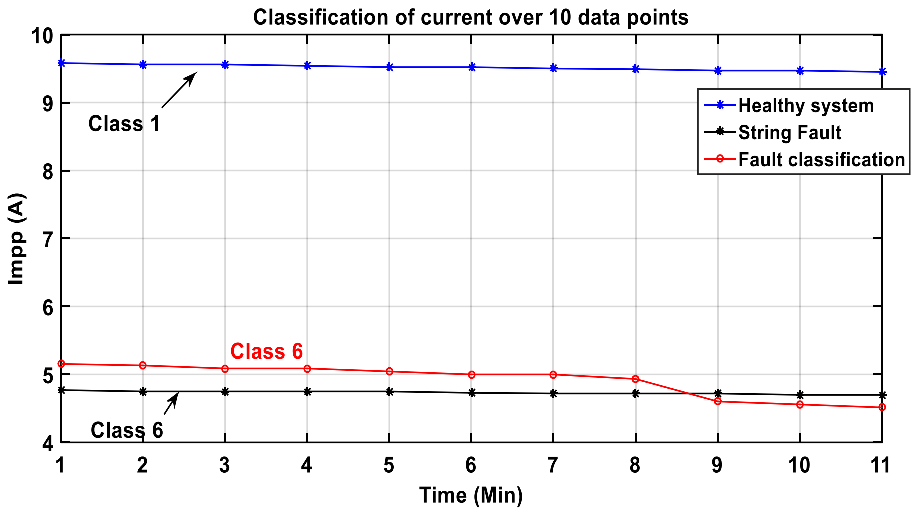

Figure 4.35 Classification of current at maximum power point in the presence of noise from an inverter, over 10 data points.

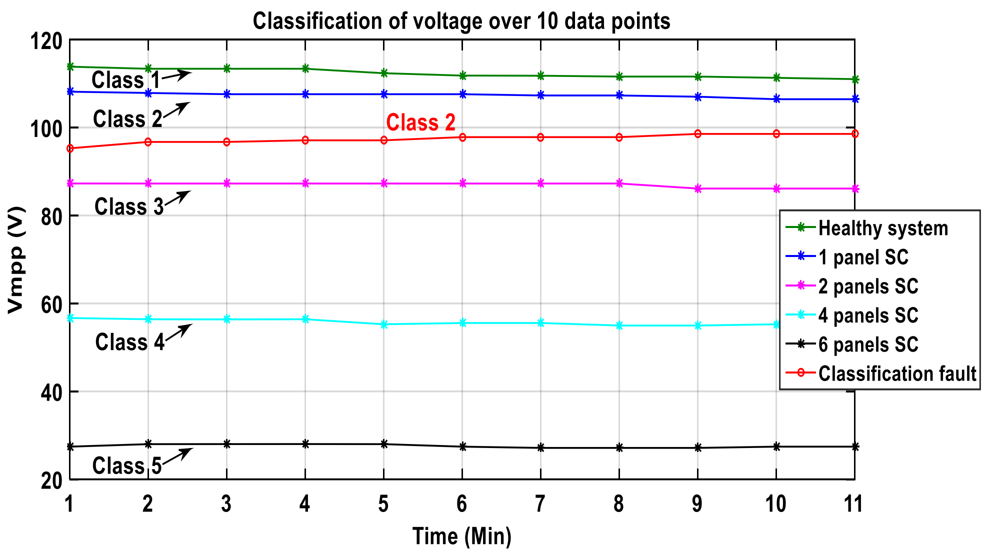

Figure 4.36 Classification of voltage at maximum power point in the presence of noise from the inverter, over 10 data points.

From Figure 4.35 and Figure 4.36 it can be observed that even though the detection time is reduced, the data to be classified is indeed well classified, and the system was able to classify it correctly.

4.11 Proposed FDD electrical-based for diagnosing shading fault

For a well and clarified explanation of the process of the FDD electrical-based techniques [163], we have opted for an approach to diagnose shading fault in a PV generator (Figure 4.37) installed on the roof of Multi-Sources-System (SMS) laboratory at Unité de Développement des Equipements Solaire (UDES) (Figure 4.38), using neural-networks (NN).

Figure 4.37 PV generator with one panel shaded of the SMS laboratory.

Figure 4.38 Multi-Sources installation (PV / Wind turbines) of the SMS laboratory.

Generally, hybrid installations (multi-sources) of the renewable energy type (Photovoltaic, Wind turbines, etc.) are subject to various faults, degradations, anomalies and damage during their lifetimes. In particular, the photovoltaic generator sometimes presents major malfunctions, which lead to degradation on the entire photovoltaic installation, or multi-sources such as that of the Systems-Multi-Sources (SMS) laboratory, in Figure 4.39.

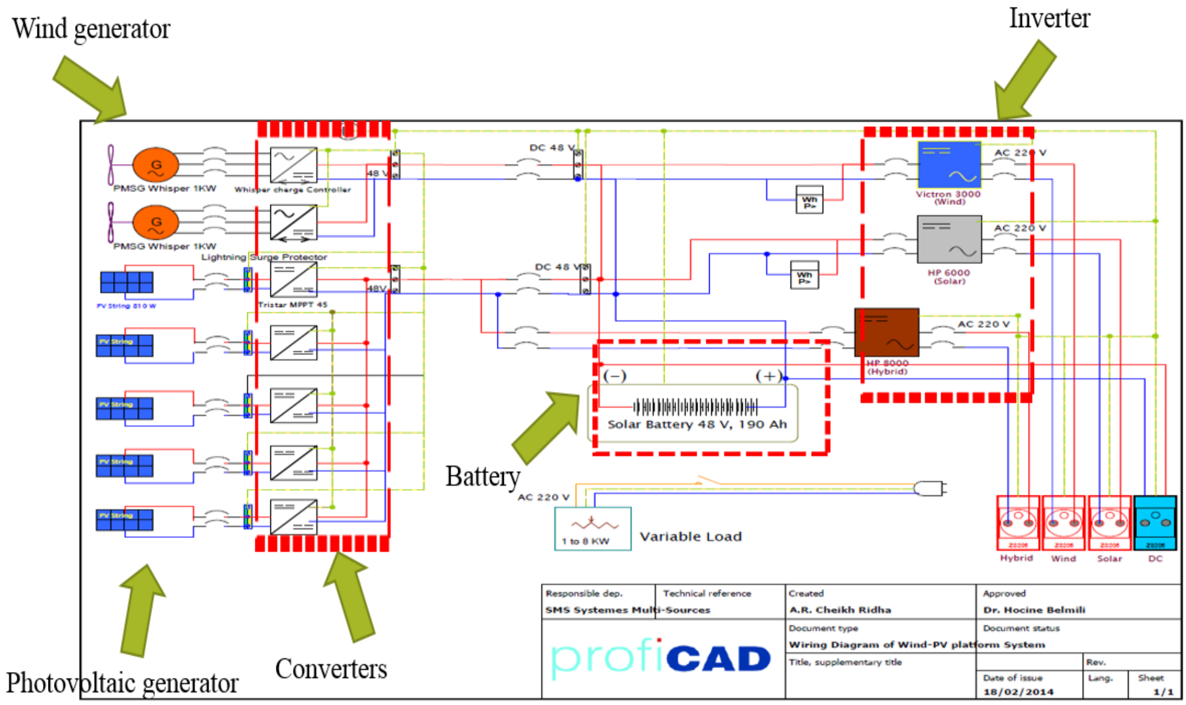

Figure 4.39 Various faults that may occur in the multi-source installation of the SMS laboratory.

The hybrid installation of the SMS laboratory is equipped with (Figure 4.39):

- 2 Wind turbines (Whisper), 1000W of each.
- 30 Suntech PV solar panels (STP-135), 135W of each, mounted for 48V.
- 5 Solar chargers (Tristar MPPT 45), connected in parallel on the DC bus (MPPT control).
- 2 Wind chargers (Whisper).
- 3 Inverters.
- Storage: 1 bank of batteries (12 * 2) 48VDC, ie 12 OPZS, 2V, mounted in 1 bank in series.

The capacity of the system is as follow:

- Overall system capacity: 6kWp

- Photovoltaic system capacity: 4kWp
- Wind system capacity: 2kWp

Figure 4.39 shows schematically the various faults that can affect the various components of the multi-source installation (PV / Wind turbine / Battery) of the SMS laboratory. Diagnosis techniques are needed to ensure fault detection, avoid dangerous risks, prevent damage and extend their lifecycle.

As there are several types of faults that can occur within the PV generator (Figure 4.40), which represents the normal current-voltage (*I-V*) characteristic curve, the one in red and those showing a fault with the other colours (degradation, shading, open-circuit, and short-circuit). Our focus was in the detection and diagnosis of shading (Figure 4.37) defects using an artificial intelligence method such as neural networks. The electrical diagnosis technique based on neural networks is developed to implement diagnostic techniques, using artificial intelligence. The proposed diagnosis technique has been developed in three main steps, providing experimental data to neural networks, the fault modelling step and the decision step. PVG power is the parameter to be processed. The descriptive schematic of the elaborated FDD electrical-based technique is presented in Figure 4.40.

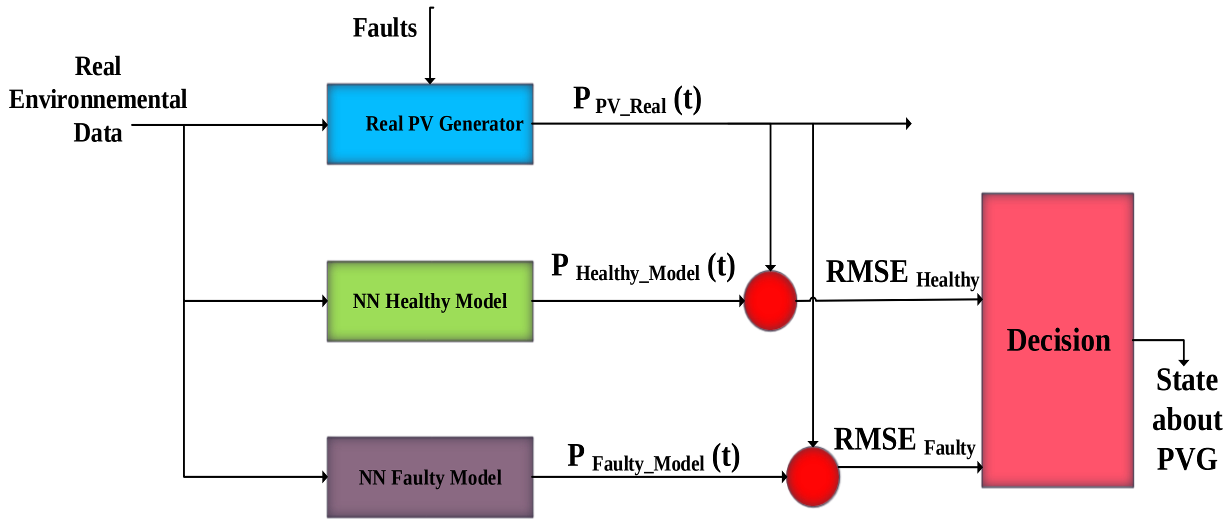

Figure 4.40 Descriptive schematic of the proposed FDD electrical-based in the PV generator.

The major steps of the developed FDD electrical-based for PVG are detailed in the following points.

a) Acquisition of real data

Some measurements have been done, through an acquisition work for obtaining real environmental (temperature and irradiance) and electrical (current and voltage from the battery) data for the PV system at SMS. They are required at the first step of PV diagnosis.

b) NN-based modelling and validation

Using a database of several days two neural-network models are created for healthy and faulty (shaded) PV generator respectively. From the introduced real data (temperature, irradiance, battery current, and battery voltage), power models for healthy and faulty PVG are elaborated (Figure 4.40).

c) Detection & localization of faults.

c.1. Reading of real data

In specific two days (11/03/2020 & 26/11/2020) for both healthy and faulty PVG respectively, read of real acquired data to be diagnosed.

c.2. Simulation using the two models

In Matlab environment, simulate of healthy and faulty models behaviour using the real data as inputs. At this step, the obtained results are illustrated in Figure 4.41 and Figure 4.42 [101].

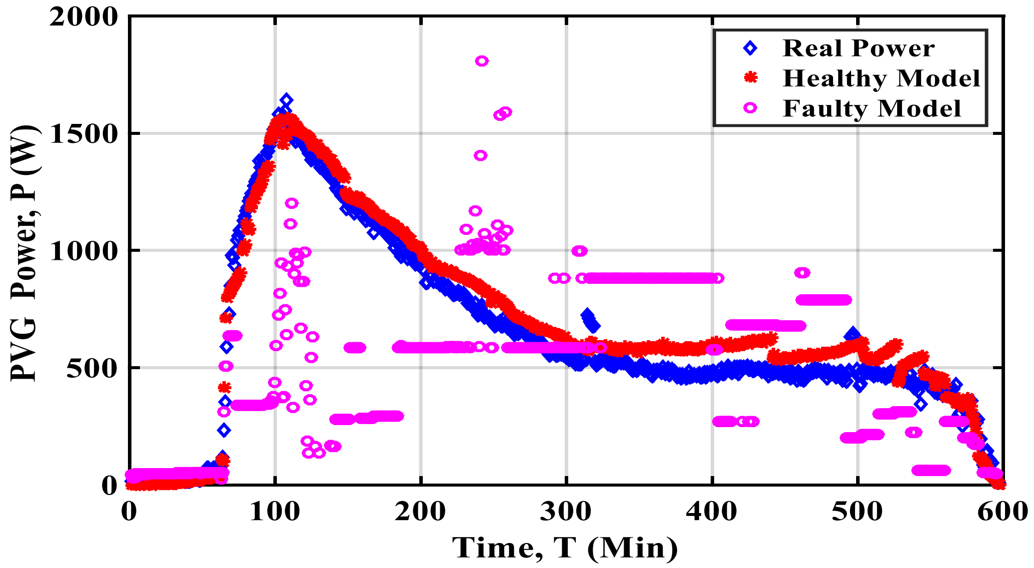

Figure 4.41 Real and modelled data for power, in a healthy PVG (11/03/2020).

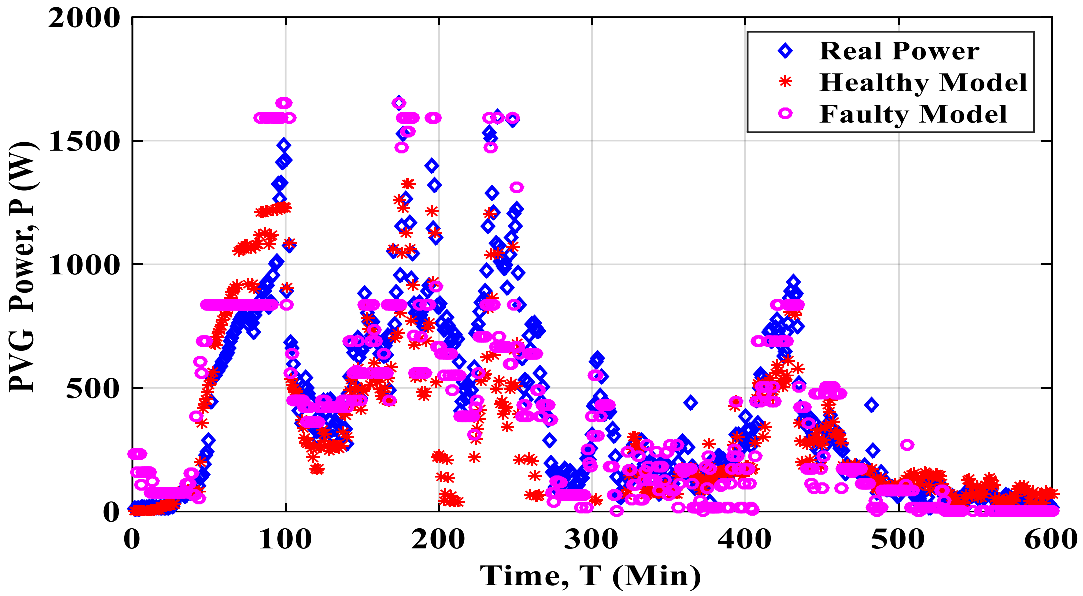

Figure 4.42 Real and modelled data for power, in a faulty PVG (shading a single PV module in the PVG) (26/10/2020).

It is observed from Figure 4.40 that the healthy generated model is the nearest one from the real data. Besides, it is observed from Figure 4.42 that the faulty (shaded) generated model is the nearest one from the real data.

c.3 Decision about diagnosis

Comparing the results of the two obtained models with the measured power of the real PVG using Root Mean Square Errors (RMSE), which is calculated between the real power and both of the healthy and faulty modeled powers through the following expression.

$$RMSE = \sqrt{\frac{1}{N}\sum_{i=1}^{N}(\mathrm{P}_{Real}(\mathrm{i}) - \mathrm{P}_{Model}(\mathrm{i}))^2} \tag{4.9}$$

Where N: is the number of data.

Based on the values of $\mathrm{RMSE}_{\mathrm{Healthy}}$ and $\mathrm{RMSE}_{\mathrm{Faulty}}$, a decision is made about the state of the PV generator, as shown in Figure 4.42 and Figure 4.43 bellow.

```
RMSE_H =

    3.2283


RMSE_F =

   19.8157

Decision about the state of system: Healthy GPV
```

Figure 4.43 RMSE command window results for healthy PVG.

```
RMSE_H =

    9.9733


RMSE_F =

    7.8278

Decision about the state of system: Faulty GPV
```

Figure 4.44 RMSE command window results for faulty PVG.

The lowest value of RMSE allows deciding the health state of the system. As in Figure 4.40, the PVG was healthy in the day of (11/03/2020) relatively to the lowest value of $RMSE_{Healthy}$ compared to $RMSE_{Faulty}$. In contrast, the PVG of Figure 4.41 was faulty in the day of (26/10/2020) relatively to the lowest value obtained for $RMSE_{Faulty}$ compared to $RMSE_{Healthy}$.

For classifying with high accuracy and effectiveness of different other faults occurring in PVG, more sophisticated techniques exist in the literature, which can be an extension of this developing technique as perspective work.

Conclusion

In this chapter, an artificial neural network has been developed in order to model different types of faults that have appeared in a photovoltaic generator. Simulation and experimental testing have been presented, the results prove the high performance of the proposed approach. We opted for this type of diagnosis method based on the calculation and comparison of the mean relative error for the voltage and current classification using the root mean square error and we obtained very satisfactory results. Even though ANNs methods are inherently statistical, they suffer from the need for a large number of unknown observations, which are not always available, and above all, they need a very important number of iterations. In [165], this problem is dealt with by providing a neural network model called PNN allowing instant learning and running even with a small number of observations [166-167]. The diagnosis by the use of PNNs have required the input layer of the various simulated faults by NANNs to have a classification on the output. The approach has proven its strength while injecting noises (*e.g* presence of perturbations from inverter) and notice the presence or absence of confusion. Besides, it does not require the entire *I-V* curve to be elaborated for telling us the decision about diagnosis, only reduced time from real collected data may suffice for the diagnosis process. The next chapter, will devote the implementation on FPGA card, for the developed NN approach.

Chapter 05

Implementation on FPGA of FDD for PVG

CHAPTER 5: Implementation on FPGA of FDD for PVG

Introduction

After studying the theory of FDD in PVG and the application of neural networks in previous chapters, this chapter will present the benefit of using such hardware implementation, which is well described in a paper by *R. L* [169] : << The great interest of building neural networks remains in the high speed processing that could be provided through massively parallel implementation >>. One would assume that the neural network models developed in computational neuroscience could be directly implemented in silicon. This assumption is false because when implementing a neural network, the designer is confined to some specific problems related to the characteristics of these algorithms such as: speed processing, precision, high memorization, parallelism, regularity and flexibility of the architecture. Nowadays, with the increasing complexity of Very Large Scale Integrated (VLSI) circuits, state of the art design is focused around high level synthesis which is a top down design methodology, that transform an abstract level such as the Very High speed integrated circuits Hardware Description Language (VHDL) into a physical implementation level a new design methodology of ANNs based upon a VHDL synthesis of the network is applied. In this chapter, we see a parametric Hardware Implementation of Artificial Neurons models using Filed Programmable Gate Array (FPGA) for diagnosing faults in PVG. The implementation is carried out with the aim of optimizing the area occupied in the FPGA circuit and increasing the rate of flexibility.

5.1 Design methodology

The proposed approach for the ANN implementation follows a top down design methodology. As illustrated in Figure 5.1, architecture is first fixed for the ANN. This phase is followed by the VHDL description of the network at the register transfer level (RTL) [170], Then this VHDL code is passed through a synthesis tool which performs logic synthesis and optimization according to the target technology. The result is a Netlist ready for place and root using an automatic FPGA place and root tool. At this level verification is required before final FPGA implementation.

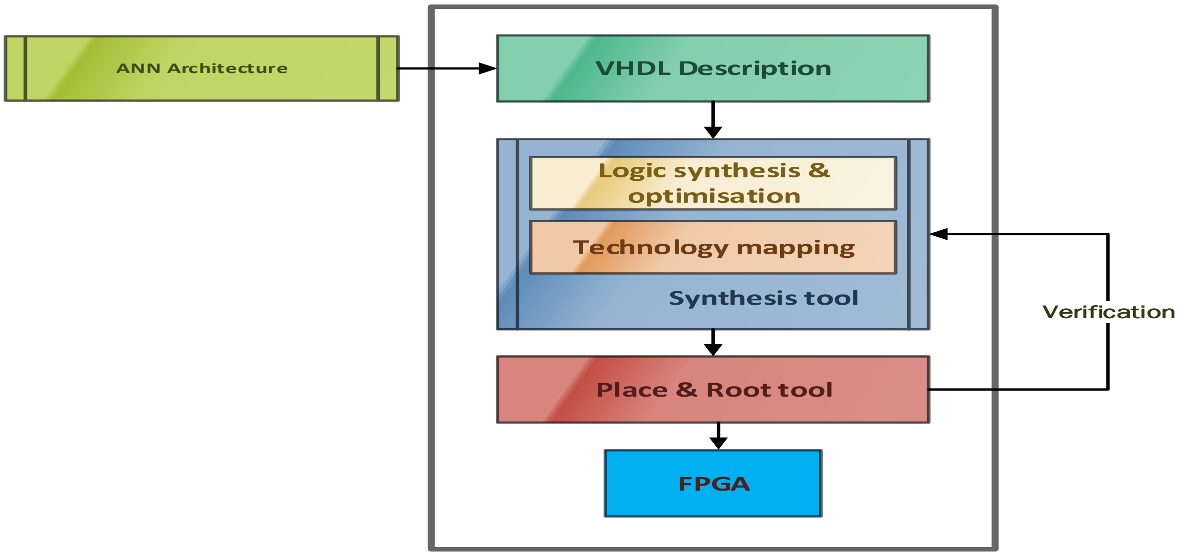

Figure 5.1 Design methodology of the ANN to be implemented in FPGA card [171].

5.2 FPGA card

Field Programmable Gate Array FPGAs, components invented by the Xilinx company, made up of a "sea" of logic gates, used for rapid and inexpensive ASIC development [172]. A brief history about FPGA development, & their characteristics, & the most fabricants in the market, and their architectures are in the next subsections.

5.2.1 History research

Programmable logic circuits appeared in the early 1980s. Developers already had "Programmable Logic Device" (PLD) circuits, which were easily configurable. The PLD have many types such as, Programmable Array Logic (PAL), Generic Array Logic (GAL), Erasable Programmable Logic Device (EPLD), Complex Programmable Logic Device (CPLD) and FPGA (Figure 5.2) [172].

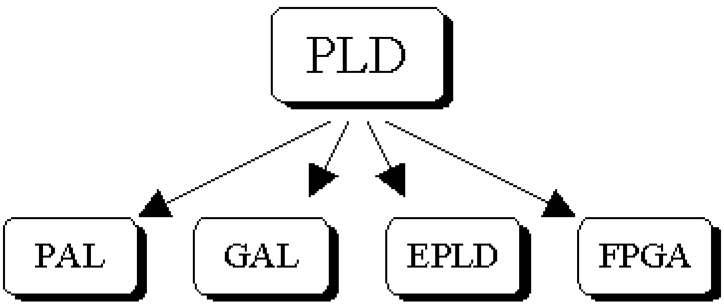

Figure 5.2 Types of PLD.

Then in 1984 *Ross Freeman, Bernie Vonderschmitt* and *Jim Barnett* founded the Xilinx Company [173]. In 1985, they introduced to the market the XC2064, the first Field Programmable Gate Array (FPGA) circuit, which is a reprogrammable integrated circuit, offering an alternative to previous approaches.

5.2.2 Characteristics of FPGA card

Among the main characteristics of FPGA circuits [173], we can mention:

- Performances.
- Time to market.
- Cost.
- Reliability.
- Long term maintenance.

5.2.3 Fabricants of FPGA card

The FPGA market is booming with dozens of manufacturers, who use more or less similar technologies for the manufacture of FPGAs. We can cite for example: Actel, Abound Logic, Atmel, Cypress, Lattice Semiconductor, Xilinx, Altera, etc (Figure 5.3). Among all these manufacturers, only two main firms have a monopoly on the market for FPGA circuits, namely Xilinx and Altera [173].

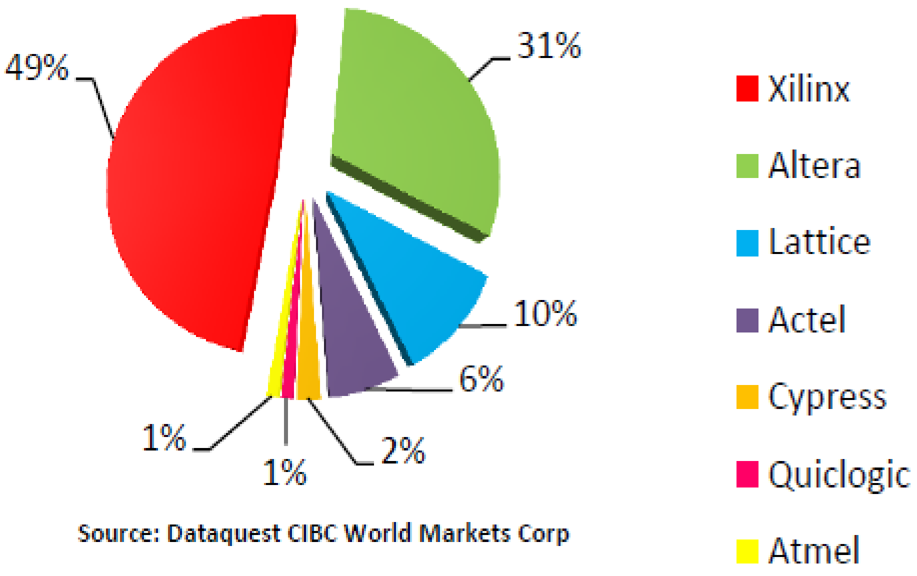

Figure 5.3 Different fabricants of FPGA.

5.2.4 General structure of FPGA card (from Xilinx)

The general structure of FPGA consists of a network of programmable configurable logic blocks (CLB) structure, of configurable input/output (IO) blocks, and interconnection matrix which surrounds the CLB and surrounds them all (Figure 5.4) [158], [172].

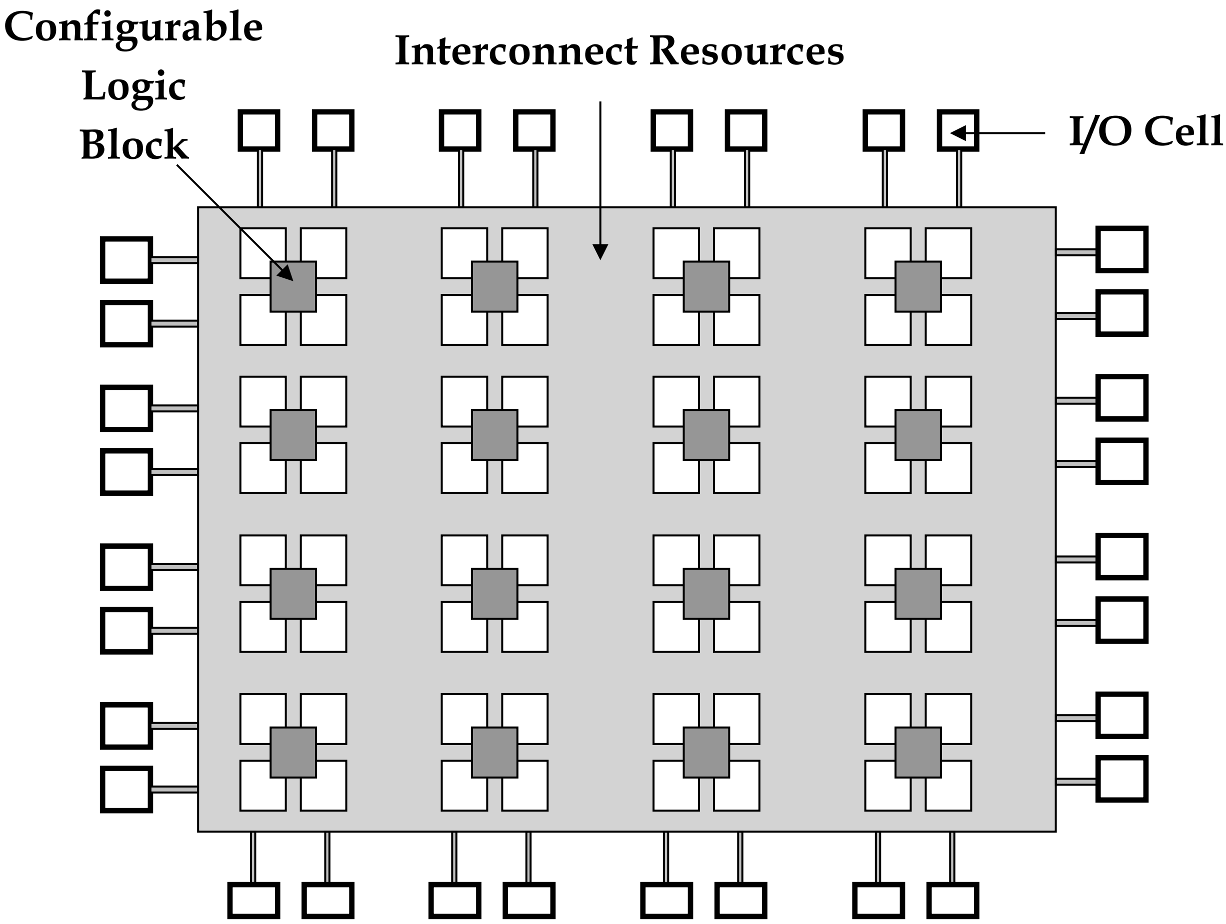

Figure 5.4 General structure of FPGA.

The architecture, adopted by Xilinx, is in the form of two layers: one layer called configurable circuit, the second is a Static Random Access Memory (SRAM) memory network layer. The so-called "configurable circuit" layer consists of a matrix of configurable logic blocks CLB making it possible to perform combinatorial functions and sequential functions. All around these configurable logic blocks, we find Inputs / Outputs blocks (IOB) whose role is to manage the inputs-outputs making the interface with the external modules (Figure 5.4).

a) CLB structure

Configurable logic blocks are the main building blocks of an FPGA (Figure 5.5). Their structure varies by manufacturer and family, several types of architectures are used by manufacturers, and some based on multiplexers (MUX), and others on look-up tables (LUT). The CLB is mainly constituted from Look-Up Table (LUT) and Flip Flop (bascule D) [172].

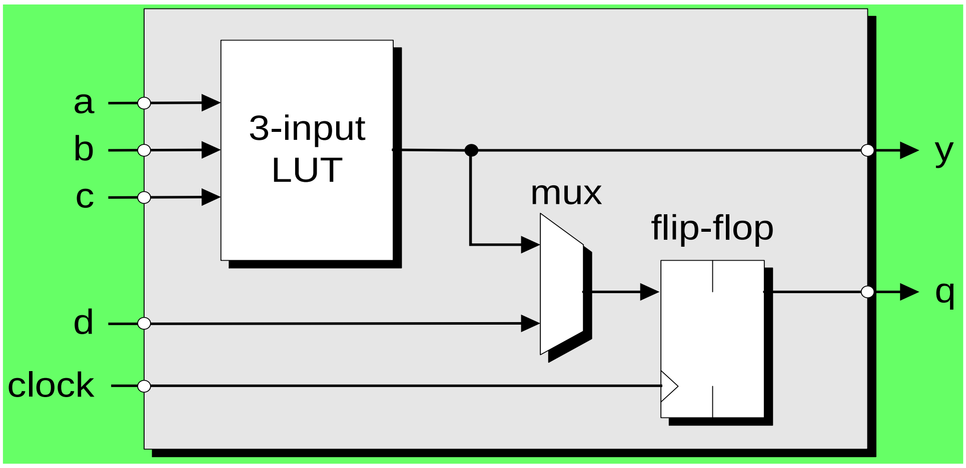

Figure 5.5 Structure of CLB.

b) Connexions resources

Internal connections in FPGA circuits are made up of metallized segments. Interconnection resources within an FPGA allow arbitrary connection of CLBs and IOBs (Figure 5.6) [174].

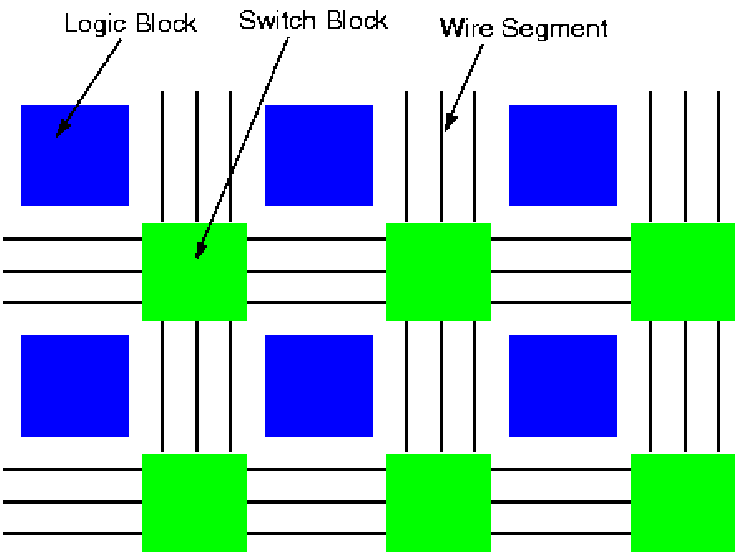

Figure 5.6 Structure of FPGA (connexions resources).

c) Inputs/Outputs blocks (IOB)

IO blocks allow internal logic to be interconnected to the input and output ports of the FPGA (Figure 5.7). These blocks are presented on the entire periphery of the FPGA circuit. Each IOB block controls a pin of the component and it can be set as input, output, and bidirectional signals [174].

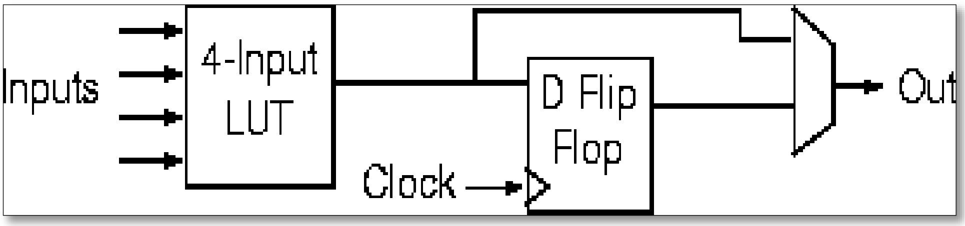

Figure 5.7 Architecture of IOB in FPGA.

5.3 VHDL

5.3.1 VHDL Description

VHDL is a modern powerful tool language: excellent visibility, high modularity, description fiability [175]. The level of VHDL abstractions are:

- Structural description.
- Behavioral description
- Data flow description.

The VHDL description of a circuit is composed of:

- Extern vision of circuit: Entity (Figure 5.8.a).
- Intern vision of circuit: Architecture (Figure 5.8.b).

a)	b)
Entity entity-name is **generic** (generic declaration); **port** (port declaration); **end** entity-name;	**Architecture** architecture_name of entity_name is **process** () –Declarative part **begin** **--** Descriptive part **end** architecture-name;

Figure 5.8 a) Top view of Entity in VHDL. b) Top view of Architecture in VHDL.

- The generic clause declares the constants which can be for the control of the structure (behavior of the entity).
- The generic port clause is used to define the circuit connections.

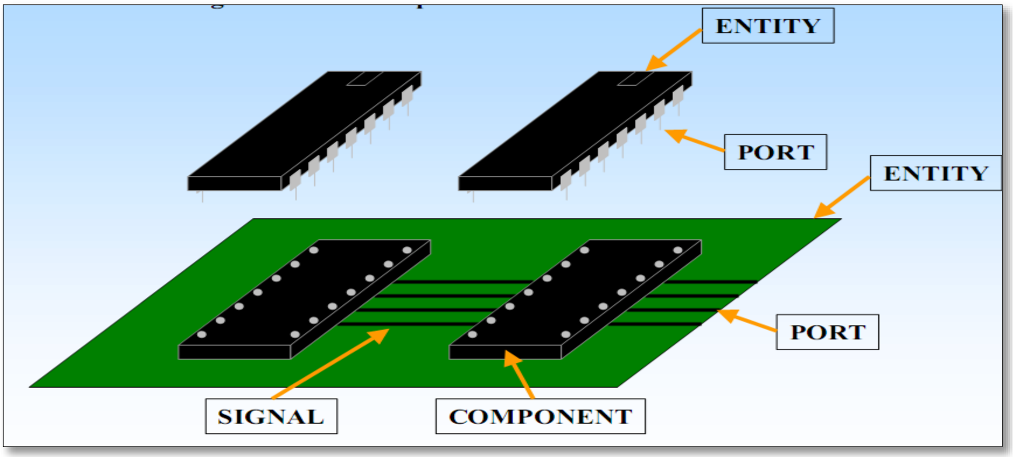

Figure 5.9 Representation of entity & architecture from software to hardware.

From a technical point of view, VHDL is a modern and powerful language characterized by its excellent readability, its high modularity, and its ease of use and the reliability of its descriptions. From an economic point of view, the VHDL tries to identify errors from the compilation, which costs less expensive.

5.4 Xilinx Ise

Xilinx ISE (Integrated Software Environment) software is a development environment for digital systems that allows you to walk through all stages of the development of an FPGA target design project (Design Entry, Design Synthesis, Design Verification (simulation), Design Implementation, Device Configuration) [176]. The hardware implementation will follow all the steps from classic design to implementation on an FPGA target, as presented in Figure 5.10.

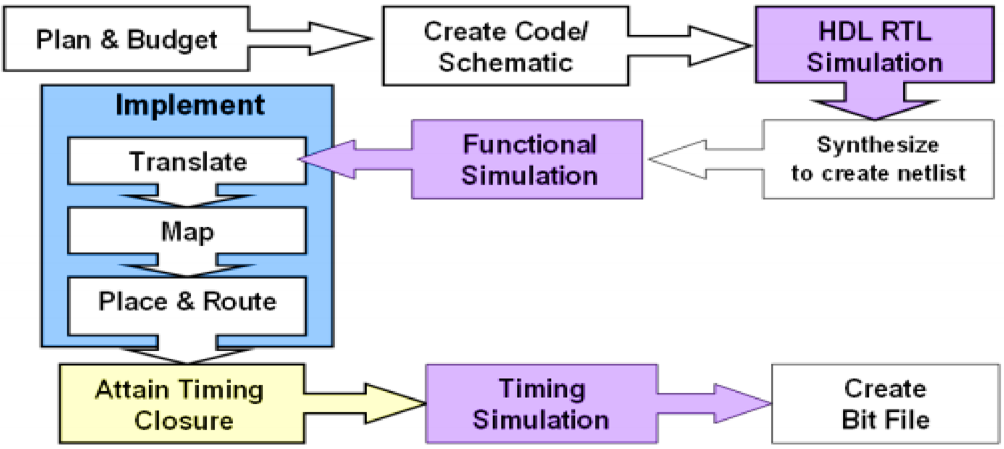

Figure 5.10 Xilinx ISE implementation main steps [177].

Designs of project can be described in three main forms: as schematics, HDLs, or state diagrams. In the following sections the modelling and digital architecture of the ANN for diagnosing faults in PVG, will be derived then the proposed parametric VHDL description.

5.5 ANN Modeling for FPGA

This section is dedicated to introduce the modeling of ANN for diagnosing faults in PVG to be implemented in FPGA. We have the three-layer feed-forward back propagation network (Figure 5.11) for implementation, which describe the main structure of our developed ANN for diagnosing faults occurring in PVG. The ANN computation can be divided in two phases: learning phase and recall phase. The learning phase performs an iterative updating of the synaptic weights based upon the error back-propagation algorithm [175]. It teaches the ANN to produce the desired output for a set of input patterns. The recall phase computes the activation values of the neurons from the output layer according to the weighted values (computed in the learning phase).

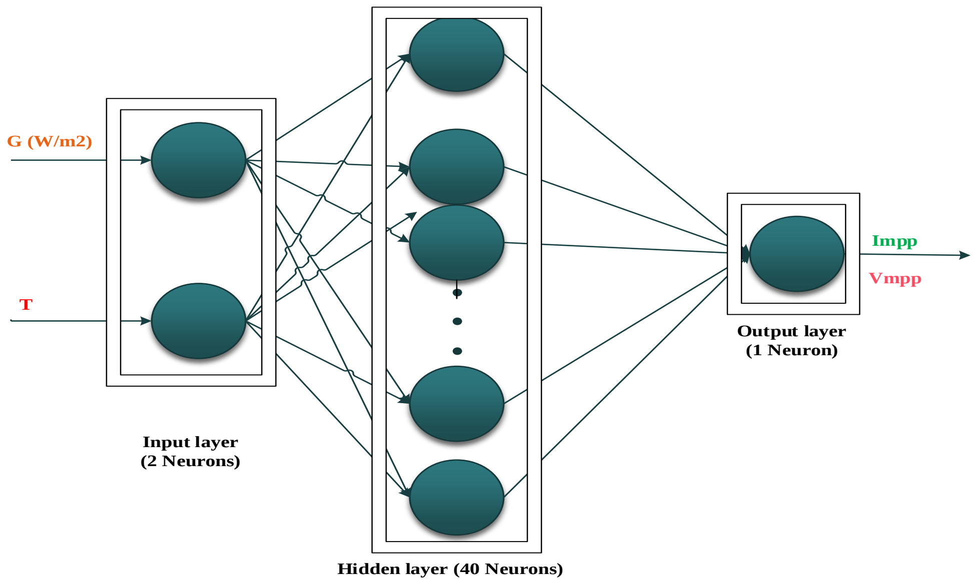

Figure 5.11 Main structure of ANN for a healthy system (feed-forward).

Training (learning) of an ANN is carried out in Matlab, as follows:

a) Initialize the weights and bias.
b) Compute the weighted sum of all processing elements from the input to output layer.
c) Starting from the output layer and going back word to the input layer adjust the weights and bias recursively until the weights are stabilized.

It is mentioned that the learning phase of this neural-network happens in Matlab (chapter above). Then, we obtain the weights and bias of the network through the use of the function (getwb(name-of-network)) and [b,iw,lw] = separatewb(net,wb).
The latter weights, are directly used in the hardware implementation.

5.6 Digital architecture of the ANN

The hardware requirements of ANNs are parallelism, performance, flexibility and their relational-ship to silicon area (in our case number of CLBs). Based upon the above ANN hardware requirements, the FPGA equivalent architectural model of the neuron of Figure 5.12 is represented by Figure 5.12.a.

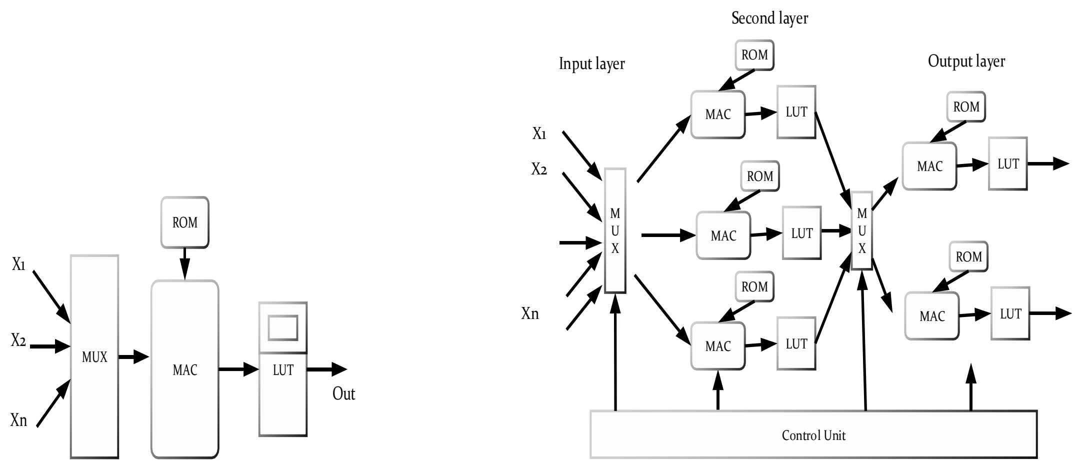

a) b)

Figure 5.12 a): Neuron hardware model. b) ANN hardware architecture.

The hardware model of neuron is mainly based on a:

- Multiply accumulate circuit (MAC) which computes the weighted sum with the following expressions:

$$\mu_i = \sum_{j=1}^{n} w_{ij} * x_i \quad (5.1)$$

Where:

w_{ij}: are the weight of connexions.

x_i: is the activation of neuron i.

- Memory circuit (ROM) where the final values of the synaptic weights are stocked.

- Look-up table (LUT) which implements the sigmoid activation function with the following expressions.

$$y_i = f(\mu_i) \tag{5.2}$$

The resulting ANN hardware architecture of Figure 5.12 is represented in Figure.12.b. (note that only the second and output layers are represented in this figure), with the following features: For the same neuron, only one MAC is used to compute the product sum. Each MAC has its own ROM of weights. The depth of each ROM is equal to the number of nodes constituting its input layer. For the same layer, neurons are computed in parallel. Computation between layers is done serially. The whole network is controlled by a unit control. As we can see, the resulting architecture exhibits a high degree of parallelism, simplicity, regularity and repeat-ness.

5.7 Parametric VHDL description of ANN

Our approach to the ANN hierarchic VHDL description is illustrated in Figure 5.13. VHDL description of the network begins by creating a **component neuron**, then a **component layer** is created and finally a **network** is described [175].

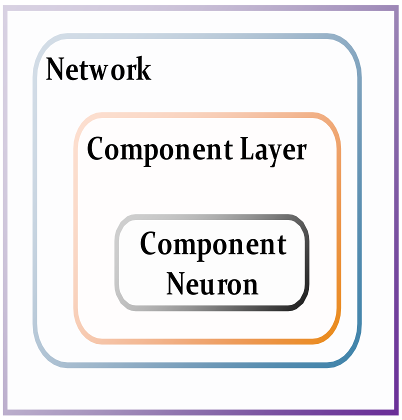

Figure 5.13 Top view of an artificial neural network parametric VHDL description.

- Component neuron is composed by a bloc of synaptic weights, a MAC component, a ROM component and a LUT component.
- Component layer is composed by a set of component neurons and multiplexers.
- A Network is composed by a set of component layer (input layer, hidden layer, and output layer).

5.7.1 Architectural description of neural component

The main components of a neural component are represented in Figure 5.14.a [158]. The hardware description of a neural component implied the MAC, ROM, and LUT (Figure 5.14.b).

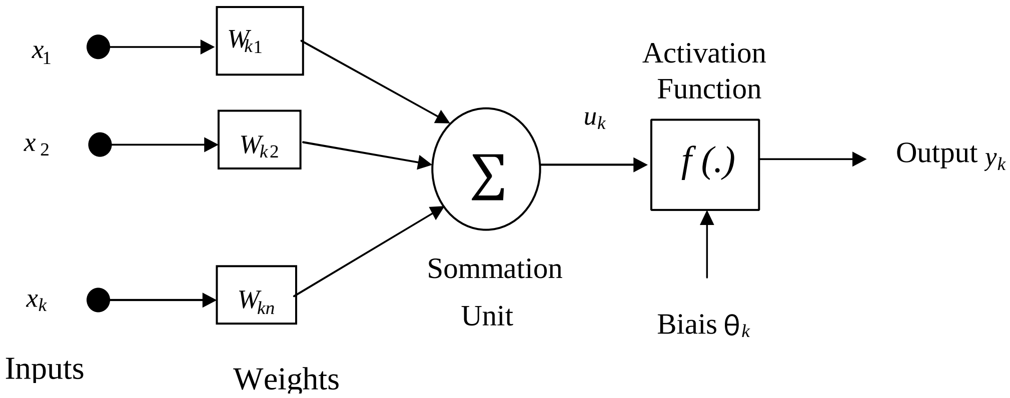

a)

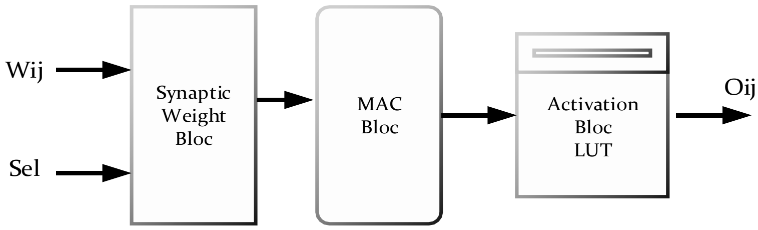

b)

Figure 5.14 Schematic representation: a) Simplified neural model; b) Equivalent neural hardware model.

The basic building block of the Feed-forward module is the neuron. It consists of a MAC block, a synaptic weight block, and an activation block, as we see in the Figure 5.14.a).

5.7.2 Architectural description of layer component:

The layer component is constituted of a neuron component with a multiplexer, which allow to aiguille the input data and transmit it to all the neurons constituting the layer. For our application, we have created three layer components: layer1, layer2, and layer3. Each of the above layer contains a number of neuron component. The hardware representation of the three layers is given in Figure 5.15 (a, b, & c).

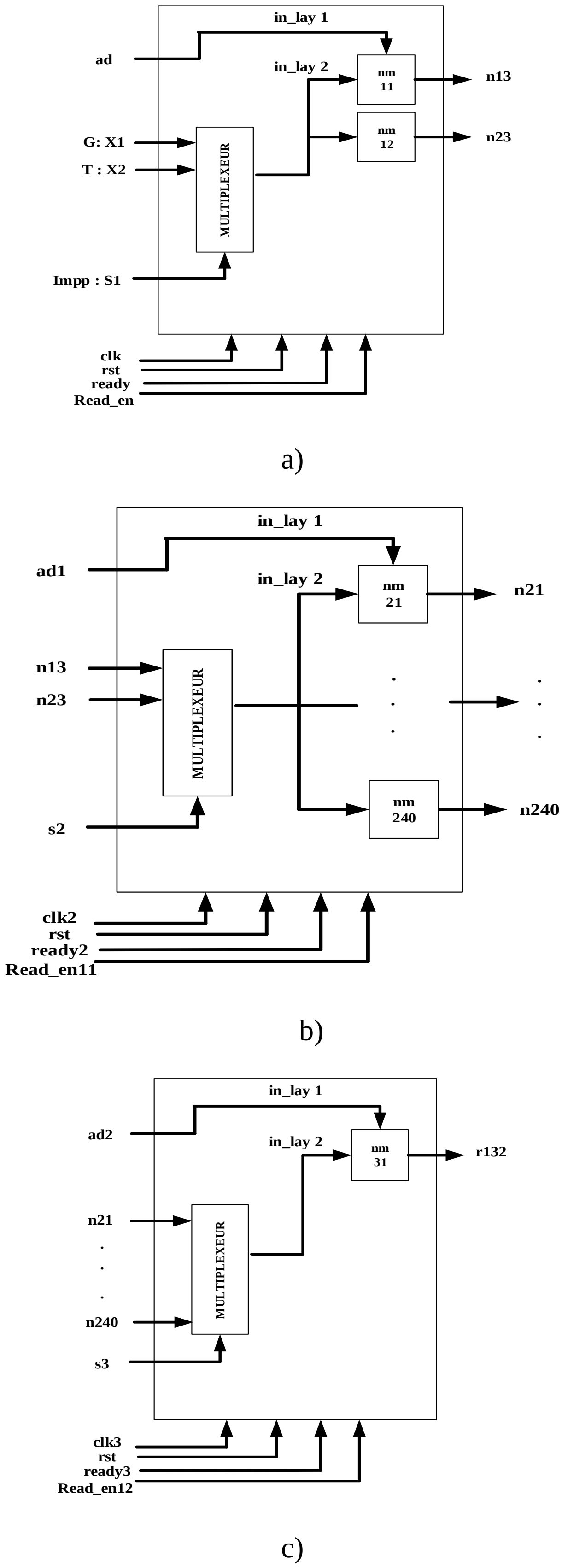

Figure 5.15 Hardware representation of the three layers: a) First layer (2 neurons); b) Second layer (40 neurons); c) Third layer (1neuron).

The developed ANN is a network of three layers with the following parameters.

- The first layer contains two neurons: 4bits (from nm11 to nm12).
- The second layer contains 40 neurons: 8bits (from nm21 to nm240).
- The third layer contains one neuron: 16bits (nm31).

Each of these layers consists of a number (N) of neurons preceded by a multiplexing block as shown in the Figure 5.16.

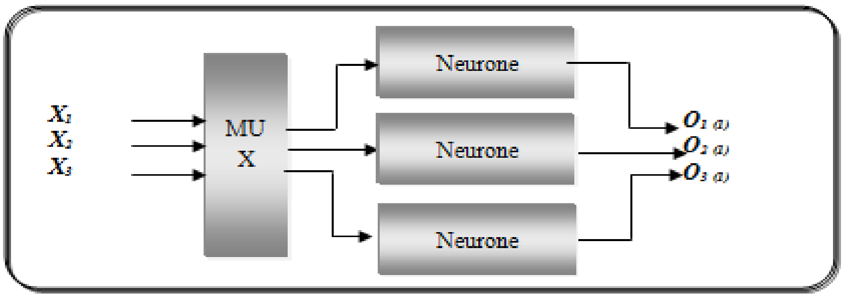

Figure 5.16 General architectural hardware representation of a layer.

5.7.3 Architectural description of neural-network Component:

From the hardware representation of a neuron with the regularity of a network, the architectural representation of a neural-network is illustrated in Figure 5.17.

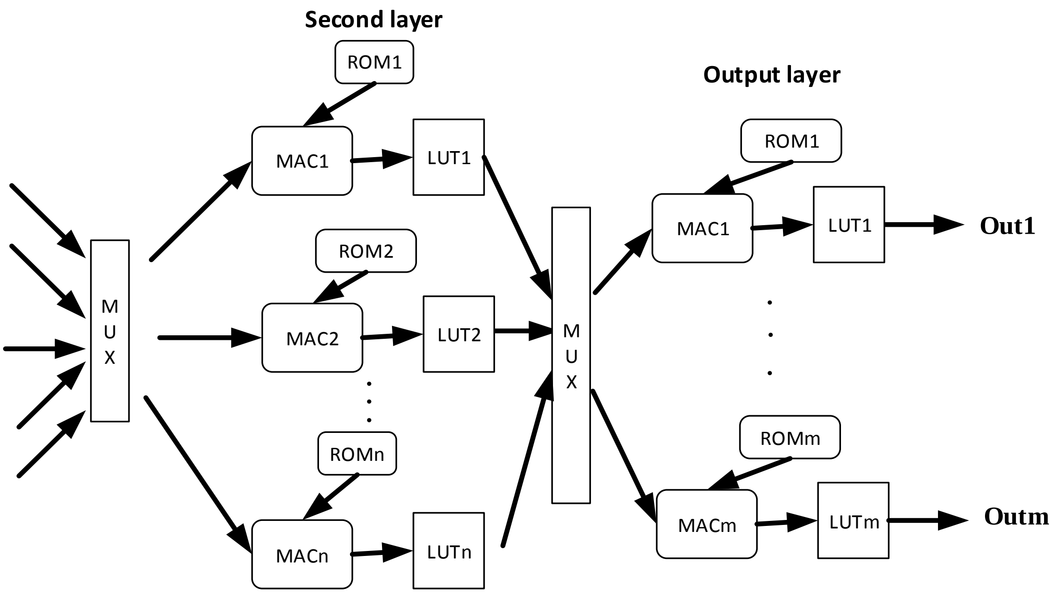

Figure 5.17 Architectural hardware representation of neural network.

The hardware representation of our neural-network is in Figure 5.18.

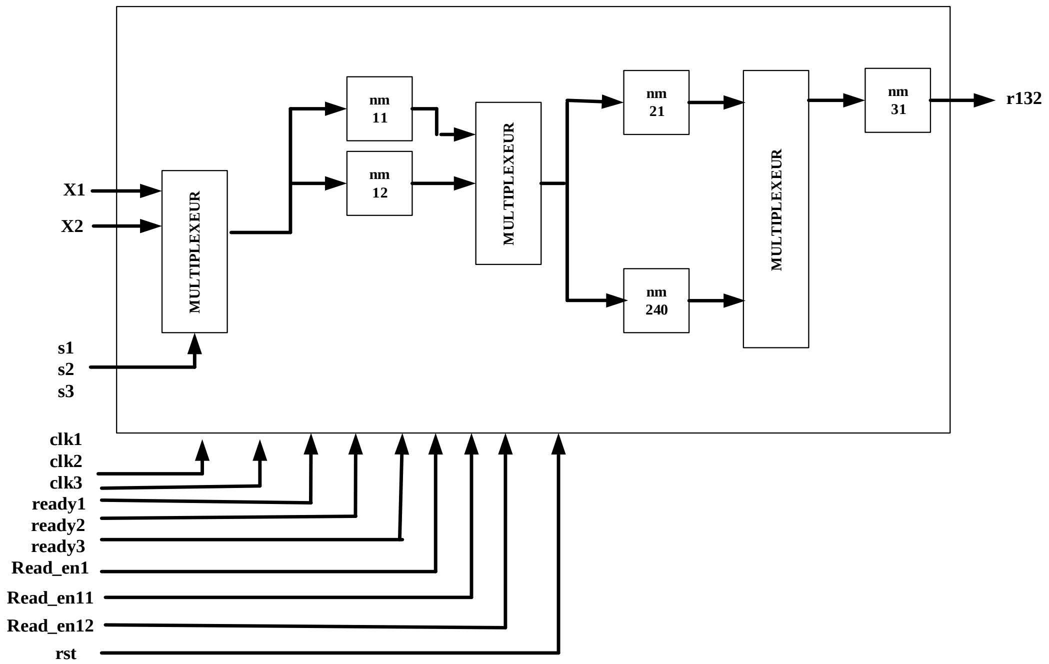

Figure 5.18 Hardware architectural representation of our neural network.

5.7.4 Case study: Implementation of ANN models for diagnosing faults in PVG

In this subsection, we focalize our interest to implement the developed neural-networks approach (modeling and validating the faults of a PVG using ANN), presented in previous chapter. The main structure of ANN is given in Figure 5.19. We have chosen to begin our implementation to the simple ANN1 for a healthy PVG.

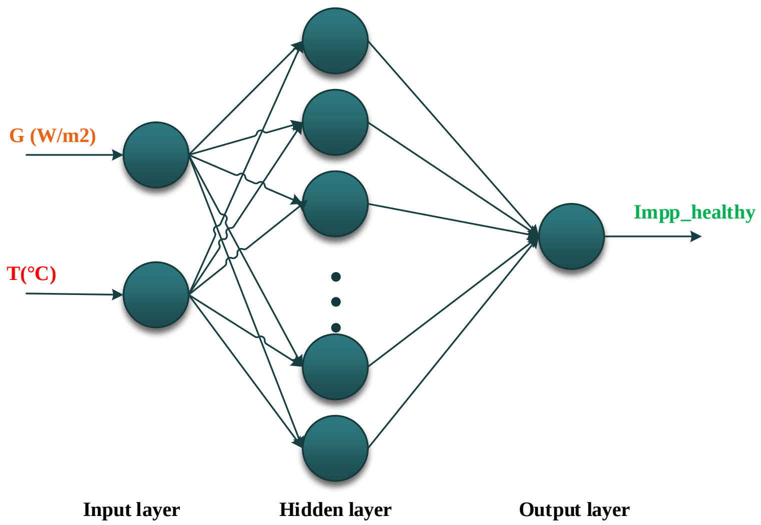

Figure 5.19 Main structure of ANN1 for a healthy system.

The ANN1 have the following characteristics:

- Type of ANN: MLP.

- Type of learning: supervised (in Matlab).
- Validation of ANN: (in Matlab).
- Type of learning algorithm: weights adjustment is using back-propagation algorithm.
- Type of transfer function: hyperbolic tangent.

There are two approaches in the hardware implementations of artificial neural networks [171]:

a) On-chip training circuits: the implementation herein integrates the learning phase and the test / generalization phase in the same circuit. This type of implementation allows flexibility and adaptability of the circuit to several applications.

b) Off-chip training circuits: the implementation herein integrates only the generalization phase. In this approach, the learning is done in software in order to generate the synaptic weights. The hardware implementation of the ANN consists in this case of loading its synaptic weights into memories and implementing the summation and activation functions.

Figure 5.20 shows the total design flow using MATLAB and Xilinx (off-chip training). The MATLAB program consists of the built and learning programs of NN. After the leaning procedure, weights data are fixed and saved to a file. Then transmit the weights to the Xilinx [178].

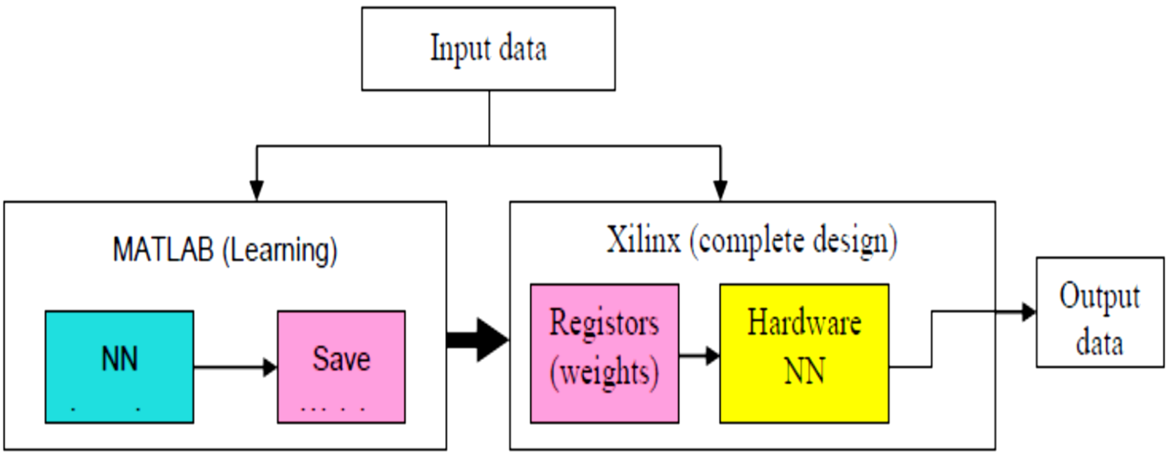

Figure 5.20 Implementation of ANN from Matlab to Xilinx ISE (Off-chip training circuits) [178].

In this work, we have used the off-chip training circuits. It is mentioned that the learning phase of this neural-network occurs in Matlab. Then, we obtain the weights of the network through the use of the function (get(name-of-network));getwb(net). The latter weights, are directly used in the hardware implementation.

5.8 Hardware representation

Having fixed architecture, the next phase is the VHDL description of the ANN. The VHDL description of our neural network begins with a neuron component, constituted of bloc of synaptic weights, MAC, ROM, and a LUT. Then, a layer component constituted of a set of neuron components.

Therefore, a VHDL description of the network is achieved. The parameters that introduce the flexibility of the network are the neurons word sizes (*n*), the number of neurons in each layer (*nb_neuron*) and component instantiation of each layer (component layer1, component layer2, and component layer3).

In what follows, we present the neuron, its internal architecture, and then we will validate by a simulation and synthesis of the results obtained for the family of FPGA circuits Virtex 5 (xc5vlx50-lff676).

5.8.1 Hardware implementation of block of synaptic weights

For synaptic weights it suffices to use a RAM to store these values, however and since we must first initialize these weights to random values and put them in RAM and then update these weights and to store them, the addition of a multiplexer is necessary at the entry of the RAM for the mixing between the values of initialization and that of the update. Thus our block of synaptic weights consists of a multiplexer and a RAM, Figure 5.21 [179].

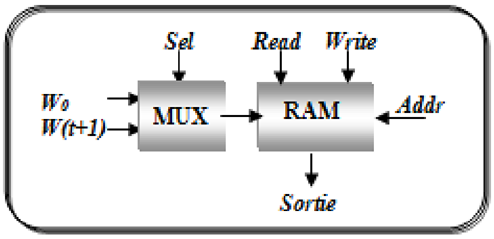

Figure 5.21 Architecture of the block of synaptic weights.

5.8.2 Hardware implementation of MAC Bloc

The MAC block realizes the weighted sum Equation (5.1). It is composed of a multiplier and an accumulator, in order to find the value of the weighted sum, we use the multiplier and the accumulator to calculate this value and a register to store it (Figure 5.22).

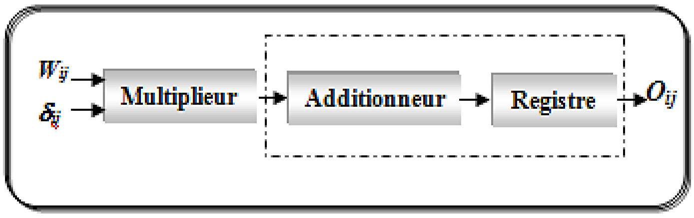

Figure 5.22 Architecture of MAC bloc.

5.8.3 Hardware implementation of Activation block (LUT)

The role of the activation function block is to take the value of the weighted sum calculated by the neuron and apply the function called Sigmoid to it, to generate the activation value of the neuron. For our network we used the sigmoid function as follows:

$$y_j = f(x_j) = \frac{1}{1+\exp(-\alpha x_j)} \quad (5.3)$$

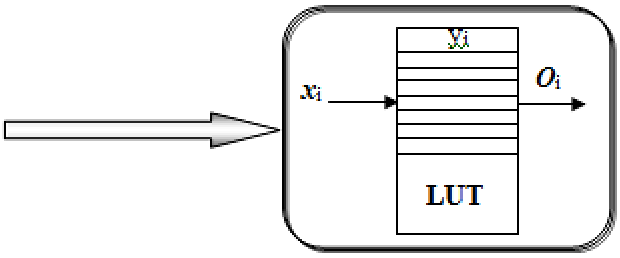

Modelling this function requires the implementation of division and exponential operations, each of these operators requires a significant number of FPGA resources. To remedy this problem we use the FPGA Look-Up-Tables (LUTs) for the modelling of this function.

In our case we are using these LUTs in ROM addressed by the value of the weighted sum and the activation values will be loaded in this ROM, so we will have the value of the weighted sum in input, and that of the activation in output. Figure 5.23 shows the plot of the sigmoid function.

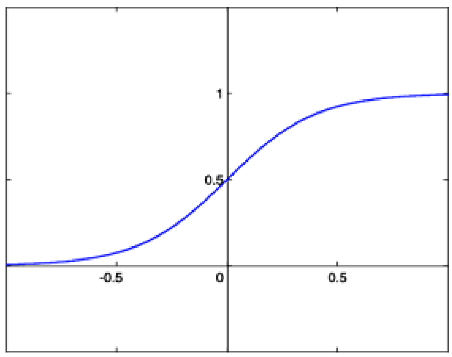

Figure 5.23 Sigmoid graph.

5.9 Synthesis and simulation of ANN in ISE

In order to validate the operation of the proposed architecture, we considered our network of size (2, 40, 1), so we have a total of 3 nodes (neurons), an input layer is used for the transfer of inputs, a layer hidden with 40 nodes and an output layer of one node. We used the FPGA ISE implementation tool from XILINX, which integrates the ISim simulation module (ISE Simulator) [180]. The algorithm mapping was done on the following FPGA circuit: Virtex-5 LX50.

5.9.1 Virtex 5

There are several families of FPGA circuits, in our study we are interested in XILINX Virtex-5 of FPGA circuits based on SRAM technology [181]. The circuit of Virtex 5 is represented in Figure 5.24. The revolution concerns the integration of memories, multipliers, processors, Digital Signal Processor (DSP) circuits in a single FPGA circuit. This evolution in the structure of FPGAs has obviously been accompanied by an evolution of development tools. More and more efficient tools were needed to take advantage of these structures, which were becoming both larger and larger, but also more and more heterogeneous [179].

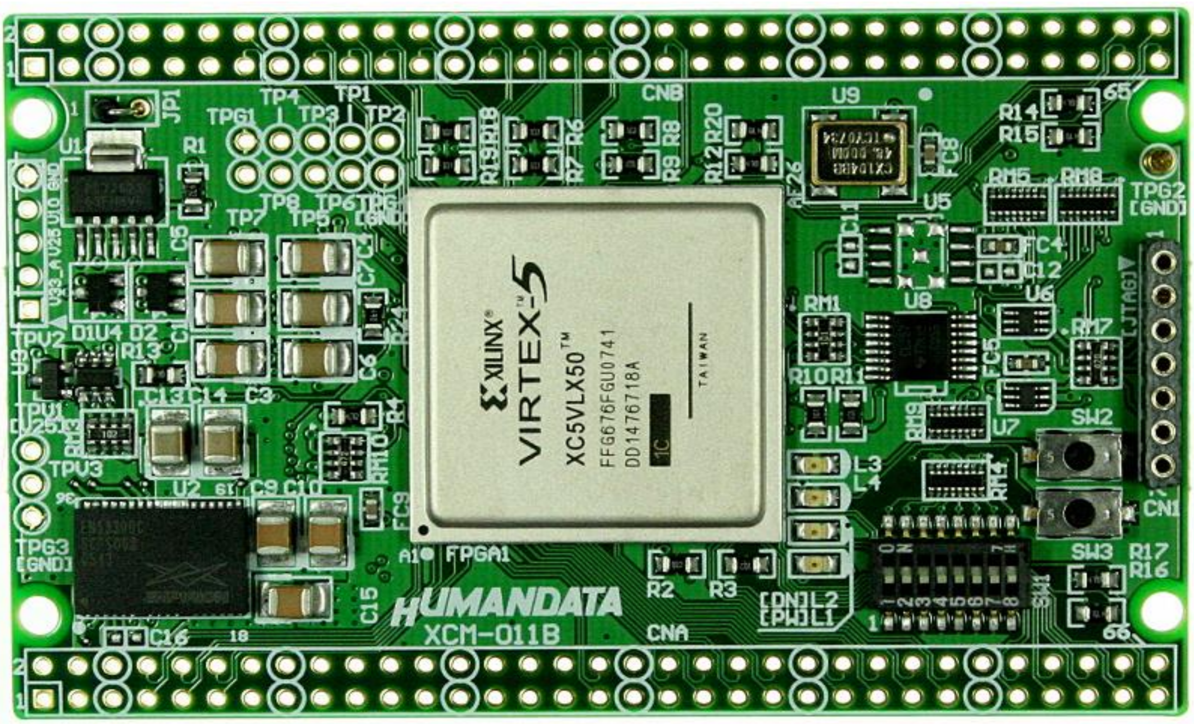

Figure 5.24 Virtex 5 LX 50.

The Virtex-5 family provides some of the most powerful devices on the FPGA market. Characterized by a clock frequency which can be increased to 550 MHz, these components are used in various applications such as telecommunications, cryptography, image processing, etc. The following figure 5.25 shows the internal architecture of Virtex-5. The latter is the 13th generation in 2006, with 6 input LUT.

Produced with a 65nm technological process with 12 metallization levels, the FPGAs of this family have a higher integration rate and allow more routing possibilities compared to previous families.

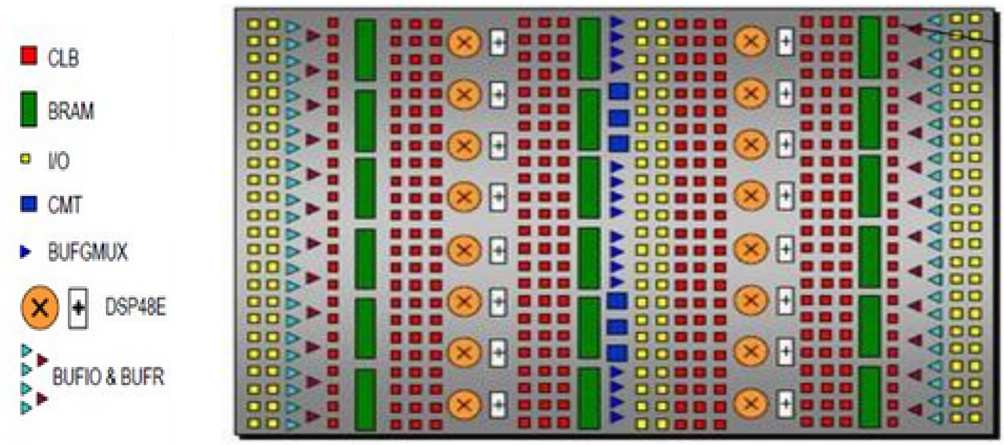

Figure 5.25 Internal architecture of the FPGA circuit of the Virtex-5 family.

The Virtex 5 family is divided into five different platforms namely LX, LXT, SXT, TXT and FXT [182]. We present below the basic components of the LX platform, intended for high performance logic applications for which the XC5VLX50 component is chosen as an implementation target in this chapter.

FPGAs circuits follow the following nomenclature information [181]:

XC5VLX50-1 FF 665 C

Temperature

C = Commercial (Tj = 0°Cto+85°C)

I = Industrial (Tj = –40°C to +100°C)

Device type

Speed

(-1, -2, -3)

Number of Pins

Package Type

Device type: the type of the family which is in our example VIRTEX-5.

Speed: the speed of the component according to the technology.

5.9.2 Synthesis results of complete neuron

In what follows, we will show the synthesis results of the neuron for the family of FPGAs xc5vlx50-lff676. After synthesis, the resulting netlist file is mapped into the FPGA Xilinx Virtex5 family circuit's for physical implementation.

Table 5.1 shows the synthesis results of a neuron that occupies different surfaces for FPGA of Virtex5LX50 (**xc5vlx50-lff676)**.

Table 5.1 Synthesis results of a neuron.

FPGA Circuit	Activation function	Resources	Used	Total	Utilisation
Virtex5LX50 (**xc5vlx50-lff676)**	Sigmoid	Slice Registres	4128	28800	14%
		Slice LUTs	1780	28800	16%
		DSP48E	1	48	1%
		I/O	110	440	25%

- **Results interpretation**

From the results obtained, we can conclude the following points:

- Each neuron consumes 1 Digital Signal Processor (DSP) to do the multiplication, this is an advantage for the implementation of large neural networks.

The xc5vlx50-1ff676 card of the Virtex-5 family with sigmoid activation function offers better performance compared to I/Os.

5.9.3 Simulation results

In what follows, the simulation results of each block constituting the neuron of the Feed-forward module [181].

- **The Mux Multiplexer has:**

- Two (2) 16-bit coded inputs (w, w_{t1}).

- A selection input coded on 1 bit (sel).

- An output coded on 16 bits (w_n).

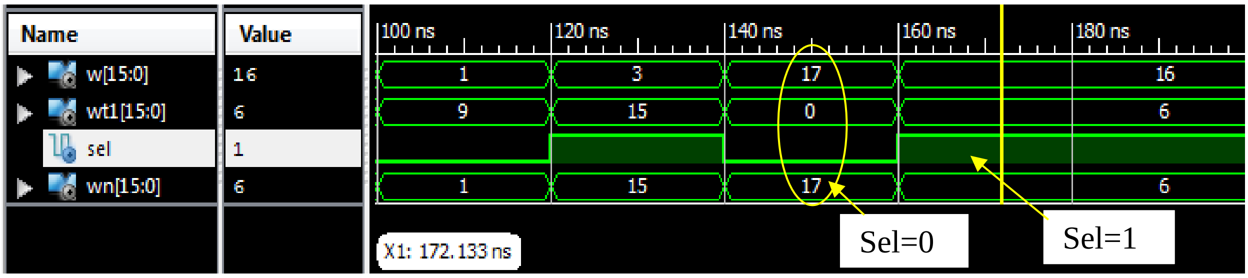

Figure 5.26 Simulation timing of a multiplexer.

Figure 5.26 shows the results of functional simulation of the multiplexer block.

The simulation results clearly show the correct operation of the multiplexer unit. For a "sel" selection input equal to 1, the "w_{t1}" input will be transmitted to the output then in the opposite case the "w" which takes over.

- **A RAM block is an 8-bit address memory (addr) has:**

  - One entry coded on 16-bit (w_n).

  - Two control signals write (write), read (read) coded on 1 bit.

  - An output coded on 16-bit (w_c).

Figure 5.27 shows the functional simulation of a RAM block.

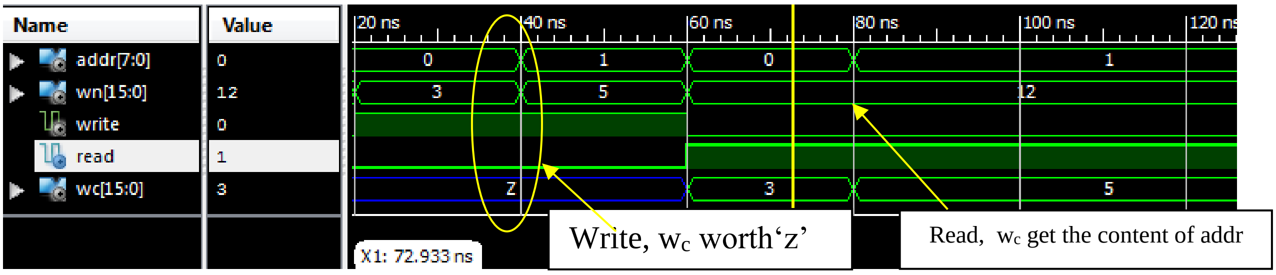

Figure 5.27 RAM simulation timing diagram.

The simulation results clearly show the correct functioning of the RAM. In the case where we are in write mode, the output is worth Z and we start to stack the addresses 0 and 1 of the RAM by the data present in input. Then, for the write mode, we recover the data stored in the addresses 0 and 1 output.

- **Multiplier Mult has:**

- Two inputs coded on 16 bits (d_{in0}, d_{in1}).

- An output coded on 16-bit (prod).

Figure 5.28 shows the functional simulation of the multiplier block.

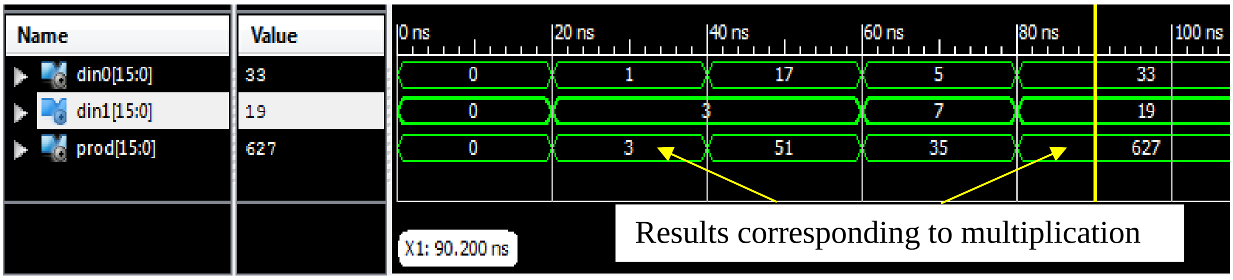

Figure 5.28 Simulation timing of a multiplier.

The simulation results clearly show the correct operation of the multiplier block. Namely, multiply the data presented at inputs “d_{in0} and d_{in1}” and present the result at output “prod”.

- **The Acc accumulator has:**

- An input coded on 16 bits (d_{in}).

- An output coded on 16 bits (doubt).

- Command signals coded on 1 bit (clock "clk", reset "" reset ").

Figure 5.29 shows the functional simulation of an accumulator.

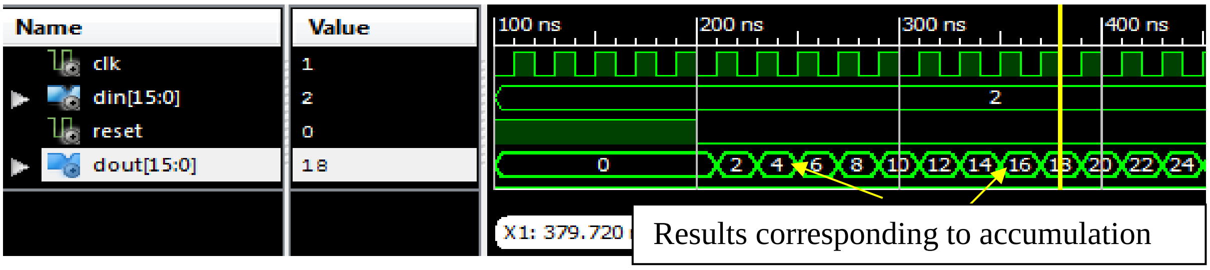

Figure 5.29 Simulation chronogram of an accumulator.

The simulation results clearly show the correct operation of the Acc block, namely adding the data present at the "d_{in}" input and outputting the result in "doubt".

• The activation block (LUT):

The Sigmoid possesses:

- An input addressed on 16 bits (a_i).
- An output coded on 16 bits (y_i).

Figure 5.30 shows the functional simulation of a sigmoid.

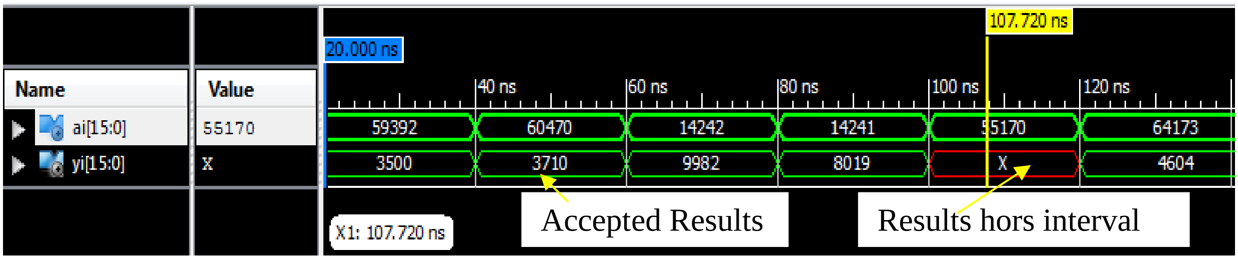

Figure 5.30 Simulation timing of a sigmoid.

We observe that the output result corresponds to the content of the sigmoid, if the value present at the input "a_i" is outside the operating interval of the function, the output "y_i" will be undefined.

• Complete neuron simulation results

Figure 5.31 shows the overall simulation of a neural network.

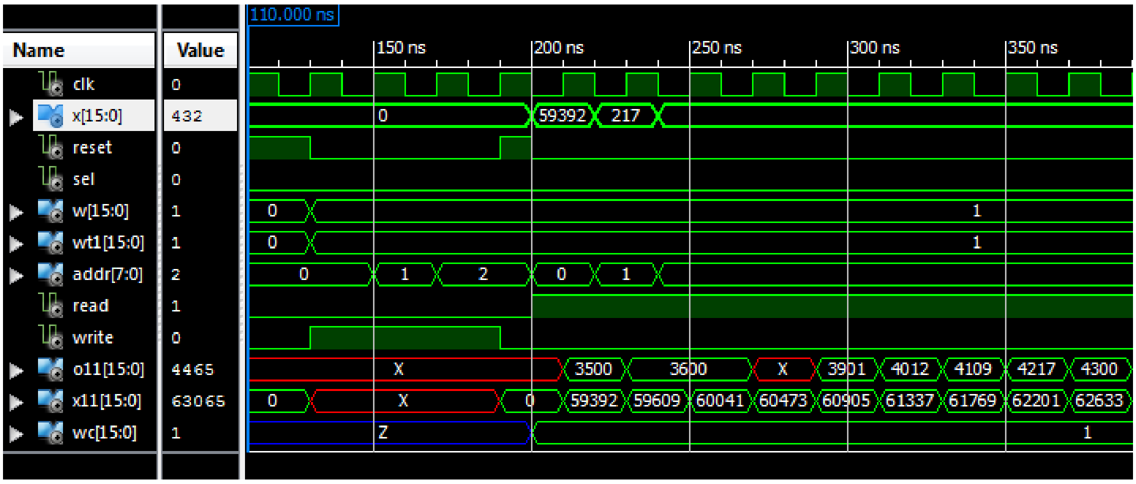

Figure 5.31 Neuron simulation timeline.

The simulation starts from 130 ns after resetting the system "reset" where we start to store the data of the synaptic weights "w_{t1} or w" (in our case w_t = w so we took sel = 0) in the RAM memory at the addresses " addr "corresponding, by choosing the write mode" write ".

After 3 clock ticks, we reset the system so that it can retrieve the stored data, then we go to read mode "read", in this phase the output of the RAM "w_c" goes from state "Z" at "1" which corresponds to the chosen synaptic weight, the latter first goes through the multiplier where it will be multiplied "w_c * x (1)" then the result will be stored in "x11" after the latter will be added to the new value "x (2) * w_c" and so on, in each clock tick if the value of x11 is outside the operating range of the sigmoid function, the result of the "O11" output of the neuron will be undefined. The "O11" output is defined by the following relation:

$$O_{11} = \sum w_c * x_i = w_c(1) * x(1) + w_c(2) * x(2) \qquad (5.3)$$

The simulation results clearly show the correct functioning of the blocks. We note that the circuit meets the required requirements, namely to multiply and then accumulate the data present in inputs.

Conclusion

Through this chapter, we have presented a synthesis methodology for FPGA implementation of a digital ANN diagnosing faults in PVG. We were interested in the study of FPGA circuits, their structures, the different circuits, the VHDL, and the ISE Xilinx software environment. The neuron being the essential nucleus of a neural network, we are therefore interested in the architecture of the latter. We first checked, validated the operation and implemented the VHDL code of the neuron architecture based on the activation function of the sigmoid type. The implementation was made on the FPGA circuit of VIRETX 5LX and before synthesis, simulation was required until the ANN meets the functional specifications. The proposed VHDL description is based on a simple, regular and parallel architecture. The use of the parametric VHDL description offers a high flexibility to the designer. These implementation results have been getting very high results quality, and good performances.

GENERAL CONCLUSION

GENERAL CONCLUSION

Commonly solar PV plants encounters failures during their life cycle, for this reason, it is necessary to detect and diagnose the PV system all the time, in order to avoid any loss of performance, and guarantee of service continuity. For the moment, artificial intelligence techniques are needed for diagnosing of the photovoltaic system and particularly the photovoltaic generator. The later are considered as the main part (the heart) of any PV plant. Automatic monitoring, supervision, detection, and diagnosis of faults that occur in solar photovoltaic generators have recently become a very important research topic. In this thesis work, an overview have been done of the main faults occurring in the PVG such as, SC, OC, LLF, GF,AF. Then, an efficient neural-network based approach have been developed for the diagnosis of failures scenarios at SC occurring in a photovoltaic generator. The developed method has been elaborated in three main steps, feeding experimental data to the neural networks, modelling of faults and decision about diagnosis. To achieve this, each imposed fault has been detected and classified. The obtained results confirm the effectiveness of the developed models to locate and identify different types of failures even with the presence of noises. The proposed fault diagnosis method can easily be generalized and applied to large scale PV plants. An implementation on FPGA card of the developed neural-network based approach for diagnosing PVG, have been done. A VHDL parametric hardware implementation have been synthesized and simulated, which gives good results.

BIBLIOGRAPHY

BIBLIOGRAPHY

[1] REN 21: RENEWABLES 2019 GLOBAL STATUS REPORT. Disponible à l'adresse: https://www.ren21.net/wp-content/uploads/2019/05/gsr_2019_full_report_en.pdf

[2] IEA PVPS report - Trends in Photovoltaic Applications 2020. Disponible à l'adresse: https://iea-pvps.org/wp-content/uploads/2020/11/IEA_PVPS_Trends_Report_2020-1.pdf

[3] JAGER-WALDAU, Arnulf. Snapshot of Photovoltaics—February 2020. Energies 2020, 13, 930; doi: 10.3390/en13040930. Disponible à l'adresse: https://doi.org/10.3390/en13040930

[4] YIHUA, Hu. WENPING, Cao. Theoretical Analysis and Implementation of Photovoltaic Fault Diagnosis. In: YIHUA, Hu. WENPING, Cao. Renewable Energy - Utilisation and System Integration. Edition, May 11th 2016, DOI: 10.5772/62057. Disponible à l'adresse: https://www.intechopen.com/books/renewable-energy-utilisation-and-system-integration/theoretical-analysis-and-implementation-of-photovoltaic-fault-diagnosis

[5] KHORSHED-ALAM, Mohamed. KHAN, Faisal. JONSON, Jay. FLICKER, Jack. A Comprehensive Review of Catastrophic Faults in PV Arrays: Types, Detection, and Mitigation Techniques. *IEEE Journal of Photovoltaics*. 2015, vol, 5, pp. 982-997. Disponible à l'adresse: DOI: 10.1109/JPHOTOV.2015.2397599.

[6] PEDRO, Branco. GONÇALVES, Francisco. COSTA, Aana Cristina. Tailored Algorithms for Anomaly Detection in Photovoltaic Systems. Energies 2020, vol, 13, p. 225, 01/02 2020. Disponible à l'adresse: https://doi.org/10.3390/en13010225

[7] QUINTANA, M. A. KING, D. L. MCMAHOM, T. J. and OSTERWALD C. R. Commonly observed degradation in field-aged photovoltaic modules, 19-24 May 2002. New Orleans, LA, USA. In Conference Record of the Twenty-Ninth IEEE Photovoltaic Specialists Conference, pp. 1436-1439. Disponible à l'adresse: 10.1109/PVSC.2002.1190879

[8] Snapshot of Global PV Markets 2020. (International Energy Agency) Report IEA-PVPS T1-37: 2020. Disponible à l'adresse: https://iea-pvps.org/wp-content/uploads/2020/04/IEA_PVPS_Snapshot_2020.pdf

[9] "PriceQuotes". *pv.energytrend.com*. Archived from the original on 26 June 2014. Retrieved 26 June 2014. (Growth of photovoltaics, from Wikipedia). Disponible à l'adresse: https://en.wikipedia.org/wiki/Growth_of_photovoltaics

[10] BOWDEN, Stuart. HONSBERG, Christiana. SCHRODER, Dieter. More's Law of Photovoltaics. Future Photovoltaics, May 2010.

[11] LUQUE, Antonio. HEGEDUS, Steven. *Handbook of Photovoltaic Science and Engineering*. Ed. John Wiley & Sons Ltd, England, 2003. Disponible à l'adresse: https://kashanu.ac.ir/Files/Content/Handbook.pdf

[12] LABOURET, Anne. CUMUNEL. Pascal, BRAUN, Jean Paul. FARRAGI, Benjamin. *Cellules solaires : Les bases de l'énergie photovoltaïque*. Ed Techniques Et Scientifiques Françaises, 5e édition DUNOD, 2010.

[13] ZAAMTA, Souad. *Réalisation d'un régulateur solaire à base de microcontrôleur pour le contrôle de l'état de charge et la protection des accumulateurs*. Mémoire de Magister. Université Larbi Ben M'hidi Oum-El-Bouaghi, 2008.

[14] http://en.wikipedia.org/wiki/File:Breakdown_of_the_incoming_solar_energy.svg

[15] YAICHE, M. R. BOUHANIK, A. BEKKOUCHE, S. M. A. BENOUAZ, T. A new modelling approach intended to develop maps of annual solar irradiation and comparative study using satellite data of Algeria. *JOURNAL OF RENEWABLE AND SUSTAINABLE ENERGY*. 2016, 8, 043702. Disponible à l'adresse: https://doi.org/10.1063/1.4958993

[16] CHRISTENSEN, Eric. Solar Energy: Photovoltaics, 2008. Disponible à l'adresse: http://pvcdrom.pveducation.org/index.html

[17] NAKAJIMA, Kazuo. USAMI, Noritaka. *Crystal Growth of Si for Solar Cells*. Advances in Materials Research. Springer Berlin Heidelberg, 2009.

[18] DELINE, Chris. PELAEZ, Silvana Ayala. MARION, Bill. SEKULIC, Bill. WOODHOUSE, Michael. STEIN, Josh. 46th IEEE Photovoltaic Specialists Conference. Bifacial PV System Performance: Separating Fact from Fiction, July 2019, Chicago. (Sandia National Labs) NREL 2019. Disponible à l'adresse: 10.13140/RG.2.2.23189.27365.

[19] POORTMANS, Jef. ARKHIPOV, Vladimir. *Thin Film Solar Cells Fabrication, Characterization and Applications*. Wiley. October 2006, 502 Pages. ISBN: 978-0-470-09127-2.

[20] SEKKAT, Zoheir. KNOLL, Wolfgang. *Photoreactive organic thin films*. Academic Press. 17th October 2002, 559 pages. ISBN: 9780080479972.

[21] RAZYKOV, T.M. FEREKIDES, C.S. MOREL, D. STEFANAKOS, E. ULLAL, H.S. UPADHYAYA, H.M. Solar photovoltaic electricity: Current status and future prospects. Solar Energy. 2011, 85, 8, 1580–1608. Disponible à l'adresse: https://doi.org/10.1016/j.solener.2010.12.002

[22] JHA, A.R. *Solar Cell Technology and Applications*. Taylor and Francis Group, 2009. Disponible à l'adresse: https://doi.org/10.1201/9781420081787

[23] KRISHNAN, Unni. KAUR, Manjot. KUMAR, Manjeet. KUMAR, Akshay. Factors affecting the stability of perovskite solar cells: a comprehensive review. Journal of Photonics for Energy, 2019, 9, 2. https://doi.org/10.1117/1.JPE.9.021001

[24] https://www.nrel.gov/pv/cell-efficiency.html (National Renewable Energy Laboratory).

[25] XIAO, Weidong. *Photovoltaic Power System: Modeling, Design, and Control*. JohnWiley & Sons Ltd. July 2017, 400 Pages. ISBN: 978-1-119-28034-7

[26] R, PATEL, Mukund. *Wind and Solar Power Systems*: *Design, Analysis, and Operation*. CRC Press. July 2005, 368 Pages. ISBN 9780849315701

[27] KALDELLIS, J. K. *Stand-alone and hybrid wind energy systems: Technology, energy storage and applications*. Woodhead Publishing. July 2010, 576 Pages. ISBN: 9781845699628

[28] BUN, Long. *Détection et localisation de défauts dans un système photovoltaïque*. Thèse de doctorat : Energie électrique. France : Université de Grenoble, 2011. Français. 207 Pages.

[29] DIAZ, P. M. EGIDO, A. NIEUWENHOUT, F. Dependability analysis of stand-alone photovoltaic systems. *Progress in Photovoltaic: Research and Applications*. 2007, vol. 15, pp. 245-264.

[30] CEC. Guidelines for the Assessment of Photovoltaic Plants. Document B, Analysis and Presentation of Monitoring Data. *Commission of the European Communities*, 1997.

[31] IEC. Photovoltaic System Performance Monitoring: Guidelines for Measurement, Data Exchange and Analysis. in International Standard IEC 61724, ed, 1998.

[32] HACHANA, Oussama. *Etude d'un système photovoltaïque en vue du diagnostic*. Thèse de Dcoctort: Electrotechnique. Algérie: Université Farhat Abbas-Sétif1, 2015. Disponible à l'adresse: http://dspace.univ-setif.dz:8888/jspui/handle/123456789/1739

[33] BOUACHA, Saida. *Study on Photovoltaic Power Plant Connected to the Distribution Network*. Thèse de Doctorat: Electronique. Algérie : Ecole Nationale Polytechnique, 2021.

[34] SANTIAGO, I. TRILLO MONTERO, D. LUNA RODRIGUEZ, J. J. MORENO GRACIA, I. M. PALACIOS GARCIA, E. J. Graphical Diagnosis of Performances in Photovoltaic Systems: A Case Study in Southern Spain. *Energies*, 2017, vol. 10, 12, p. 1964. Disponible à l'adresse: https://doi.org/10.3390/en10121964

[35] DHIPATYA SYAHINDRA, Kianda. MA'ARIF, Samsul. ANINDITO WIDAYAT, Aditya. FAKHRUL FAUZI, Ahmad. ADHI SETIAWAN, Eko / 2nd International Conference on Power, Energy and Electrical Engineering (PEEE 2020). *Solar PV System Performance Ratio Evaluation for Electric Vehicles Charging Stations in Transit Oriented Development (TOD) Areas*, E3S Web of Conferences, 2021, Vol. 231, 02002. Disponible à l'adresse: https://doi.org/10.1051/e3sconf/202123102002

[36] LINDIG, S. KAAYA, I. WEISS, K. MOSER, D. TOPIC, M. Review of Statistical and Analytical Degradation Models for Photovoltaic Modules and Systems as Well as Related Improvements. *IEEE Journal of Photovoltaics*, 2018, vol. 8, p. 1773-1786. Disponible à l'adresse: 10.1109/JPHOTOV.2018.2870532

[37] LAUKAMP, H. SCHOEN, T. RUOSS, D. Reliability Study of Grid Connected PV Systems: Field Experience and Recommended Design Practice. *Report IEA-PVPS T7-08*. 2002 p. 31. Disponible à l'adresse: https://iea-pvps.org/wp-content/uploads/2020/01/rep7_08.pdf

[38] HAEBERLIN, Heinrich. GRAF, J. D. FACHHOCHSCHULE, Berner / 2nd World Conference on Photovoltaic Solar Energy Conversion. *Gradual Reduction of PV Generator Yield due to Pollution*. Vienna, Austria, Published 1998. Disponible à l'adresse: http://www.vipclean.it/files/evtdoc-14.pdf

[39] DELINE, Chris / 35th IEEE Photovoltaic Specialists Conference. *Partially shaded operation of multi-string photovoltaic systems*. Honolulu, HI, USA, 2010. pp. DOI: 000394-000399.

[40] SILVERMAN, Timothy. J. DECEGLIE, M. G. SUBEDI, I. PODRAZA, N. J. SLAUCH, I. M. FERRY, V. E. Reducing Operating Temperature in Photovoltaic Modules. *IEEE Journal of Photovoltaics*. 2018, vol. 8, pp. 532-540.

[42] COELLO, M. BOYLE, L. Simple Model for Predicting Time Series Soiling of Photovoltaic Panels. *IEEE Journal of Photovoltaics*. 2019, vol. 9, pp. 1382-1387. DOI: 10.1109/JPHOTOV.2019.2919628

[43] MELLIT, Adel. TINA, G. M. KALOGIROU, S. A. Fault detection and diagnosis methods for photovoltaic systems: A review. *Renewable and Sustainable Energy Reviews*. 2018, vol. 91, pp. 1-17. Disponible à l'adresse: https://doi.org/10.1016/j.rser.2018.03.062

[44] PILLAI, Dhanup. S. RAJASEKAR, N. A comprehensive review on protection challenges and fault diagnosis in PV systems. *Renewable and Sustainable Energy Reviews*. 2018, vol. 91, pp. 18-40. Disponible à l'adresse: https://doi.org/10.1016/j.rser.2018.03.082

[45] MEYER, E. L. DYK, E. E. v. Assessing the reliability and degradation of photovoltaic module performance parameters. *IEEE Transactions on Reliability*. 2004, vol. 53, pp. 83-92. DOI: 10.1109/TR.2004.824831

[46] JONES, Russel. K. BARAS, Abdulaziz. AL SAEERI, Abdullah. AL QAHTANI, Aymen. AL AMOUDI, Ahmed. AL SHAYA, Yousef. ALODAN, Maher. Optimized Cleaning Cost and Schedule Based on Observed Soiling Conditions for Photovoltaic Plants in Central Saudi Arabia. *IEEE Journal of Photovoltaics*. 2016, vol. 6, pp. 730-738. DOI: 10.1109/JPHOTOV.2016.2535308

[47] GUERRIERO, P. DALIENTO, S. Toward a Hot Spot Free PV Module. *IEEE Journal of Photovoltaics*. 2019, vol. 9, pp. 796-802. DOI: 10.1109/JPHOTOV.2019.2894912

[48] WOYTE, A. NIJS, J. BELMANS, R. Partial shadowing of photovoltaic arrays with different system configurations: literature review and field test results. *Solar Energy*. 2003, vol. 74, pp. 217-233. https://doi.org/10.1016/S0038-092X(03)00155-5

[49] KING, D. QUINTANA, M. KRATOCHVIL, J. ELLIBEE, D. HANSEN, B. Photovoltaic module performance and durability following long-term field exposure. *Progress in Photovoltaics: Research and Applications*. 2000, vol. 8, pp. 241-256. Disponible à l'adresse: http://www.irantahgig.ir/wp-content/uploads/30329.pdf

[50] MUNOZ, M. A. ALONSO-GARCIA, M. C. VELA, Nieves. CHENLO, F. Early degradation of silicon PV modules and guaranty conditions. *Solar Energy*. 2011, vol. 85, pp. 2264-2274. Disponible à l'adresse: http://oa.upm.es/10081/2/doi.10.1016.j.solener.2011.06.011.pdf

[51] KONTGES, M. KURTZ, S. PACKARD, C. JAHN, U. BERGER, K. KATO, K. Review of Failures of Photovoltaic Modules. Report IEA-PVPS T13-01:2014. Disponible à l'adresse: https://www.sunsniffer.de/images/imge_slide/IEA-PVPS_T13-01_2014_Review_of_Failures_of_Photovoltaic_Modules_Final_.pdf

[52] PEI, Tingting. HAO, Xiaohong. A Fault Detection Method for Photovoltaic Systems Based on Voltage and Current Observation and Evaluation. *Energies*. 2019, 12, 1712; doi: 10.3390/en12091712. https://doi.org/10.3390/en12091712

[53] KAPLANI, Eleni. Degradation Effects in sc---Si PV Modules Subjected to Natural and Induced Ageing after Several Years of Field Operation. *Journal of Engineering Science and Technology Review*. 2012, vol. 5, 4, 18-23. Special Issue on Renewable Energy Systems. DOI: 10.25103/jestr.054.04

[54] BROOKS, William. Field Guide for Testing Existing Photovoltaic Systems for Ground Faults and Installing Equipment to Mitigate Fire Hazards. NREL/SR-5D00-65050, October 2015. Disponible à l'adresse: https://www.nrel.gov/docs/fy16osti/65050.pdf

[55] FLICKER, Jack. JOHNSON, Jay. Photovoltaic Ground Fault Detection Recommendations for Array Safety and Operation. *Solar Energy*. 2016, Vol. 140, pp. 34-50. DOI: 10.1016/j.solener.2016.10.017

[56] ZHAO, Ye. DE PALMA, Jean François. MOSESIAN, Jerry. LYONS, Robert. LEHMAN, Brad. Line–Line Fault Analysis and Protection Challenges in Solar Photovoltaic Arrays. *IEEE Transactions on Industrial Electronics*. SEPTEMBER 2013, Vol. 60, NO. 9. DOI: 10.1109/TIE.2012.2205355

[57] YI, Zhehan. ETEMADI, Amir H. 2016 IEEE Power and Energy Society General Meeting (PESGM). A Novel Detection Algorithm for Line-to-Line Faults in Photovoltaic (PV) Arrays Based on Support Vector Machine (SVM). 2016. Boston, MA, USA. DOI: 10.1109/PESGM.2016.7742026. ISSN: 1944-9933.

[58] XIONGA, Qing. JIA, Shengchang. LIUA, Xiaojun. FENG, Xianyong. ZHANGA, Fan. ZHUA, Lingyu. GATTOZZI, Angelo L. HEBNER, Robert E. Detecting and localizing series arc fault in photovoltaic systems based on time and frequency characteristics of capacitor current. *Solar Energy*. 2018, vol. 170, p. 788-799. https://doi.org/10.1016/j.solener.2018.06.004

[59] WEERASEKARA, Medhawa. *DC Arc Faults In Photovoltaic Systems*. Thesis: Electrical Engineering & Computer Science. Queensland University of Technology, 2019. Disponible à l'adresse: https://eprints.qut.edu.au/130681/1/Madhawa_Weerasekara_Thesis.pdf

[60] PIERDICA, R. MALINVERNI, E. PICCININI, F. PAOLANTI, M. FELICETTI, A. ZINGARETTI, P. Deep convolutional neural network for automatic detection of damaged photovoltaic cells. *ISPRS - International Archives of the Photogrammetry, Remote Sensing and Spatial Information Sciences*. 05/30 2018, Vol. XLII-2, pp. 893-900. DOI: 10.5194/isprs-archives-XLII-2-893-2018

[61] VENKATESH S, Naveen. SUGUMARAN, V. Fault diagnosis of visual faults in photovoltaic modules: A Review. *International journal of green energy*. 2021, Vol. 18, - Issue 1. https://doi.org/10.1080/15435075.2020.1825443

[62] JEON, Hyewon. *Thermal image analysis for fault detection and diagnosis of PV systems*. Thesis. Indiana: West Lafayette, May 2020.

[63] NATARAJAN, Karuppiah. PRAVEEN KUMAR, B. SAMPATH KUMAR, Vankadara. Fault Detection of Solar PV system using SVM and Thermal Image Processing. *International journal of renewable energy research*. June 2020, Vol.10, No.2. Disponible à l'adresse: https://www.ijrer.org/ijrer/index.php/ijrer/article/view/10775/pdf

[64] PLATON, Radu. MARTEL, J. WOODRUFF, N. CHAU, T. Y. Online Fault Detection in PV Systems. *IEEE Transactions on Sustainable Energy*. 2015, Vol. 6, pp. 1200-1207. DOI: 10.1109/TSTE.2015.2421447

[65] APPIAH, A. Y. ZHANG, X. AYAWLI, B. B. K. KYEREMEH, F. Review and Performance Evaluation of Photovoltaic Array Fault Detection and Diagnosis Techniques. *International Journal of Photoenergy*. 2019, vol. 2019, p. 19. https://doi.org/10.1155/2019/6953530. Disponible à l'adresse: https://downloads.hindawi.com/journals/ijp/2019/6953530.pdf

[66] VERGURA, Silvano. ACCIANI, Guiseppe. AMORUSO, Vitantonio. PATRONO, Guiseppe. E. VACCA, F. Descriptive and Inferential Statistics for Supervising and Monitoring the Operation of PV Plants. *IEEE Transactions on Industrial Electronics*. 2009, vol. 56, pp. 4456-4464. DOI: 10.1109/TIE.2008.927404

[67] TAKASHIMA, Takumi. YAMAGUCHI, Junji. ISHIDA, Masayoshi / 33rd IEEE Photovoltaic Specialists Conference. Fault detection by signal response in PV module strings, 11-16 May 2008, San Diego, CA, USA. IEEE ,2008, pp. 1-5. DOI: 10.1109/PVSC.2008.4922843

[68] JOHNSON, Jay. KUSZMAUL, Scott. BOWER, Ward. SCHOENWALD, David. Using PV module and line frequency response data to create robust arc fault detectors. SAND2011-6307C, 2011. Disponible à l'adresse: https://www.osti.gov/servlets/purl/1119759

[69] CHOUDER, Aissa. *Analysis, diagnosis and fault detection in photovoltaic systems*. Thesis: doctorals. Spain: Universitat Politècnica de Catalunya, 2010.

[70] DA SILVA, Mário Filipe Aires. *Analysis of new indicators for Fault detection in grid connected PV systems for BIPV applications*. Thesis: GEOGRAPHICAL, GEOPHYSICAL AND ENERGY ENGINEERING. Portugual: UNIVERSIDADE DE LISBOA, 2014. Disponible à l'adresse: https://core.ac.uk/download/pdf/32329402.pdf

[71] KANG, Byung Kwan. KIM, Seung Tak. BAE, Sun Ho. PARK, Jung Wook. Diagnosis of Output Power Lowering in a PV Array by Using the Kalman-Filter Algorithm. *IEEE Transactions on Energy Conversion*. 2012, vol. 27, pp. 885-894. DOI: 10.1109/TEC.2012.2217144

[72] CHOUDER, Aissa. SILVESTRE, Santiago. Automatic supervision and fault detection of PV systems based on power losses analysis. *Energy Conversion and Management*. 2010, Vol. 51, pp. 1929-1937. https://doi.org/10.1016/j.enconman.2010.02.025

[73] MIWA, Masaki. YAMAKA, S. KAWAMURA, H. OHNO, H. KAWAMURA, H / IEEE 4th World Conference on Photovoltaic Energy Conference. *Diagnosis of a Power Output Lowering of PV Array with a (-dI/dV)-V Characteristic*, Waikoloa, HI, USA , 7-12 May 2006, IEEE, pp. 2442-2445. ISSN: 0160-8371. DOI: 10.1109/WCPEC.2006.279703.

[74] CHINE, W. MELLIT, A. LUGHI, V. MALEK, A. SULLIGOI, G. MASSI PAVAN, A. A novel fault diagnosis technique for photovoltaic systems based on artificial neural networks. *Renewable Energy*. 2016, Vol. 90, pp. 501-512. https://doi.org/10.1016/j.renene.2016.01.036

[75] BERMEJO, Jesus Ferrero. FERNANDEZ, Juan Francisco Gomez. FOLIVENCIA POLO, Fernando Augustin. CRESPO MARQUEZ, Adolfo. A Review of the Use of Artificial

Neural Network Models for Energy and Reliability Prediction. A Study of the Solar PV, Hydraulic and Wind Energy Sources. *Applied Sciences*. 2019, Vol. 9, p. 1844. DOI: 10.3390/app9091844

[76] MELLIT, Adel. KALOGIROU, Soteris. A. Artificial intelligence techniques for photovoltaic applications: A review. *Progress in Energy and Combustion Science*. 2008, Vol. 34, pp. 574-632. https://doi.org/10.1016/j.pecs.2008.01.001

[77] YUCHUAN, W. QINLI, L. YAQIN, S / International Conference on Mechatronics and Automation. *Application of BP neural network fault diagnosis in solar photovoltaic system*. Changchun, China, 9-12 Aug. 2009. IEEE, pp. 2581-2585. DOI: 10.1109/ICMA.2009.5246742

[78] HWANG, Hye Rin. KIM, Berm Soo. CHO, Tae Hyun. LEE, In Soo. Implementation of a Fault Diagnosis System Using Neural Networks for Solar Panel. *International Journal of Control Automation and Systems*. 2019, Vol. 17, pp. 1050-1058.

[79] SYAFARUDDIN, KARATEPE, E. HIYAMA, T / 6th International Conference on Intelligent System Applications to Power Systems. *Controlling of artificial neural network for fault diagnosis of photovoltaic array*, Hersonissos, Greece, 25-28 Sept. 2011. IEEE. 18 November 2011, pp. 1-6. DOI: 10.1109/ISAP.2011.6082219

[80] ZHAO, Ye. YANG, Ling. LEHMAN, Brad. DE PALMA, Jean. François. MOSESIAN, Jerry. LYONS, Robert / in 2012 Twenty-Seventh Annual IEEE Applied Power Electronics Conference and Exposition (APEC). *Decision tree-based fault detection and classification in solar photovoltaic arrays*, Orlando, FL, USA, 5-9 Feb. 2012. IEEE, 09 March 2012. pp. 93-99. DOI: 10.1109/APEC.2012.6165803

[81] ZAKI A. Sayed. ZHU, Honglo. YAO, Jianxi. / International Conference on Sustainable and Renewable Energy Engineering (ICSREE 2019). *Fault detection and diagnosis of photovoltaic system using fuzzy logic control*. E3S Web Conf., 2019, Vol. 107, p. 02001. https://doi.org/10.1051/e3sconf/201910702001

[82] ZHAO, Qiang. SHAO, Shuai. LU, Lingxing. LIU, Xin. ZHU, Hong Lu. A New PV Array Fault Diagnosis Method Using Fuzzy C-Mean Clustering and Fuzzy Membership Algorithm. *Energies*, 01/19 2018, Vol. 11, p. 238. https://doi.org/10.3390/en11010238

[83] BONSIGNORE, Luca. DAVARIFAR, Mehrdad. RABHI, Abdelhamid. TINA, Giuseppe. M. ELHAJJAJJI, Ahmed. Neuro-Fuzzy Fault Detection Method for Photovoltaic Systems. *Energy Procedia*, 2014, Vol. 62, pp. 431-441. https://doi.org/10.1016/j.egypro.2014.12.405

[84] LIAO, Zhenguai. WANG, DAZHENG. TANG, Liangliang. REN, Jinli. ZHUMING . Liu. A Heuristic Diagnostic Method for a PV System: Triple-Layered Particle Swarm Optimization–Back-Propagation Neural Network. *Energies*, MDPI, 2017, Open Access Journal, Vol. 10(2), pp. 1-11. https://doi.org/10.3390/en10020226

[85] PRADEEP KUMAR, B. P. ILANGO, G. S. REDDY, M. J. B. CHILAKAPATI, N. Online Fault Detection and Diagnosis in Photovoltaic Systems Using Wavelet Packets. *IEEE Journal of Photovoltaics*. 2018, vol. 8, pp. 257-265. 10.1109/JPHOTOV.2017.2770159

[86] WU, Yue. CHEN, Zhicong. WU, Lijun. LIN, Peijie. CHENG, Shuying. LU, Peimin. An Intelligent Fault Diagnosis Approach for PV Array Based on SA-RBF Kernel Extreme Learning Machine. *Energy Procedia*, 2017, Vol. 105, pp. 1070-1076. https://doi.org/10.1016/j.egypro.2017.03.462

[87] HACHANA, Oussama. TINA, Giuseppe Marco. HEMSAS, Kamel Eddine. PV array Fault Diagnostic Technique for BIPV Systems Oussama 2016. *Energy and Buildings*. 2016, Vol. 126, 15, pp. 263-274. https://doi.org/10.1016/j.enbuild.2016.05.031

[88] SERA, D. TEDORESCU, R. RODRIGUEZ, P / in 34th Annual Conference of IEEE Industrial Electronics. *Photovoltaic module diagnostics by series resistance monitoring and temperature and rated power estimation*, Orlando, FL, USA, 10-13 Nov. 2008. IEEE. 23 January 2009, pp. 2195-2199. DOI: 10.1109/IECON.2008.4758297

[89] BASTIDAS RODRIGUEZ J. D. FRANCO, E. PETRONE, G. RAMOS PAJA, C. A. SPAGNUOLO, G. Quantification of photovoltaic module degradation using model based indicators. *Mathematics and Computers in Simulation*, 2017, Vol. 131, pp. 101-113. https://doi.org/10.1016/j.matcom.2015.04.003

[90] LIN, Hanwei. CHEN, Zhicong. WU, Lijun. LIN, Peijie. CHENG, S. On-line Monitoring and Fault Diagnosis of PV Array Based on BP Neural Network Optimized by Genetic Algorithm. *Springer, Cham*, 2015. https://doi.org/10.1007/978-3-319-26181-2_10

[91] TINA, Giuseppe Marco. COSENTINO, Fabio. VENTURA, Cristina. Monitoring and Diagnostics of Photovoltaic Power Plants. *Renewable Energy in the Service of Mankind*. 2016, Vol. II, pp. 505-516. https://doi.org/10.1007/978-3-319-18215-5_45

[92] BRESSAN, Mickael. EL BASRI, Youssef. GUTIEREZ, Alonso. ALONSO, Corinne. A shadow fault detection method based on the standard error analysis of I-V curves. *Renewable Energy*. *Elsevier*. 2016, 99, pp.1181-1190. DOI: 10.1016/j.renene.2016.08.028

[93] FADHEL, S. DELPHA, Claude. DIALLO, Demba. BAHRI, I. MIGAN, A. TRABELSI, M. MIMOUNI, M.F. PV shading fault detection and classification based on I-V curve using principal component analysis: Application to isolated PV system. *Solar Energy, Elsevier*. 2019, Vol. 179, pp.1-10. https://doi.org/10.1016/j.solener.2018.12.048

[94] DAVARIFAR, M. RABHI, A. HAJJAJI, A. KAMAL, E. DANESHIFAR, Z. Partial / 3rd International Conference on Renewable Energy Research and Applications. *Shading Fault Diagnosis in PV System With Discrete Wavelet Transform (DWT)*, Milwakuee, USA, 19-22 Oct 2014. IEEE: 22 January 2015. ISBN:978-1-4799-3795-0

[95] SAYFARUDDIN, ZINGER, Donald S. Review on Methods of Fault Diagnosis in Photovoltaic System Applications. *Journal of Engineering Science and Technology Review*. 2019, 12 (5) 53 – 66. DOI: 10.25103/jestr.125.07

[96] CHEN, Ling. HAN, Wei. LI, Hai-Tao. XU, Zi-Kun. ZHANG, Jing-Wei. CAO, Xiang. Long distance wireless fault diagnosis for photovoltaic modules based on back propagation neural network. *The International Journal of Electrical Engineering & Education*. 2020. https://doi.org/10.1177/0020720920940601

[97] ARMIJO, Kenneth M. JOHNSON, Jay. HIBBS, Michael. FRESQUEZ, Armando / 2014 IEEE 40th Photovoltaic Specialists Conference (PVSC). *Characterizing Fire Danger from Low-Power Photovoltaic Arc-Faults*. SAND2014-4593C. DOI: 10.1109/PVSC.2014.6925658

[98] AL HOUSANI, Mohammed. BICER, Yusuf. KOC, Muammer. Assessment of Various Dry Photovoltaic Cleaning Techniques and Frequencies on the Power Output of CdTe-Type Modules in Dusty Environments. *Sustainability*. 2019, 11, 2850; doi: 10.3390/su11102850. https://doi.org/10.3390/su11102850

[99] SARAVANAN, V. DARVEKAR, S. Solar Photovoltaic Panels Cleaning Methods: A Review. *International Journal of Pure and Applied Mathematics*. 2018, Vol. 118 No. 24.

[100] CHEDDADI, Youssef. CHEDDADI, Hafsa. CHEDDADI, Fatima. ERRAHIMI, Fatima. ESSBAI, Najia. Design and implementation of an intelligent low-cost IoT solution for energy monitoring of photovoltaic stations. *SN Applied Sciences, Springer,* 2020. https://doi.org/10.1007/s42452-020-2997-4. Disponible à l'adresse: https://link.springer.com/content/pdf/10.1007/s42452-020-2997-4.pdf

[101] TCHOKETCH KEBIR, Selma. CHEGGAGA, Nawal. AIT CHEIKH, Mohamed Salah. HADDADI, Mourad. RAHMANI, Hachemi. A comprehensive study of diagnosis faults techniques occurring in photovoltaic generators. *Engineering Review*. 2021, Vol. 41, No. 03. Disponible à l'adresse: https://doi.org/10.30765/er.1714

[102] IZADIAN, A. POURTAHERIAN, A. MOTAHARI, S / IEEE Energy Conversion Congress and Exposition (ECCE) . *Basic Model and Governing Equation of Solar Cells used in Power and Control Applications*, Raleigh, NC, USA, 15-20 Sept. 2012. IEEE, 12 November 2012. DOI: 10.1109/ECCE.2012.6342639

[103] TIAN, Hongmei. MANCILLA DAVID, Fernando. ELLIS, Kevin. MULJADI, Eduard. JENKINS, Peter. A cell-to-module-to-array detailed model for photovoltaic panels. *Solar Energy*. 2012, Vol. 86, 2695–2706. https://doi.org/10.1016/j.solener.2012.06.004

[104] KENNETH, L. KENNERUD. Analysis of Performance Degradation in CdS Solar Cells. *IEEE Transactions on aerospace and electronic systems*. 1969, Vol. AES-5, NO. 6, 912 – 917. DOI: 10.1109/TAES.1969.309966

[105] MA, Jieming. *Optimization Approaches for Parameter Estimation and Maximum Power Point Tracking (MPPT) of Photovoltaic Systems*. Thesis: Doctor in Philosophy. Royume Uni: University of Liverpool. August 2014. Disponible à l'adresse: https://livrepository.liverpool.ac.uk/2006662/1/MaJie_Aug2014_2002783.pdf

[106] SAHA, Chitta. AGBU, Naomi. JINKS, Robert. HUDA, Nazmul. Review article of the solar PV parameters estimation using evolutionary algorithms. *MOJ Solar and Photoenergy Systems*. 2018, Vol. 2. No. 2, p.66–78. DOI: 10.15406/mojsp.2018.02.00026

[107] BASHAHU, M. HABYARIMANA, A. Review and test of methods for determination of the solar cell series resistance. *Pergamon, Renewable Energy, Elsevier.* 1995, Vol. 6(2), pages 129-138. DOI: 10.1016/0960-1481(94) E0021-V.

[108] TCHOKETCH KEBIR, Selma. HADDADI, Mourad. AIT CHEIKH, Mohamed Salah/ 3rd International Conference on Control, Engineering & Information Technology CEIT. *An Overview of Solar Cells Parameters Extraction Methods*, Tlemcen, Algeria, 25-27 May 2015. IEEE proceedings, 03 September 2015. **DOI:** 10.1109/CEIT.2015.7232987

[109] TCHOKETCH KEBIR, Selma. A summary of methods to get parameters values of photovoltaic cells/panels". Revue des Energies Renouvelables du CDER : JREEN -20-07-022 : (Journal of Renewable Energies (Revue des Energies Renouvelables)), Volume 23, numéro 1, novembre 2020. Disponible à l'adresse: https://www.asjp.cerist.dz/en/article/133867

[110] DUFFIE, John A. BECKMAN, A. William. *Solar Engineering of Thermal Processes*. Book, Second Edition, John Wiley & Sons, INC, June 1980. Chap 23. (P 777). Disponible à l'adresse:https://www.sku.ac.ir/Datafiles/BookLibrary/45/John%20A.%20Duffie,%20William%20A.%20Beckman(auth.)-Solar%20Engineering%20of%20Thermal%20Processes,%20Fourth%20Edition%20(2013).pdf

[111] GHANI, F. ROSENGARTEN, G. DUKE, M. CARSON J.K. The numerical calculation of single-diode solar-cell modelling parameters. *Renewable Energy*. 2014, Vol. 72, 105-112. https://doi.org/10.1016/j.renene.2014.06.035

[112] HUAN-LIANG, T. Insolation-oriented model of photovoltaic module using Matlab/Simulink. *Solar Energy*. 2010, Vol. 84, 1318–1326. Disponible à l'adresse: https://www.tarjomefa.com/wp-content/uploads/2018/08/TarjomeFa-F1005-English.pdf

[113] CARRERO, C. RAMIREZ, D. RODRIGUEZ, J. PLATERO, C.A. Accurate and fast convergence method for parameter estimation of PV generators based on three main points of the I-V curve. *Renewable Energy*. 2011, Vol. 36, 2972-2977. Disponible à l'adresse: http://www.sciencedirect.com/science/article/pii/S0960148111001698

[114] ORIOLI, Aldo DI GANG, Alessandra. A procedure to calculate the five-parameter model of crystalline silicon photovoltaic modules on the basis of the tabular performance data. *Applied Energy*. 2013, Vol. 102, 1160–1177. Disponible à l'adresse: http://www.sciencedirect.com/science/article/pii/S0306261912004813

[115] MUHAMMAD, Fahmi F. KARIM SANGAWI, Ali W. HASHIM, Suhairul. GHOSHAL, S. K. ISAM, K. ABDULLAH, Shilan. HAMEED. Simple and efficient estimation

of photovoltaic cells and modules parameters using approximation and correction technique. *PLoS ONE*. 2019, Vol. 14, 5, e0216201. https://doi.org/10.1371/journal.pone.0216201

[116] DI PIAZZA, Maria Carmela. LUNA, Massimiliano. PETRONE, Giovanni. SPAGNUOLO, Giovanni. Translation of the Single-Diode PV Model Parameters Identified by Using Explicit Formulas. *IEEE Journal of Photovoltaics*. July 2017, Vol. 7, Issue: 4. DOI: 10.1109/JPHOTOV.2017.2699321

[117] KASHIF, Ishaque. ZAINAL, Salam. HAMED, Taheri. Simple, fast and accurate two-diode model for photovoltaic modules. *Solar Energy Materials & Solar Cells*. 2011, Vol.95, 586–594. DOI: 10.1016/j.solmat.2010.09.023

[118] CABESTANY, J. CASTANIER, Louis. Evaluation of solar cell parameters by nonlinear algorithms. *J. Phys. D: Appl. Phys*. 1983, Vol.16, 2547.

[119] EASWARAKHANTHAN, T. BOTTIN, J. BOUHOUCH, I. BOUTRIT, C. Nonlinear Minimization Algorithm for Determining the Solar Cell Parameters with Microcomputers. *International Journal of Solar Energy*. 1986, Vol.6, N°.1. https://doi.org/10.1080/01425918608909835

[120] AYODELE, T.R. OGUNJUYIGBE, A.S.O. EKOH, E.E. Evaluation of numerical algorithms used in extracting the parameters of a single-diode photovoltaic model. *Sustainable Energy Technologies and Assessments*. 2016, Vol.13, 51–59. https://doi.org/10.1016/j.seta.2015.11.003

[121] RASHEDI, E. NEZAMABADI, H. SARYAZDI, S. GSA: a gravitational search algorithm. *Information sciences*. 2009, Vol. 179, pp. 2232-2248. https://doi.org/10.1016/j.ins.2009.03.004

[122] CHENA, Meng-Hui. CHANG, Pei-Chann. WU, Jheng-Long. A population-based incremental learning approach with artificial immune system for network intrusion detection. *Engineering Applications of Artificial Intelligence*. 2016, Vol. 51, N°C. pp 171–181. https://doi.org/10.1016/j.engappai.2016.01.020

[123] BENI, Gerrardo. WANG, Jing. Swarm intelligence in cellular robotic systems, in Robots and Biological Systems: Towards a New Bionics. *Springer*. 1993, pp. 703-712. DOI: 10.1007/978-3-642-58069-7_38

[124] KASHIF, Ishaque. ZAINAL, Salam. HAMED, Taheri. SHAMSUDIN, Amir. A critical evaluation of EA computational methods for Photovoltaic cell parameter extraction based on two diode model. *Solar Energy*. September 2011, Volume 85, Issue 9, Pages 1768-1779. https://doi.org/10.1016/j.solener.2011.04.015

[125] KASHIF, Ishaque. ZAINAL, Salam. An improved modeling method to determine the model parameters of photovoltaic (PV) modules using differential evolution (DE). *Solar Energy*. 2011, Vol. 85, p.2349–2359. https://doi.org/10.1016/j.solener.2011.06.025

[126] ZAGROUBAA, M. SELLAMI, A. BOUICHA, M. KSOURI, M. Identification of PV solar cells and modules parameters using the genetic algorithms: Application to maximum power extraction. Solar Energy. 2010, Vol.84 p.860–866. https://doi.org/10.1016/j.solener.2010.02.012

[127] AL HAJRI, M.F. EL NAGGAR, K.M. ALRASHIDI, M.R. AL OTHMAN, A.K. Optimal extraction of solar cell parameters using pattern search. *Renewable Energy*. 2012, Vol.44, p.238-245. DOI: 10.1016/j.renene.2012.01.082

[128] EL NAGGAR, K.M. AL RASHIDI, M.R. ALHAJRI, M.F. AL OTHMAN, A.K. Simulated Annealing algorithm for photovoltaic parameters identification. *Solar Energy*. 2012, Vol.86, p.266–274. DOI: 10.1016/j.solener.2011.09.032

[129] YURTKURAN, Alkın. KUCUKOGLU, İlker / 16th International Conference on Clean Energy (ICCE). Comparative study of physics-inspired meta-heuristic algorithms for the solar cell parameter identification problem. 2018.

[130] ASKARZADEH, A. REZAZADEH, A. Parameter identification for solar cell models using harmony search-based algorithms. *Solar Energy*. 2012, Vol. 86, N. 11, p.86:3241–9. https://doi.org/10.1016/j.solener.2012.08.018

[131] RAJASEKAR NEERAJA, N. KRISHMA KUMAR, Rini Venugopala. Bacterial Foraging Algorithm based solar PV parameter estimation. *Solar Energy*. November 2013, Vol. 97, P. 255-265. https://doi.org/10.1016/j.solener.2013.08.019

[132] QUN, Niu. HONGYUN, Zhang. KANG, Li. An improved TLBO with elite strategy for parameters identification of PEM fuel cell and solar cell models. *International Journal of Hydrogen Energy*. 2014, Vol.39, N°8. https://doi.org/10.1016/j.ijhydene.2013.12.110

[133] BOUALI, Chaabane. SCHULTE, Horst. MAMI, Abdelkader. A High Performance Optimizing Method for Modelling Photovoltaic Cells and Modules Array Based on Discrete Symbiosis Organism Search. *Energies*. 2019, Vol.12, p.2246. Doi:10.3390/en12122246

[134] JACOBA, Basil. BALASUBRAMANIANA, Karthik. SUDHAHAR BABU, Ta S. AZHARUDDINA, Mohammed. RAJASEKAR, N. Solar PV modelling and Parameter Extraction using Artificial Immune system. *Energy Procedia*. 2015, Vol.75, p.331 – 336. https://doi.org/10.1016/j.egypro.2015.07.375

[135] QIN, Hengsi. W KIMBALL, Jonathan / IEEE Power and Energy Conference at Illinois. *Parameter Determination of Photovoltaic Cells from Field Testing Data using Particle Swarm Optimization*, 25-26 Feb. 2011, Urbana, IL, USA. IEEE, 28 March 2011.

[136] JUN SOON, Jing. LOW, Kay-Soon. Photovoltaic Model Identification Using Particle Swarm Optimization with Inverse Barrier Constraint. *IEEE Transactions on power electronics*. 2012, Volume: 27, Issue: 9 . DOI: 10.1109/TPEL.2012.2188818

[137] ASKARZADEH, Alireza. REZAZADEH, Alireza. Extraction of maximum power point in solar cells using bird mating optimizer-based parameters identification approach. *Solar Energy*. 2013, Vol. 90, p. 123–133. DOI: 10.1016/j.solener.2013.01.010

[138] ASKARZADEH, Alireza. REZAZADEH, Alireza. Artificial bee swarm optimization algorithm for parameters identification of solar cell models. *Applied Energy*. 2013, Vol.102, p. 943–949. https://doi.org/10.1016/j.apenergy.2012.09.052

[139] DAMANSYAH. ROBANDI, Imam / 3rd International Conference on Control, Automation and Robotics (ICCAR). *Photovoltaic Parameter Estimation Using Grey Wolf Optimization*, 24-26 April 2017. IEEE, 08 June 2017, Nagoya, Japan. DOI: 10.1109/ICCAR.2017.7942766

[140] DIEGO, Oliva. MOHAMED, Abd El Aziz. ABOUL, Ella Hassanien. Parameter estimation of photovoltaic cells using an improved chaotic whale optimization algorithm. *Applied Energy*. 2017, Vol.200. N°.C, p.141–54. DOI: 10.1016/j.apenergy.2017.05.029

[141] GUO, Lei. MENG, Zhuo. SUN, Yize. WANG, Libia. Parameter identification and sensitivity analysis of solar cell models with cat swarm optimization algorithm. *Energy Convers Manage*. 2016, Vol.108, p. 520–8. DOI: 10.1016/j.enconman.2015.11.041

[142] SANDROLINI, L. ARTIOLI, M. REGGIANI, U. Numerical method for the extraction of photovoltaic module double-diode model parameters through cluster analysis. *Applied Energy*. 2010, Vol.87, 442–451. https://doi.org/10.1016/j.apenergy.2009.07.022

[143] DHANUP, S. PILLAI, N. RAJASEKAR. Metaheuristic algorithms for PV parameter identification: A comprehensive review with an application to threshold setting for fault detection in PV systems. *Renewable and Sustainable Energy Reviews*. 2017, Vol.82, N°3, p. 3503-3525. https://doi.org/10.1016/j.rser.2017.10.107

[144] CHEN, Zhicong. LIJUN, Wu. PEIJIE, Lin. YUE, Wu. SHUYING, Cheng. Parameters identification of photovoltaic models using hybrid adaptive Nelder-Mead simplex algorithm based on eagle strategy. *Appl Energy*. 2016, Vol.182, p.47–57. DOI: 10.1016/j.apenergy.2016.08.083

[145] ABDUL HAMID, Nurul Farhana. ABD RAHIM, Nasrudin, SELVARAJ, Jeyraj. Solar cell parameters identification using hybrid Nelder-Mead and modified particle swarm optimization. *J Renew Sustain Energy*. 2016, Vol. 8, 015502. https://doi.org/10.1063/1.4941791

[146] HACHANA, Oussama. HEMSAS, K E. TINA, G M. VENTURA, C. Comparison of different metaheuristic algorithms for parameter identification of photovoltaic cell/module. *J Renew Sustain Energy*. 2013, Vol. 5. https://doi.org/10.1063/1.4822054

[147] ALI MUGHAL, Muhammad. MA, Qishuang. XIAO, Chunyan. Photovoltaic Cell Parameter Estimation Using Hybrid Particle Swarm Optimization and Simulated Annealing. *Energies*. 2017, Vol. 10, 1213. Doi: 10.3390/en10081213

[148] UCINSKI, D. Optimal Measurement Methods for Distributed Parameter System Identification: CRC Press. August 27, 2004. ISBN 9780367393984

[149] TCHOKETCH KEBIR, Selma. AIT CHEIKH, Mohamed Salah. HADDADI, Mourad. A detailed step-by-step electrical parameters identification method for photovoltaic generators using a combination of two approaches. *Advances in Science, Technology and Engineering Systems Journal*. 2018, Vol. 3, No. 4, p.45-52.

[150] TCHOKETCH KEBIR, Selma. Study of a new hybrid optimization-based method for obtaining parameters values of solar cells. In: *Solar cells*. IntechOpen, 2020. DOI: 10.5772/intechopen.93324

[151] LAWSON, Charles L. HANSON, Richard J. *Solving Least Squares Problems*. Society for Industrial and Applied Mathematics. Classics in applied mathematics, 1975. SIAM e-books. Philadelphia, Pa, Englewood Cliffs, NJ: Prentice-Hall. ISBN: 978-0-89871-356-5

[152] WHITTLE, Peter. SARGENT, Thomas J. *Least-square approximation*. In: Prediction and Regulation by Linear Least-Square Methods. 2nd ed. Minneapolis: University of Minnesota Press, 1983. Pp.46-55.

[153] LOURAKIS, Manolis. A Brief Description of the Levenberg-Marquardt Algorithm Implemened by levmar. *Crete, Greece: Institute of Computer Science, Foundation for Research and Technology – Hellas (FORTH*). 2005.

[154] DKHICHI, F. OUKARFI, B. Levenberg-Marquardt algorithm for parameter identification of solar cell model. In: Conference Paper. June 2014. pp.781-788.

[155] LUGER, F George. *Artificial Intelligence Structures and Strategies for Complex Problem Solving*. ADDISON WESLEY. Fifth edition published, 2005.

[156] HAYKIN, Simon. *Neural Networks: A comprehensive foundation*. Pearson Education, 2005.

[157] ISAAC ABIODN, Oludare. JANTAN, Aman, ESTHER OMOLARA, Abiodun. VICTORIA DADA, Kemi. ABD ELATIF MOHAMED, Nachaat. ARSHAD, Humaira. State-of-the-art in artificial neural network applications: A survey. *Heliyon*. 2018, Vol.4 e00938. https://doi.org/10.1016/j.heliyon.2018.e00938

[158] BENBOUCHAMA, Cherrad. *Contribution à l'implémentation des réseaux de neurones artificiels sur hardware reconfigurable FPGA*. Thèse de doctorat : Electronique. Algerie : Ecole Nationale Polytechnique, 2008.

[159] Fundamentales in neural networks : Artificial Intelligence. AI course, https://www.myreaders.info/htm/artificial_intelligence.html

[160] TCHOKETCH KEBIR, Selma. CHEGGAGA, Nawal. ILINCA, Adrian. BOULOUMA, Sabri. An Efficient Neural Network-Based Method for Diagnosing Faults of PV Array. *Sustainability* 2021, *13*(11), 6194; https://doi.org/10.3390/su13116194.

[161] CHOUDER, Aiassa. SILVESTRE, Santiago. Automatic supervision and fault detection of PV systems based on power losses analysis. *Energy Conversion and Management*. 2010, vol. 51, pp. 1929-1937, 2010/10/01. https://www.academia.edu/29169405/Automatic_supervision_and_fault_detection_of_PV_systems_based_on_power_losses_analysis

[162] CHOUDER, Aissa. SILVESTRE, Santiago. TAGHEZOUIT, Billal. KARATEPE, Engin. Monitoring, modelling and simulation of PV systems using LabVIEW. *Solar Energy*. 2013, Vol. 91, 337–349.

[163] SOBHANI TEHRANI, Ehsan. KHORASANI, Khashayaer. *Fault Diagnosis of Nonlinear Systems Using a Hybrid Approach*. Springer: Control and Information Sciences. 2009, Chapitre 2.

[164] CHINE, W. MELLIT, A. LUGHI, V. MALEK, A. SULLIGOI, G. MASSI PAVAN, A. A novel fault diagnosis technique for photovoltaic systems based on artificial neural networks. *Renew. Energy*. 2016, 90, 501–512. DOI: 10.1016/j.renene.2016.01.036

[165] SPECHT, Donald F. Probabilistic neural networks. *Neural Networks*. 1990, vol. 3, pp. 109-118, 1990/01/01/. https://doi.org/10.1016/0893-6080(90)90049-Q

[166] PARZEN, Emanuel. On Estimation of a Probability Density Function and Mode. *Ann. Math. Statist*. 1962, Vol. 33, pp. 1065-1076. Disponible à l'adresse: https://bayes.wustl.edu/Manual/parzen62.pdf

[167] BURRASCANO, P. Learning vector quantization for the probabilistic neural network. *IEEE Transactions on Neural Networks*. February 1991, Vol.2, N°.4: 458-61.

[168] KIM, Moon W. AROZULLAH, Mohamed. Generalized probabilistic neural network based classifiers. *In: IJCNN International Joint Conference on Neural Networks*. 1992, vol.3, 648-653.

[169] LIPPMAN, Richard P. An Introduction to computing with Neural Nets. I*EEE ASSP Magazine.* April 1987, pp. 4 -22.

[170] AIRIAU, R. BERGE, J. M. OLIVE, V. Circuit Synthesis with VHDL. Kluwer Academic Publishers. Disponible à l'adresse: https://link.springer.com/content/pdf/bfm%3A978-1-4615-2760-2%2F1.pdf

[171] lZEBOUDJEN, N. FARAH, A. TITRI, S. BOUMERIDJA, H. Digital Implementation of Artificial Neural Networks: From VHDL Description to FPGA Implementation. 1999.

[172] KARTOUT, Hadjira. *Implémentation de l'Algorithme Cordic sur un FPGA (Field Programmable Gate Array) Application au Modèle de PARK*. Mémoire de Magister : Physique Appliquée. Algerie : École Normale Superieure De Kouba, 2009.

[173] TITRI, Sabrina. *Circuits reconfigurables pour la gestion de l'énergie dans les systèmes photovoltaïques*. Thèse de doctorat : Electronique. Algérie : Ecole Nationale Polytechnique, 2018.

[174] K A HAMDAN, Muhammad. *VHDL auto-generation tool for optimized hardware acceleration of convolutional neural networks on FPGA (VGT)*. Graduate states and dissertations. United State: Iowa State University, 2018. https://lib.dr.iastate.edu/etd/16368

[175] TITRI, Sabrina. Synthèse et simulation d'un réseau de neurone décrit en VHDL. *Rapport d'activité*, CDTA, Alger, 2003.

[176] DEKEYSER, Jean Luc. DIDACTICIEL D'INITIATION À L'ENVIRONNEMENT DE CONCEPTION FPGA. Version, 2.1. Automne 2012.

[177] Introduction to Xilinx ISE 8.2i. University of Pennsylvania, Digital Design Laboratory.

[178] ABDU ALJABAR, Rana D. Design and Implementation of Neural Network in FPGA. *Journal of Engineering and Development*. Sep. 2012, Vol. 16, No.3, ISSN 1813- 7822.

[179] IZEBOUDJEN Nouma. *Plateforme pour l'implémentation des réseaux de neurones sur FPGA : Application à l'algorithme de la retro-propagation du gradient (RPG)*. Thèse de doctorat : Electronique. Algérie : Ecole Nationale Polytechnique, 2013/2014.

[180] ISE 10.1 Quick Start Tutorial. http://www.xilinx.com/support. Disponible à l'adresse : https://www.xilinx.com/support/documentation/application_notes/xapp1085-7s-isolation-design-flow-ise-14-4.pdf

[181] GLARIZA, Abdelwaheb. Implémentation des réseaux de neurones artificiels sur circuit FPGA en utilisant la représentation en virgule fixe. Mémoire de master : Electronique. Algérie : Université Saad Dahleb de Blida1, 2014.

[182] DS100 - Virtex-5 Family Overview (v5.1). https://www.xilinx.com/support/documentation/data_sheets/ds100.pdf

[182] https://www.xilinx.com/publications/matrix/Virtex5_Family_FPGAs.pdf

APPENDIX

APPENDIX

- **Calcul of GHI :**

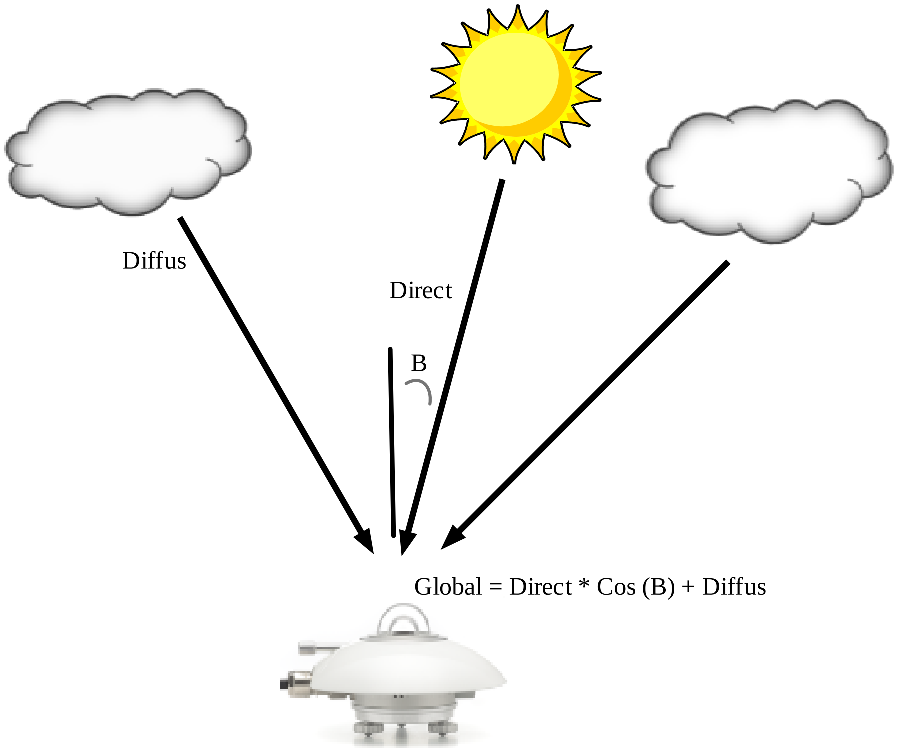

Figure 6.1 Calculation of the Global horizontal irradiation (GHI).

Solar simulator

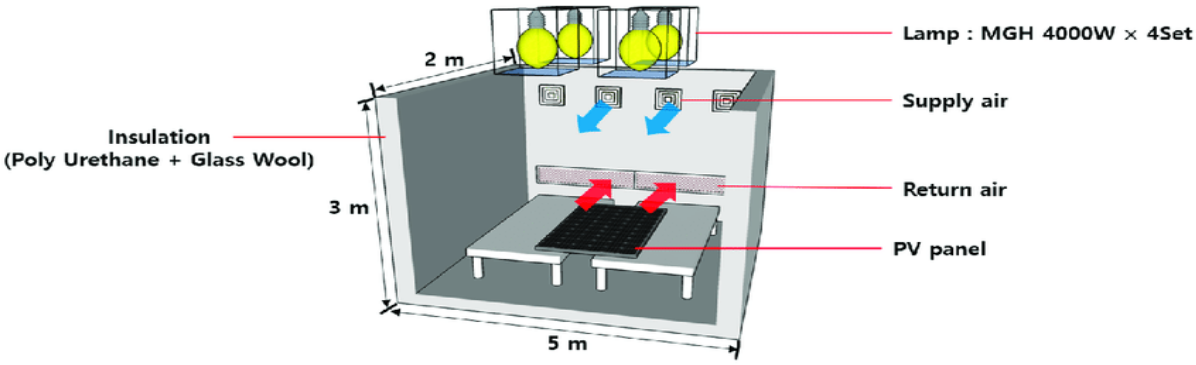

Figure 6.2 Solar Simulators for PV module testing.

PV panel's datasheet: PS250P-AC (250W)

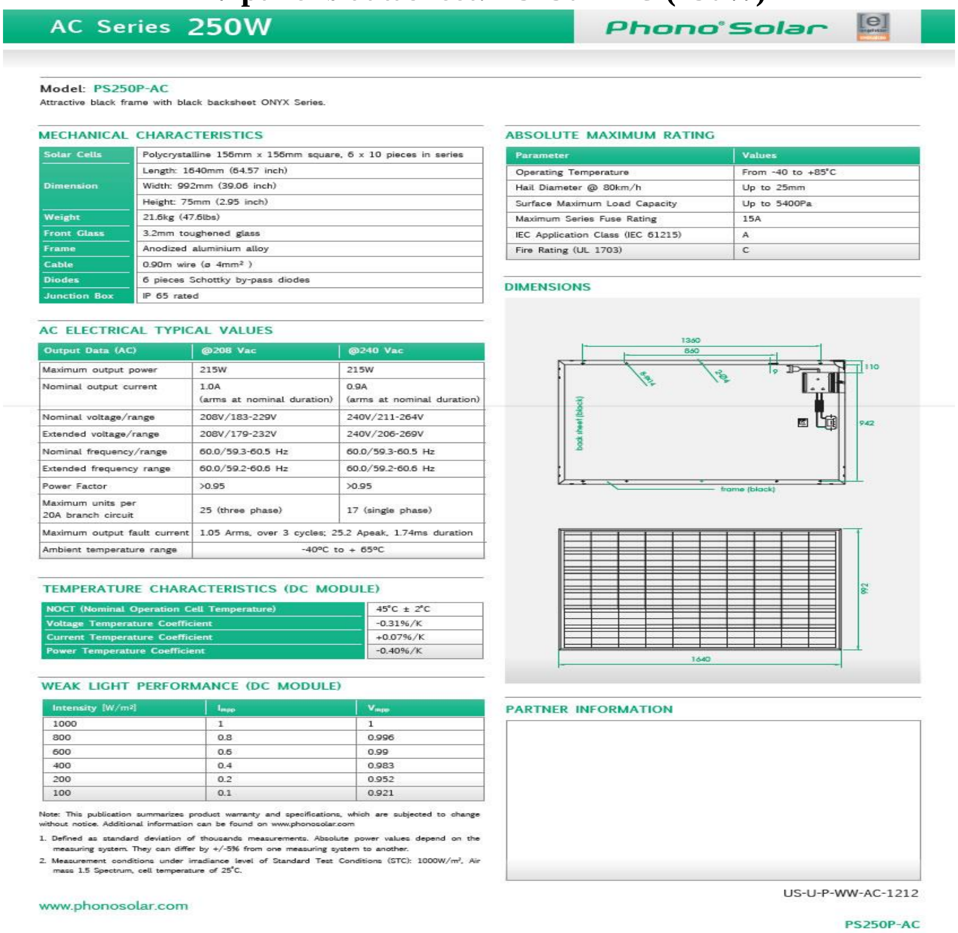

AC Series 250W

Phono Solar

Model: PS250P-AC

Attractive black frame with black backsheet ONYX Series.

MECHANICAL CHARACTERISTICS

Solar Cells	Polycrystalline 156mm x 156mm square, 6 x 10 pieces in series
Dimension	Length: 1640mm (64.57 inch)
	Width: 992mm (39.06 inch)
	Height: 75mm (2.95 inch)
Weight	21.6kg (47.6lbs)
Front Glass	3.2mm toughened glass
Frame	Anodized aluminium alloy
Cable	0.90m wire (ø $4mm^2$)
Diodes	6 pieces Schottky by-pass diodes
Junction Box	IP 65 rated

ABSOLUTE MAXIMUM RATING

Parameter	Values
Operating Temperature	From -40 to +85°C
Hail Diameter @ 80km/h	Up to 25mm
Surface Maximum Load Capacity	Up to 5400Pa
Maximum Series Fuse Rating	15A
IEC Application Class (IEC 61215)	A
Fire Rating (UL 1703)	C

AC ELECTRICAL TYPICAL VALUES

Output Data (AC)	@208 Vac	@240 Vac
Maximum output power	215W	215W
Nominal output current	1.0A (arms at nominal duration)	0.9A (arms at nominal duration)
Nominal voltage/range	208V/183-229V	240V/211-264V
Extended voltage/range	208V/179-232V	240V/206-269V
Nominal frequency/range	60.0/59.3-60.5 Hz	60.0/59.3-60.5 Hz
Extended frequency range	60.0/59.2-60.6 Hz	60.0/59.2-60.6 Hz
Power Factor	>0.95	>0.95
Maximum units per 20A branch circuit	25 (three phase)	17 (single phase)
Maximum output fault current	1.05 Arms, over 3 cycles; 25.2 Apeak, 1.74ms duration	
Ambient temperature range	-40ºC to + 65ºC	

DIMENSIONS

TEMPERATURE CHARACTERISTICS (DC MODULE)

NOCT (Nominal Operation Cell Temperature)	45°C ± 2°C
Voltage Temperature Coefficient	-0.31%/K
Current Temperature Coefficient	+0.07%/K
Power Temperature Coefficient	-0.40%/K

WEAK LIGHT PERFORMANCE (DC MODULE)

Intensity [W/m²]	I_{mpp}	V_{mpp}
1000	1	1
800	0.8	0.996
600	0.6	0.99
400	0.4	0.983
200	0.2	0.952
100	0.1	0.921

PARTNER INFORMATION

Note: This publication summarizes product warranty and specifications, which are subjected to change without notice. Additional information can be found on www.phonosolar.com

1. Defined as standard deviation of thousands measurements. Absolute power values depend on the measuring system. They can differ by +/-5% from one measuring system to another.
2. Measurement conditions under irradiance level of Standard Test Conditions (STC): 1000W/m², Air mass 1.5 Spectrum, cell temperature of 25°C.

www.phonosolar.com

US-U-P-WW-AC-1212

PS250P-AC

Figure 6.3 Datasheet of PV panel parameters.

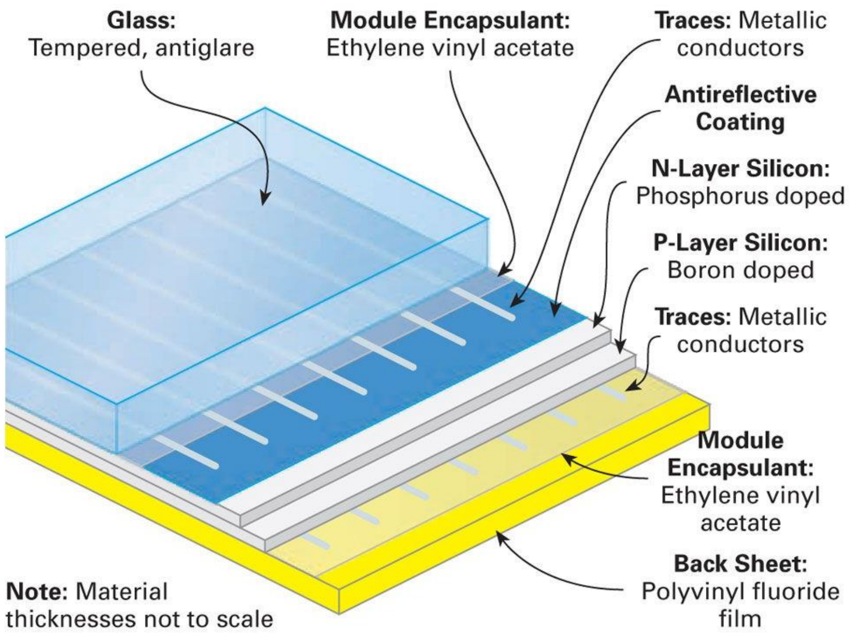

Figure 6.4 Constitution and anatomy of a PV panel.

Figure 6.5 Laboratory for PV module testing.

❖ **FLIR camera for inspection of PV panels**

In the field of research and development, thermal imaging cameras are an established tool for evaluating solar cells and panels. However, the use of thermal imaging cameras for solar panel evaluation is not restricted to the field of research. Uncooled thermal imaging cameras are currently being used more and more for solar panel quality controls before installation and regular predictive maintenance check-ups after the panel has been installed. Because these affordable cameras are handheld and lightweight, they allow a very flexible use in the field.

Figure 6.6 FLIR picture.

❖ **I-V test curve tracers**

Figure 6.7 PV analyser (Solmetric).

❖ **Drones**

Figure 6.8 Drones.

Drones are used to monitor solar site construction or to conduct regular assessments. The integration of infrared imaging and artificial intelligence (AI) algorithms, allow to identify deterioration, damage and other abnormalities in an early stage.

- **Agilent 34970A card for data acquisition**

The Keysight 34970A data acquisition / data logger switch consists of a three-slot mainframe with a built-in 6 1/2 digit digital multimeter. Each channel can be configured independently to measure one of 11 different functions without the added cost or hassles of signal-conditioning accessories. Choose from eight optional plug-in modules to create a compact data logger, full-featured data acquisition system or low-cost switching unit. On-module screw-terminal connections eliminate the need for terminal blocks and a unique relay maintenance feature counts every closure on every switch for easy, predictable relay maintenance. Our most popular module 34901A features a built-in thermocouple reference and 20 two-wire channels.

Figure 6.9 Agilent Card.

- **Pyranometer**

Figure 6.10 Pyranometer.

❖ K-type thermocouple

Type K Thermocouple (Nickel-Chromium / Nickel-Alumel): The type K is the most common type of thermocouple. It's inexpensive, accurate, reliable, and has a wide temperature range. The type K is commonly found in nuclear applications because of its relative radiation hardness. Maximum continuous temperature is around 1,100C.

Figure 6.11 K -type thermocouple.

ACHEIVEMENTS OF PAPERS AND CONFERENCES

Achievements of papers and conferences

1. Publication

- **Selma Tchoketch Kebir,** Nawal Cheggaga, Mohamed Salah Ait Cheikh, Mourad Haddadi. "A comprehensive study of diagnosis techniques for faults occurring in photovoltaic generators". *Engineering Review, Vol. XX, Issue X, XX-XX, 14.01.2021. DOI: 10.30765/er.1714.*
- **Selma Tchoketch_Kebir,** Nawal Cheggaga, Adrian Ilinca, and Sabri Boulouma. "An Efficient Neural Network-Based Method for Diagnosing Faults of PV Array". *Sustainability 2021, 13, 6194. https://doi.org/10.3390/su13116194.*
- **Selma Tchoketch_Kebir**. Study of a New Hybrid Optimization-Based Method for Obtaining Parameter Values of Solar Cells. http://dx.doi.org/10.5772/intechopen.93324
- **Selma TCHOKETCH KEBIR**. A summary of methods to get parameters values of photovoltaic cells/panels". Revue des Energies Renouvelables du CDER : JREEN -20-07-022 : (Journal of Renewable Energies (Revue des Energies Renouvelables)), Volume 23, numéro 1, novembre 2020. https://www.asjp.cerist.dz/en/article/133867.
- Billel Boumaaraf, Houria Boumaaraf, Mohamed El-Amine Slimanic, **Selma Tchoketch_Kebir**, Mohamed Salah Ait-cheikha, Khaled Touafek. Performance evaluation of a locally modified PV module to a PV/T solar collector under climatic conditions of semi-arid region. Mathematics and Computers in Simulation 167 (2020) 135–154.
- **Selma Tchoketch Kebir**, Mohamed Salah Ait Cheikh, Mourad Haddadi. "A detailed step-by-step electrical parameters identification method for photovoltaic generators using a combination of two approaches". Adv. Sci. Technol. Eng. Syst. J. 3(4), 45-52 (2018);
- Gul Filiz Tchoketch Kebir, Cherif Larbes, Adrian Ilinca, Thameur Obeidi, and **Selma Tchoketch Kebir**. "Study of the Intelligent Behavior of a Maximum Photovoltaic Energy Tracking Fuzzy Controller". Energies 2018, 11, 3263; doi:10.3390/en11123263.

2. Communication

- CEIT'2015 (3rd International Conference on Control, Engineering & Information Technology) 25-27 May 2015, Tlemcen, Algeria
  S.TCHOKETCH KEBIR, M.HADDADI, M.S. AIT CHEIKH. "An Overview Of Solar Cells Parameters Extraction Methods". IEEE proceeding.

- ICEE'2017 (5th International Conference on Electrical Engineering) 29-31 October 2017, Boumerdes, Algeria
  S.TCHOKETCH KEBIR, M.S. AIT CHEIKH, M.HADDADI, B.BOUMAARAF. "Step by step parameters identification for photovoltaic generator". IEEE proceeding
- M. Hatti (Ed.): "Renewable Energy for Smart and Sustainable Cities", **Selma Tchoketch Kebir**, Mohamed Salah Ait Cheikh, and Mourad Haddadi, "A Set of Smart Swarm-Based Optimization Algorithms Applied for Determining Solar Photovoltaic Cell's Parameters", Springer Nature America, Inc, ICAIRES 2018, LNNS 62, pp. 384–399, 2019.